Space-Based Solar Power

Conceptual and Preliminary Design of a Scalable SBSP System for a Lunar Demonstration Mission

Hobie Köster 4652312

Delft University of Technology

TU Delft

Preface

First of all, I would like to thank my supervisor, Angelo Cervone, for his invaluable guidance. Next, I would like to thank my family and friends for their unwavering support and understanding during the course of this journey.

Hobie Köster 4652312
Delft, January 2025

Cover image [103].

Summary

Space-Based Solar Power (SBSP) is an innovative concept first introduced by Dr. Peter Glaser in the 1960s. The concept is based on the ability to deliver power from space using a wireless power transmission method. This technology could supply energy 24/7 to remote locations using the virtually inexhaustible energy source, the Sun. Despite its promising potential, SBSP experienced significant technical and economic challenges at the time of its invention.

Beyond Earth-based applications, SBSP holds a great potential for extraterrestrial use, especially on the Moon. The long lunar night, lasting around 15 Earth days, makes it difficult to effectively deploy traditional solar panels. SBSP could provide a reliable energy solution for lunar habitats, powering life support systems and other critical systems. Furthermore, the Moon acts as an ideal testbed for refining SBSP technologies, preparing it for potential Martian applications.

This thesis focuses on designing a conceptual SBSP system for a lunar demonstration mission. In particular, it investigates system architecture, power transmission techniques and subsystem trade-offs for a promising SBSP system design. The research also aims to address the mission objectives of the lunar demonstration mission, optimal transmission methods, redundancy measures and scalability for future operations.

The SBSP lunar demonstration mission aims to validate the solar power generation, transmission, thermal control and communication functionalities in the lunar environment while assessing scalability, redundancy, orbital maneuverability and long-term operational sustainability. Further, the mission is to validate the Power Management and Distribution (PMAD) subsystem.

Laser Power Transmission (LPT) is the preferred power transmission technique due to its compact design, higher power density and lower deployment costs, which makes it more fitting within mass, volume and budget constraints. RF SBSP has a higher end-to-end efficiency and technical maturity (TRL 6) but faces challenges in deployment complexity due to its modular nature. Laser SBSP enables a more practical, precise and cost-effective solution for the lunar demonstration mission.

The optimal SBSP lunar demonstration mission consists of a Frozen Polar Low Lunar Orbit, a one-year mission delivering 3 kW via laser transmission onto the lunar receiver. The End-of-Life strategy will be a controlled lunar impact.

The SBSP conceptual design consists of the following subsystems and their respective components. Two deployable MegaFlex solar arrays are used for energy collection. The Laser Power Transmission (LPT) subsystem utilizes a custom laser unit combining multiple low-power lasers together with a custom beam director for precisely pointing the beam. The PMAD subsystem includes SSUs, DCSUs, MBSUs, DDCUs, BCDUs, and Li-ion batteries for power conditioning, distribution and storage. The Thermal Control subsystem incorporates cold plates, active fluid loops, and a radiator for heat management. The ADCS subsystem relies on two star trackers, four sun sensors, and two 3-axis fiber optic gyroscopes, and for control it uses four reaction wheels and eight hydrazine thrusters for stability and maneuvers. The On-Board Computer (OBC) is the ICDE-NG by Airbus, coming with integrated hardware redundancy. Telecommunication subsystem features one high-gain (X-band) and two low-gain (S-band) antennas, two transponders, and an RFDU for communication. The Structure utilizes a primary sandwich core with honeycomb panels as its skin. Finally, Propulsion includes four hydrazine thrusters, two titanium propellant tanks, a helium pressurant tank, pressure regulators, pipes, and valves for the orbital insertion and End-of-Life maneuvers.

Including margins, the 3 kW SBSP system will have a total mass of 4057.43 kg, with a dry mass of 2596.03 kg. In total, the MegaFlex arrays will be able to generate 15772 W with a total area of 72.78 m^2. The satellite has a length of 3.67 m. The total spacecraft bus can hold a volume of 17.80 m^3, while all internal components only hold up to 4.58 m^3 in volume, excluding the active fluid loop.

The system sizing model outputs align reasonably with the reference 40 kW SBSP system, displaying a 35.6% mass difference mainly due to different assumptions during subsystem design. Key variations come from potentially different PMAD architecture, radiator design and system efficiency assumptions.

Scaling the SBSP system results in significant increases in mass, power requirements and subsystem scaling as power output and mission duration grow. Further, the specific power for larger systems decreases. Large-scale systems face feasibility challenges due to launcher payload limits and reduced mass efficiency. Hence, deploying multiple smaller SBSP systems provide a redundant and flexible alternative for supporting lunar habitats.

Concluding, a laser-based SBSP system capable of delivering 3 kW of power from LLO to the surface was identified as a promising demonstration mission, with scalable and redundant subsystems designed to support future operations up to 45 kW. Despite the promising solutions in the design, key assumptions regarding the LPT, PMAD and TCS subsystems require further detailed development and optimization to ensure system feasibility and performance.

Contents

Nomenclature

Abbreviations

Abbreviation	Definition
ACS	Attitude Control System
ADCS	Attitude Determination and Control System
ADS	Attitude Determination System
ATCS	Active Thermal Control System
BCDU	Battery Charge Discharge Unit
BOL	Begin-of-Life
CFRP	Carbon Fiber Reinforced Polymer
CMG	Control Moment Gyroscopes
COTS	Commercial Off-The-Shelf
CPL	Capillary Pumped Loops
CSS	Coarse Sun Sensor
CSP	Concentrated Solar Power
DC	Direct Current
DCSU	Direct Current Switching Unit
DDCU	Direct Current to Direct Current Converter Unit
DLR	Deutsches Zentrum für Luft- und Raumfahrt
DSS	Deployable Space Systems
EIRP	Effective Isotropic Radiated Power
EOL	End-of-Life
ESA	European Space Agency
EU	Electronics Unit
FOG	Fiber Optic Gyroscope
HEFLO	Highly Elliptical Frozen Lunar Orbit
HGA	High Gain Antenna
ICDE-NG	Integrated Control and Data Equipment - Next Generation
IMU	Inertial Measurement Unit
IR	Infrared
ISS	International Space Station
LAU	Laser Assembly Unit
LEO	Low Earth Orbit
LGA	Low Gain Antenna
LHP	Loop Heat Pipes
LLO	Low Lunar Orbit
LOI	Lunar Orbit Insertion
LPT	Laser Power Transmission
MBSU	Main Bus Switching Unit
MGA	Medium Gain Antenna
MLI	Multi-Layer Insulation
MPT	Microwave Power Transmission
MBSU	Main Bus Switching Unit
NASA	National Aeronautics and Space Administration
Nd YAG	Neodymium-doped Yttrium Aluminum Garnet

Abbreviation	Definition
NLR	Nederlandse Lucht- en Ruimtevaartlaboratorium
OH	Optical Head
OBC	On-Board Computer
OBDH	On-Board Data Handling
PMAD	Power Management and Distribution
PV	Photovoltaic
RF	Radio Frequency
RFDU	Radio Frequency Distribution Unit
RLV	Reusable Launch Vehicles
ROSA	Roll-Out Solar Array
RW	Reaction Wheel
RWA	Reaction Wheel Assembly
RWU	Reaction Wheel Unit
S/C	Spacecraft
SBSP	Space Based Solar Power
SERT	SSP Exploratory Research and Technology
SPS	Solar Power Satellite
SSU	Sequential Shunt Unit
TC	Telecommand
TCS	Thermal Control System
TM	Telemetry
TLI	Trans-Lunar Injection
TRL	Technological Readiness Level
TT&C	Telemetry, Telecommand and Control
WDE	Wheel Drive Electronics box
WPT	Wireless Power Transmission

Symbols

Symbol	Definition	Unit
A	Cross-sectional area of the structure	[m^2]
A_{exposed}	Exposed surface area of the satellite	[m^2]
A_{MLI}	Area of the Multi-Layer Insulation (MLI) material	[m^2]
A_{radiator}	Required radiator area	[m^2]
A_{rect}	Area of the four rectangular sides of the satellite	[m^2]
A_{square}	Area of the two square sides of the satellite	[m^2]
A_{SA}	Solar array area required to meet power demand	[m^2]
$A_{\text{spot,min}}$	Minimum spot size	[m^2]
A_{total}	Total area of the skin panels	[m^2]
a	Semi-major axis of the elliptical orbit	[km]
C_{battery}	Required battery capacity	[Ah]
D_{BD}	Required beam director diameter	[m]
D_{HGA}	HGA diameter	[m]
$D_{\text{pressurant tank}}$	Pressurant tank diameter	[m]
$D_{\text{propellant tank}}$	Propellant tank diameter	[m]
D_{ref}	Reference diameter	[m]
D_{spot}	Spot size diameter	[m]
D_t	Transmitter diameter	[m]
d	Spot size diameter	[m]
DOD	Depth of discharge	[-]
E_{battery}	Total battery energy	[Wh]
E_{required}	Energy required during eclipse	[Wh]

Symbol	Definition	Unit
$EIRP$	Effective isotropic radiated power	[dBm]
$\left(\frac{E_b}{N_o}\right)_{\text{received}}$	Received energy per bit to noise density ratio	[dB]
$\left(\frac{E_b}{N_o}\right)_{\text{required}}$	Required energy per bit to noise density ratio	[dB]
e_{MLI}	Specific weight of the MLI material	[kg/m^2]
e_{density}	Energy density of the battery	[Wh/L]
e_{specific}	Specific energy of the battery	[Wh/kg]
F_{axial}	Axial force experienced by the spacecraft	[N]
F_{lateral}	Lateral force encountered during launch	[N]
G_{HGA}	HGA gain	[dBic]
G_{R}	Ground station antenna gain	[dBic]
g	Gravitational acceleration (9.81 m/s^2)	[m/s^2]
h	Orbital altitude above lunar surface	[km]
I	Moment of inertia	[kg·m^2]
I_{albedo}	Albedo irradiance from the lunar surface	[W/m^2]
I_{moon}	Lunar infrared radiation in LLO	[W/m^2]
I_{solar}	Solar irradiance on the lunar satellite	[W/m^2]
I_{sun}	Solar irradiance at 1 AU	[W/m^2]
I_{sp}	Specific impulse of the propulsion system	[s]
L	Distance between the transmitter and receiver	[m]
L	Length of the satellite	[m]
L_{a}	Atmospheric loss	[dB]
L_{margin}	Link margin	[dB]
L_{receiver}	Receiver internal losses	[dB]
L_{space}	Free-space path loss	[dB]
L_{max}	Maximum beaming distance	[m]
L_{Moon}	Radius of the Moon	[km]
M_{Al}	Mass of the aluminum honeycomb core	[kg]
M_{base}	Mass of base fluid loop	[kg]
$M_{\text{component}}$	Mass of PMAD component	[kg]
$M_{\text{core,CFRP}}$	Mass of the CFRP core	[kg]
$M_{\text{core,Al}}$	Mass of the aluminum honeycomb core	[kg]
M_{core}	Total mass of the core structure	[kg]
M_{CFRP}	Mass of the CFRP sheets	[kg]
M_{dry}	Dry mass of the spacecraft	[kg]
$M_{\text{dry+margin}}$	Dry mass of the spacecraft with margin	[kg]
M_{FL}	Mass of the total fluid loop	[kg]
M_{gas}	Mass of the pressurant gas	[kg]
M_{helium}	Molecular weight of helium	[g/mol]
M_{heater}	Mass of the heater for the spacecraft bus	[kg]
$M_{\text{heater,SA}}$	Mass of the heater for the solar array	[kg]
M_{laser}	Mass of one laser	[kg]
M_{lateral}	Bending moment caused by lateral loads	[N·m]
M_{LAU}	Mass of one LAU	[kg]
M_{LPT}	Mass of the combined LAUs	[kg]
M_{MLI}	Mass of the MLI material	[kg]
M_{panels}	Total mass of the skin panels	[kg]
M_{sat}	Satellite mass	[kg]
$M_{\text{structure}}$	Total structural mass of the SBSP satellite	[kg]
M_{tank}	Total mass of the combined propellant and pressurant gas tanks	[kg]
$M_{\text{tank,he}}$	Mass of the pressurant gas tank	[kg]
M_{P}	Required propellant mass	[kg]
m_{BD}	Estimated mass of beam director	[kg]

Symbol	Definition	Unit
m_{battery}	Battery mass	[kg]
m_{SA}	Mass of one solar array	[kg]
m_{ref}	Reference mass	[kg]
N	Number of lasers	[-]
N_0	System noise density	[dBm/Hz]
n_{axial}	Axial load factor	[—]
n_{lateral}	Lateral load factor	[—]
n_{helium}	Number of moles of helium	[mol]
P_{base}	Base heat rejection power	[W]
P_{density}	Maximum power density of receiver	[kW/m^2]
P_d	Power required during daylight	[W]
P_e	Power required during eclipse	[W]
P_{ecl}	Power consumed during eclipse	[W]
P_{f}	Final pressure of the helium gas	[Pa]
P_{heaters}	Required heater power	[W]
$P_{\text{in,comp}}$	Input power to the component	[W]
P_{i}	Initial pressure of the helium gas	[Pa]
P_{laser}	Output power of each laser	[W]
P_{output}	Output power required from each LAU	[W]
P_{prop}	Internal pressure of the propellant tank	[Pa]
P_{R}	Received power	[dBm]
P_{required}	Required heat rejection power	[W]
P_{SA}	Effective power generated by the solar array	[W]
$P_{\text{SA,tot}}$	Total power generated by the solar array, accounting for degradation factors	[W]
$P_{\text{SA,eff}}$	Effective power generated by the solar array	[W]
$P_{\text{sys,i}}$	Power consumed by the i-th internal subsystem	[W]
$P_{\text{transmitted}}$	Transmitted power	[W]
P_{T}	Transmitted power	[dBm]
P_{tank}	Pressure in the propellant tank	[Pa]
p_{specific}	Specific power of the solar array	[W/kg]
p_{specific}	Specific power of the component	[W/kg]
Q_{albedo}	Heat absorbed from albedo radiation	[W]
Q_{moon}	Heat absorbed from lunar IR radiation	[W]
$Q_{\text{heaters,SA}}$	Power required by the heaters for the solar array	[W]
Q_{solar}	Heat absorbed from direct solar radiation	[W]
$Q_{\text{PMAD,ecl}}$	PMAD heat generation during non-operational phase	[W]
Q_{total}	Total heat load	[W]
Q_{external}	Heat absorbed from external sources	[W]
Q_{internal}	Heat generated internally by the SBSP system	[W]
$Q_{\text{int,SA}}$	Internal heat generated by the solar panels	[W]
$Q_{\text{rad,SA}}$	Heat radiated into space by the solar arrays	[W]
Q_{radiated}	Heat radiated out into space	[W]
R_{SA}	Required radius of the solar array	[m]
R	Data rate	[bps]
R_{tank}	Average radius of the cylindrical structure	[m]
$R_{\text{tank,he}}$	Radius of the pressurant gas tank	[m]
R_{Moon}	Radius of the Moon	[km]
R_{tank}	Radius of the propellant tank	[m]
r_{spot}	radius of spot size	[m]
r_t	radius of transmitter aperture	[m]
r_{apoapsis}	Apoapsis radius of the elliptical orbit	[km]
r_{orbit}	Orbital radius for a circular orbit	[km]

Symbol	Definition	Unit
$r_{\text{periapsis}}$	Periapsis radius of the elliptical orbit	[km]
SF	Safety factor	[—]
T	Temperature of radiating surface	[K]
T_{i}	Initial temperature of the helium gas	[K]
T_{radiator}	Operating temperature of radiator	[K]
T_{SA}	Temperature of the solar array	[K]
$T_{\text{SA,hot}}$	Equilibrium temperature of the solar array in the hot case	[K]
$T_{\text{sat,hot}}$	Equilibrium temperature of satellite in the hot case	[K]
$T_{\text{sat,cold}}$	Equilibrium temperature of satellite in the cold case	[K]
t_{aluminum}	Thickness of the aluminum honeycomb layer	[m]
t_{CFRP}	Thickness of the CFRP material	[m]
t_d	Daylight duration	[h]
t_e	Eclipse duration	[h]
t_{tank}	Thickness of the propellant tank	[m]
$t_{\text{tank,he}}$	Thickness of the pressurant gas tank	[m]
V_{Al}	Volume of the aluminum honeycomb core	[m^3]
V_{bat}	Battery voltage	[V]
V_{battery}	Battery volume	[m^3]
V_{CFRP}	Volume of the CFRP sheets	[m^3]
$V_{\text{component}}$	Volume of one PMAD component	[m^3]
V_{SA}	Volume of one solar array	[m^3]
V_{laser}	Volume of one laser	[m^3]
V_{LAU}	Volume of one LAU	[m^3]
V_{LPT}	Volume of the combined LAUs	[m^3]
V_{tank}	Volume of the propellant tank	[m^3]
$V_{\text{tank,he}}$	Volume of the pressurant gas tank	[m^3]
$v_{\text{apoapsis, new}}$	Orbital velocity at apoapsis in the new elliptical orbit	[km/s]
v_{orbit}	Orbital velocity for a circular orbit	[km/s]
v_{specific}	Specific power density of the solar array	[kW/m^3]
α_{surface}	Absorptivity of the surface material	[-]
α_{SA}	Absorptivity of the solar array coating	[-]
β	Elevation angle	[degrees]
θ	divergence half-angle	[rad]
ΔV	Required change in velocity (delta-v)	[km/s]
ϵ	Emissivity of satellite surface	[-]
$\epsilon_{\text{radiator}}$	Emissivity of radiator	[-]
σ	Stefan-Boltzmann constant	[W/m2K^4]
η_d	Daytime efficiency of the power system	[-]
$\eta_{\text{sys,i}}$	thermal efficiency of the i-th internal subsystem	[-]
η_e	Nighttime efficiency of the power system	[-]
η_{charge}	Charge efficiency of the battery	[-]
$\eta_{\text{discharge}}$	Discharge efficiency of the battery	[-]
$\eta_{\text{distribution}}$	Efficiency of power distribution	[-]
$\eta_{\text{power conditioning}}$	Power conditioning efficiency	[-]
η_{SSU}	Efficiency of the SSU	[-]
η_{DCSU}	Efficiency of the DCSU	[-]
η_{BCDU}	Efficiency of the BCDU	[-]
η_{Bat}	Efficiency of the battery system	[-]
η_{MBSU}	Efficiency of the MBSU	[-]
η_{DDCU}	Efficiency of the DDCU	[-]
γ	Specific heat ratio of helium	[-]
σ_{axial}	Axial stress in the structure	[Pa]
σ_{titanium}	Yield strength of titanium material	[Pa]

Symbol	Definition	Unit
λ	Wavelength	[m]
μ	Lunar gravitational parameter	[km^3/s^2]
$\rho_{component}$	Density of one PMAD component	[kg/m^3]
$\rho_{titanium}$	Density of titanium	[kg/m^3]
η_{aging}	Aging degradation factor for solar arrays	[-]
η_{degrad}	Combined degradation factor for solar arrays (aging, shadowing, and temperature effects)	[-]
η_{shadow}	Shadowing degradation factor for solar arrays	[-]
η_{temp}	Temperature degradation factor for solar arrays	[-]
τ	Shear stress in the aluminum honeycomb material	[Pa]

List of Figures

List of Tables

1

Introduction to Space-Based Solar Power

In this chapter, an introduction on Space Based Solar Power (SBSP) will be given. First, the background of SBSP will be elaborated. Then, the potential of SBSP as a renewable energy will be addressed. Next, the lunar SBSP applications will be elaborated. At last, the objectives and research questions of the thesis will be listed and discussed.

1.1. Background and Overview of SBSP

In the late 1960s, Dr. Peter Glaser invented the concept of the 'solar power satellite' (SPS). The SPS, or now more commonly referred as a SBSP system, is a concept that tries to tackle the challenge of providing large-scale energy for humanity. By positioning a large platform containing photovoltaics panels in space in a high Earth orbit, the system continuously collects and converts solar energy into electricity [54]. The generated power is then used to run a wireless power transmission (WPT) system. A WPT system is capable of transmitting the captured solar energy to the receivers on Earth. Figure 1.1 depicts the transmission procedure in a clear overview. One of the potential, major advantages of SBSP is that a much greater energy-efficiency can be achieved compared to terrestrial solar power due to the absence of nighttime for a SBSP system.

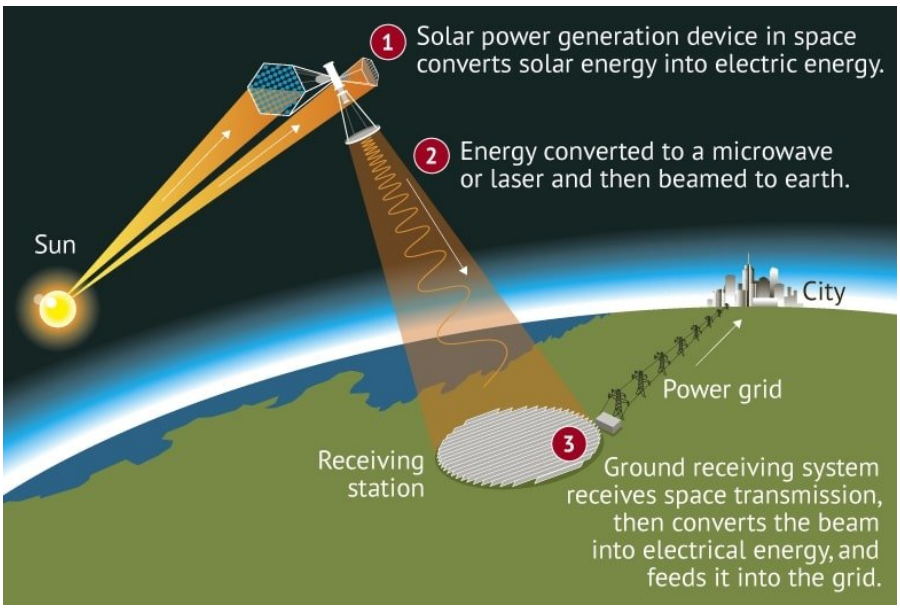

Figure 1.1: Illustration of the transmission procedure of solar power to the ground [2].

At the time of invention, SBSP was technically complex and unlikely to be economically feasible. The overall technology maturity was very low and the system had lots of excessive mass due to the need for large high-voltage power management and distribution (PMAD) components. Additionally, the total cost of a SBSP system would require immense investments, potentially exceeding the total cost of the ISS, making the project financially demanding. At last, in order to assemble the SBSP system, hundreds of astronauts and thousands of robots were required, a feature that at that time was still considered to be part of science fiction. For these reasons, the SBSP idea was put on hold and shelved. According to Manskins [54], some of the above mentioned issues were addressed by NASA's SSP studies and the SSP Exploratory Research and Technology (SERT) Program. However, according to Mankins, other concerns around SBSP still remained:

- Poor efficiency of key devices (amplifiers, PV cells, etc.);
- The required large-scale integration of key systems (PMAD, thermal management, etc.);
- Inadequate capabilities in space robotics and autonomy;
- The need for Reusable Launch Vehicles (RLV) prior to launching an initial SBSP system;
- The lengthy R&D phase required for an initial SBSP pilot plant (estimated at 20-25 years or more).

Now, decades after the invention of the technology, SBSP has gained more and more interest by governments worldwide. Thanks to companies like Spacex, the cost per launch has dramatically reduced. Furthermore, the growing affordability of Photovoltaic (PV) technology has made SBSP even more appealing and feasible. The field of robotics has undergone significant advancements in autonomous technology compared to the technological capabilities available in the 60s. These combined factors have attenuated and even mitigated some of the previous concerns surrounding SBSP. Thus, it comes as no surprise that countries with a significant presence in space are reigniting their interest in SBSP.

1.2. Potential of SBSP as a Renewable Energy Source

General solar power holds a great promise as a renewable energy source. Using the virtually inexhaustible solar energy source, the Sun, solar power offers a sustainable and renewable alternative to finite and environmentally harmful energy sources such as coal, oil and natural gas. Solar power can be generated using two designs; terrestrial solar power and SBSP.

1.2.1. Advantages and potential of SBSP

One of the main advantages of SBSP is that it is capable of capturing solar energy in space, where sunlight is abundant and does not experience the negative effects of atmospheric interference or geographical limitations. In contrary, terrestrial solar power systems are subjected to fluctuations in weather patterns and daylight hours. Comparing SBSP to terrestrial solar power, it becomes clear that SBSP could continuously harvest solar energy 24 hours per day, depending on the specific orbit and its corresponding eclipse period. Hence, SBSP is considered to be a more reliable and consistent power supply option than terrestrial solar power. However, it is important to note that while SBSP systems avoid atmospheric interference during energy capture, the transmission phase can still be affected by atmospheric conditions. The precise influence of the atmospheric conditions on the transmission method depends on the type of beam frequency used.

The strategy to invest in multiple renewable energy sources simultaneously, and thereby enhancing the energy security and independence for a nation, has been actively pursued by countries all over the world. In addition to wind energy, nuclear energy and terrestrial solar energy, SBSP will make a great contribution to the renewable energy portfolio of a country. When a country has the ability to generate power from space, it will be able to reduce their reliance on finite and geopolitically sensitive energy sources.

Finally, SBSP will further develop the economic growth and innovation in (space related) technology. Initiating a mega project like SBSP will not only create new employment opportunities but will also require the development of innovative solutions for intricate challenges that will arise during the project. A nation that can undertake the construction such a colossal structure in space not only showcases its

capabilities to the rest of the world but also sets a precedent for pioneering innovation and future space exploration.

1.2.2. Disadvantages of SBSP

Despite the advantages, SBSP also comes with several disadvantages when compared to terrestrial PV systems. For instance, the cost of developing, launching and deploying an SBSP system in space is significantly higher than installing terrestrial PV systems. Moreover, the cost of maintenance and repairs are substantially higher for SBSP than for terrestrial systems.

A major technical problem for SBSP is efficiently transmitting power from space to Earth without significant losses. The system should be highly efficient to minimize the losses during transmission and have proper thermal control systems to reject the generated heat. From that point of view, terrestrial PV systems are less complex and thus more reliable compared to SBSP. The same holds for the antenna alignment with the ground receiver. This activity still is a critical factor in the overall SBSP operation and remains technically challenging.

Environmental and safety concerns for SBSP could be the result of deploying large SBSP systems in orbit. The risk of space debris could pose hazards for other satellites and space missions and the transmitting beam could be harmful when in contact with humans. Alternatively, terrestrial solar power has no ability to cause such danger for other space missions or humans.

Developing a SBSP will be accompanied by complex problems that, if not properly managed, can cause significant disadvantages over terrestrial PV systems. However, when these problems are effectively dealt with, the benefits of SBSP can outweigh the benefits of terrestrial PV systems.

1.3. Lunar SBSP Applications

Initially, the focus of SBSP development has primarily been towards Earth-based applications, due to the range of potential benefits it could provide to the energy sector. Especially SBSP technology utilizing Microwave Power Transmission (MPT) systems are exhibiting potential for Earth-based applications but come at a high cost. Alternatively, researchers have started to study the potential of SBSP for other applications than Earth-based power generation [25] [37]. By expanding the scope of SBSP applications to include other celestial bodies, the overall technological maturity of SBSP can be accelerated, unlocking greater potential for the technology.

1.3.1. SBSP for Lunar Habitats

The Moon presents an interesting opportunity for testing and operating SBSP systems, addressing the unique challenges of power supply for lunar missions. The extended lunar night, which lasts approximately 15 Earth days [50], creates significant limitations for traditional solar panels. Thus, establishing a robust power grid on the Moon requires alternative and complementary energy solutions. SBSP systems, alongside nuclear power and traditional solar panels, offer the potential to establish a diverse and robust power generation portfolio, ensuring the reliability and resilience needed to sustain remote habitats and human missions.

SBSP systems are a good candidate for addressing the energy needs of the permanently shadowed regions and polar areas on the Moon. In these regions, conventional solar panels face challenges due to limited or uneven sunlight exposure. SBSP systems can transmit solar power from orbiting satellites to surface receivers, providing consistent and scalable power to support critical operations, including life support, scientific instruments and resource extraction technologies.

1.3.2. Lunar SBSP as a Gateway to Mars

The Moon also acts as a great proving ground for SBSP technologies that may one day be used for Martian exploration or colonization. The proximity of the Moon to Earth enables for iterative testing and refinement of SBSP systems in a realistic environment. Establishing a presence on the Moon once again using SBSP systems can validate the operational reliability, efficiency and safety of the technology, which could pave the way for their use in more distant and challenging locations such as the red planet.

1.4. Thesis Objectives

The thesis will focus on the design of a lunar SBSP system purposed for a demonstration mission. The thesis shall investigate a possible design for a lunar SBSP system determined via trade-off analysis. Therefore, the research question for the thesis will be as follows:

Research Question:
What is a promising conceptual design for a lunar-based SBSP demonstration mission, covering system architecture, transmission techniques, and corresponding SBSP subsystems?

From the main research question, a series of sub-questions have been derived to investigate specific aspects of the lunar SBSP design. Answering these questions will contribute to the understanding of the complexities involved in designing and implementing a successful lunar SBSP demonstration mission. The sub-questions are listed below:

- **SQ-1:** What are the mission objectives for the lunar SBSP demonstration mission guaranteeing a successful mission?
- **SQ-2:** What is the most effective method for transmitting solar power to the lunar surface?
- **SQ-3:** What redundancy and reliability measures should be integrated into the design of a lunar SBSP system to ensure mission success?
- **SQ-4:** How can the design of a lunar SBSP demonstration mission be scaled up for future SBSP operations on the Moon?

The scope of this thesis focuses exclusively on the space segment of the SBSP project, specifically the satellite. While an SBSP project can be divided into three segments; the Space Segment, the Receiver Segment and the Ground Segment, this thesis only focuses on the conceptual/preliminary design of the satellite. The Receiver Segment should undergo its own design study to ensure the SBSP project is fully prepared and ready for operations. For instance, the receiver could be integrated into a lunar rover, enabling the demonstration of WPT practices while simultaneously studying other aspects of the lunar environment.

1.4.1. Importance of the demonstration mission

The demonstration mission for SBSP on the Moon will be a critical milestone towards a sustainable and continuous supply of energy on extraterrestrial sites such as the Moon, which will help establish a full scale lunar habitat.

The demonstration mission will be essential for proving the feasibility and reliability of SBSP technology under actual lunar conditions. Simulations and laboratory tests provide valuable insights but will never be able to fully replicate the unique challenges of the lunar environment, such as extreme temperature variations and long-term exposure to cosmic radiation. A successful demonstration on the Moon would validate the system's design, operational capabilities and durability, providing evidence that SBSP can function effectively in the harsh Moon environment.

Furthermore, the mission will offer valuable data to the designers to iterate and optimize the SBSP system. Necessary adjustments can be made to improve system efficiency, reliability and scalability. Unforeseen issues could arise during the demonstration mission, which allows for the development of robust solutions before full-scale deployment.

Finally, a demonstration mission will help build confidence among stakeholders, including space agencies, commercial partners and policymakers. The demonstration of SBSP on the Moon will showcase its potential to provide continuous and reliable power for lunar bases. Such success could catalyze investment and collaboration, propelling the maturity of SBSP technology exponentially.

Several conceptual designs of SBSP systems for lunar applications have been proposed in literature. Cougnet et al. have proposed a SBSP system at the Earth-Moon L2 position, capable of transmitting 40 kW to the lunar surface [25]. Furthermore, Soto et al. have investigated various orbital solutions for SBSP systems around the Moon, taking into account orbits such as frozen orbits, repeat ground track orbits and also Lagrangian points [86]. Additionally, they make a comparison between deploying a single satellite versus a constellation. However, these studies focus on large-scale operational systems rather than small-scale demonstration missions. No specific lunar demonstration missions for SBSP were identified in existing literature.

This gap in the current literature highlights the uniqueness of the proposed demonstration mission in this thesis, which focuses on demonstrating the feasibility of SBSP under lunar conditions at a smaller, more manageable scale. This thesis aims to bridge the gap between conceptual designs and full-scale deployment.

2

Lunar Demonstration Mission

In Chapter 2, the mission objectives and stakeholders for the demonstration mission will be identified. Consequently, stakeholder requirements will be aligned with the mission's goals. From the mission objectives and stakeholder analysis, the system requirements will be defined.

2.1. Need Statement and Mission Objectives

The need statement and the mission objectives have been derived in the next subsections. The need statement represents the underlying need that forms the basis for this mission. From the need statement, the mission objectives can be determined.

2.1.1. Need Statement

SBSP technology has advanced to the point where conceptual technologies have been successfully demonstrated through experiments and research. Now, it is desired to validate these SBSP subsystems in a representative environment to ensure their practical application and reliability. The following need statement represents the need for a SBSP lunar demonstration mission:

"There is a need to validate the feasibility, efficiency, and sustainability of Space-Based Solar Power technology in the lunar environment to provide a reliable, renewable energy source for future lunar operations and establish a foundation for broader applications in space exploration and terrestrial energy systems."

2.1.2. Mission Statement

The demonstration mission for a lunar SBSP system has resulted in a mission statement. The mission statement defines the purpose of the mission and effectively communicates the definition of the mission to customers and stakeholders. The mission statement for the lunar SBSP demonstration mission is the following:

"Demonstrate the feasibility and effectiveness of Space-Based Solar Power generation and wireless energy transmission from lunar orbit to a designated receiver on the lunar surface, validating the system's capability for future continuous and reliable power delivery, and ensuring scalability, redundancy, and long-term operational sustainability."

From the mission statement, a list of more detailed goals can be derived that break down the key aspects of the mission into focused, actionable objectives. These objectives provide a comprehensive framework to assess the various aspects of the SBSP lunar demonstration mission, ensuring that all critical factors are addressed and the system's potential for future continuous power delivery is validated. Seven goals with thirteen mission objectives have been identified and are depicted in Table 2.1. The mission objectives encompass the critical aspects of the full SBSP system design, from which the mission requirements can be derived.

Goals	Objectives
1. Demonstrate solar power generation and transmission capabilities.	1.1. Validate the efficiency and performance of the solar power generation system in the lunar environment. 1.2. Assess the impact of the lunar environmental factors (e.g., temperature) on power generation. 1.3. Demonstrate the effective transmission of the generated solar power from the satellite to the lunar surface receiver. 1.4 Measure and analyze the efficiency and accuracy of power transmission.
2. Assess system scalability and redundancy.	2.1. Evaluate the system's ability to scale up for increased power generation and transmission. 2.2. Ensure the system can maintain functionality in the event of an individual component failure.
3. Perform the orbital manoeuvres to achieve the appointed orbits.	3.1. Achieve and maintain optimal satellite positioning for effective power generation and transmission.
4. Validate the thermal control functionalities.	4.1. Ensure effective thermal regulation to maintain satellite functionality.
5. Validate the functionality of the power management system	5.1. Optimize the balance between power generation, storage and transmission by monitoring power usage and adjust to optimize efficiency.
6. Validate the functionality of the communications system	6.1. Ensure robust communication between satellite, the lunar receiver and Earth ground control. 6.2 Ensure timely transmission of control signals and telemetry data.
7. Demonstrate long-term operational sustainability	7.1. Demonstrate the system's ability to operate sustainably over an extended period. 7.2. Identify and address any long-term operational challenges.

Table 2.1: Goals and Objectives for the SBSP Lunar Demonstration Mission.

2.2. Stakeholder Analysis

The stakeholder analysis identifies and evaluates the numerous groups that have showed interest in the SBSP lunar demonstration mission. Potential stakeholders for the demonstration mission include space agencies, commercial aerospace companies, energy firms, government and policy makers, research and academic institutions and the general public. Each stakeholder could have an impact on the planning, execution and eventually the success of the mission.

The stakeholder analysis has resulted in a list of potential stakeholders shown in Table 2.2 that could impact the SBSP lunar demonstration mission. Each stakeholder has been assigned to a stakeholder ID. The distinction between active and passive stakeholders has also been noted in the analysis, where active stakeholders are individuals, entities or other systems which will actively interact with the ”system” once operational and in use. Passive stakeholders can be seen as groups, standards, protocols or procedures which will also influence the success of the system.

The space agencies will award the project contract to one or multiple contractors. The contractor(s) will conceptualize, develop and test the design in house while the agencies actively supervise the project as a customer. The launcher company will be responsible for launching the system into the desired orbit, where after the contractor(s) ensure full deployment of the system in the correct lunar orbit.

Energy firms may feel drawn to this project as it offers an opportunity to take part in the rapidly expanding space industry. By investing in an energy source for a potential future moon base, the energy firms can align themselves with a clean and innovative future, which could enhance their brand and be beneficial for their overall business standing. Governments and policy makers will have a passive influence on the project by establishing laws and policies for any moon activities. Research institutions could be given access to the results of the demonstration mission, allowing them to conduct independent analyses and provide valuable insights for the future of SBSP. The general public could

be engaged through transparent communication about the mission progress and benefits. This could spark a widespread support and interest in space exploration and renewable energy technologies.

Type	Stakeholder	ID	A/P
Customer	Space Agencies (ESA, NASA)	STK-01	Active
Contractor	Commercial Aerospace Companies (Airbus, Thales Alenia Space, OHB)	STK-02	Active
Launcher	Commercial Launcher Companies (SpaceX, Blue Origin, Arianespace)	STK-03	Active
Investor	Energy Firms (Vattenfall, Shell, BP)	STK-04	Passive
Government	Government and Policy Makers (European Commission, US Congress)	STK-05	Passive
Research	Research and Academic Institutions (TU Delft etc.)	STK-06	Passive
Public	General Public (Citizens, Environmental Groups)	STK-07	Passive

Table 2.2: Principal System Stakeholders for the SBSP Lunar Demonstration Mission.

2.2.1. Mission Requirements

Stakeholder expectations have been derived and set up from their individual needs. These expectations have been converted into mission requirements and are displayed in Table 2.3. Each mission requirement represents a general requirement for the system and can be traced back to their respective stakeholders.

Table 2.3: Mission requirements with their corresponding ID, stakeholder and rationale.

ID	Stakeholder	Requirement	Rationale
MR-01	STK-01	The mission shall comprise of a space segment, a receiver segment, and a ground segment.	A complete SBSP system demonstration requires all three segments to validate end-to-end functionality.
MR-02	STK-01	The mission shall not exceed a cost of **<TBD>** euros.	Ensures financial feasibility and alignment with the budget constraints of stakeholders.
MR-03	STK-01	The mission shall have a minimum duration of **<TBD>** months.	Allows for adequate time to test performance across varying lunar conditions and operational scenarios.
MR-04	STK-01	The mission shall incorporate an End-of-Life procedure.	Minimizes space debris and ensures compliance with sustainability guidelines.
MR-05	STK-01	The mission shall demonstrate wireless power transmission in flight.	Validates the core objective of the SBSP system: power delivery to a receiver.
MR-06	STK-01	The system shall deliver a minimum power of **<TBD>** W to the receiver.	Establishes baseline power delivery to demonstrate feasibility for future scalability.
MR-07	STK-01	The system shall deliver a maximum power of **<TBD>** W to the receiver.	Demonstrates the ability to meet power needs of specific systems on the lunar surface.
MR-08	STK-01	The system shall deliver continuous and reliable power for a period of **<TBD>** minutes.	Validates reliability for consistent power delivery, important for operational use.
MR-09	STK-01	The mission shall follow a detailed validation campaign.	Ensures that all subsystems are thoroughly tested and performance metrics are captured.
MR-10	STK-02	The system shall be designed, integrated, and tested in the facilities of the contractor.	Ensures centralized management and quality control of the development process.
MR-11	STK-02	The system shall use COTS components for all subsystems.	Reduces costs and development time while leveraging proven technology.
MR-12	STK-02	The system shall be able to independently point the transmitting beam at the ground receiver.	Ensures accurate power delivery despite orbital motion or misalignments.
MR-13	STK-02	The system shall be able to withstand the harsh lunar environment for the complete duration of the mission.	Validates the robustness of the system against extreme temperature variations and radiation.
MR-14	STK-02	The system shall be able to communicate with the ground segment during the individual validation actions.	Enables real-time monitoring and troubleshooting of system performance.

Continued on next page...

Table 2.3 continued from previous page: Mission requirements with their corresponding ID, stakeholder and rationale.

ID	Stakeholder	Requirement	Rationale
MR-15	STK-02	The system shall have incorporated redundant components for all critical functionalities to eliminate single points of failure.	Increases reliability and mission success probability by addressing component failures.
MR-16	STK-02	The system shall be able to generate all necessary power to support its operations.	Ensures self-sufficiency during all mission phases.
MR-17	STK-02	The system shall be able to achieve a lunar orbit.	A prerequisite for positioning the SBSP system for power transmission validation.
MR-18	STK-02	The system shall be able to determine its attitude and position with an accuracy of **<TBD>**.	Ensures precise attitude and stability for power transmission and orbit maintenance.
MR-19	STK-02	The system shall be able to maintain its lunar orbit to perform the validation campaign.	Ensures the continuation of the demonstration of SBSP performance.
MR-20	STK-02	The system shall maintain the temperature of all critical components within their specified operating temperature ranges.	Prevents damage or performance degradation due to thermal extremes.
MR-21	STK-02	The system shall be able to transfer all TT&C and performance data to the ground segment.	Ensures comprehensive data collection for mission evaluation and optimization.
MR-22	STK-03	The system shall not exceed a mass of **<TBD>** kg.	Maintains compatibility with the payload capacity of the potential launcher and minimizes launch costs.
MR-23	STK-03	The system shall not exceed the dimensions of the payload bay of the designated launcher.	Ensures physical compatibility with the launcher for safe transportation.
MR-24	STK-06	The mission shall provide all test results to assess the scalability of the system.	Supports evaluation of the system's potential for larger-scale applications.
MR-25	STK-07	The mission shall ensure that no irreversible damage is inflicted on historically significant and scientifically valuable regions on the lunar surface.	Complies with international guidelines for preservation of lunar heritage.
MR-26	STK-02	The TT&C system shall incorporate a signal-to-noise ratio larger or equal to **10**.	Ensures reliable communication and data transfer under lunar conditions.

2.2.2. System Architecture

With the mission objectives and requirements now established, the next task is to determine the high-level system architecture. The high-level system architecture comprises of three primary segments: the space segment, the receiver segment and the Earth ground segment. A visualization of the system architecture has been depicted in Figure 2.1, where each segment is presented with their interactions between the other segments. Note that this is a very generic system architecture but does provide enough insights to continue the development process.

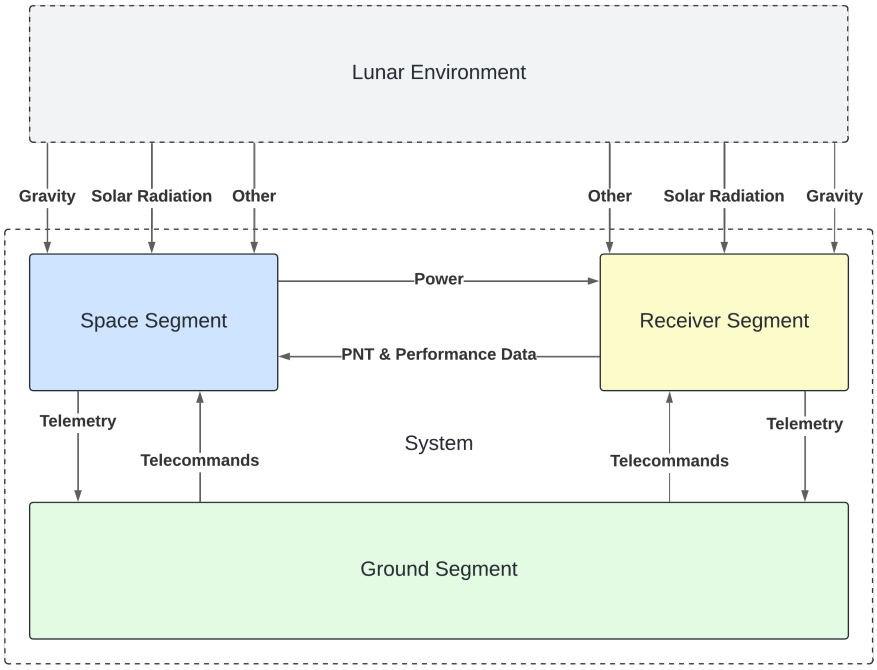

Figure 2.1: The high-level system architecture of the SBSP system.

From Figure 2.1, it becomes apparent that the success of the demonstration mission depends on three segments. It is assumed that the ground segment on Earth is based on already existing infrastructure. Specific functionalities and software packages do have to be developed but this will not be included in the scope of this thesis. The remaining two segments, the space segment and the receiver segment, will have to be developed from scratch to ensure the success of the mission. Yet, it has been determined that only the space segment, otherwise known as the solar power satellite, will be part of the thesis scope. The primary reason for this decision stems from the fact that designing the solar power satellite by itself will already be a challenging and time-consuming task. For the rest of the thesis, it will be assumed that the receiver has landed on a (as of now, not yet determined) location on the Moon and is ready to receive power. However, any technological challenges for landing the receiver on the Moon will not be solved during this thesis.

3

Conceptual Design Trade-offs

3.1. Wireless Power Transmission Trade-off

The first section will analyze the trade-off between laser and RF SBSP for a lunar demonstration mission. First, the trade-off criteria and respective weights have to be determined where after a trade-off table can be generated to visualize the trade-off. The best candidate for the lunar demonstration mission will follow from the wireless power transmission trade-off and sets the foundation for the lunar demonstration mission trade-off.

3.1.1. Types of Wireless Power Transmission

The two most commonly considered power transmission methods are Radio Frequency (RF) Power Transmission and Laser Power Transmission (LPT). RF power transmission uses electromagnetic waves in the radio frequency spectrum to wirelessly transfer power. It is a reasonably mature and proven technology which can enable efficient power transfer over long distances with relatively low attenuation in space. The downside is the need for large antennas and rectennas, which increase system mass and complexity.

Laser Power Transmission use highly focused optical or near-infrared light to transfer power. These systems would allow for compact antennas and receivers due to their ability to deliver concentrated power with lower beam divergence. However, LPT systems face challenges such as atmospheric attenuation and lower overall efficiency.

3.1.2. Criteria and Weights

A set of criteria has been selected to evaluate the performances of Wireless Power Transmission (WPT) options for a lunar demonstration mission. The criteria are based on technical, operational, economical and safety factors that influence the mission. The criteria are listed below with their corresponding weights and rationale in Table 3.1. Each input for a specific criteria will be rated as one of the following: *Excellent, Good, Medium, Low*.

Criteria	Rationale	Weight
Transmission Efficiency	High transmission efficiency is important to ensure that a significant proportion of the transmitted power is delivered to the receiver.	2
Beam Precision	High beam precision is desired as it reflects in the ability to precisely deliver the power onto the receiver, minimizing power losses.	2
Mass and Volume	The mass and volume of the space segment are critical factors in a SBSP mission. A higher mass reflects in a higher launch cost and each launcher has a fixed payload volume, limiting the space available.	3
Power Density	The power density indicates the amount of power transmitted per unit area. High power density reflects in a smaller receiver size which is particularly valuable in the lunar environment.	3
Technical Maturity	The technical maturity indicates whether the WPT system is close to being reliable deployed for operational use.	3
Safety and Health Risks	The safety and health risks correspond to the potential risks associated with the operation of the WPT system.	1
Cost	The cost to operate the WPT system incorporates the development, deployment and operational expenses regarding the WPT system.	2
Feasibility	The feasibility assesses the practicality of implementing the WPT system within a given time frame, resources and technical constraints. A high feasibility suggests that the WPT system can be realistically achieved.	4
Scalability	The scalability assesses the potential of the WPT system to be expanded for larger-scale operations in the future.	4

Table 3.1: WPT trade-off criteria with the corresponding rationale and weight.

3.1.3. Evaluation of WPT Trade-off Criteria

The key criteria will be systematically evaluated in the context of SBSP using laser or RF WPT. The results are then transferred to the trade-off table, producing a clear comparison of the advantages and disadvantages of laser and RF SBSP.

Efficiency

The efficiencies of both WPT options have been derived from a paper written by Reynolds [74]. In the paper, a comparison between the state-of-the-art power transmission methods is provided. A laser SBSP system would have an end-to-end efficiency of roughly 8.3% whereas RF SBSP can achieve an end-to-end efficiency of 11%. From previous research, it was determined that RF SBSP systems incorporated a significantly higher *theoretical* end-to-end efficiency of approximately 45% [56]. Yet, in practice, achieving such an efficiency turned out to be infeasible due to various losses.

Beam Precision

Laser systems offer a precision of 1-10 μrad according to Grandidier et al.[37]. This accuracy enables the system to accurately and efficiently deliver power to the lunar receiver. In contrast, RF systems incorporate a much lower beam accuracy, especially when such a system consists of a large number of modules. This leads to energy dispersion and creates the need for a larger receiver area to capture all transmitted power. In this case, laser SBSP holds a significant advantage over RF SBSP, since it can beam power with a greater precision, mitigating any potential accuracy losses.

Mass and Volume

After evaluating the mass and volume of both options, laser SBSP seems to offer distinct advantages over RF SBSP. Laser SBSP comes with a compact design and is characterized by smaller transmitters and rectennas which minimizes payload size and the total mass of the system. This is particular important for efficient launch and deployment of the system. The compactness reduces complexity in deployment logistics, potentially lowering overall mission costs. In contrary, RF SBSP comes with larger and modular components which poses challenges to meet payload limitations and most likely will require more complex deployment strategies. Numerous launches will be required to transport all modules to the moon, where after each module must be integrated into the full RF SBSP. Thus, the compactness of laser SBSP makes it the preferred choice when considering mass and volume constraints for lunar missions.

Power Density
The power density of a laser SBSP system show more beneficial performance due to its ability to produce a highly focused beam with low divergence. The focused beam allows for a significant portion of the transmitted beam to be concentrated onto a small receiver area on the lunar surface, resulting in a relatively high power density. For example, a Mars laser SBSP system was characterized with a power density of 144.4 W/m^2 (at an altitude of 17000 km) by Cougnet et al. [25]. The relatively high power density not only increases the overall system efficiency but also enables the deployment of smaller receivers on the lunar surface. RF SBSP systems use transmission beams with larger wavelengths resulting in greater beam divergence which make it more difficult to achieve comparable power densities at the receiver. Mankins et al. have evaluated the power densities of Earth based RF SBSP systems where the power density range from 1 - 100 W/m^2 [56]. This low power density requires a larger rectenna area compared to laser SBSP, highlighting the clear advantage of laser SBSP systems in maximizing power density and optimizing power transmission for a lunar demonstration mission. Additionally, RF SBSP presents another significant challenge: the need for large amounts of transmitted power to achieve sufficiently high power densities for efficient rectenna operations, which could render RF systems infeasible for a lunar demonstration mission.

Technical Maturity
The technical maturity of RF SBSP systems have an advantage over laser SBSP systems with a Technical Readiness Level (TRL) of 6. Jaffe et al. have established that RF is at TRL 6 [47], indicating that RF SBSP has been demonstrated in relevant environments and are thus closer to operational deployment with lower risk and fewer unknowns. Laser SBSP has obtained the technical maturity of TRL 5, indicating that the technology has been validated in a relevant environment but that it yet has to be fully demonstrated in the relevant environment. The slightly higher level of technical readiness makes the RF systems more attractive for near-term missions due to the fact that it has already been proven in flight. Alternatively, this would be a good opportunity for laser SBSP to reach TRL 6.

Safety and Health Risks
RF SBSP systems are more beneficial when evaluating the safety and health risks for both options. This option shows relatively low safety risks even at high power levels, is less likely to cause acute injuries to humans and requires simpler safety measures compared to laser SBSP systems. Therefore, this is labeled as ”Excellent” since it does not pose any real threats to humans. Laser SBSP systems pose high safety risk due to their intense, focused beams and require strict safety protocols for when a fully operational base is present on the lunar surface. However, since the purpose for this design is a demonstration mission and therefore will have no direct contact with humans while operational, this is labeled as ”Medium”. In fact, it can serve as a great test ground to validate laser SBSP safety protocols, ensuring the safety of a future fully operational SBSP system around the Moon. But still, in terms of safety and health risks, the RF SBSP system is more suitable for operational use.

Cost
The cost for laser and RF systems is based on the development, deployment and operational costs. It should be noted that the total cost will depend on the required power output but an accurate comparison between the two options can still be provided. Firstly, laser SBSP will come with lower deployment costs due to its size and thus requiring fewer launches compared to RF SBSP systems. Alternatively, it can be suggested that laser SBSP will require higher initial development costs than RF SBSP, primarily because laser SBSP is at a TRL of 5 whereas RF SBSP is at TRL 6. RF SBSP systems will be joined by higher deployment costs due to their larger, modular components. Numerous launches will be necessary in order to get every module in orbit around the Moon. Next, the time to integrate each module into a full RF SBSP system will be much more costly than launching a single laser SBSP around the Moon. Hence, despite the initial expenses, laser SBSP systems are more cost-effective compared to RF SBSP systems.

Feasibility
In assessing the feasibility for laser and RF SBSP, laser SBSP shows to be the more practical choice. Laser SBSP systems are compatible with existing launchers and are accompanied by manageable receiver sizes. This greatly reduces the mission complexity. Although hazardous, laser SBSP could

use the demonstration mission to also demonstrate its safety protocols for future full-scale applications. Finally, laser SBSP is a more cost-effective solution where a single launch per SPS aligns well within budgeting constraints typical of lunar missions. On the other hand, RF SBSP systems need multiple launches to fully deploy the system, which could adversely impact the mission's budget constraints. Therefore, laser SBSP offers a more optimal solution that balances practicality, safety and cost-effectiveness for the lunar demonstration mission.

Scalability
When analyzing the scalability of both options, it becomes clear that both can be expanded effectively from a technical engineering standpoint. Despite being limited to a certain power output, laser SBSP systems can be significantly scaled up to a constellation configuration. RF SBSP can be scaled up to larger power outputs than laser SBSP due to the system's modular nature, but the increase in number of modules would cause even higher deployment costs. Incorporating that with a constellation of RF SBSP systems, and the total cost of the project will skyrocket. Therefore, laser SBSP shows greater scalability potential, primarily due to the relatively low cost for deploying a constellation around the Moon. Such a constellation configuration could offer a continuous power supply to a future lunar base.

3.1.4. Comparison of Laser and RF SBSP

To illustrate the trade-off in WPT options, an example will be examined where both laser and RF SBSP systems operate under identical mission characteristics. This comparative analysis aims to evaluate how each system performs when meeting specific mission requirements. By exploring these examples, a better understanding of the implications and benefits of either WPT options should be obtained. The main focus will lie on the antenna and rectenna sizes and the corresponding number of launches that are required to transport it to the lunar environment. The following mission characteristics are defined:

- **Orbit Altitude:** 100 km
- **Solar Irradiance:** 1361 W/m^2
- **Power Output:** 10 kW
- **Photovoltaic efficiency:** 30%
- **Transmission Efficiency:** Laser: 8.3%, RF: 11%

To assess the transmitter and rectenna sizes, Equation 3.1 should be used. It calculates the spot size diameter, D_{spot} of the transmitting beam which directly indicates what size the rectenna should be to capture all transmitted power. Next, λ represents the wavelength of the respective beam and L equals the distance between the transmitter and the rectenna. At last, the spot size can be written as a function of the transmitter diameter D_{t}.

$$D_{\text{spot}}(D_t) = D_t + \frac{2.44\lambda L}{D_t} \tag{3.1}$$

Laser SBSP Example
The laser SBSP system has a transmitting efficiency of 8.3%. Ensuring that 10 kW of power is transmitted to the receiver on the ground, the power subsystem should supply approximately 120 kW of power to the transmitting subsystem. Accounting for the 30% efficiency of the photovoltaic cells, a total solar panel area of 294 m^2 is required. A laser SBSP system located in a 100 km orbit around the Moon is assumed to use a 1064 nm laser to transmit its power. When finding the minimum spot size parameter using the derivative of Equation 3.1, a transmitter diameter of 0.51 m is found with corresponding spot size diameter of 1.02 m. From this result, it can be suggested that the full laser SBSP system will fit in a single launcher, with clever unfolding mechanisms for the solar panels and thermal control subsystems.

RF SBSP Example
The RF SBSP system has a slightly higher transmitting efficiency of 11% while using a 5.8 GHz beam. Again, ensuring that 10 kW of power reaches the ground, the power subsystem should supply roughly 90.9 kW of power to the transmitting arrays. Calculating the solar panel area with the corresponding PV efficiency results in an area of 223 m^2. In this case, RF SBSP holds the advantage of deploying smaller solar panels, reducing the mass of the system. However, when calculating the spot size diameter again using the derivative of Equation 3.1, a transmitter diameter of 112.34 m is found with a

corresponding spot size diameter of 224.68 m is found. This in itself will not fit in a payload bay of any existing launchers. Thus, only two options could realize this solution. Either a cleverly designed unfolding mechanism should be integrated into the system, allowing it to potentially fit in a single launcher or the system should incorporate a modular design. The latter will require multiple launches and thus will be more costly than laser SBSP. Not to forget the fact that a receiver with a minimum diameter of 224.68 m is required to harvest the power on the Moon. This on its own will require a number of launches only to get a proper receiver on the lunar surface.

A plot has been computed to display the relationship between the spot size on the ground and the transmitter diameter for various altitudes, for both laser and RF SBSP. Each subplots depicts how the spot size decreases as the transmitter diameter increases, where the different lines represent altitudes of 100 km, 500 km, 1000 km, 1500 km and 2000 km. This visualization shows the trade-off between the transmitter size and the spot size at different altitudes and can be considered insightful for the WPT trade-off for a SBSP system around the Moon. It can be concluded that RF SBSP faces a significant trade-off between the transmitter size and the rectenna size. However, it is highly probable that no practical balance can be achieved between these two parameters.

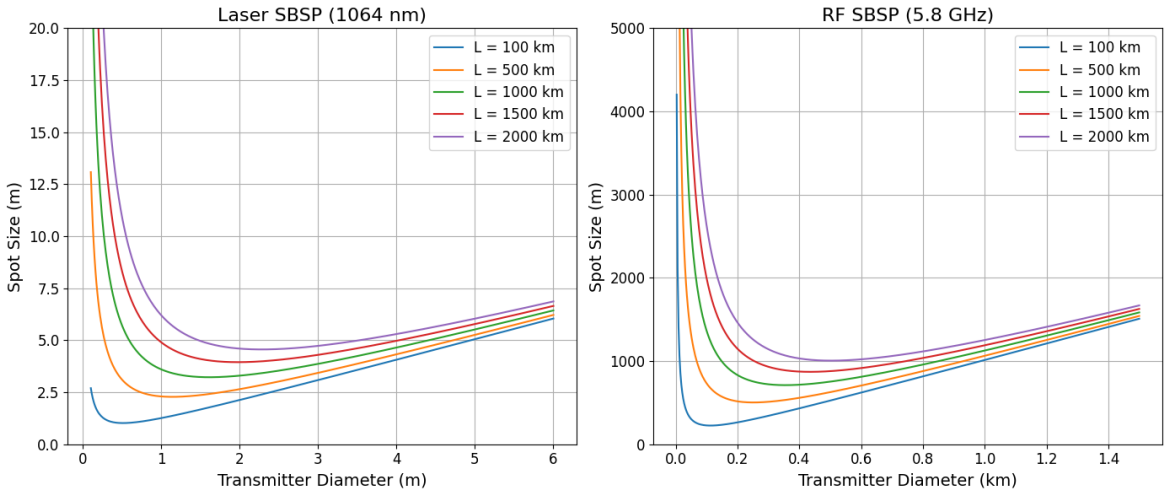

Figure 3.1: The relationship between the spot size and the transmitter diameter for various altitudes.

To summarize the comparison of both options, a readable table has been provided. Table 3.2 contains the relevant parameters that were used and resulted from the comparison. Note, the referred power densities in Section 3.1.3 should not be compared with this example, as those reference systems had different power output requirements and orbital altitudes.

Parameter	Laser SBSP	RF SBSP
Orbit altitude	100 km	100 km
Solar irradiance	1361 W/m^2	1361 W/m^2
Power output	10 kW	10 kW
Transmission efficiency	8.3%	11%
Required power supply	120 kW	90.9 kW
Photovoltaic efficiency	30%	30%
Total solar panel area	294 m^2	223 m^2
Spot size diameter	1.02 m	224.68 m
Transmitting aperture size	0.51 m	112.34 m

Table 3.2: Summary of the comparison of laser and RF SBSP.

3.1.5. WPT Trade-off Table

All criteria for the WPT trade-off have been evaluated for the WPT options. The trade-off table presented in Table 3.3 has integrated the various criteria essential for the lunar demonstration mission. The height of each row represents the weight of the respective criteria. Notably, the RF SBSP option has scored ”Low” in both the beam precision and mass and volume criteria. This is primarily because these characteristics of RF SBSP significantly increase the cost and complexity of the mission, rendering it infeasible to be completed given the budget and timeline. Finally, the laser SBSP offers superior beam precision, power density and a smaller transmitter and rectenna size, making it a more viable and effective solution for the challenges of a lunar demonstration mission. To conclude, the laser SBSP option scores higher overall at 76 points, compared to the RF SBSP at 40 points, making laser SBSP the more favorable option.

Option / Criteria	**Laser SBSP**	**RF SBSP**
Efficiency	8.3% [74]	11% [74]
Beam Precision	1-10 μrad [37]	Very low for modular RF systems
Mass and Volume	Compact system. Relatively small transmitter and receiver	Large transmitter and receiver. Often designed to be highly modular
Power Density	Highly focused energy beam. Relatively low beam divergence	Low power density due to large beam divergence
Technical Maturity	TRL 5 [87][47]	TRL 6 [47]
Safety and Health Risks	High risk at high power	Low risk at high power
Cost	Single launch per SPS. Relatively low cost	>1 launches per SPS. Relatively high cost
Feasibility	Full laser SPS would fit in an existing launcher. Receiver size is manageable	Highly modular RF system requires numerous of launches. Large receiver in order of kms required
Scalability	Individual laser SPS could be scaled. A constellation can be deployed	Highly modular design allows for great scalability of single SPS.

Excellent = 4	Good = 3	Medium = 1	Low = 0

Table 3.3: Trade-off matrix for laser and RF SBSP for a lunar demonstration mission.

3.2. Demonstration Mission Trade-off

The following stage of the conceptual design phase involves initiating the trade-off analysis for the demonstration mission. Consequently, a sequence of different mission characteristics are traded off. As a result, a final configuration will be crowned as the most optimal mission for the lunar demonstration mission.

3.2.1. Trade-off Sequence

The trade-off analysis for the lunar demonstration mission structured such that every critical characteristic of the demonstration mission is being evaluated. This structured approach ensures a proper comparison of different mission parameters. The trade-off is divided into three stages:

- **Types of Orbits**
- **Mission Duration**
- **Delivered Power**

3.2.2. Receiver Site

The receiver site for the SBSP system is proposed to be Shackleton Crater, near the lunar south pole. This location is of significant international interest due to its near-continuous sunlight on the crater rim and potential water ice deposits within. As a likely site for future lunar bases, Shackleton Crater is an ideal candidate for deploying a robust SBSP system to support long-term habitation and exploration. SBSP could contribute to the lunar power grid as one of the possible energy solutions, enhancing its resilience and ensuring reliable power for diverse applications. The receiver site will play an important role in determining a suitable solution for the demonstration mission.

3.2.3. Types of Orbits

Firstly, the types of orbits should be evaluated to understand the advantages and disadvantages of each orbit. A list of potential orbits is proposed after which the accompanied criteria that will be used to assess each orbit are depicted. The potential lunar orbits are as follows:

- **Equatorial Low Lunar Orbit (LLO)**: A circular orbit at low altitudes (typically 50–100 km) above the Moon's equator, with an inclination near 0°. This orbit provides close proximity for precise power delivery. Its low altitude minimizes the effect of beam divergence but requires frequent station-keeping.
- **Frozen Polar Low Lunar Orbit (LLO)**: A low-altitude orbit (50–100 km) that passes over the lunar poles, with an inclination of 90°. This allows global surface coverage over time and contact with potential lunar bases stationed on the poles of the Moon. The "frozen" aspect minimizes orbital perturbations, reducing fuel requirements for station-keeping.
- **Highly Elliptical Frozen Lunar Orbit (HEFLO)**: A highly elliptical orbit balances observation proximity and lower energy consumption, and the frozen characteristic ensures long-term stability with minimal adjustments. Long ground visibility but varying altitudes at different moments in the orbit.
- **Earth-Moon L2 Halo Orbit**: A quasi-stable orbit around the Earth-Moon Lagrange Point 2. This orbit provides continuous visibility of the Moon's far side and stable thermal and radiation conditions, making it ideal for communication or relay purposes. The distance between L2 and the lunar surface is quite substantial, making precise beam pointing highly complex.
- **Sun-Synchronous Lunar Orbit**: An orbit designed to continuously be exposed to sunlight. This is useful for missions requiring consistent lighting conditions, such as imaging or energy harvesting. A downside to this orbit is the periodic regional coverage, making continuous power transmission difficult.

Each lunar orbit exhibits characteristics that could be beneficial for the lunar demonstration mission. However, several disadvantages can also be listed. The suitability of each orbit will be traded off using the criteria listed in Table 3.4. Each criteria has received a weight to determine its significance for a SBSP lunar demonstration mission.

Criteria	Rationale	Weight
Stability	Crucial to maintain consistent power transmission performance and avoid frequent orbit corrections.	4
Orbital Impact on Power Transmission	The power transmission is influenced by distance from the receiver and power beam accuracy.	5
Scalability	The potential for expanding the satellite constellation to meet increasing demands for coverage and redundancy.	4
Ground Visibility	The ground visibility duration reflects the ability to beam power for a longer duration.	3
Applicability	This measures how well the orbit is aligned with the specific mission sites or areas of interest. The major area of interest is the Shackleton's Crater on the South Pole.	3

Table 3.4: Orbit trade-off criteria with the corresponding rationale and weight.

A trade-off matrix has been generated in Table 3.5. As a result, the weighted scores of each option can be computed. The best orbit option for a lunar demonstration mission appears to be the Frozen Polar LLO at 73 points, offering strong performance in stability, power transmission and scalability as well as good visibility of the lunar South Pole. At a second place comes the Highly Elliptical Frozen Lunar Orbit at 61 points, showcasing a strong stability and ground visibility but moderate performance in orbital impact on power transmission.
The various orbits have been evaluated against a range of weighting scenarios in a sensitivity analysis. This is done to assess the sensitivity of each orbit type to these changes in criteria weights. A total of 10 scenarios, including the baseline scenario and nine additional scenarios have been listed below with a brief description of their respective priorities.

- **Original:** Baseline scenario with the initial weights.
- **Scenario A:** Priority on Stability. Emphasizes maintaining a stable orbit.
- **Scenario B:** Priority on Power Transmission Efficiency. Focuses on the efficiency and accuracy of power transmission.
- **Scenario C:** Scalability focused. Prioritizes the potential to expand the satellite constellation.
- **Scenario D:** Ground Visibility Priority. Ensures longer durations of ground visibility.
- **Scenario E:** Applicability focused. Aligns with specific mission sites such as the lunar South Pole.
- **Scenario F:** High Risk Tolerance. Accepts higher risks for greater benefits.
- **Scenario G:** Low Risk Tolerance. Prefers safer, more stable approaches.
- **Scenario H:** Scalability and Flexibility priority. Emphasizes the ability to expand and adapt the satellite constellation.
- **Scenario I:** Long Term mission focus. Prioritizes extended mission durations.

Figure 3.2 reveals that the Frozen Polar LLO consistently outperforms the other orbits across all weighting scenarios, showcasing itself as the most reliable choice for the lunar demonstration mission. The Highly Elliptical Frozen Lunar Orbit also performs great, particularly for scenarios where extended ground visibility is demanded such as Scenario G. In conclusion, the Frozen Polar LLO performs exhibits steady, optimal behaviour for all scenarios and is thus the best solution for the lunar demonstration mission.

Orbit Type / Criteria	**Equatorial LLO**	**Frozen Polar LLO**	**Highly Elliptical Frozen Lunar Orbit**	**L2 Halo Orbit**	**Sun Synchronous Lunar Orbit**
Stability	Low stability due to high perturbations caused by mascons on the Moon	A frozen orbit using an 86 ° inclination cancels out most of the perturbations	Orbits exist where periapsis height stays relatively constant over time[53]	An L2 halo orbit is unstable and needs $\approx$ 83-141 m/s ΔV/year [67][100]	Low stability. Requires active station-keeping for maintaining its path
Orbital Impact on Power Transmission	Efficient, accurate but short power transmission due to low altitude	Efficient, accurate but short power transmission due to low altitude	Varying efficiency and accuracy due to varying altitudes	Low efficiency due to long distance but continuous availability	High efficiency due to predictable periods of power transmission
Scalability	High scalability. Easy to expand to increase revisit freq.	High scalability. Extra polar LLOs with extra sats can increase revisit freq.	High scalability. Extra HEFLOs with extra sats can increase revisit freq.	Low scalability. Minimal feasibility for expanding to a constellation	Moderate scalability. Periodic regional coverage with higher # of satellites
Ground Visibility	Frequent short passes due to low altitude	Frequent short passes due to low altitude	Long visibility periods at apogee	Constant visibility if receiver lands on far side of the Moon	Moderate visibility duration with large time intervals
Applicability	Low applicability. No frequent access to lunar South Pole	High applicability. Frequent access to lunar South Pole	High applicability. Frequent access to lunar South Pole	Low applicability. No consistent sight of lunar South Pole	Medium applicability. Periodic coverage of lunar South Pole

Excellent = 4	Good = 3	Medium = 1	Low = 0

Table 3.5: Trade-off matrix for the types of orbits for a lunar demonstration mission.

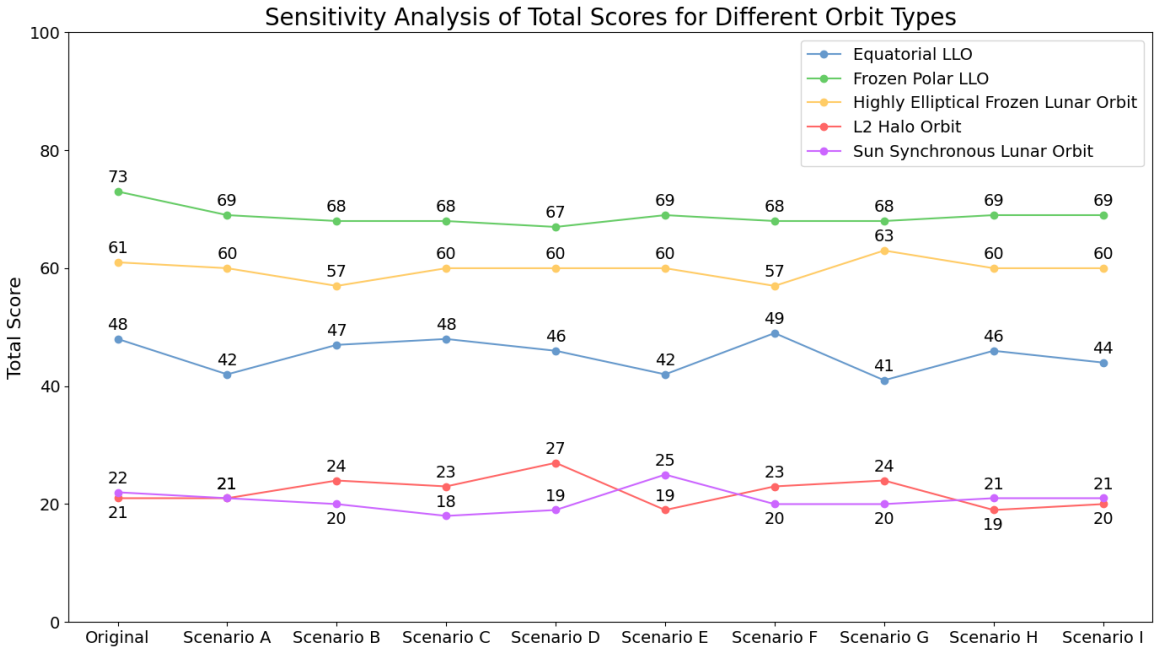

Figure 3.2: The results of each scenario in the sensitivity analysis for the orbit trade-off.

3.2.4. Mission Duration

When planning the SBSP lunar demonstration mission, a number of duration options offer varying benefits and challenges. All options are listed below with a brief description.

- **Short-Term Mission (6 Months):** A 6 month duration allows for rapid deployment and quick assessment of the initial system performance but may limit the scope of the technological demonstration due to its short duration.
- **Medium-Term Mission (1 Year):** A one-year duration presents a more balanced approach, in which the full system can be demonstrated and insightful data can be collected. One year is enough time to evaluate the reliability and performance of the system while costs and resources are managed effectively.
- **Long-Term Mission (3 Years):** A three-year mission would allow for even more in-depth analysis and extended technology validation. It enables more sustained operations and a more detailed performance assessment, but will increase the environmental risks and total cost of the mission.
- **Extended Mission (5+ Years):** This duration would be beneficial for long-term research on the performance degradation of SBSP subsystems. However, this entails higher costs and significant challenges in maintaining the spacecraft functional for such an extended period of time.

The criteria used in the mission duration trade-off have been listed in Table 3.6 with their respective weights and corresponding rationale.

Criteria	Rationale	Weight
Orbital Stability Over Time	Crucial for missions as it defines how much ΔV is required to maintain the desired orbit over time.	4
Radiation Exposure	The lunar environment comes with higher levels of radiation compared to Earth orbits. This exposure directly affects the S/C electronics and materials leading to higher chances of failure over time.	3
Cost	The cost of the mission is directly linked to the mission duration via operational costs and any other costs that help the S/C stay in orbit for a longer duration.	3
Technological Demonstration	The primary purpose of the mission is to demonstrate the new technologies in a real-world environment. A longer mission duration allows for more extensive validation but should also consider the effectiveness of an extended mission lifetime.	5

Table 3.6: Mission duration trade-off criteria with the corresponding rationale and weight.

Table 3.7 displays the trade-off matrix in which each criteria for a mission duration has been compared. After the computation of the weighted scores of each option, a favorable mission duration can be suggested. The Medium-Term Mission of 1 year has the highest score of 48 points as it provides a good balance between stability, radiation exposure, cost and the ability to demonstrate the SBSP technology sufficiently. Very close behind is the Short-Term Mission of 6 months following with a score of 45 points. This option scores excellent in all but lacks in technological demonstration duration. Both the Long-Term and Extended Mission appear to face higher cost and stability challenges over time, despite offering strong potential for extensive technological demonstration opportunities.

Mission duration / Criteria	**Short-Term Mission (6 Months)**	**Medium-Term Mission (1 Year)**	**Long-Term Mission (3 Years)**	**Extended Mission (5+ Years)**
Orbital Stability Over Time	High stability with low ΔV requirements	High stability with manageable ΔV requirements	High stability with higher ΔV requirements	Requires significant effort for stability management. Potential high risk
Radiation Exposure	Low radiation risk due to limited exposure time	Moderate radiation risk requiring effective radiation protection	High radiation risk. Requires robust protective measures and careful planning	Very high radiation risk. Advanced shielding and protective strategies
Cost	Cost-effective. Minimal operational expenses	Reasonable cost for duration, with balanced budget requirements	Elevated cost. Requires significant budget allocation	Very high cost. Needs a substantial budget investment
Technological Demonstration	Basic demonstration. Insufficient for extensive validation	Sufficient time for a demonstration. Enables the refining of SBSP technology	Extensive time for in-depth testing of SBSP technology. Detailed system assessment	Extensive technology demonstration. Long-term research on performance degradation.

Excellent = 4	Good = 3	Medium = 1	Low = 0

Table 3.7: Trade-off matrix for the mission duration for a lunar demonstration mission.

A sensitivity analysis has been conducted to examine how changes in the weights of various criteria impact the total scores of different mission duration options. In total, 10 scenarios were analyzed, including the baseline scenario and nine variants where the weighting has been modified. Each scenario shows how the changes in weighting affect the overall evaluation of the mission duration options:

- **Original**: Baseline scenario with the initial weights.
- **Scenario A**: Increased emphasis on Technological Demonstration, reduced focus on Cost.
- **Scenario B**: Higher priority on Orbital Stability, reduced emphasis on Radiation Exposure.
- **Scenario C**: Greater focus on Cost management, balanced attention to other criteria.
- **Scenario D**: Equal weighting across all criteria but radiation exposure, maintaining a balanced approach.
- **Scenario E**: Increased focus on Orbital Stability and Technological Demonstration, reduced emphasis on Cost and Radiation Exposure.
- **Scenario F**: Emphasis on Orbital Stability and Radiation Exposure, with a reduced focus on Technological Demonstration.
- **Scenario G**: Balanced focus on Orbital Stability and Radiation Exposure, with strong emphasis on Technological Demonstration.
- **Scenario H**: Increased focus on Cost and Technological Demonstration, with reduced emphasis on Orbital Stability.
- **Scenario I**: Equal assessment across all criteria, providing a uniform approach.

The various scenarios have been converted into different weightings of the criteria. These weightings have been used to compute the total scores for each mission duration option in each scenario. The

results are depicted in Figure 3.3. From this sensitivity analysis, a few conclusion can be derived. The Medium-Term mission maintains a high performance across a range of scenarios, highlighting its versatility. Meanwhile, the Short-Term mission performs optimal in scenarios where lower cost and complexity are prioritized but is less effective when focus is put on the Technological Demonstration aspect. Based on this information, it can be stated that the Medium-Term mission is a more reliable option where a combination of short-term efficiency and long-term performance is essential.

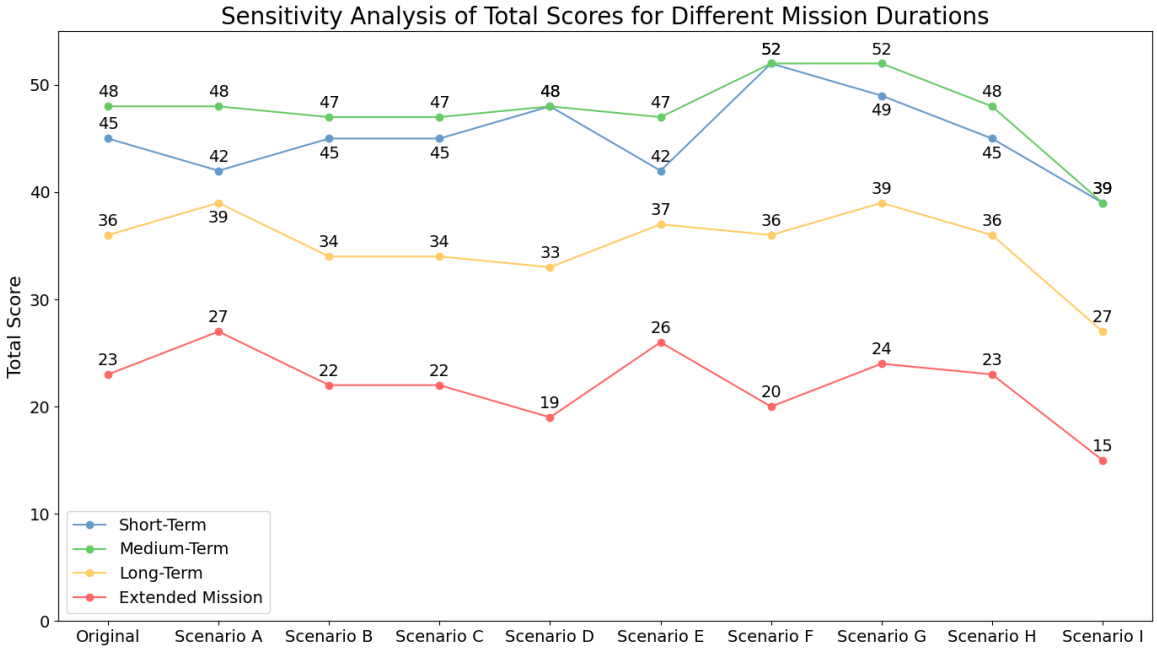

Figure 3.3: The results of each scenario in the sensitivity analysis for the mission duration trade-off.

3.2.5. Delivered Power

For the SBSP lunar demonstration mission, the choice of delivered power to the ground receiver substantially influences the feasibility and objectives of the mission. Moreover, determining a delivered power directly affects the size of the satellite. Consequently, each power level is accompanied with distinct benefits and challenges. Four options have been listed with their respective implications:

- **Low Power (1 kW):** Delivering 1 kW of power to a ground receiver offers a straightforward demonstration of the power transmission technology. It allows for testing the fundamental aspects of the system with lower complexity and cost. However, it cannot fully showcase the capabilities of high-power transmission.
- **Medium Power (3 kW):** A delivery power of 3 kW enables a good balance between demonstrating the transmission technology and managing operational complexities. It allows for a more comprehensive evaluation of the SBSP system performance, providing valuable data for scaling up to higher power levels.
- **High Power (5 kW):** A 5 kW power level offers the ability to support more substantial applications such as powering larger systems. Additionally, it allows for a more robust performance evaluation and its ability to handle higher energy demands. This does introduce increased system complexity, cost and thermal management challenges.
- **Very High Power (10 kW):** Delivering 10 kW of power would allow for large-scale demonstrations, potentially powering large lunar infrastructure or equipment. Furthermore, it allows for a detailed assessment regarding the system's ability to handle high power levels, including thermal management and laser durability. But it also comes with a significant complexity and cost and might surpass the optimal scope for a demonstration mission focused on initial technology validation.

In order to assess each power level option, a set of criteria with respective weights and corresponding rationale have been provided in Table 3.8.

Criteria	Rationale	Weight
System Complexity	Complexity affects both design and operational aspects. Important but manageable with good engineering and planning.	3
System Mass	Mass impacts launch costs and spacecraft performance. It is critical parameter in spaceflight.	4
Thermal Management	Effective thermal management is crucial for system reliability and performance but can often be designed around with appropriate engineering solutions.	3
Technological Demonstration	The primary goal of a demonstration mission is to validate technology. Thus, the effectiveness of technological demonstration is a top priority.	5
Cost	Cost is significant in mission planning, influencing budget constraints and overall mission feasibility.	4
Feasibility	Feasibility determines practical execution, including ease of implementation and operational risk.	4

Table 3.8: Trade-off criteria for power delivery with corresponding rationale and weight.

In Table 3.9, a trade-off matrix has been generated with the results of the delivery power trade-off. After computing the weighted scores of each option, the 3 kW (Medium Power) option scores the highest in the trade-off with 77 points, showing that this option offers the optimal balance between all trade-off criteria. The 1 kW option is also a strong contender at 74 points, but is only slightly surpassed by the 3 kW option. The 5 kW and 10 kW options are less favorable due to their higher complexity, mass, and cost. Notably, the thermal management of the 3 kW power level states it requires more space for thermal control systems and is marked as *Excellent*, yet the 1 kW power level is only marked as *Good*. This decision stems from the idea that a proper thermal control system with a certain degree of complexity should be in place in order to fully assess the future scalability of the system.

Delivered Power / Criteria	**Low Power (1 kW)**	**Medium Power (3 kW)**	**High Power (5 kW)**	**Very High Power (10 kW)**
System Complexity	Simple system design, low complexity	Moderately complex system design	Increased complexity in design and implementation	High complexity; high TRL required
System Mass	Low mass; minimizes launch cost	Moderate mass; manageable launch cost	Higher mass; increased launch cost	Very high mass; significant launch cost
Thermal Management	Minimal thermal components needed. Limited complexity	Requires more space for thermal control systems	Requires a more complex thermal control system	Requires extensive thermal control solutions
Technological Demonstration	Basic demonstration. Shows functionality of laser SBSP. Not a realistic scenario	More robust testing in a more realistic power scenario	High performance evaluation. Limited usage for delivered power	Excessive power for demonstration scope
Cost	Low cost due to simple, low-power components	Moderate cost	Higher cost due to more demanding components	Very high cost due to complexity and power level
Feasibility	Highly feasible due limited complexity and relatively low mass	Feasible but increased cost and complexity	Feasible but more demanding than a power level of 3 kW	Challenging with current technology

Excellent = 4	Good = 3	Medium = 1	Low = 0

Table 3.9: Trade-off matrix for delivered power options for a SBSP lunar demonstration mission.

Finally, a sensitivity analysis has been executed which evaluates how changes in the weights of various criteria affect the total scores of different power delivery options. The impact of adjusting these weights has been assessed across several scenarios. In total, nine scenarios have been used in the analysis, including a baseline scenario and eight variants where weights for specific criteria are adjusted. Each scenario reflects how changes in weighting affect the comparative performance of the power delivery options:

- **Original**: Baseline scenario with initial weightings for all criteria.
- **Scenario A**: Emphasizes System Complexity while reducing emphasis on Feasibility.
- **Scenario B**: Prioritizes Thermal Management over Cost.
- **Scenario C**: Focuses on increasing Technological Demonstration, with a reduced focus on System Mass.
- **Scenario D**: Shifts focus to System Mass and reduces emphasis on Technological Demonstration.
- **Scenario E**: Enhances the importance of System Complexity while decreasing the weight on Cost.
- **Scenario F**: Increases emphasis on Thermal Management and decreases focus on System Mass.
- **Scenario G**: Prioritizes Feasibility over Technological Demonstration.

- **Scenario H**: Focuses on Cost while reducing the weight given to Technological Demonstration.

The analysis utilizes the total scores computed using the weighting under different scenarios. The results have been visualized in Figure 3.4, showcasing how each power delivery option performs relative to the others as criteria weights are varied. The sensitivity analysis reveals that the 3 kW power delivery option generally outperforms the 1 kW option across most scenarios. However, there are specific scenarios where the 1 kW option shows superior behaviour, albeit with a very small difference of one point compared to the 3 kW option. Scenario D, G and H all have in common that the weighting of Technological Demonstration criteria is decreased by one. This common factor underscores the critical nature of the technological demonstration aspect in the trade-off for the lunar demonstration mission. Thus, the sensitivity analysis confirms that the 3 kW option is a more balanced solution among the criteria considered. This makes the 3 kW option a more robust and adaptable choice for the lunar demonstration mission.

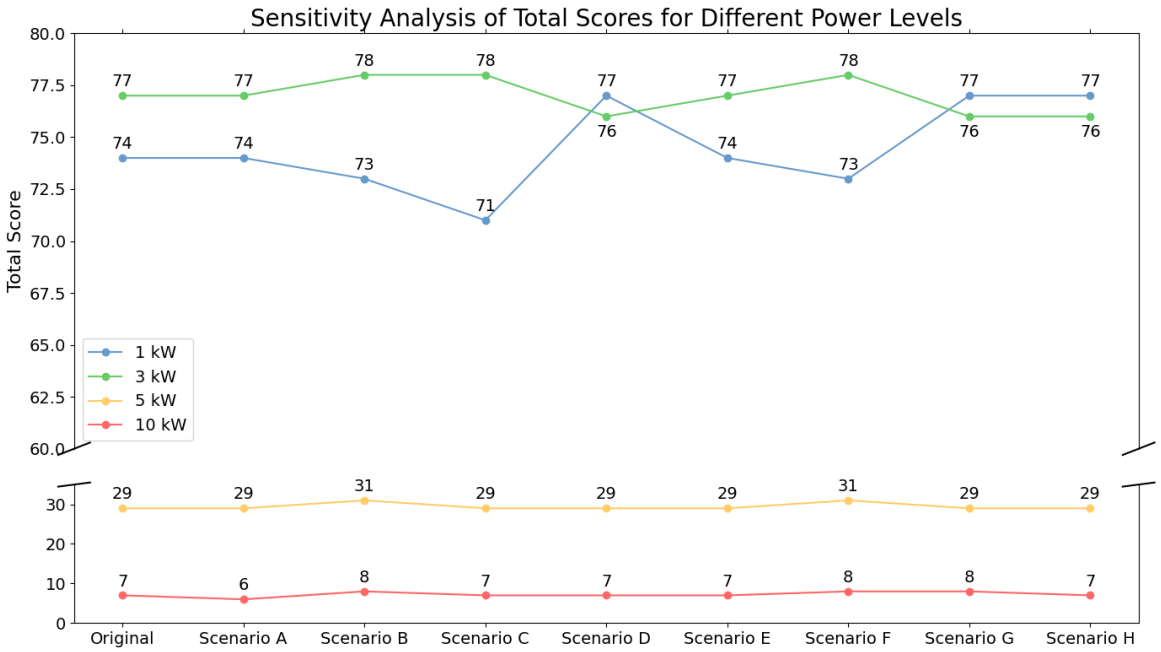

Figure 3.4: The results of each scenario in the sensitivity analysis for the delivered power trade-off.

3.2.6. End of Life Disposal Options

The End of Life (EoL) strategy for the SBSP satellite in LLO must consider environmental sustainability, operational safety, and future lunar mission needs. Two primary options for disposal are evaluated: a controlled lunar surface impact and transfer to a graveyard orbit. Both approaches have unique advantages and challenges, which are examined below.

Controlled Lunar Impact

A controlled lunar impact involves directing the satellite to a pre-selected, geologically insignificant crater on the Moon's surface. This method ensures definitive disposal of the satellite and eliminates any contribution to long-term orbital debris. By targeting a desolate region, interference with potential scientific or exploration sites is minimized. Additionally, an impact can offer scientific opportunities, such as studying the plume ejected during the collision, as demonstrated by the LCROSS mission.

However, lunar impacts can introduce contamination to the surface, potentially complicating astrobiological studies or future research objectives. While the Moon is considered devoid of life, care must be taken to avoid historically significant or scientifically valuable regions.

Graveyard Orbit

Transferring the satellite to a graveyard orbit places it in a stable, high-altitude trajectory outside operational LLO regions. This approach preserves the lunar surface from physical contamination and leaves

it undisturbed for future exploration. Additionally, a well-designed graveyard orbit can remain stable for hundreds or thousands of years, depending on the Moon's gravitational perturbations.

Despite its advantages, graveyard orbits pose challenges. The Moon's irregular gravitational field (mascons) can destabilize orbits over time, potentially returning the satellite to operational regions or resulting in an uncontrolled lunar impact. Furthermore, as lunar activity increases, graveyard orbits may contribute to orbital congestion, necessitating long-term debris mitigation strategies.

Recommended End of Life Strategy
Based on the evaluation, a controlled lunar impact is proposed as the preferred EoL strategy for the SBSP satellite. This approach aligns with long-term orbital debris mitigation principles and ensures that the satellite will not pose a risk to future operations in lunar orbit. By targeting a geologically insignificant crater in a desolate region, contamination and interference with exploration activities are minimized.

The controlled lunar impact offers the most environmentally responsible solution, given the absence of a lunar biosphere and the increasing importance of debris-free orbital regions for sustainable lunar exploration.

Delta-V Calculation for Lunar Impact at Apoapsis
To calculate the ΔV required for a satellite in a 100 km lunar orbit to perform an EoL maneuver leading to a lunar impact, the burn is assumed to occur at apoapsis. The initial orbit is circular, and the maneuver transitions the orbit into an ellipse with periapsis intersecting the Moon's surface.
The given parameters are:

- Lunar radius: $R_{\text{Moon}} = 1,737\,\text{km}$,
- Orbital altitude: $h = 100\,\text{km}$,
- Orbital radius: $r_{\text{orbit}} = R_{\text{Moon}} + h = 1,837\,\text{km}$,
- Lunar gravitational parameter: $\mu = 4904.869\,\text{km}^3/\text{s}^2$.

The initial orbital velocity for a circular orbit is given by:

$$v_{\text{orbit}} = \sqrt{\frac{\mu}{r_{\text{orbit}}}} \tag{3.2}$$

Substituting the values:

$$v_{\text{orbit}} = \sqrt{\frac{4904.869}{1837}} \approx 1.634\,\text{km/s}. \tag{3.3}$$

The semi-major axis of the resulting elliptical orbit is:

$$a = \frac{r_{\text{periapsis}} + r_{\text{apoapsis}}}{2} = \frac{R_{\text{Moon}} + r_{\text{orbit}}}{2} = \frac{1737 + 1837}{2} = 1787\,\text{km}. \tag{3.4}$$

The orbital velocity at apoapsis in the elliptical orbit is calculated using the vis-viva equation:

$$v_{\text{apoapsis, new}} = \sqrt{\mu \left(\frac{2}{r_{\text{apoapsis}}} - \frac{1}{a} \right)}. \tag{3.5}$$

Substituting the values:

$$v_{\text{apoapsis, new}} = \sqrt{4904.869 \left(\frac{2}{1837} - \frac{1}{1787} \right)} \approx 1.586\,\text{km/s}. \tag{3.6}$$

The required ΔV is the difference between the new apoapsis velocity and the initial circular velocity:

$$\Delta V = v_{\text{orbit}} - v_{\text{apoapsis, new}} = 1.634 - 1.586 \approx 0.048\,\text{km/s} \approx 48\,\text{m/s} \tag{3.7}$$

3.2.7. Optimal Configuration for the Lunar Demonstration Mission

After the thorough trade-off analysis has been conducted, the optimal configuration for the SBSP lunar demonstration mission can be determined. Based on the evaluated criteria and weighted scores for different mission characteristics, the following configuration in Table 3.10 can be identified as most optimal:

	Configuration
Type of Orbit	Frozen Polar Low Lunar Orbit (LLO)
Mission Duration	Medium-Term Mission (1 Year)
Delivered Power	Medium Power (3 kW)
End of Life Strategy	Controlled Lunar Impact
Transmission Method	Laser

Table 3.10: Mission Characteristics for the Lunar Demonstration Mission.

This configuration holds a balance between the various criteria used throughout the trade-off analysis. The Frozen Polar LLO provides high orbital stability, efficient and accurate power transmission due to low altitude and offers the opportunity to scale the configuration to a constellation. Moreover, the lunar South Pole can be frequently accessed to provide power to a major area of interest, the Shackleton's Crater. The Medium-Term Mission of one year allocates sufficient time for a comprehensive technological demonstration while managing cost and risks. The Medium Power level of 3 kW enables a realistic assessment of the system performance, while managing the cost and system complexity and mass. A 3 kW power level also maintains a good overall mission feasibility. Finally, as concluded in the WPT trade-off analysis, the SBSP system will utilize a laser for its power transmission method.

3.2.8. Mission Timeline

Building upon the preliminary mission characteristics outlined in Table 3.10, a conceptual timeline is proposed to organize the mission into distinct phases defined by specific planned events. These durations represent preliminary estimates that provide a foundational structure for the mission.

The mission allocates two five-month periods for technology demonstration, ensuring sufficient time to assess the system performance under real operational conditions. During these phases, the SBSP system will transmit power, collect data, and evaluate long-term operational reliability. In the Table 3.11, these two operational phases are divided by data analysis and optimization activities. These efforts aim to refine system performance and address potential areas for improvement, ensuring the demonstration achieves its objectives effectively. The ten key mission events are outlined in Table 3.11, providing a high-level mission planning for the lunar demonstration mission.

Event	**Description**	**Duration**
1. Launch into an Earth Parking Orbit	Utilizing one of the available launchers.	1 week
2. Deployment of the space segment	Deploying of the solar arrays and antennas, testing of components required for TLI.	1 day
3. Trans-lunar Injection	Launcher provides ΔV for the TLI.	1 week
4. Lunar Orbit Insertion	Space segment performs a LOI burn.	1 day
5. Deployment of power transmitter components	Ensuring that every required component is deployed for power transmission.	1 week
6. Space segment initial testing	Test the integration of the satellite in lunar orbit.	3 weeks
7. Operational Demonstration Phase	Transmit power to the receiver and gather the demonstration data.	5 months
8. Data Analysis and Optimization Phase	Assess system performance and implement optimizations based on data analysis.	1 month
9. Extended Operational Phase	Continue the power transmitting procedure with the optimized satellite.	5 months
10. End of life and decommissioning phase	Shutting down the spacecraft.	2 weeks

Table 3.11: Event sequence for the mission.

Now that the lunar demonstration mission characteristics have been defined via a detailed trade-off analysis, the next step is to determine which conceptual SBSP design is most suitable for this demonstration mission. This decision will be made via a SBSP conceptual design trade-off analysis. Once the most optimal concept has been selected, the preliminary design phase will be initiated where a more detailed SBSP system design will be established.

4

SBSP Conceptual Design Trade-Off Analysis

Chapter 4 will contain the conceptual trade-off for each relevant subsystem in a SBSP system. The adhered trade-off sequence is determined such that each trade-off sets the foundation for the next subsystem trade-off. Hence, power related subsystems will be analyzed first after which the relevant subsystems are evaluated.

4.1. Power Generation System Trade-off

The power generation system will act as the first trade-off in this design study. This system plays an integral role in supplying 3 kW to the ground receiver.

4.1.1. Power Generation System Objectives

Before investigating the power generation trade-off, a number of clear objectives for the subsystem have to be established. These objectives will guide the following trade-off by providing a baseline for the trade-off criteria. Table 4.1 has depicted the list of objectives.

ID	Objective
PGEN-01	The power generation system should generate enough power to meet the demand of the SBSP system.
PGEN-02	The power generation system should be as lightweight and compact as possible without compromising system performance.
PGEN-03	The power generation system should convert solar energy into power as efficiently as possible to minimize losses.
PGEN-04	The power generation system shall be characterized with a high Technology Readiness Level (TRL) to increase the system reliability.

Table 4.1: Power generation system objectives with a corresponding ID.

4.1.2. High-End Power Generation System Trade-off

The power generation subsystem holds the functionality to generate a stream of power for every power-consuming subsystem in the satellite. This can be done the conventional way, by employing photovoltaic panels or solar arrays. Alternatively for SBSP systems, Concentrated Solar Power (CSP) can be used to partially feed direct solar-pumped lasers and partially feed heat converters for powering the other subsystems. A benefit of CSP is that it bypasses the solar energy to electrical conversion which, in the end, allows for a greater laser system efficiency [95]. In total, four power generation options are analyzed in the trade-off:

- **Photovoltaic Panels:** Traditional solar panels that use silicion-based solar cells to convert sunlight directly into electricity. These panels are relatively outdated and less efficient than advanced PV panels but have been widely used on older spacecraft like the ISS.
  - *Existing Spacecraft:* International Space Station (ISS) [57], Vanguard 1 [61].
- **Concentrated Solar Power:** A power generation method that focuses sunlight directly into direct solar-pumped lasers using mirrors and/or lenses.
  - *Existing Spacecraft:* Conceptual stage, has not yet been implemented on any operational spacecraft. Among others proposed in SBSP concepts [95].
- **Advanced PV Panels:** Solar cells that consist of multiple layers (i.e. multi-junction cells) to capture a larger spectrum of sunlight, resulting in higher efficiency.
  - *Existing Spacecraft:* UltraFlex arrays on Phoenix Mars Lander [64], Juno.
- **Thin-Film Solar Cells:** Lightweight and flexible solar cells that can be integrated onto a range of surfaces. This has the benefit of offering a lower mass alternative to traditional PV panels.
  - *Existing Spacecraft:* Hubble Space Telescope [31], IKAROS [48].

Next, a set of criteria with corresponding weightings have been determined in Table 4.2. For the Power Generation Trade-off, both the *Efficiency* and *Mass and Volume* criteria have been deemed as most important because it influences both the maximum power output and the total mass and volume of the subsystem.

Criteria	Rationale	Weight
Efficiency	Essential for maximizing the power output from the solar arrays.	5
Operational Reliability	The power generation system must withstand the extreme temperature variations and radiation exposure of the lunar environment.	3
Mass and Volume	Efficient use of mass and volume is critical due to launch constraints and overall spacecraft design.	5
Subsystem Complexity	The complexity of the subsystem impacts the ease of deployment and integration of the power generation system with other spacecraft systems.	3
Cost	The cost of developing and manufacturing the power generation system significantly impacts the overall mission budget.	4
Technology Readiness Level (TRL)	The TRL indicates the maturity and reliability of the technology.	4

Table 4.2: Trade-off criteria for the power generation subsystem with corresponding rationale and weight.

As a result, a trade-off matrix for the power generation trade-off has been generated in Table 4.3. After analyzing the matrix, it can be suggested that CSP is not yet developed enough to be implemented in this SBSP demonstration mission. The technology lacks the required TRL and thus the required reliability to make the mission a success. Continuing, the most suitable option for the power generation unit is the *Advanced PV Panel* option with a total score of 76 points. Number two in the trade-off is the *Photovoltaic Panels* option with a total score of 56 points. The difference between the two options is notably the higher efficiency of the advanced PV panels.

Power Generation / Criteria	**Photovoltaic Panels**	**Concentrated Solar Power**	**Advanced PV Panels**	**Thin-Film Solar Cells**
Efficiency	15-20%[43]	Can be used with direct solar-pumped lasers, resulting in $\approx$ 50% [95]	Up to 34% [43]	7-18% [8]
Operational Reliability	Reliable performance over time. Susceptible to degradation from radiation.	In conceptual stage for space applications. Lack of operational data.	Strong performance. Excellent in dealing with high radiation and thermal cycles.	Not as reliable as traditional PVs. More prone to radiation degradation.
Mass and Volume	Relatively high mass and volume. Rigid structures require more mass & volume.	Heavy and bulky equipment. Mirrors, lenses and structural support.	Lightweight panels due to multi-junction cells. Reduced mass and volume.	Offer lightest and most compact option. Thin, flexible design best for low mass and volume.
Subsystem Complexity	Relatively simple and well-understood mechanical design.	Complex mirrors must focus sunlight directly into the laser modules.	Relatively simple and well-understood mechanical design.	Thin-film cells itself are quite simple. Unfolding mechanisms can be quite complex.
Cost	Mature manufacturing processes. Cost-effective for space missions.	Very high cost. Space-based CSP is still in the conceptual phase.	More costly due to complex manufacturing processes. High cost materials.	Lower material cost but specialized manufacturing and deployment methods.
Technology Readiness Level (TRL)	Widely used and thoroughly tested. Minimal risk.	Not proven in space environments. Primarily proposed in concepts.	Widely used and thoroughly tested. Minimal risk.	Moderately high TRL. Tested in experimental and limited space missions.

Excellent = 4	Good = 3	Medium = 1	Low = 0

Table 4.3: Trade-off matrix for power generation options in a SBSP lunar demonstration mission.

A sensitivity analysis has been conducted to assess the fluctuations in the trade-off results. Including the original weighting scenario, ten scenarios have been listed below:

- **Original**: Baseline scenario with initial weightings for all criteria.
- **Scenario A**: Emphasizes Efficiency as the highest priority while slightly reducing emphasis on Mass and Volume.
- **Scenario B**: Prioritizes Operational Reliability over Mass and Volume to ensure durability in the lunar environment.
- **Scenario C**: Focuses on Cost-conscious approach by reducing emphasis on Mass and Volume, making cost the top priority.
- **Scenario D**: Shifts focus to Compact Design, giving the highest weight to Mass and Volume, with moderate importance on Efficiency and Reliability.
- **Scenario E**: Enhances the importance of Subsystem Complexity by reducing weight on Efficiency and Mass and Volume.

- **Scenario F**: Emphasizes Technology Readiness Level (TRL) to prioritize mature and reliable technologies over other criteria.
- **Scenario G**: Adopts a Balanced Weighting approach, giving equal importance to most criteria with slight variations.
- **Scenario H**: Combines a high emphasis on Efficiency and Operational Reliability while reducing importance on Cost and TRL.
- **Scenario I**: Prioritizes Cost and Compactness by focusing on Cost and Mass and Volume, with lower emphasis on Efficiency.

These scenarios have been plotted in Figure 4.1. For each scenario, the *Advanced PV Panels* outperform every other option. Only in scenario C and I do the *Photovoltaic Panels* and *Advanced PV Panels* perform similarly, but regardless, the advanced PV option seems to be a more suitable option for the SBSP system.

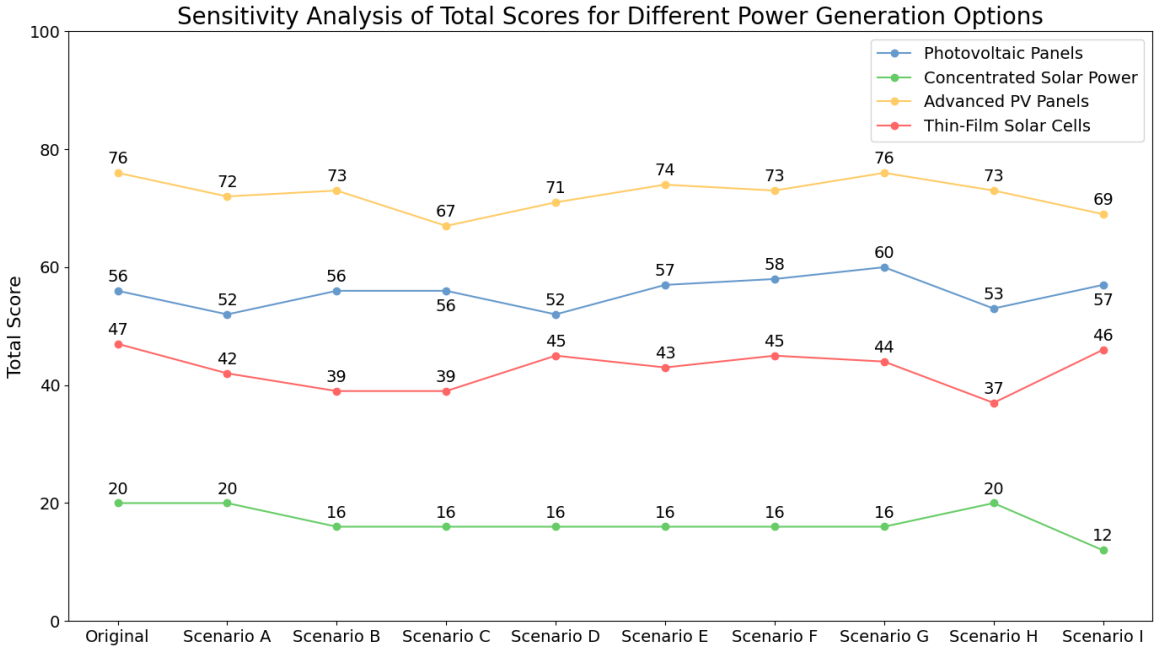

Figure 4.1: The results of each scenario in the sensitivity analysis for the Power Generation trade-off.

4.1.3. Advanced PV Panels Trade-off

In the previous high-end power generation trade-off, the conclusion was drawn that the *Advanced PV Panels* was the most suitable option for the demonstration mission. The next step is to analyze existing advanced solar panel options and perform a trade-off analysis to determine the best COTS solution for the demonstration mission. Four power generation COTS have been proposed.

- **UltraFlex**: The UltraFlex array is a circular, ultra-lightweight, and deployable solar array technology designed for space applications. UltraFlex has incorporated high power-to-weight ratios and excellent stowage efficiency in its design [3]. Originally developed by ATK, UltraFlex has been used on NASA's Mars missions, demonstrating its reliability in harsh environments. A characteristic feature of the UltraFlex array is its fan-like deployment seen in Figure 4.2, which ensures a compact launch configuration with a large deployed surface area.
- **MegaFlex**: MegaFlex is an advanced solar array system developed by Northrop Grumman (formerly Orbital ATK) for high-power space applications. Based on the same principles as UltraFlex, it is designed to provide significantly more power, up to hundreds of kilowatts [59]. MegaFlex arrays hold great potential as they are scalable, lightweight, and capable of supporting large spacecraft and long-duration missions. MegaFlex has integrated an accordion-like deployment mechanism, seen in Figure 4.3, which allows for a compact stowage volume, making it ideal for deep space and large satellite applications.

- **ROSA (Roll-Out Solar Array)**: ROSA is a flexible, roll-out solar array developed by Deployable Space Systems (DSS) shown in Figure 4.4. It deploys unrolling the array from a compact cylindrical stowed configuration. ROSA is designed to offer high power generation capabilities with minimal mass and stowage volume [73]. It has been successfully operating on the International Space Station (ISS) and is considered a key technology for future space missions requiring large, lightweight, and efficient solar arrays.
- **DLR Boom Arrays**: Designed by the German Aerospace Center (DLR), Boom Arrays are deployable solar arrays that use a lightweight and compact boom structure to support the with solar cell integrated solar sails shown in Figure 4.5. These arrays are designed to provide efficient power generation for small satellites and spacecraft but can also be scaled up to 500 kW. The DLR Boom Arrays offer a balance between structural rigidity and flexibility, allowing for efficient deployment in space while maintaining stability during operation. This technology is primarily attractive for missions where weight and volume constraints are critical. As of now, the Deployable Boom Array is still in the conceptual design phase.

Figure 4.2: ATK Orbital's UltraFlex Array [64].

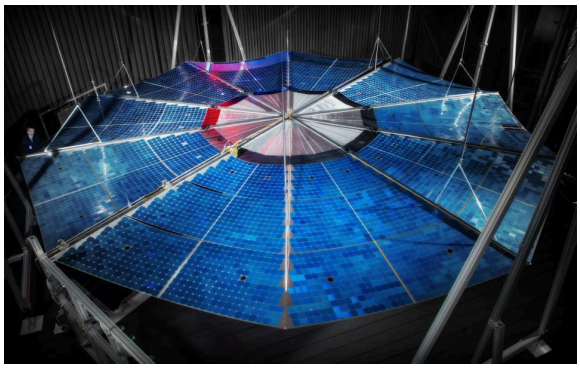

Figure 4.3: Northrop Grumman's (formerly ATK) MegaFlex Array [62].

Figure 4.4: DDS's ROSA Array [27].

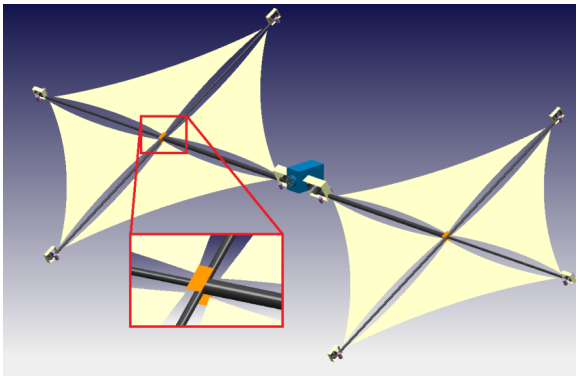

Figure 4.5: DLR's Deployable Boom Array [94].

Figure 4.6: The included Advanced PV Panel options in the detailed trade-off.

The criteria used in the COTS power generation trade-off have been slightly altered to focus more on the specific performance parameters of the COTS systems.To be precise, the *Power Generation* criterion has been added to ensure the system is capable of delivering the required power to each subsystem in the SBSP satellite. Additionally, this criterion is used to assess the scalability of the power generation system. It is important to note that most of the evaluated options are not modular solar arrays; scaling these systems can only be achieved by increasing the area of the two solar arrays mounted on each side of the satellite. The ROSA option is the only exception, which offers a modular design and can be scaled by adding additional units. However, this is at the cost of a much higher complexity. Furthermore, the *Operational Reliability* option has been removed from the criteria list for

two reasons: (1) it is assumed that the *Advanced PV Panels* have somewhat similar reliability features based on the previous trade off and (2) the subsystem complexity also indirectly reflects the reliability of each option. The more complex an option is, the higher the change of a part malfunctioning, and thus the lower the overall reliability is of that option. The full list of criteria is depicted in Table 4.4.

Criteria	Rationale	Weight
Efficiency	Essential for maximizing the power output from the solar arrays.	5
Power Generation	The power generation system must be able to provide the required total power of the SBSP system	4
Mass and Volume	Efficient use of mass and volume is critical due to launch constraints and overall spacecraft design.	5
Subsystem Complexity	The complexity of the subsystem impacts the ease of deployment and integration of the power generation system with other spacecraft systems. Also affects the reliability of the COTS.	4
Cost	The cost of developing and manufacturing the power generation system significantly impacts the overall mission budget.	3
Technology Readiness Level (TRL)	The TRL indicates the maturity and reliability of the technology.	3

Table 4.4: Trade-off criteria for the COTS power generation subsystem with corresponding rationale and weight.

In Table 4.5, the four advanced solar panel options have been traded off against the list of criteria in Table 4.4. It should be noted that finding the relevant COTS characteristics was quite challenging as not every parameter is publicly available. Therefore, some parameters have been qualitatively estimated. In the end, performing the trade-off went smoothly and resulted in the following outcome. The UltraFlex COTS option scores a ”Low” for the Power Generation criterion as it can only provide a maximum power of 15 kW Begin-Of-Life (BOL) per wing. When recalling the example in Table 3.2, it can be stated that a maximum power generation of 30 kW power will not suffice for this particular lunar demonstration mission, because the example in Table 3.2 necessitates a required power supply of 90 to 120 kW and not even to mention that the UltraFlex COTS does not allow for any significant scalability of the SBSP system. Next, the DLR Boom Arrays option has scored a ”Low” for the TRL criterion. The arrays designed by DLR are still in the conceptual design phase and are not ready for in-flight demonstration yet. Implementing the DLR arrays for the lunar demonstration mission would heighten the overall risks of the mission.

With the elimination of these two options, the MegaFlex and ROSA options now stand out as the only two prominent choices. MegaFlex offers a significant power generation capability, with a two-wing system capable of producing up to 500 kW. Furthermore it demonstrates excellent mass and volume efficiency, with over 100 W/kg and 40 kW/m^3 at the End-Of-Life (EOL) [59]. A downside of this technology is the lower TRL of approximately 5+ [59], indicating that is has not yet been proven in-flight.
On the other hand, ROSA features an innovative roll-out mechanism, providing a balance of power generation between 1-30 kW for a single wing and up to 400+ kW for a Mega-ROSA configuration [73]. Its superior efficiency of up to 34% and its operation aboard the ISS signifies its maturity and reliability with a high TRL. This solution is also assumed to be more cost-effective with a lower cost per watt than the MegaFlex solution. ROSA’s disadvantage is that for higher power configurations the Mega-ROSA solution has to be employed which sparks up the complexity and potentially the volume of the system.

The results of the trade-off table conclude that the MegaFlex option is more favourable than ROSA. The MegaFlex option scored in total 85 points. ROSA obtained a total score of 80 points. With a difference of only five points it is obviously of paramount importance to conduct a sensitivity analysis to see the behaviour of the trade-off results when changing the weights of the criteria.

Power Generation / Criteria	UltraFlex	MegaFlex	ROSA	DLR Boom Arrays
Efficiency	27% [3]	29% [59]	34% [40]	TF: 10-20%. MJ: 20-30% [94].
Power Generation	Wing sizes up to 15 kW BOL [3].	A two-wing system up to 500 kW [59].	Single wing: 1-30 kW. Mega-ROSA: 20-400+ kW [73].	Wing sizes up to 500+ kW [94].
Mass and Volume	> 150 W/kg BOL. > 40 kW/m^3 [3].	> 100 W/kg EOL. > 40 kW/m^3 EOL [59].	100-120 W/kg. 40 kW/m^3 [73].	For 2.5 kW: 220 W/kg. For 500 kW: 140 W/kg [94].
Subsystem Complexity	Low complexity. Deploys each wing separately.	Employs UltraFlex deployment strategy.	Higher complexity with Mega-ROSA. Innovative roll-out mechanism.	High complexity Intricate deployment mechanism. Each wing has 4 boom elements.
Cost	A 1.8 m diameter array costs (2011) $20 million [88]. $5700 per W.	Assumed to have a similar cost as Ultraflex but at a lower TRL.	Six iROSA units cost $103 million [76]. $488 per W.	Higher cost due to development and deployment complexity.
Technology Readiness Level (TRL)	High TRL. Flown on Mars Phoenix Lander [64].	Moderate TRL of 5+. Not yet proven in-flight.	High TRL. Operating onboard the ISS.	Low TRL. Still in conceptual phase at DLR.

Excellent = 4	Good = 3	Medium = 1	Low = 0

Table 4.5: Trade-off matrix for advanced deployable solar array options in a SBSP lunar demonstration mission.

For the sensitivity analysis, the following set of weighting scenarios have been determined to assess the validity of the trade-off analysis:

- **Original**: Baseline scenario with initial weightings for all criteria.
- **Scenario A**: Emphasizes Efficiency as the highest priority, with a slightly reduced focus on Mass and Volume.
- **Scenario B**: Prioritizes Power Output to ensure high energy transmission, with moderate emphasis on Mass and Volume and reduced focus on Efficiency.
- **Scenario C**: Focuses on a Cost-conscious approach by making Cost the top priority, with reduced emphasis on Efficiency and Subsystem Complexity.
- **Scenario D**: Shifts focus to Compact Design, giving the highest weight to Mass and Volume while maintaining a balanced approach to Subsystem Complexity and TRL.
- **Scenario E**: Enhances the importance of Subsystem Complexity and TRL by slightly reducing the focus on Efficiency and Cost.
- **Scenario F**: Emphasizes TRL to prioritize mature and reliable technologies over other criteria, with reduced focus on Efficiency, Power Output, and Mass and Volume.

- **Scenario G**: Adopts an Equal Weighting approach, giving equal importance to all criteria to ensure a balanced decision-making process.
- **Scenario H**: Combines high emphasis on Efficiency and Mass and Volume while reducing the importance of Cost and TRL.
- **Scenario I**: Prioritizes Cost and Compact Design by focusing on Cost and Mass and Volume, with lower emphasis on Efficiency and TRL.

Using the range of weighting scenarios, a sensitivity analysis has been conducted and is displayed in Figure 4.7. The sensitivity analysis shows that both the MegaFlex and ROSA COTS options perform very similar in almost every scenario. In scenario C, the cost-conscious approach, ROSA is even a more suitable solution. Nevertheless, in almost every scenario MegaFlex appears to be the primary solution for the SBSP system. Concluding, the ROSA system consistently demonstrated strong performance across multiple scenarios, proving it to be a highly promising solution. However, the MegaFlex system ultimately prevailed. Additionally, more specific performance characteristics were available for the MegaFlex system. This additional data will simplify integrating MegaFlex into the overall design, giving it an edge in the selection process, despite near-equal performance of both ROSA and MegaFlex.

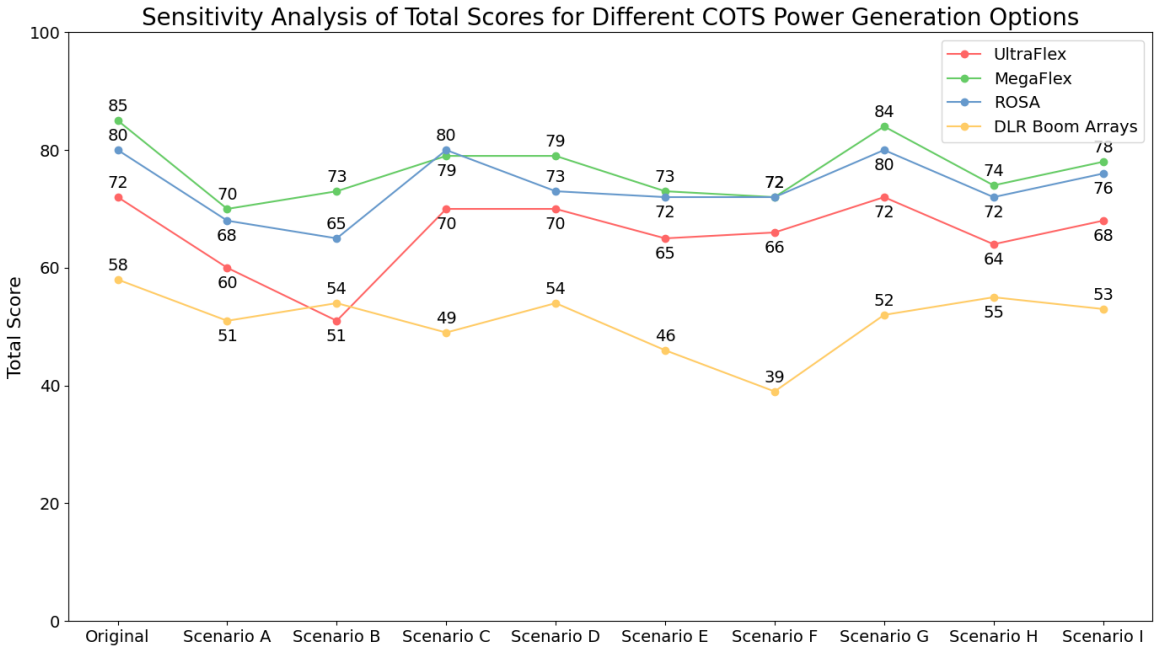

Figure 4.7: The results of each scenario in the sensitivity analysis for the COTS Power Generation trade-off.

4.2. Laser Power Transmission System Trade-off

The second subsystem trade-off will cover the Laser Power Transmission (LPT) system. This system is responsible for ensuring the transmission of the power generated by the power generation system. The LPT can be classified as the payload of the satellite, as its primary function aligns most with the mission objective of the SBSP system.

4.2.1. Laser Power Transmission System Objectives

To initiate the high-end LPT trade-off, it is useful to first determine the LPT system objectives. A list of six objectives has been compiled below in Table 4.6, focusing on the system's primary tasks along with secondary, non-critical objectives, including ensuring the implementation of safety mechanisms.

ID	Objective
LASER-01	The laser transmission system should efficiently transmit the generated power from the satellite to the lunar ground receiver.
LASER-02	The laser transmission system should operate reliably in the harsh space environment, including temperature extremes and radiation exposure.
LASER-03	The laser transmission system should be capable of transmitting power to the receiver during periods of ground visibility.
LASER-04	The laser transmission system should be compact and lightweight to optimize integration with the spacecraft and minimize launch costs.
LASER-05	The laser transmission system should be designed to minimize beam divergence.
LASER-06	The laser transmission system should include safety mechanisms to prevent unintended beam exposure to unintended targets.

Table 4.6: Laser transmission system objectives with a corresponding ID.

4.2.2. High-End Laser Power Transmission System Trade-off

The first action in the LPT system trade-off involves determining the most suitable laser technology for the SBSP system. Given the variety of available laser types, this first trade-off will reduce the amount of Commercial Off-The-Shelve (COTS) laser systems available and thus simplify the COTS LPT trade-off in Section 4.2.3. Three types of potential laser technologies have been assessed and are shortly described below:

- **Flashlamp Solid-State Lasers:** This type of laser employs a crystal of Neodymium-doped Yttrium Aluminum Garnet (Nd YAG) as the gain medium and are pumped by flashlamps. These lasers are known for high power output and are widely deployed in industrial, medical and military operations. These lasers tend to be bulkier and less efficient compared to diode-pumped systems.
- **Diode Solid-State Lasers:** This type of laser also uses a Nd YAG crystal as the gain medium but uses semiconductor diodes as the pump source, which holds a more efficient energy conversion and a more compact design. Widely used in telecommunications and medical applications.
- **Fiber Lasers:** These lasers also utilize semiconductor diodes as the pump source but use a doped optical fiber as the gain medium. This allows for higher beam quality and efficiency. This type of laser is used in cutting, welding, telecommunications and military operations.

In Table 4.7, the list of criteria with their respective weights for the LPT system trade-off has been compiled. These criteria will ensure a comprehensive analysis of the three laser technologies. Both *Efficiency* and *Mass and Volume* have been deemed as critical criteria for the LPT trade-off as these system characteristics affect the total system efficiency and the total system mass and volume.

Criteria	Rationale	Weight
Efficiency	Ensuring efficient power transmission to the receiving station and minimizing excess heat.	5
Operational Reliability	The LPT system must be able to operate reliably over extended periods in the harsh space environment, ensuring consistent power transmission.	3
Mass and Volume	Mass and volume must be minimized for meeting launch constraints and launching and deploying the system in space.	5
Cost	The cost of developing, manufacturing, and deploying the laser system is directly related to the overall project budget and feasibility.	3
Technology Readiness Level (TRL)	The TRL indicates the maturity of the laser technology, which is directly related to the risk and reliability of the system in space operations.	4

Table 4.7: Trade-off criteria for the laser subsystem with corresponding rationale and weight.

The trade-off matrix for the LPT system trade-off has been generated in Table 4.8. The three laser technology options have been analyzed for the criteria in the table. As a result, the *Fiber Lasers* option is outperforming the other two laser options with a total score of 70 points. The *Diode Solid-State Lasers* option has only one point less, 69 points and is also a suitable candidate for the design. Fiber lasers hold the potential for a high efficiency beam and are considered to be highly reliable with excellent beam quality. Weaponized systems by i.e. Raytheon could lay the foundation for a laser system tailored for power transmission purposes. All options show a high TRL for laser usage in space but this level is not specifically for power transmission tasks. LPT has been demonstrated at low power levels onboard the ISS [87] but the lunar demonstration mission is vastly more complex than the achievement onboard the ISS.

A sensitivity analysis has been conducted to assess the impact of different weighting scenarios. The following list of scenarios has been used:

- **Original**: Baseline scenario with initial weightings for all criteria.
- **Scenario A**: Emphasizes Efficiency as the highest priority.
- **Scenario B**: Moderate emphasis on Efficiency and TRL.
- **Scenario C**: Focuses on a Cost-conscious approach by making Cost the top priority, with reduced emphasis on Efficiency and Reliability.
- **Scenario D**: Shifts focus to Compact Design, giving the highest weight to Mass and Volume while maintaining a balanced approach to other criteria.
- **Scenario E**: Enhances the importance of Operational Reliability and Mass and Volume by reducing the focus on Cost and Efficiency.
- **Scenario F**: Emphasizes TRL to prioritize mature and reliable technologies over other criteria.
- **Scenario G**: Adopts an Equal Weighting approach, giving equal importance to all criteria to ensure a balanced decision-making process.
- **Scenario H**: Combines high emphasis on Efficiency while reducing the importance of Cost and TRL.
- **Scenario I**: Prioritizes Cost and Reliability by focusing on Cost and Operational Reliability, with lower emphasis on Efficiency.

Laser Type / Criteria	**Flashlamp Solid-State Lasers**	**Diode Solid-State Lasers**	**Fiber Lasers**
Efficiency	Very low efficiency (Nd lasers, 0.1-2% [70])	High efficiency (up to 50%) [68].	High efficiency (30-50%) [28].
Operational Reliability	Flashlamp degrade over time; regular replacement. More heat generation.	More efficient; generate less heat. Lower degradation.	Highly reliable, robust in harsh environments. Excellent beam quality. Minimal degradation.
Mass and Volume	Relatively high mass and volume. Bulky flashlamp. Lower efficiency; affects thermal system mass.	Compact and lightweight system [68] with reduced cooling needs.	A 15 kW Raytheon fiber laser has a laser system mass of ≈530 kg [72]. Compact design.
Cost	Lower initial cost but higher long-term operational cost.	Moderate cost with better efficiency. Lower operational cost.	High cost, though most cost-effective over time.
Technology Readiness Level (TRL)	High TRL. Proven in various space missions. But not for power transmission.	High TRL. Used in various space missions. But not for power transmission.	Moderate TRL. Gaining acceptance in space applications [26].

Excellent = 4	Good = 3	Medium = 1	Low = 0

Table 4.8: Trade-off matrix for laser types in a SBSP system.

The results of the sensitivity analysis have been plotted in Figure 4.8. It can be stated that the Fiber Lasers and the Diode Solid-State Lasers are competing for first place. In some scenarios, the Diode Solid-State Lasers are performing better than the Fiber Lasers such as in Scenario C where cost is more important and efficiency and reliability are reduced. The Flashlamp Solid-State Lasers option stays the least favourable option throughout the sensitivity analysis. Despite being the best solution in some scenarios, the Diode Solid-State Laser option is not the most suitable option as the Fiber Laser is on average a more suitable option as this option scores on average higher than the Diode Solid-State Lasers.

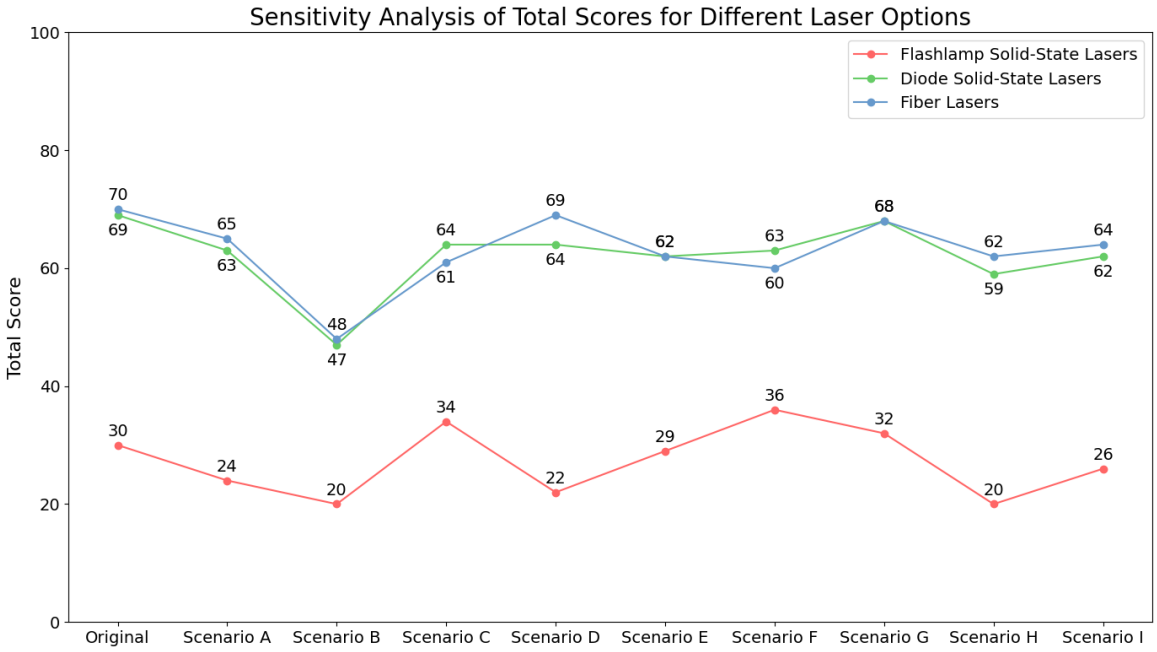

Figure 4.8: The results of each scenario in the sensitivity analysis for the Laser Power Transmission trade-off.

4.2.3. COTS Laser Power Transmission System Trade-off

The second trade-off will build on the result of the high-level LPT trade-off and covers the use of COTS for the LPT system. Hence, three types of fiber lasers have been listed to participate in the trade-off analysis.

- **Raytheon HEL6 Fiber Laser:** A high-power fiber laser system capable of delivering 15 kW up to 50 kW of output power [72]. Known for its robust design, the HEL6 is optimized for defensive military operations but lacks publicly available performance data such as efficiency. Included in the design is a 70 kg beam director capable of of rotating at a maximum slew rate of 3 rad/s. The HEL6 design could face potential challenges in environmental adaptability due to its robust design for operations on Earth. But still, the HEL6 laser system could act as a foundation for further development of a scaled down, space-based HEL6 system.
- **Raycus 3000W Global-Series CW Fiber Laser:** A compact and efficient fiber laser with a nominal output power of 3 kW. It offers moderate efficiency of 30% and is noted for its small size and low weight [71]. However, its environmental adaptability is limited due to its reliance on a stock water cooling system and narrow operating temperature range of 10-40°C. A separate beam director should be incorporated to accurately point the beam.
- **Combined Lower Power Lasers:** A system that integrates multiple lower-power lasers to achieve the desired output of around 3 kW. This approach offers high efficiency and flexibility in scaling but can lead to increased complexity in beam quality management and integration, as well as potential bulkiness due to the number of lasers used. This option also needs an additional beam director to accurately steer the beam. Furthermore, this option would require additional design steps to converge to a functioning LPT system.

In Table 4.9, the set of criteria is depicted which will be used to evaluate the performance of the three COTS laser options. The main focus is put on the overall efficiency of the laser, mass and volume efficiency and its potential to scale to output larger quantities of power. The ”Cost” criterion is not included in this trade-off, as it is very challenging to estimate the cost of these systems. This is particularly true for the Raytheon laser, which is a proprietary product of a private company, and for the combined lower-power lasers, as this solution represents a conceptual estimation rather than a commercially available system. Furthermore, both solutions will need to be converted to a space-graded product which is not reflected in the cost for terrestrial use.

Criteria	Rationale	Weight
Efficiency	Essential for minimizing power consumption and heat dissipation.	5
Power Output	Directly affects the capability to meet the 3 kW power transmission requirement.	4
Operational Reliability	Ensures that the laser system can function consistently and effectively over long periods in the harsh space environment.	4
Mass and Volume	Critical for adhering to launch constraints.	5
Environmental Adaptability	Determines how well the system can handle extreme temperature fluctuations and space conditions, crucial for reliable space operations.	3
Integration Complexity	Influences the ease of integrating the laser system with other subsystems.	2
Thermal Management Complexity	Affects how easily the system can manage and dissipate heat.	3
Beam Quality and Control	Ensures that the transmitted beam meets the required precision and coherence for effective power transmission and operational accuracy.	4
Radiation Hardness	Assesses the ability to withstand the radiation in space.	3
Scalability	Reflects how easily the system can be expanded or adjusted to meet varying power requirements or mission needs.	4

Table 4.9: Trade-off criteria for the laser subsystem with corresponding rationale and weight.

The trade-off analysis for the COTS laser systems has identified the *Combined Lower Power Lasers* option as the optimal choice, with the *Raytheon HEL6 Fiber Laser* following in second place. The decision to choose the set of low power lasers is based on several factors. When the laser system consists of bundles of lasers, it enhances the system reliability through inherent redundancy. Multiple low power laser units can provide a safety net. If one laser unit fails, other can continue to operate. This feature mitigates the laser system becoming a ”Single-Point-of-Failure”.

Moreover, this system can be designed to handle extreme environments and radiation exposure experienced in lunar orbit. Unlike COTS components such as the HEL6 laser and the Raycus laser, which have not been designed to operate under these conditions, the combined set of low power lasers can be assumed to incorporate robust features that enhance their performance and durability in such demanding environments.

However, in practice, space agencies are likely to contract established aerospace companies, like Raytheon, for the development of the laser system. The main advantage of this approach is that Raytheon can leverage their existing terrestrial systems, like the HEL6 laser, as a foundation for the space-based laser. They can redesign it to meet the strict requirements to operate reliably in the harsh environment of space. Therefore, another possible solution is to select the HEL6 laser and clearly state the assumptions made about the missing performance characteristics. This could allow for a balance between proven technology and addressing the unique challenges of the space environment.

Nevertheless, the *Combined Lower Power Laser* option is selected and will be implemented in the SBSP design because it offers more opportunities to design for redundancy. This will require a design based on conceptual ideas and will be further elaborated in Chapter 5. To validate the results of the trade-off, a sensitivity analysis has been conducted which resulted in Figure 4.9. In the plot, the combination of low power lasers is the superior option for every scenario, validating the results of the trade-off analysis.

Laser Type / Criteria	**Raytheon HEL6 Fiber Laser**	**Raycus 3000W Global-Series CW Fiber Laser**	**Combined Lower Power Lasers**
Efficiency	Efficiency data not available, but likely moderate (∼30%).	Moderate efficiency (30%) based on commercial specs [71].	High efficiency (30-50%) depending on selected lasers.
Power Output	A 15 kW laser and a 50 kW laser [72].	Nominal output power 3 kW [71].	Achieves 3 kW by combining multiple lasers.
Operational Reliability	Unclear reliability in harsh environments. Likely not able to handle lunar environment.	Limited by mild temperature ranges. Incorporates a water cooling system.	High reliability due to redundancy and multiple units.
Mass and Volume	Laser module, beam director and laser power module weigh a combined 530 kg [72]. Combined volume of 1 m^3.	Compact dimensions (485×172×727 mm) with weight <55 kg. Does not include beam director.	Varies with the number of combined lasers; can be bulky. Does not include beam director.
Environmental Adaptability	Not designed with lightweight materials in mind. Might malfunction due to temperature fluctuations.	Low adaptability. Narrow temperature range. Stock water cooling does not function in space.	Moderate to high adaptability. Lasers can be selected based on characteristics.
Integration Complexity	Moderate due to absence relevant data. System itself seems robust and adaptable.	Very complex to integrate because it comes with a stock water cooling system.	Moderately high complexity (more components, complex integration).
Thermal Management Complexity	Moderate complexity. Lack of detailed thermal management data. Likely requires some integration effort.	High complexity with integrated water cooling. Operating temperature range of 10-40°C.	Low to moderate complexity. Scalable cooling can be customized for each laser unit.
Beam Quality and Control	Most likely very good but little data known about beam accuracy except slew rate.	Beam quality of 1.5∼2 (mm x mrad) [71]. Separate beam director required.	Maintaining a coherent beam with combined low power lasers can be challenging.
Radiation Hardness	Unclear radiation tolerance; likely moderate based on standard military-grade components.	Very likely to have low radiation resistance due to COTS design for Earth practices.	Moderate to high. Depends on selected lasers and corresponding space performance.
Scalability	Great scalability due to higher power laser systems.	Good scalability by adding multiple laser units.	Highly scalable by adding or reducing the number of lasers.

Excellent = 4	Good = 3	Medium = 1	Low = 0

Table 4.10: Trade-off matrix for different fiber laser types for a space-based laser power transmission system.

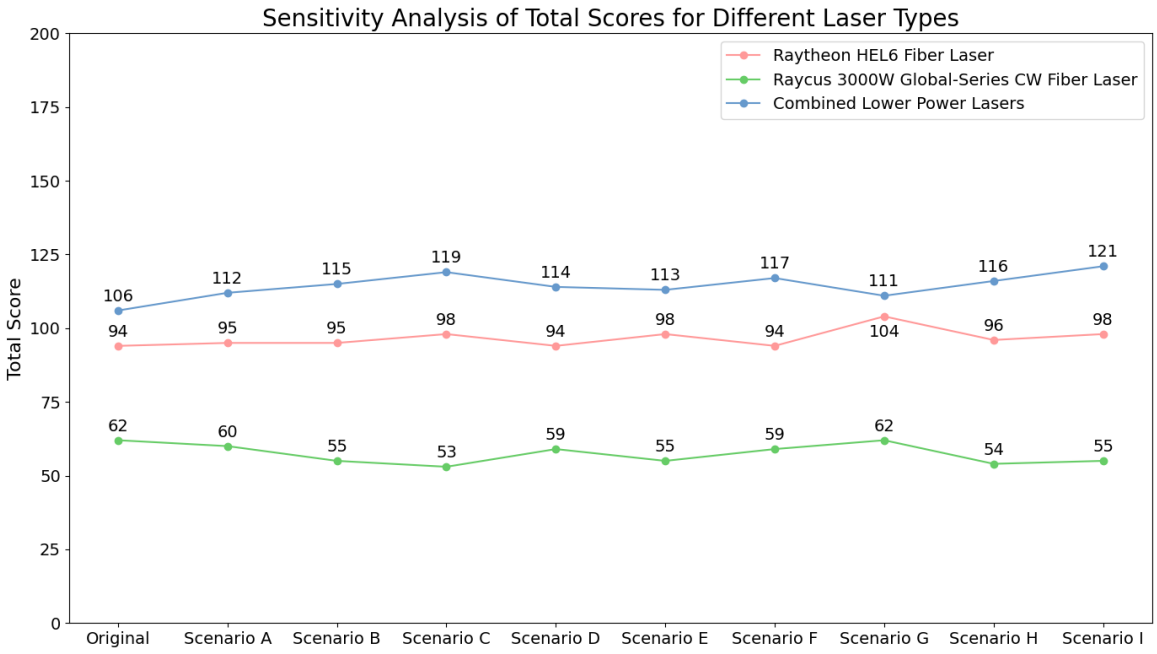

Figure 4.9: The results of each scenario in the sensitivity analysis for the Laser COTS trade-off.

4.3. Power Management and Distribution System Trade-Off

The Power Management and Distribution (PMAD) subsystem is a vital part of the SBSP system. It ensure the conditioning, control and distribution of the electrical power throughout the satellite. This section discusses the trade-offs associated with the various components of the PMAD subsystem. As the SBSP mission goal is to transmit power via a laser to a lunar receiver, the PMAD subsystem is what integrates the power-demanding subsystem, such as the laser and solar arrays, together. Moreover, it must also supply the other onboard subsystems.

4.3.1. Power Management and Distribution System Objectives

The objectives of the PMAD subsystem provide a framework to evaluate the system performance and effectiveness. In total, five objectives have been identified in Table 4.11 and each function is essential which the PMAD must fulfill to ensure reliable power management and distribution.

ID	Objective
PMAD-01	The PMAD system should provide stable and reliable energy storage to support operations during eclipse periods.
PMAD-02	The PMAD system should manage power distribution effectively to ensure all subsystems receive the necessary voltage and current.
PMAD-03	The PMAD system should incorporate redundancy to enhance reliability and fault tolerance in power management.
PMAD-04	The PMAD system should maintain optimal thermal performance to prevent overheating of components.
PMAD-05	The PMAD system should enable monitoring and control of power flow to maximize efficiency and adapt to changing operational conditions.

Table 4.11: PMAD system objectives with a corresponding ID.

4.3.2. General PMAD Architecture

The first step is to create good overview of a typical PMAD subsystem. In Figure 4.10, a typical PMAD architecture is depicted with their corresponding efficiencies [109]. This high-end overview of the PMAD architecture accurately represents PMAD systems onboard of conventional satellites. However, the SBSP is not a conventional satellite; its power consumption will significantly exceed the typical few kilowatts seen in most satellites. Its consumption profile aligns more with the International Space Station than with any other modern satellite, especially when considering future scalability plans.

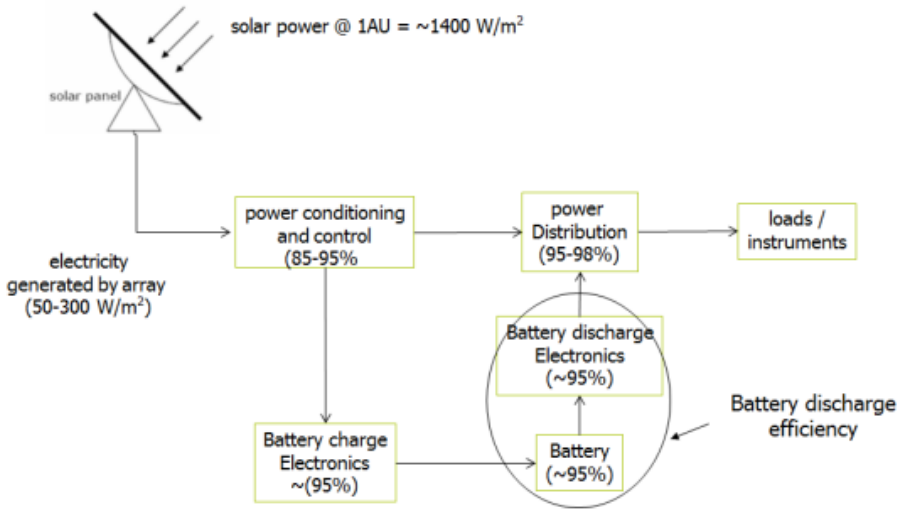

Figure 4.10: Example of the PMAD system architecture [109].

Hence, evaluating the PMAD subsystem of the ISS would offer valuable information regarding the SBSP PMAD design. It more accurately serves as a practical reference for managing substantial power demands in space. Although the equipment onboard the ISS might not be the most modern technology, it has been reliably proven in-flight. Therefore, this PMAD architecture will act as a foundation for the SBSP system. From there, a more tailored solution will be designed. In Figure 4.11, the PMAD system of the ISS is depicted.

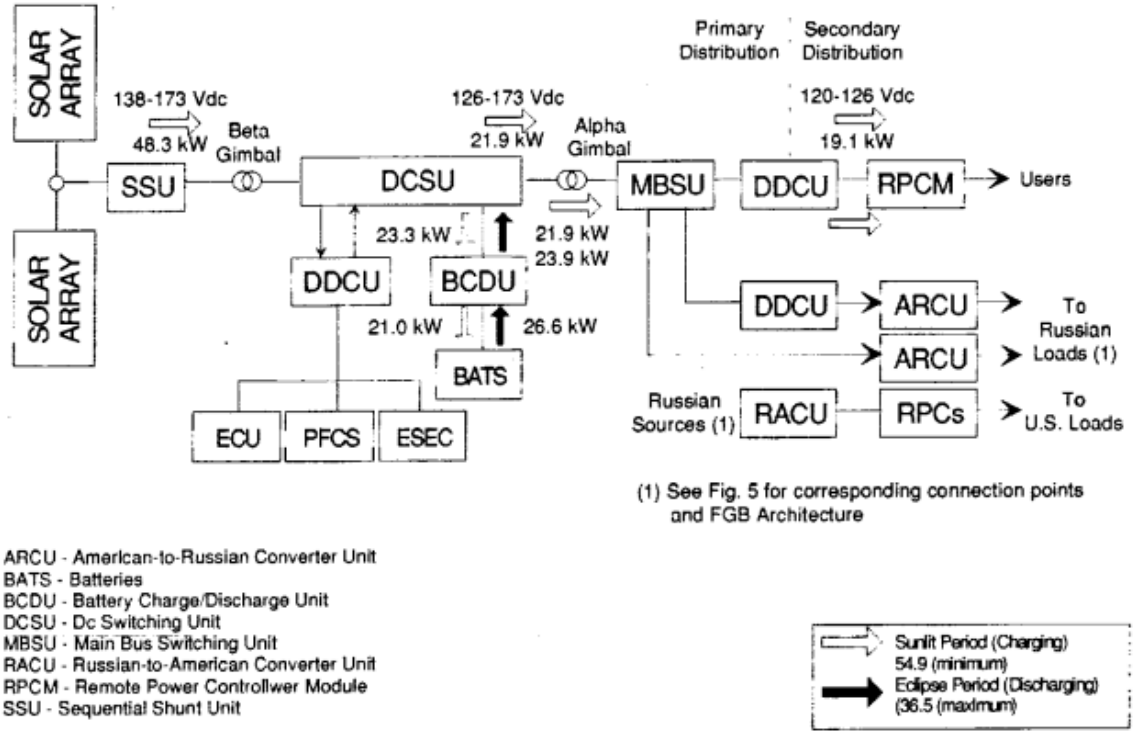

Figure 4.11: The Single-Channel Power Flow Diagram of the ISS [35].

From the ISS architecture, it can be observed that a ”Primary Power System” and a ”Secondary Power System” is used onboard. The Primary Power System is used for power generation, storage and distribution at a voltage range of 137 to 173 volts direct current (Vdc). The Secondary Power System operates at 123 to 126 Vdc and is used to supply power to user loads [20]. For the SBSP design, the system can be divided into two categories; the power supply to the laser and the power supply to the rest of the subsystems. This method could potentially utilize the same configuration as the ISS, using two DC-current (as most subsystems are compatible with DC-current) power channels. To further understand the power flow of the ISS, each relevant component will be elaborated below.

- **Sequential Shunt Unit (SSU):** The primary power regulation device controlling the photovoltaic output. Output is by design a consistent source of 160 Vdc based upon a programmable setpoint. During orbit, the output voltage often times is greater than the ISS demands. By shunting and un-shunting solar array strings, the SSU is capable of maintaining a consistent output voltage.
- **Direct Current Switching Unit (DCSU):** Main purpose of the DCSU is routing power between the solar arrays, batteries and downstream MBSUs and DDCUs. Also provides fault protection. DCSU holds a mass of 108 kg [20].
- **Battery Charge Discharge Unit (BCDU):** The BCDU is managing the charge and discharge of each battery. Each unit onboard of the ISS weights 106.6 kg and can charge 8.4 kW and discharge 6.6 kW [20].
- **Main Bus Switching Unit (MBSU):** The MBSU distributes primary power from the power channels downstream towards the DDCUs and other loads. Output voltage from 133 to 177 Vdc. One unit weighs 99.8 kg (220 pounds) [20].

- **Direct Current to Direct Current Converter Unit (DDCU):** The DDCU is responsible for DC power conversion, in this case primary power into secondary power. The secondary power has a voltage of 124.5 Vdc $\pm$1.5 Vdc. The primary power usually is 160 Vdc. Three versions exist of the DDCU; DDCU-E (external), DDCU-I (internal) and DDCU-HP (heatpipe version). For the SBSP system, the external DDCU-E could be implemented. This unit weighs 58.5 kg [20].

In Figure 4.11, the initial total power generated in one power channel is 48.3 kW. On the other hand, the SBSP system would need to generate approximately 10 kW for a 30% efficient laser system. For the sake of this example, let us assume the other subsystems consume at a maximum 5 kW. Assuming the power is distributed over two separate channels in the SBPS system, a total power of 7.5 kW would need to be managed and distributed, which is only 15% of one power channel onboard of the ISS. Despite the significant difference in scale, this type of architecture holds great potential for the SBSP system. To make this architecture feasible, a set of assumptions regarding the PMAD components must be established to justify it:

- **Assumption 1:** The mass of the components scale linearly with the percentage of power that passes through them, with the ISS performance being 100%. The batteries in the PMAD subsystem will be sized differently, elaborated in Section 5.3.1.
- **Assumption 2:** Using the density of a component, the new volume can be computed using the new mass of said component.
- **Assumption 3:** The efficiency characteristics of each component are assumed to be constant.

Using these assumptions, a PMAD architecture specifically for this SBSP design can be established.

4.3.3. PMAD Architecture in the SBSP System

At this stage, the full SBSP system has not yet been finalized, as trade-offs for several key subsystems have not been conducted. However, based on the current understanding of the needs of a SBSP system, a general SBSP PMAD architecture can be proposed. The proposed PMAD architecture, shown in Figure 4.12, follows a redundant configuration designed to ensure continuous power to all onboard systems. The architecture consists of two parallel power flow channels, each equipped with a MegaFlex solar array and an SSU. The two parallel power flow channels ensure the redundancy in the power generation, such that the satellite is still able to function when one solar array malfunctions.

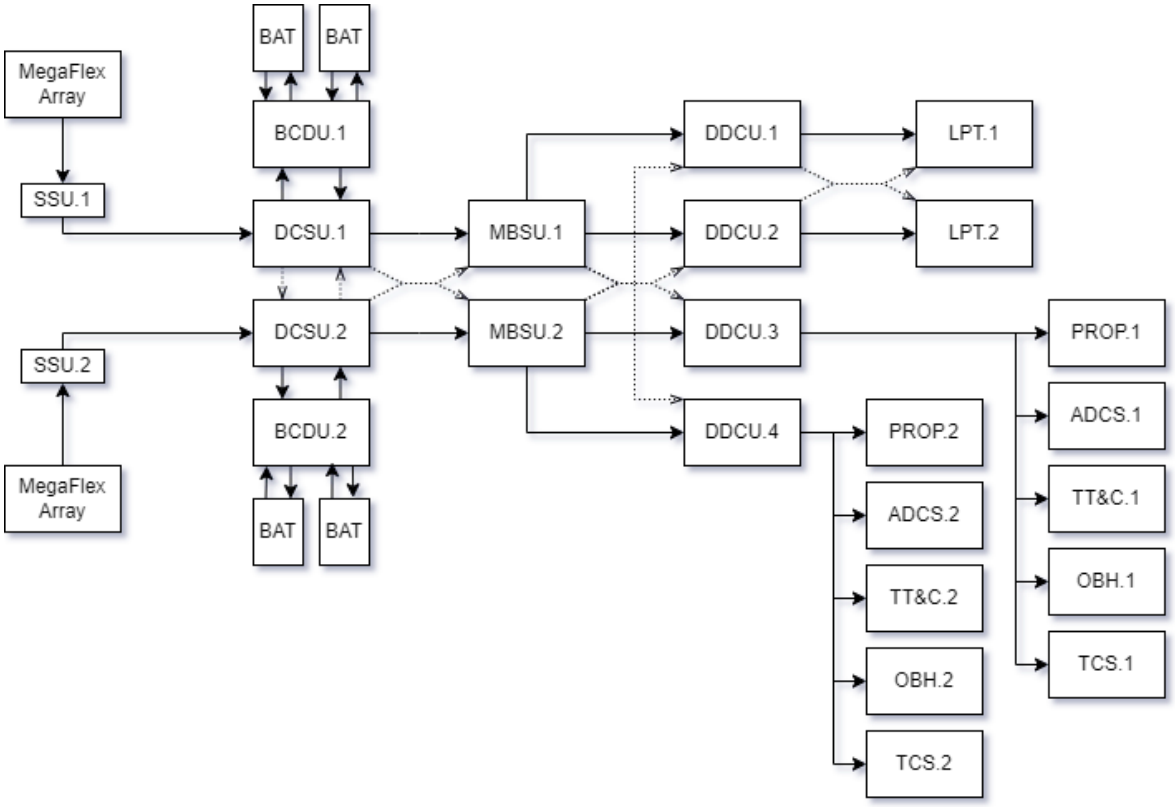

Figure 4.12: The PMAD Architecture of the full SBSP system.

The generated power is fed into the DCSUs, which routes the power towards the BCDUs and downstream to the MBSUs. The BCDUs manage the charge and discharge cycles of the batteries, storing power for when solar power is unavailable during lunar eclipse. At the heart of the PMAD system are two MBSUs, both responsible for the central management and power distribution across the spacecraft. Each MBSU routes power downstream towards several DDCUs which convert the bus voltage to the appropriate voltage levels required for each subsystem.

Redundancy has been integrated at various levels in the PMAD architecture to meet the high reliability requirements of the SBSP system. The two power flow channels add the first level of redundancy. Similarly, the dual MBSUs and BCDUs offer further resilience by preventing Single-Point-of-Failures within the primary power distribution chain. Moreover, the DDCUs have been arranged in pairs to provide fault isolation and failover support for the downstream subsystems. The dotted lines between the DCSUs, MBSUs and DDCUs represent cross-connections for load-sharing and redundancy. In the event of a component failure, the remaining component can reroute power, ensuring uninterrupted power distribution to the subsystems.

4.3.4. Battery Trade-off

Different batteries can be implemented in the SBSP system. The battery types that will be contesting are Nickel-Hydrogen (Ni-H2) and Lithium-Ion (Li-ion) batteries. These technologies will be evaluated using several performance criteria listed in Table 4.12. The criteria assess multiple factors such as energy density, cycle life and self-discharge rate, all of which affect the overall mission performance.

Criteria	Rationale	Weight
Energy Density	Determines the total energy storage capacity per unit mass.	5
Self-Discharge Rate	Affects how much power is lost during storage, influencing long-term energy availability.	3
Cycle Life	Assesses how many charge-discharge cycles the battery can withstand.	5
Storage Life	Defines the periods of inactivity without significant degradation, which is important for mission planning and delays.	4
Overcharge Tolerance	Determines the ability of the battery to handle overcharging, which could lead to damage during charging cycles and improving safety.	3
Total Energy Storage	Total energy storage of existing, proven in-flight batteries.	4

Table 4.12: Battery Trade-off Criteria with Corresponding Rationale and Weight

The trade-off analysis between Ni-H2 and Li-ion batteries, shown in Table 4.13, reveals the clear advantages of Li-ion technology for the lunar SBSP system. With a total score of 88 points, Li-ion batteries outperform Ni-H2, which scored only 64 points in total, in multiple key criteria. Specifically, in Energy Density, Self-Discharge Rate and Total Energy Storage it performs more optimal.

The higher energy density indicates that a Li-ion battery will be much more mass efficient than a Ni-H2 battery. Even more so when considering that Ni-H2 batteries have a significantly lower power density than Li-ion batteries. While Ni-H2 batteries outperform Li-ion batteries in terms of cycle life and proven reliability (implemented on the ISS), their lower energy density and higher self-discharge rate make the Li-ion battery a more suitable option. In conclusion, the Li-ion battery will be used as the power storage device onboard the SBSP system.

Battery Type / Criteria	**Nickel-Hydrogen (Ni-H2)**	**Lithium-Ion (Li-Ion)**
Energy Density	30 Wh/kg [1].	100-200 Wh/kg [1].
Self-Discharge Rate	7% per day [1].	<0.05% per day [1].
Cycle Life	60,000-75,000 cycles [1].	58,000 cycles [1].
Storage Life	4 years [1].	6 years [1].
Overcharge Tolerance	Controlled by 2 Fault-Tolerant design [1].	Controlled by design [1].
Total Energy Storage	8 kW-hr (Two ORUs) [1].	15 kW-hr (One ORU) [1].

Excellent = 4	Good = 3	Medium = 1	Low = 0

Table 4.13: Trade-off analysis for Nickel-Hydrogen and Lithium-Ion batteries.

4.4. Thermal Control System Trade-off

The Thermal Control System (TCS) is a critical subsystem in the SBSP design, and is assigned with the task to ensure that all systems onboard operate within their required temperature ranges. The TCS is of paramount importance for maintaining the performance and longevity of space-based systems, especially when dealing with high-power subsystems such as lasers. Besides lasers, the generated heat of the other subsystems in the SBSP system must also be managed to ensure optimal performance. This section explores the key objectives for the TCS where after various trade-off options are presented and analyzed.

4.4.1. Thermal Control System Objectives

The primary objectives of the Thermal Control System are listed in Table 4.14. In total, six objectives have been identified and set a foundation for the trade-off analysis.

ID	Objective
TCS-01	The TCS should efficiently dissipate all heat generated by the laser and other subsystems to maintain operational temperatures within safe limits.
TCS-02	The TCS should maintain stable operating temperatures across all spacecraft components, ensuring they remain within their specified thermal operational ranges.
TCS-03	The TCS should be designed to minimize mass and volume, optimizing the spacecraft's overall efficiency and cost-effectiveness.
TCS-04	The TCS should minimize thermal gradients across the spacecraft to avoid structural stresses and potential misalignment of sensitive instruments.
TCS-05	The TCS should incorporate redundancy in critical components to ensure continuous operation in the event of a failure.
TCS-06	The TCS should be capable of sustaining long-term operation throughout the mission duration, with minimal degradation in performance.

Table 4.14: Thermal Control System objectives with a corresponding ID.

4.4.2. Heat Transportation Thermal Control System Trade-off

The TCS is a complex subsystem within spacecrafts as it encompasses a range of components and technologies to manage heat effectively. The TCS typically comprises three main components:

- **Heat Collection:** These components capture the heat from numerous spacecraft components. Usually, this entails heat sinks, cold plates and other mechanisms to absorb the heat from sources within the spacecraft.
- **Heat Transportation:** Components that ensure that the absorbed heat is transported from the collection point to the radiators for rejection into space.
- **Heat Rejection:** The last step involves dissipating heat into space through radiators that are often designed to be deployable to be as volume efficient as possible.

Among these components, the heat transportation method is particularly critical. This method directly influences the overall performance of the TCS. It is assumed that heat collection will be done via heat sinks and the heat rejection via a set of deployable radiators. Given its central role in the TCS, a range of options for heat transportation are considered in the trade-off, each with its own advantages and disadvantages. The primary heat transportation options are as follows:

- **Loop Heat Pipes (LHPs):** LHPs are advanced thermal management devices utilizing a closed-loop system to transfer heat from an evaporator to a condenser. Its functionality relies on the phase change of the working fluid and capillary action to circulate the fluid and transfer heat efficiently. Considered a passive system and has a high reliability due to the absence of moving parts. Uses a sintered powder metallic wick with pore sizes on the order of 1 μm [24]. As of now, LHPs can transfer 10 kW of heat [85].

- **Active Fluid Loops with Pumps:** This method employs a closed-loop system with mechanical pumps to circulate a coolant such as ammonia through heat exchangers, transporting heat from the collection point to the radiators. This allows for design flexibility and can be adapted to various mission profiles. Easier to design and integrated compared to LHPs and can accommodate a range of heat loads. On the ISS, an Active Thermal Control System (ATCS) is installed and can handle thermal loads up to 70 kW [19].
- **Capillary Pumped Loops (CPLs):** CPLs also employ a capillary action to transport heat without mechanical pumps. It involves the same principle as LHPs but instead uses a polyethylene wick with pore sizes on the order of 15 μm [24].

These three heat transportation options will be analyzed in a trade-off. To accurately assess the options, a set of criteria is derived based on the TCS objectives. The criteria are depicted in Table 4.15 with their corresponding weights.

Criteria	Rationale	Weight
Heat Transportation Capability	Measures the system's ability to transfer and reject heat efficiently, crucial for managing high thermal loads.	5
Power Consumption	Indicates the amount of power the system consumes, affecting overall energy usage and efficiency.	3
Mass and Volume	Critical for meeting launch constraints and ensuring that the system is space-efficient.	5
System Complexity	Reflects the ease or difficulty of integrating, operating, and maintaining the system. Lower complexity generally implies easier integration and operation.	4
Reliability	Assesses the system's ability to perform consistently under the harsh space environment and over extended periods.	4
Cost	Includes the development, manufacturing, and deployment costs, which impact the overall project budget.	3
Scalability	Determines the system's ability to handle increased heat loads or be adapted for different missions or scales.	4

Table 4.15: Trade-off criteria for the thermal control system with corresponding rationale and weight.

Table 4.16 contains the TCS trade-off matrix. The *Active Fluid Loops with Pumps* option has turned out to be the most suitable option, ending with a total score of 87 points. In second place is the *Loop Heat Pipes* option with 71 points. At last, is the *Capillary Pumped Loops* option with 57 points. The Active Fluid Loop option has shown better performance in its heat transportation capability and scalability compared to the other options while also performing relatively well for the other criteria. While the LHP option promises great performance for a passive system it might not suffice given the amount of heat the system has to transport. Combined with the system complexity and scalability, the LHP seemed not like the optimal solution for a SBSP system, where the TCS is considered a highly critical system.

TCS / Criteria	**Loop Heat Pipes (LHPs)**	**Active Fluid Loops with Pumps**	**Capillary Pumped Loops (CPLs)**
Heat Transportation Capability	Can handle high heat-loads. A few watts up to 10 kW (experimental) [85]. Effective for long-distance heat transfer.	High transfer capability. Depends on pump and pipe size. Up to 70 kW on the ISS [19].	No comparable heat transfer found for CPL. Assumed to be lower than maximum LHP heat transfer.
Power Consumption	Classified as passive system. Requires Starter Heater to initiate flow [24].	Relatively high power consumption due to mechanical pumps.	Classified as a passive system. Requires Starter Heater to initiate flow. Needs additional pre-heating [24].
Mass and Volume	Relatively compact and lightweight compared to their heat transfer capacity.	Can be heavier compared to LHPs due to mechanical pumps and fluid reservoirs.	Relatively compact and lightweight compared to their heat transfer capacity.
System Complexity	Startups often take several hours before flow circulation starts [24]. But no moving parts.	Moderate complexity due to pumps, valves and plumbing.	Startups often take several hours before flow circulation starts [24]. But no moving parts.
Reliability	High reliability, with no moving parts. Proven technology [85].	Lower reliability due to moving parts which can fail. Operating on the ISS [19].	High reliability, with no moving parts. But CPL design is complex. Fails if radiator cannot reject all heat.
Cost	High cost due to design and manufacturing complexity.	Moderate cost due to more robust design but more components.	High cost due to design and manufacturing complexity.
Scalability	Moderate scalability. Limitations on capillary action over very long distances.	Excellent scalability. Can be adjusted based on pump and pipe size. Up to 70 kW on ISS [19].	Moderate scalability. Limitations on capillary action over very long distances.

Excellent = 4	Good = 3	Medium = 1	Low = 0

Table 4.16: Trade-off analysis for different heat transportation systems in thermal control systems.

Next, a sensitivity analysis is done to assess the validity of the trade-off results. Hence, a set of weighting scenarios have been proposed below:

- **Original**: Baseline scenario with balanced emphasis across all criteria.
- **Scenario A**: Focus on heat transportation capability and power consumption for high energy efficiency.
- **Scenario B**: Prioritizes minimizing power consumption and system complexity to save resources.
- **Scenario C**: Emphasizes cost-effectiveness and compact design, ideal for limited budgets and space.
- **Scenario D**: A balance between reliability and scalability for long-term, robust systems.
- **Scenario E**: Low complexity and moderate reliability for a straightforward, maintainable design.
- **Scenario F**: Focuses on high reliability for critical missions where uptime is essential.
- **Scenario G**: Equal weighting across all criteria for a balanced, neutral approach.
- **Scenario H**: Emphasizes heat transportation capability and cost for an efficient, cost-conscious system.
- **Scenario I**: Focus on compact design and scalability, ideal for modular, expandable systems.

The scenarios are depicted in Figure 4.13. The results show that the *Active Fluid Loops with Pumps* option outperforms the other options in each scenario. Only in scenario A and B does it drop in points, closely to the LHP option. These scenarios penalize active thermal control systems, hence the drop in points. But nevertheless, the *Active Fluid Loops with Pumps* option has been chosen for the SBSP design based on the TCS trade-off analysis.

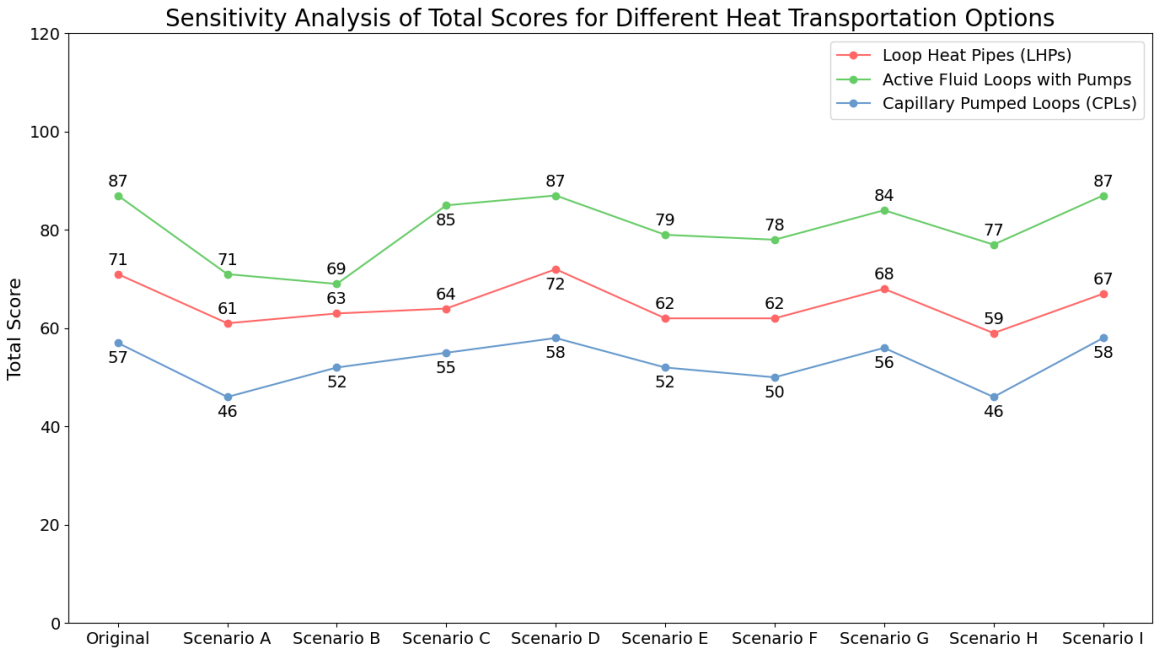

Figure 4.13: The results of each scenario in the sensitivity analysis for the Thermal Control System trade-off.

4.5. Attitude Determination and Control System Trade-off

The Attitude Determination and Control System (ADCS) plays an important role in guaranteeing that the satellite maintains its proper orientation throughout the mission. Specifically for a lunar SBSP system, it must ensure precise pointing for power transmission while also ensuring stability in the harsh lunar environment. The purpose of this trade-off analysis is to evaluate different ADCS configurations by comparing available options.

4.5.1. Attitude Determination and Control System Objectives

In Table 4.17, the key objectives for both the attitude determination and control systems have been presented. Here, the emphasize lies on precision, reliability, power consumption and mass and volume efficiency. These objective serve as a foundation for the following trade-offs.

ID	Objective
ADCS-01	The ADCS should accurately determine the spacecraft's orientation using on-board sensors.
ADCS-02	The ADCS should maintain spacecraft attitude stability, ensuring precise pointing for instruments and communication antennas.
ADCS-03	The ADCS should provide accurate attitude adjustments to accommodate mission needs, such as maneuvering or re-pointing.
ADCS-04	The ADCS should minimize fuel and power consumption during attitude maneuvers to extend the spacecraft's operational life.
ADCS-05	The ADCS should minimize both mass and volume to optimize spacecraft design and reduce launch costs.
ADCS-06	The ADCS should be capable of continuous operation throughout the mission, maintaining high precision and reliability.

Table 4.17: Attitude Determination and Control System objectives with corresponding ID.

The ADCS trade-off is structured into two major parts: the *Attitude Determination System* trade-off and the *Attitude Control System* trade-off. By adhering to this structure, both functions of the ADCS are thoroughly analyzed.

4.5.2. Attitude Determination System Trade-off

The Attitude Determination System (ADS) is responsible for accurately determining the orientation of the spacecraft during all phases of the mission. For a lunar SBSP system, this translates to ensuring precise attitude information to support accurate pointing and control. In the document provided by NASA, various ADS options are outlined [92]. These options will be analyzed in the ADS trade-off and are listed below with a brief description:

- **Star Tracker:** A high-precision sensor that registers images of star fields and compares them to an onboard catalog to determine the orientation of the spacecraft. Star Trackers are highly accurate but can be affected by bright celestial objects like the Sun, Earth or the Moon. A set of Hydra Star Trackers is displayed in Figure 4.14.
- **Sun Sensor:** A sensor that measures the angle between the spacecraft and the Sun, shown in Figure 4.15. It is popular for its accuracy and reliability and consumes little power. However, it can only operate when the Sun is visible, making it ineffective during eclipses.
- **Horizon Sensor:** A sensor typically used in Earth-orbiting spacecraft to determine attitude by detecting the Earth's horizon. It works by identifying the sharp contrast between the Earth's surface and the surrounding space, often via a contrast in IR spectrum. The Digital Earth Sensor by SITAEL is depicted in Figure 4.16.
- **Gyroscope:** An inertial measurement unit (IMU) that uses gyroscopes to determine the angular velocity of the spacecraft. It provides continuous attitude data but suffers from drift over time. Therefore it requires periodic corrections using external references. A Fiber Optic Gyroscope (FOG) sensor is shown in Figure 4.17.

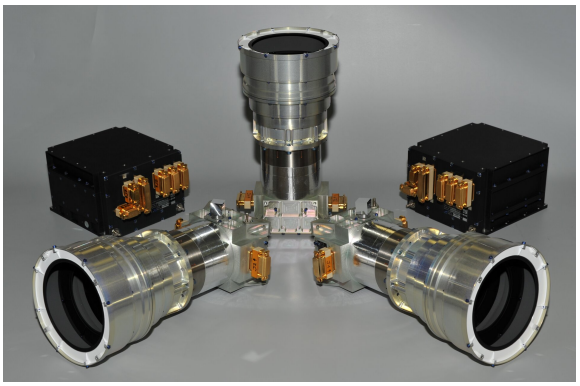

Figure 4.14: Hydra Star Tracker [32].

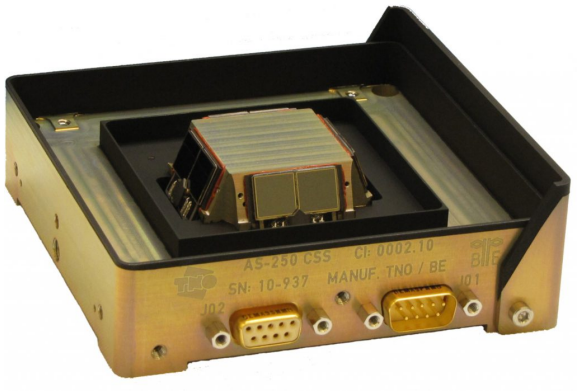

Figure 4.15: Coarse Sun Sensor [79].

Figure 4.16: Digital Earth Sensor [83].

Figure 4.17: 3-Axis Fiber Optic Gyroscope sensor [45].

A clear conclusion can already be drawn, which is that the Magnetometer sensor will not be effective in lunar orbit, as the Moon lacks a magnetic field for the sensor to detect and determine the attitude of the spacecraft. Alternatively, the other three sensory options show great potential for a lunar mission. Hence, four configurations using different sensor combinations are proposed for further evaluation in the ADS trade-off. The configurations are as follows:

- **Configuration A: 4 Coarse Sun Sensors, 2 Horizon Sensors and 2 3-axis FOGs.** This configuration combines four low complexity sun sensors and two horizon sensors with two highly accurate 3-axis FOGS. Emphasizes relative low cost and the relative low complexity of the sensors.
- **Configuration B: 2 Star Trackers and 2 3-axis FOGs.** This combination leverages the high accuracy of two Star Trackers for precise attitude determination and two highly accurate FOGs. This combination is more accurate compared to Config. B but will also be more costly. May lack redundancy for when the Star Trackers are exposed to sunlight.
- **Configuration C: 2 Star Trackers and 2 Coarse Sun Sensors.** This configuration employs two Star Trackers for accurate positioning and two Coarse Sun Sensors for quick attitude updates during sunlight exposure, though it may lack redundancy and robustness without FOG equipment.
- **Configuration D: 2 Star Trackers, 4 Coarse Sun Sensors and 2 3-axis FOGs.** This comprehensive configuration combines the strengths of two Star Trackers and two Coarse Sun Sensors with two 3-axis FOGs, providing high accuracy, fast responsiveness, and improved reliability for maintaining spacecraft attitude during lunar operations.

Each ADS configuration is assessed using a set of criteria depicted in Table 4.18. The focus of the ADS trade-off has been put on the Accuracy, Mass and the overall Redundancy of the ADS component. The reason being that these criteria affect the total performance of the SBSP system as well as the mass budget of the spacecraft.

Criteria	Rationale	Weight
Accuracy	The ability to precisely determine the attitude of the spacecraft, essential for achieving mission-specific pointing requirements.	5
Power Consumption	Reflects the energy demands of the sensors, impacting the power budget.	4
Mass	Evaluates the mass of each configuration, directly affecting the mass budget and potential launch costs.	4
Redundancy	Assesses the inclusion of backup components to ensure continuous system functionality in case of failures.	5
Environmental Constraints	Considers the system ability to function reliably under various space conditions.	4
Cost	Reflects the total cost of the sensor configuration, which affects the total cost of the spacecraft.	3

Table 4.18: Trade-off criteria for Attitude Determination Systems with corresponding rationale and weight.

The trade-off analysis has resulted in the trade-off matrix shown in Table 4.19. *Configuration D* emerged as the most suitable option for the ADS onboard the lunar SBSP system with a total score of 83 points. Primarily, due to its exceptional pointing accuracy and its high degree of redundancy and robustness. Including both the sun sensors and star trackers together with the robust FOGs provide a versatile combination of attitude determination methods. This will enhance the system reliability in the challenging lunar environment. In second place is *Configuration A* with 74 points, valued for its low power consumption, low mass and its low cost while still maintaining a reliable option with redundancy features. *Configuration B* has obtained third place with 62 points, providing an option using both star trackers and FOGs. However, this configuration lacks the robustness ann additional redundancy features provided by the by the low complexity sun sensors. At last, *Configuration C* showed the lowest potential, scoring 52 points, due to its lower redundancy. In fact, this configuration turned out to include insufficient redundancy measures for continuous and reliable 3-axis attitude determination.

In conclusion, Configuration D utilizing four Coarse Sun Sensors, two Star Trackers and two 3-axis Fiber Optic Gyroscopes (FOG) provides a well-rounded balance of sensor capabilities, redundancy and reliability. Sun sensors and star trackers provide complementary attitude determination methods, which mitigate the risk of sensor failure or inaccuracies in operational conditions. Additionally, the two FOGs are capable of maintaining accurate attitude determination during dynamic phases in the mission. This combination makes Configuration D more adaptable and robust which is highly desired for the SBSP system. The additional redundancy ensures even if one sensor type is temporarily compromised, the system can still maintain accurate attitude determination.

Configuration / Criteria	**Configuration A: 4 Coarse Sun Sensors, 2 Horizon Sensors and 2 FOGs**	**Configuration B: 2 Star Trackers and 2 FOGs**	**Configuration C: 2 Star Trackers and 2 Coarse Sun Sensors**	**Configuration D: 2 Star Trackers, 4 Coarse Sun Sensors and 2 FOGs**
Accuracy	Medium. Combines sun sensors and horizon sensors for quick updates with FOGs for precise measurements.	Excellent. Dual star trackers with additional FOGS ensure high accuracy for attitude determination.	Good. Star trackers provide high accuracy, but sun sensors are less accurate compared to FOGs.	Excellent. Combines multiple sensor types for optimal accuracy. Star Trackers and FOGs offer high accuracy.
Power Consumption	Sun sensor: 4x 0-3 W. Horizon sensor: 2x 2 W. 3-axis FOG: 2x 8 W (BOL) In total maximum 32 W.	Star Tracker: 2x 5-20 W. 3-axis FOG: 2x 8 W (BOL) In total maximum 56 W.	Sun sensor: 2x 0-3 W. Star Tracker: 2x 5-20 W. In total maximum 46 W.	Sun sensor: 4x 0-3 W. Star Tracker: 2x 5-20 W. 3-axis FOG: 2x 8 W (BOL). In total maximum 68 W.
Mass	Sun sensor: 4x 0.1-2 kg. Horizon sensor: 2x 0.4 kg. 3-axis FOG: 2x 1.4 kg. In total maximum 11.6 kg.	Star Tracker: 2x 2-5 kg. 3-axis FOG: 2x 1.4 kg. In total maximum 12.8 kg.	Sun sensor: 2x 0.1-2 kg. Star Tracker: 2x 2-5 kg. In total maximum 14 kg.	Sun sensor: 4x 0.1-2 kg. Star Tracker: 2x 2-5 kg. 3-axis FOG: 2x 1.4 kg. In total maximum 20.8 kg.
Redundancy	Sun sensors and Horzion sensors provide redundancy while FOGs. add additional robustness.	Star trackers are the only type which rely on external reference data. FOGs might not provide enough redundancy.	This configuration lacks redundancy. Sun sensors are not enough for 3-axis attitude determination.	Includes multiple sensors for robust performance and enhanced reliability.
Environmental Constraints	Sun sensors need direct sunlight. Horizon sensors can be disturbed by the Sun or Earth.	Star trackers may be affected by bright celestial bodies such as the Sun, Earth or the Moon.	Combination of config. A and B. Both sensors operate while other sensor is ineffective.	Similar to config. C but FOGs help mitigate environmental constraints.
Cost	Moderate cost. Three different sensors offer balanced cost.	Moderate cost. Star trackers and FOGs drive up costs significantly.	Moderate cost. Star trackers and sun sensors offer a balanced total cost.	High cost. Comprehensive configuration increases costs but reflects in enhanced performance.

Excellent = 4	Good = 3	Medium = 1	Low = 0

Table 4.19: Trade-off analysis for ADS configurations.

In this case, a sensitivity analysis has been performed and the results are shown in Figure 4.18. Except for scenario C, Configuration D outperforms all other configurations in every weighting scenario. Scenario C, where the focus is on minimizing mass and cost, Configuration A actually performs better than Configuration D due to its lower sensor cost and reduced mass. However, this scenario does not prioritize high accuracy sensors which is desired in this lunar SBSP demonstration mission. While Configuration A may be more efficient in terms of mass and cost, it lacks the accuracy necessary for mission-critical operations. Therefore, Configuration D remains the best choice overall, offering the required accuracy, reliability and redundancy to ensure mission success.

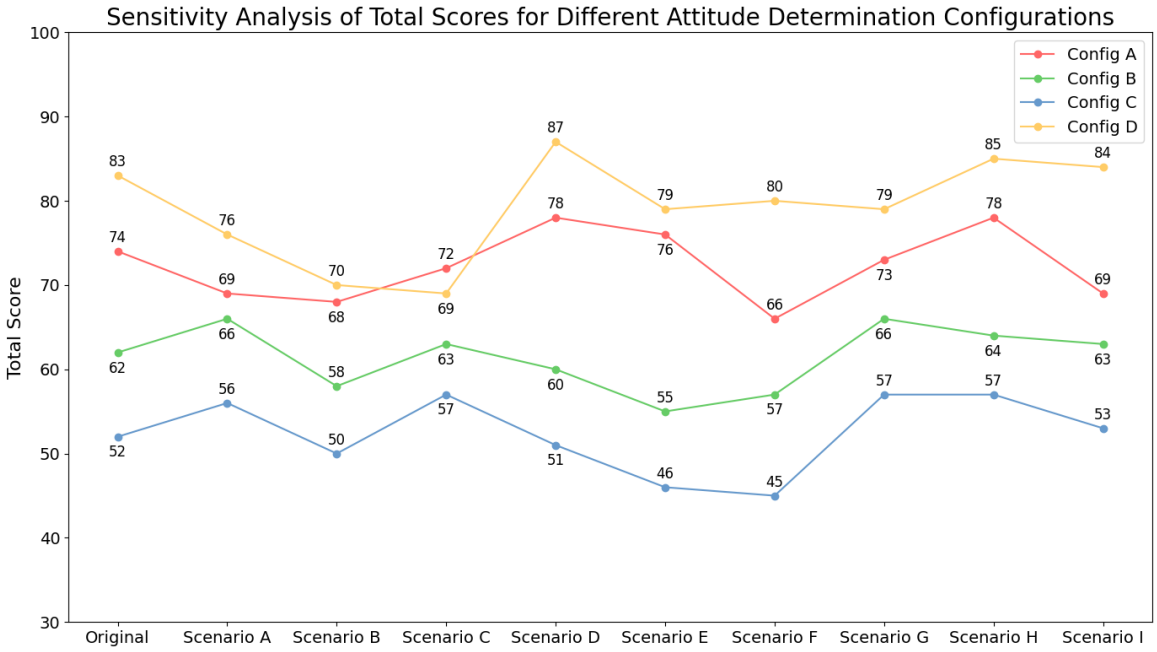

Figure 4.18: The results of each scenario in the sensitivity analysis for the Attitude Determination Configuration trade-off.

4.5.3. Attitude Control System Trade-off

The Attitude Control System (ACS) is operated with the purpose of maintaining the orientation of the spacecraft during all phases of the mission. For a SBSP lunar demonstration mission, this translates into maintaining precise control of the spacecraft to ensure optimal pointing accuracy while operating in a challenging lunar environment. In the document provided by NASA, numerous ACS options have been provided [92]. These options will be analyzed in the trade-off and are listed below with a short description:

- **Reaction Wheels:** Reaction wheels are rotating devices and are mounted on orthogonal axes. By varying the speed of the wheels, the spacecraft can rotate in the opposite direction due to the conservation of angular momentum. Provide smooth and precise control for small to medium attitude adjustments which makes it ideal for fine pointing. Reaction wheels are commonly deployed in long-duration missions. However, reaction wheels require periodic momentum dumping when they saturate due to the buildup of angular momentum. A visualization is presented in Figure 4.19.
- **Control Moment Gyroscopes (CMGs):** CMGs are gimbaled spinning wheels capable of providing large torques by tilting the axis of the spinning wheel to change the orientation of the spacecraft. Compared to reaction wheels, they can generate significantly more torque which makes them ideal for fast, agile maneuvers. However, this comes with several disadvantages. CMGs are mechanically complex, consume more power, and have a shorter lifespan due to mechanical stress on their gimbals. A CMG system is shown in Figure 4.20.
- **Thrusters:** Thrusters expel mass to generate a reaction force that changes the spacecraft's attitude. They provide high torque and responsiveness, making them suitable for large maneuvers or rapid attitude changes. A disadvantage of thrusters is that they consume propellant, limiting their long-term use. They are best for short-duration, high-torque needs such as orbit insertion, major re-orientations, or momentum dumping. A bipropellant thruster is shown in Figure 4.21.

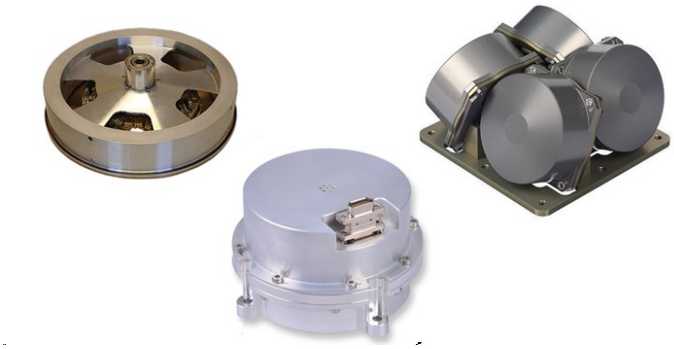

Figure 4.19: Reaction Wheels [78].

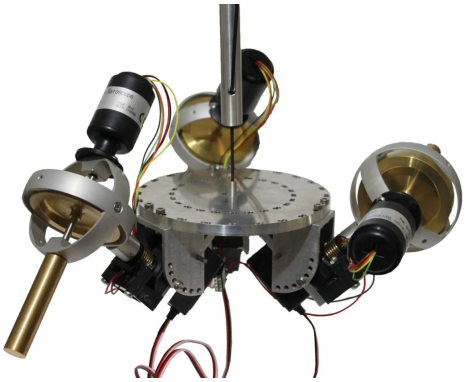

Figure 4.20: Control Moment Gyroscopes (CMGs) [39].

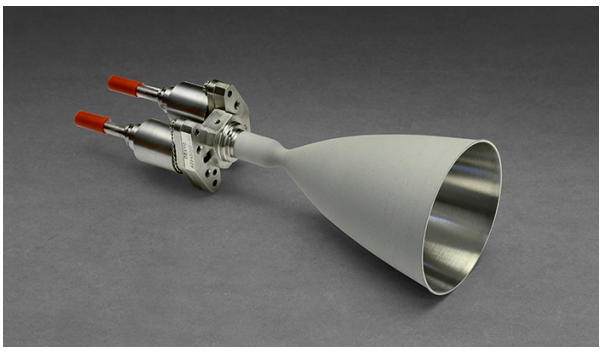

Figure 4.21: Europa Bipropellant Thruster [94].

In order to assess each ACS option thoroughly, a set of criteria has been determined and is depicted in Table 4.20. The Control Capability, Mass and Reliability are deemed as most critical criteria as they directly influence the pointing accuracy performance as well as the mass and power budgets of the overall SBSP system.

Criteria	Rationale	Weight
Control Capability	Measures the ability to provide precise and sufficient torque for spacecraft attitude control.	5
Power Consumption	Reflects the amount of power consumed by the system, impacting the power budget of the spacecraft.	4
Mass	Reflects the weight of the system which affects the overall spacecraft mass budget and launch costs.	5
Slew Rate	Assesses its ability to achieve rapid reorientation maneuvers, which might be desired for missions requiring agile spacecraft.	3
Environmental Constraints	Considers the ability to function reliably in different space environments (e.g., momentum dumping, lack of magnetic field).	4
Reliability	Reflects the ability to perform consistently over the mission duration without failure.	5
Cost	Encompasses the total costs of the Attitude Control component, impacting the overall mission budget.	3

Table 4.20: Trade-off criteria for Attitude Control Systems with corresponding rationale and weight.

The trade-off analysis has resulted in the trade-off matrix shown in Table 4.21. The *Reaction Wheels* option has turned out to be the most suitable option for the ACS onboard the SBSP system with a total score of 97 points. The primary reasons being its high pointing accuracy as well as its reliability. Second in line is the *Control Moment Gyros* options with 89 points. The *Thrusters* options is in third place with 84 points. The thrust levels provided for the thrusters are included because these systems are inherently required to offload angular momentum from the reaction wheels or CMGs. While the comparison between torque and thrust levels might not be direct, the thrusters play a critical role in maintaining the long-term attitude stability of the spacecraft by compensating for momentum buildup. Their capability to provide control over a wider range of magnitudes, including precise adjustments and large-scale corrections, complements the other systems rather than replacing them.

It should be noted that the paper by NASA states that the *Zero Momentum* ACS method is described as the most accurate and precise method [92]. This feature is considered highly critical in the SBSP design for ensuring highly accurate laser beam pointing performance. Using three reaction wheels, it can achieve a typical accuracy of $\pm 0.0001°$ to $\pm 1°$, depending on its sensors and processors. A limitation for this method is the lifetime of the dedicated sensors as well as the wheel bearings of the reaction wheels. Furthermore, it is concluded that additional thrusters should be included in the design used for slewing and momentum dumping. But a limitation for this action is the propellant usage which can be high. Hence, the *Zero Momentum* ACS method has been chosen for the SBSP system design utilizing four reaction wheels (one extra for redundancy) and two thruster loops, each comprising of four thrusters (one for redundancy) leading to a combined total of eight thrusters.

Attitude Control / Criteria	**Reaction Wheels**	**Control Moment Gyros (CMGs)**	**Thrusters**
Control Capability	Max. torques of 0.01 to 1 Nm. ±0.0001° to ±1°.	Max. torques of 25 to 500 Nm. ±0.001° to ±1°.	Hot Gas: 0.5 to 9000 N. Cold Gas: <5 N. ±0.1° to 5°.
Power Consumption	Varies with speed: 10 to 100 W.	90 to 150 W.	Depends on specific thruster.
Mass	2 to 20 kg.	>10 kg.	Depends on specific thruster. Requires propellant mass.
Slew Rate	Slew rates from 0.05 deg/s (LEO orbital rate) to 0.5 deg/s.	High slew rate from 0.05 deg/s to >0.5 deg/s.	High slew rate from 0.05 deg/s to >0.5 deg/s.
Environmental Constraints	Functions well in space. Will require periodic momentum dumping when they saturate.	Perform well in lunar environment. Periodic momentum dumping required.	None. Thrusters operate well in the vacuum of space.
Reliability	Very reliable. Wear over time can reduce reliability. Reported lifetime of 10-15 years [63].	More complex which affects its reliability. Recorded lifetime of 10 years [81].	Generally reliable but its lifespan is limited by amount of available propellant.
Cost	Medium to high cost. Increase with need for redundant wheels.	Among the most expensive options due to complexity and high-performance.	Medium to high cost. Depends on propulsion type. Chemical or electric propulsion.

Excellent = 4	Good = 3	Medium = 1	Low = 0

Table 4.21: Trade-off analysis for different Attitude Control systems.

The results of the ACS trade-off have to be justified by performing a sensitivity analysis. Again, a set of scenarios has been generated where each scenario highlights different criteria. The scenario's have been listed below:

- **Original**: Baseline scenario with balanced emphasis across all criteria, ensuring a well-rounded evaluation.
- **Scenario A**: Focus on control capability and power consumption to optimize performance while minimizing energy use.
- **Scenario B**: Prioritizes power consumption and slew rate, aiming for energy efficiency and faster reorientations.
- **Scenario C**: Emphasizes cost-effectiveness and low mass, making it ideal for budget-conscious and lightweight systems.
- **Scenario D**: A balance between reliability and environmental constraints, ensuring robustness in harsh environments.
- **Scenario E**: Focus on low complexity and moderate reliability for a straightforward, easily maintainable system.
- **Scenario F**: Prioritizes high reliability for critical missions where system uptime and durability are essential.
- **Scenario G**: Equal weighting across all criteria for a neutral, balanced approach in system evaluation.
- **Scenario H**: Emphasizes control capability and reliability, ideal for missions requiring precise control and system longevity.
- **Scenario I**: Focus on high control capability and environmental constraints, ensuring system adaptability in challenging conditions.

Observing and analyzing the results in Figure 4.22, it becomes evident that the *Reaction Wheels* option indeed is the superior option regarding the ACS for the SBSP system. The CMG option and the *Thruster* option alternate in their total points in the sensitivity analysis but realistically these two systems cannot be compared as the thrusters complement the other two options . But the overall results from the ACS sensitivity analysis justify the decision for the *Zero Momentum* method using four reaction wheels and additional thrusters for momentum dumping.

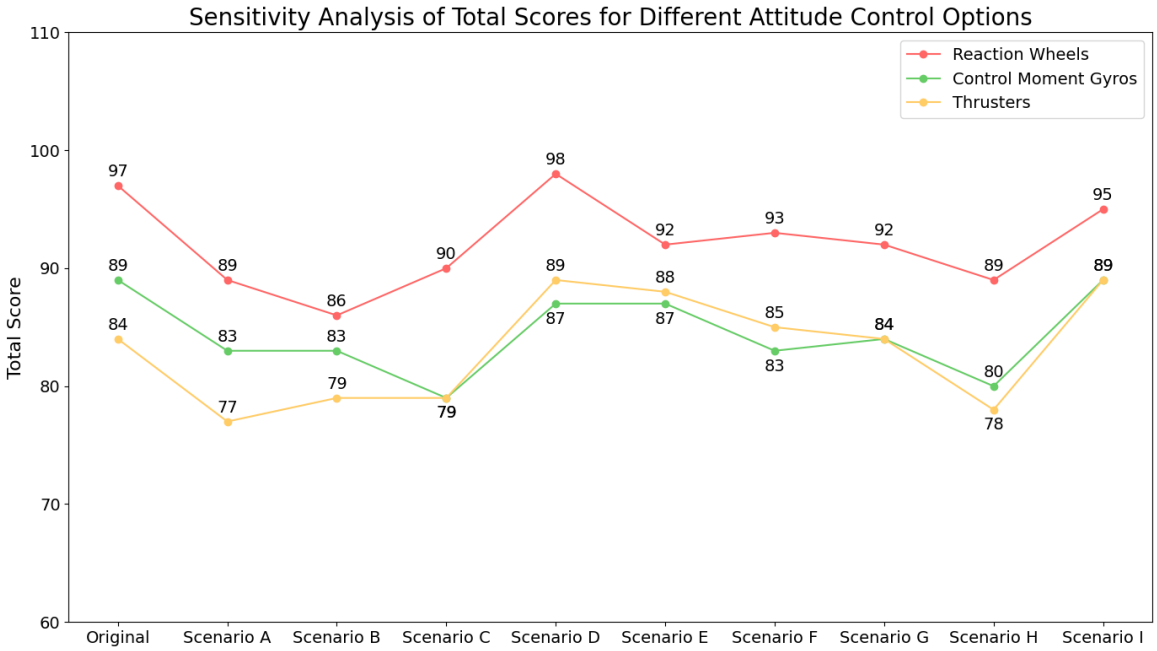

Figure 4.22: The results of each scenario in the sensitivity analysis for the Attitude Control System trade-off.

4.5.4. ADCS Summary

The ADCS Summary table shown in Table 4.22 provides an overview of the components selected for the ADCS of the SBSP system. The table lists the primary sensors and actuators that will be used in the SBSP design to ensure proper a proper spacecraft attitude at all times. The amount of sensors and actuators has been determined based on comparisons with previous satellite designs and relevant case studies (i.e. the Lunar Reconnaissance Orbiter (LRO) [46], the LUNARSAT [9] and the case study by NASA [92]).

ADS	**Component**	
	2 Star Trackers	Provides high-precision attitude determination using star field imaging.
	4 Coarse Sun Sensors	Low-power sensor that determines the orientation of the spacecraft when the Sun is visible.
	2 3-axis Fiber Optic Gyroscopes (FOGs)	The FOG is capable of providing extremely high-performance rotation sensing data.
ACS	**Component**	
	4 Reaction Wheels	Allow continuous control of the spacecraft attitude. One extra wheel included for redundancy.
	8 Thrusters	Used for large-scale maneuvers and momentum dumping.

Table 4.22: Summary of the ADS and ACS components selected for the spacecraft ADCS.

4.6. On-Board Computer System Trade-off

The On-Board Computer (OBC) system is responsible for managing and coordinating the numerous operations required to ensure a successful mission. It takes the role as the central processing unit for the spacecraft by integrating data from multiple subsystems, executing onboard software and handling the communication with the ground segment. The OBC functions as the brain of the spacecraft, orchestrating its operations and ensuring seamless integration between various subsystems. Given its central role, the OBC requires a detailed analysis and design to fully realize its capabilities. However, due to the scope of this project, achieving an extensive design for the OBC is not feasible. Instead, the focus will be put on selecting an appropriate COTS OBC component which will provide estimates for mass, power and volume. This will set the stage for more detailed development in the future phases of the SBSP system design.

4.6.1. On-Board Computer System Objectives

Despite the preliminary nature of the OBC design, a set of objectives can be established. These objectives provide the foundation for evaluating the OBC performance and capabilities such that, even at this early stage, the system requirements are well-defined. In Table 4.23, seven objectives for the OBC system have been compiled.

ID	Objective
OBC-01	The OBC should provide sufficient processing capability to handle all spacecraft operations and payload data processing requirements.
OBC-02	The OBC should offer adequate memory capacity to support data handling and software operations throughout the mission.
OBC-03	The OBC should support a variety of communication interfaces to ensure compatibility with other spacecraft subsystems.
OBC-04	The OBC should ensure reliable software operation with fault detection and correction capabilities to handle errors and maintain system integrity.
OBC-05	The OBC should operate within the power budget of the spacecraft, with efficient power consumption to optimize energy use.
OBC-06	The OBC should be compact and lightweight, fitting within the mass and volume constraints of the spacecraft to optimize design and reduce launch costs.
OBC-07	The OBC should provide redundancy for critical components to enhance reliability and minimize the risk of mission failure.

Table 4.23: On-Board Computer (OBC) subsystem objectives with corresponding ID.

4.6.2. On-Board Computer System COTS Trade-off

The COTS trade-off analysis for the OBC system involves assessing existing OBC components which have been proven in-flight on previous spacecraft missions. Hence, a number of OBC components have been selected to participate in the trade-off analysis. These components have been found online using SatSearch [80] where a large number of OBCs can found. Among these options, three potential OBCs have been selected that were promising in terms of performance. The following three options were chosen:

- **ICDE-NG:** The *Integrated Control and Data Equipment - Next Generation*, in short ICDE-NG, is an on board computer for multi-purpose applications developed by Airbus Defence & Space [7], shown in Figure 4.23. It is a 32-bit based fully redundant On-Board Computer and is composed of ERC32 Processor (up to 16 MIPS), high memory capability including in-flight programmable EEPROM. Further it includes, a TC/TM module which is able to process ESA standard TC/TM packets up to 1 Mbit uplink and 10 Mbit downlink. Holds full redundancy due to its internal cross-strapped architecture. Has been operational in the Galileo System Test Bed V2, LISA Pathfinder and ARSAT projects.
- **FERMI Deep Space On-Board Computer:** The FERMI OBC is a rad-hard avionics unit purposed for deep space and mission-critical applications developed by Argotec [11], and is depicted in Fig-

ure 4.24. It works in cooperation with the customizable on-board software, providing full spacecraft and payload control. The component holds a volume of 0.4U and typically consumes 5 W of power. It is primarily suitable for small satellite platforms where focus is put on volume and power constraints. It features a Dual-Core LEON3FT SPARC V8 Processor with fault-tolerant memory controller.

- **SpaceCloud iX5-106:** The SpaceCloud iX5-106 is designed as the most power-efficient and reliable computer technology made by Unibap [101], shown in Figure 4.25. It features an AMD Steppe Eagle Quad-core x86-64 CPU and an AMD Radeon GPU combined with SATA SSD Storage. When fully equiped, the iX5-106 has the capacity for trillions of computer operations per second (TOPS).

The inclusion of the FERMI Deep Space On-Board Computer and the SpaceCloud iX5-106 in this trade-off analysis is based on their advanced capabilities and unique features, despite being originally designed for CubeSat platforms. While these systems are optimized for smaller spacecraft, their compact size, high computational performance, and low power consumption make them appealing for specific subsystems of a larger spacecraft.

Figure 4.23: The ICDE-NG OBC developed by Airbus Defense and Space [7].

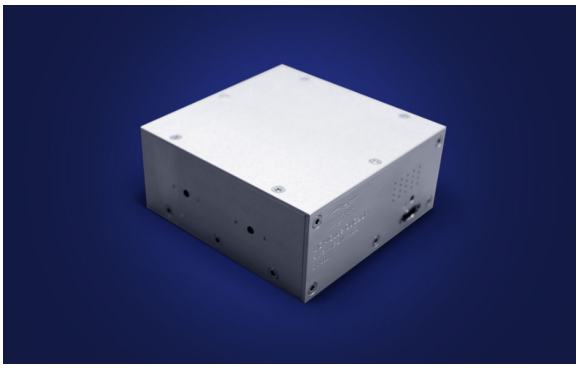

Figure 4.24: The FERMI OBC developed by Argotec [11].

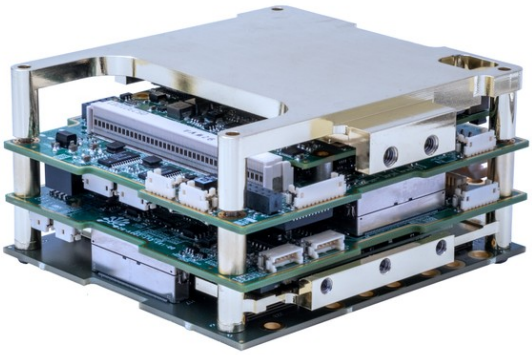

Figure 4.25: The SpaceCloud iX5-106 OBC developed by Unibap [101].

Based on the objectives defined for the OBC subsystem, a set of key criteria has been generated to guide the selection and evaluation process. These criteria, shown in Table 4.24, are determined to ensure that the OBC meets the subsystem objectives [80]. Each criteria evaluates an important aspect of the OBC performance such as processing capability and its available memory. With these criteria, a systematic trade-off analysis can be performed which will results in the most suitable OBC component for the SBSP system.

Criteria	Rationale	Weight
Processing Capability	Reflects the ability of the computing unit to manage all essential operations, including controlling subsystems like attitude, communication, and power distribution, as well as handling payload data processing.	5
Memory (Storage and RAM)	Refers to the capacity and types of memory required to support data storage and operational software. Both volatile and non-volatile memory types are necessary for handling real-time operations and long-term data retention.	4
Interoperability	Evaluates how well the OBC can communicate with other spacecraft subsystems via different interfaces (e.g., USB, I2C) and the number of available ports to connect external systems.	4
Reliability	Measures the ability of the OBC to perform consistently and without failure throughout the mission. Includes operating in harsh space environments	5
Power Consumption	Considers the energy consumption of the OBC, which, though typically low, must be efficient to conserve power for other mission-critical systems.	3
Mass and Volume	Ensures that the OBC fits within the spacecraft's mass and volume constraints, helping avoid excessive redesign or increased launch costs.	4
Temperature Operating Range	Assess the ability of the OBC to operate effectively within a specified temperature range.	4
Cost	Assess the overall cost of the OBC, affecting the cost budget.	3

Table 4.24: Trade-off criteria for On-Board Computer (OBC) system with corresponding rationale and weight.

These criteria have been used to assess the three OBC options in Table 4.25 which led to the following results. The ICDE-NG OBC emerged as the most suitable option for the SBSP system with a total score of 99 points. Its available interface designs and operational reliability were the primary reasons for this status. Furthermore, its size and power consumption was considered good as well as its processing capability and available memory. In second place, the SpaceCloude iX5-106 OBC scored a total of 94 points. While it showed superior computational power and making it a strong candidate for high-performance tasks, it was less optimal in terms of reliability and interoperability compared to the ICDE-NG. Lastly, the FERMI Deep Space OBC scored the lowest total score of 87 points. While it is a robust, rad-hard unit intended for deep space missions, its primary design focus on smallsats limited its applicability to the SBPS system. Its interoperability was deemed ”Low” as it was tailored more for smallsats and cubesats. Therefore, it might not fully meet the requirements of a larger, more complex SBSP system.

Additionally, a sensitivity analysis has been performed to assess the validity of the trade-off results. As a result, a set of weighting scenarios have been generated and listed below. These weighting scenarios have been used to compute the plot in Figure 4.26. From this plot, a conclusion can be drawn. Specifically, the ICDE-NG developed by Airbus Defense and Space outperforms the other two OBC options in all weighting scenarios but Scenario A which is focusing more on a cost-effective approach. Hence the following statement is made regarding the OBC subsystem.

The ICDE-NG OBC has been selected to be integrated into the preliminary design of the SBSP system. Its mass, volume and power characteristics will be used during the early design phases to provide a realistic estimate of the impact of the OBC subsystem on the lunar satellite. If the project advances into the detailed design of the SBSP system, more precise and mission-specific OBC parameters will need to be established and validated to meet the final system requirements.

OBC / Criteria	ICDE-NG	FERMI Deep Space	SpaceCloud iX5-106
Processing Capability	ERC32 Processor running at 14 MIPS (up to 16 MIPS) at 20 MHz. MIL-STD-1553B interface at 1 MHz for reliable subsystem communication [7].	Dual-Core LEON3FT SPARC V8 Processor with fault-tolerant memory controller [11].	Unibap Qseven e2160 compute module. AMD Steppe Eagle Quad-core x86-64 CPU. AMD Radeon GPU Several TOPS [101].
Memory (Storage and RAM)	Up to 8 MB of SRAM plus extra 2 MB for redundancy. Up to 12.6 Gbits of SDRAM. 1 MB of SRAM and 1 MB of EEPROM, all EDAC protected [7].	A 16 GB ECC-corrected mass memory. 256 Mbyte SDRAM, EDAC-protected. 20 Mbit EEPROM + 5 Mbit EEPROM [11].	2 GB DDR3 ECC. 2 x120 GB SATA SSD.
Interoperability	Available interface designs of most AOCS equipment. Reduces design time and technical risk [7]	Primarily used in SmallSats. For SBSP system might not suffice.	Less I/O interfaces than ICDE-NG. Might not suffice for all SBSP subsystems
Reliability	Operational in orbit on several satellites since 2007 (i.e. LISA Pathfinder) [7]. Full redundancy; cross-strapped architecture.	Operated on board of ARGOMOON and LICIACube [11].	TLR of 9 [101]. Deployed in LEO. Might not operate in lunar orbit.
Power Consumption	Power consumption of 35 W (with 2 redundant I/O modules). Power bus 18 V - 50 V [7].	Power consumption of 5 W [11].	Power consumption of 10 - 30 W, depending on settings. 12 V voltage supply [101].
Mass and Volume	13.6 kg. 307 x 242 x 263 mm^3. [7]	0.4U [11]. No mass found.	0.226 kg. 100 x 100 x 50 mm^3. [101]
Temperature Operating Range	-25 to +50 °C. [7]	No thermal constraints found. Assumed to operate under harsh conditions.	-14 to +70°C [101].
Cost	Relatively high cost due to larger size and I/O modules.	Relatively low cost due to smaller size.	Relatively low cost due to smaller size.

Excellent = 4	Good = 3	Medium = 1	Low = 0

Table 4.25: Trade-off analysis for different On-Board Computers COTS.

The list of scenarios used in the sensitivity analysis is presented below:

- **Original:** Balanced weighting across all criteria, with a slight emphasis on Processing Capability, Reliability, and Temperature Operating Range.
- **Scenario A:** Focus on Processing Capability, Memory and Cost to ensure strong computational performance and storage capacity for an affordable price, with less emphasis on other factors.
- **Scenario B:** Prioritizes Memory and Interoperability to support systems that require extensive data handling and strong interfacing capabilities.
- **Scenario C:** Focus on Reliability and Mass and Volume, emphasizing robustness and the physical constraints of the spacecraft.
- **Scenario D:** Reliability and Temperature Operating Range are prioritized to ensure dependable operation in challenging environmental conditions, with less emphasis on Cost.
- **Scenario E:** Emphasis on Power Consumption to manage energy efficiency, with a balanced approach across other criteria.
- **Scenario F:** Reliability and Temperature Operating Range take precedence, ensuring high durability and operability across extreme thermal conditions.
- **Scenario G:** Equal weighting across all criteria, representing a scenario where no single criterion is prioritized over others.
- **Scenario H:** Focus on Processing Capability and Reliability, ensuring the system can handle high computational demands while maintaining robust performance.
- **Scenario I:** Prioritizes Interoperability and Temperature Range, ensuring compatibility with other systems and stable operation across a wide range of temperatures.

The following sensitivity analysis using the different weighting scenarios led to the plot shown in Figure 4.26.

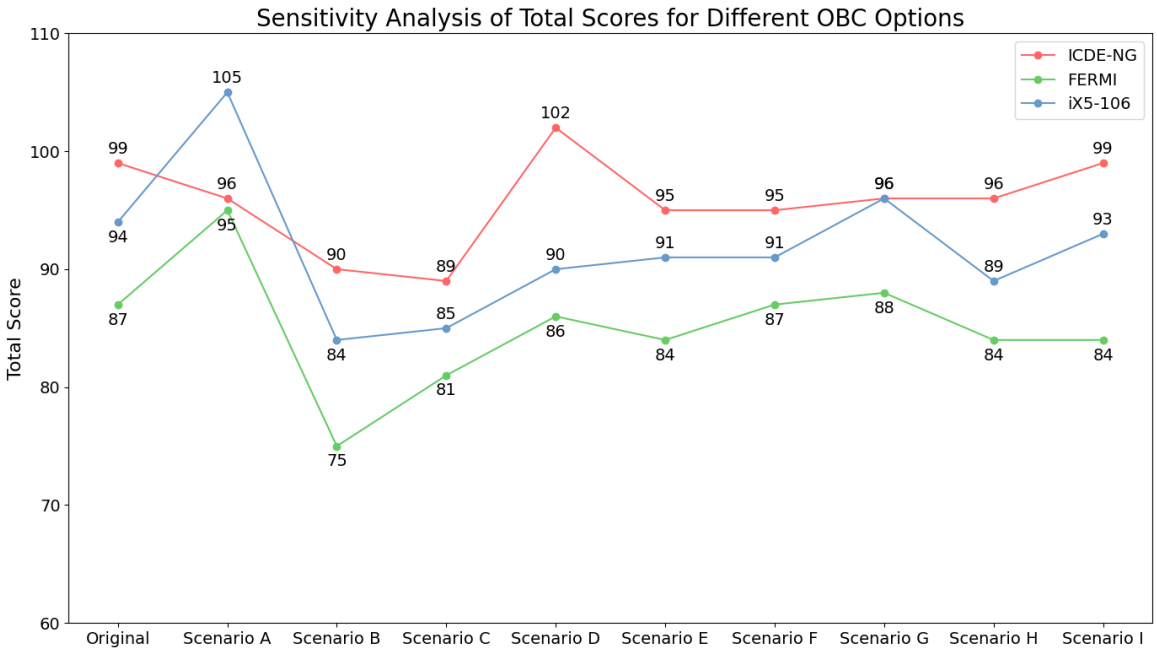

Figure 4.26: The results of each scenario in the sensitivity analysis for the On-Board Computer System trade-off.

4.7. Telecommunications System Trade-off

The Telecommunications subsystem of the lunar SBSP system is to provide reliable and efficient communication between the satellite and Earth. It should be capable of handling both telemetry and command (TM/TC) functions as well as high data-rate payload downlinks. In this section, the general architecture of the Telecommunications subsystem will be evaluated. Furthermore, a few component trade-offs will be performed to guide the preliminary design phase of the Telecommunications system. First, the overall objectives of the Telecommunications subsystem are determined.

4.7.1. Telecommunications System Objectives

The Telecommunications subsystem has to fulfil various tasks to ensure that the SBSP system is capable of communicating with the ground segment on Earth. Hence, the objectives are outlined for this subsystem in Table 4.26. These objectives collectively ensure that the Telecommunications subsystem is capable of meeting the demands of the lunar SBSP mission, providing reliable and high quality communications capabilities.

ID	Objective
TTC-01	The telecommunications system should ensure reliable and high-quality data transmission for high data-rate applications, such as payload data downlink.
TTC-02	The telecommunications system should provide sufficient gain and directivity to maintain effective communication over long distances and ensure robust signal strength.
TTC-03	The system should be designed to operate efficiently within the power budget, minimizing power consumption while maintaining performance.
TTC-04	The antennas should be compact and lightweight to fit within the mass and volume constraints of the satellite, optimizing the overall design and reducing launch costs.
TTC-05	The telecommunications system should ensure compatibility with ground stations and other spacecraft subsystems, including reliable interfaces for telemetry and command.
TTC-06	The system should include redundancy for critical components to enhance reliability and minimize the risk of communication failures during the mission.

Table 4.26: Telecommunications system objectives with corresponding ID.

4.7.2. Telecommunications System Architecture

A schematic of a typical TT&C subsystem has been presented in Figure 4.27. In this case, the subsystem has integrated two Low-Gain Antennas (LGA) with hemispherical coverage, two transponders each consisting of a transmitter and receiver and two command decoders and a radio frequency network and diplexers [109]. The TT&C subsystem is connected to rest of the system via the On-Board Data Handling (OBDH) subsystem.

- The Tele-Command (TC) signal from the ground station is gathered by an LGA after which it is applied to both receiver inputs via the diplexer. A diplexer is device that distributes the signal.
- The receiver out put the TC signal to the active decoder where the TC data is recovered and sent to the OBDH.
- The active transmitter computes a downlink carrier phase and frequency in line with the uplink carrier.
- Additionally, uplink signal contains the ranging signal and is demodulated by the receiver after which it is transmitted back to the ground with the telemetry (TM) signal.

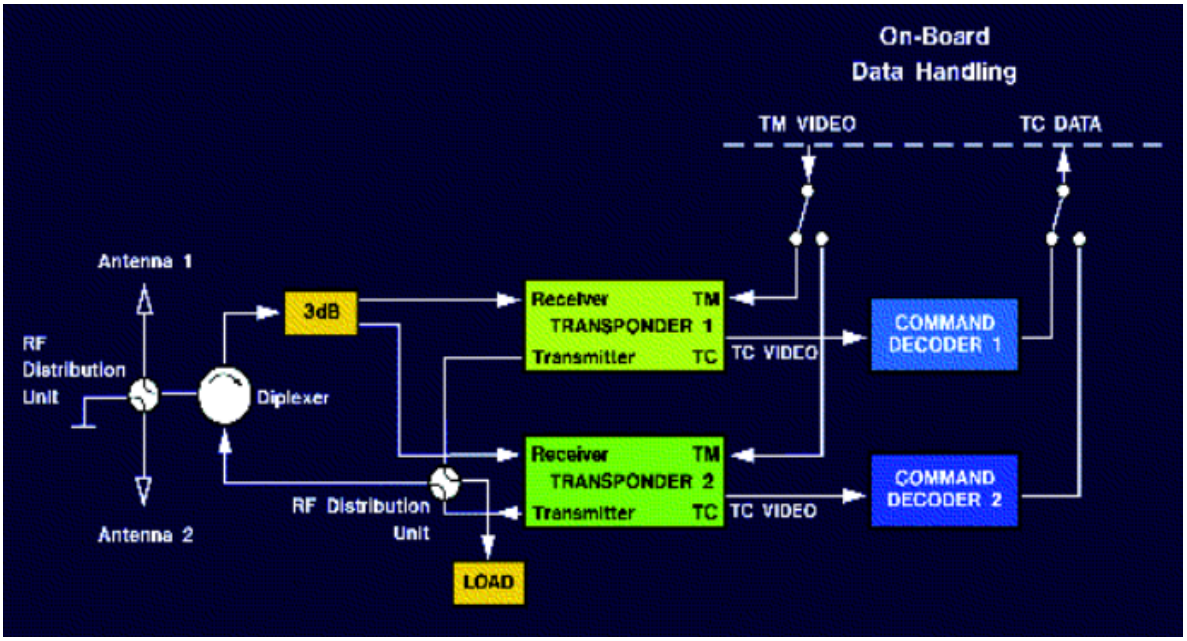

Figure 4.27: A typical TT&C System Architecture [109]

One feature is not shown in Figure 4.27 but will be implemented in the design. Usually the high data-rate payload downlinks are transmitted via a High-Gain Antenna (HGA) as these antennas are designed to provide substantial signal amplification and directivity. This ensures efficient transmission and reception of data over long distances, which is highly applicable for lunar satellites. A comparison table between the HGA and LGA is presented in Table 4.27 to showcase both advantages and disadvantages. Note, this table does not act as a trade-off table but as an overview displaying the characteristics of the LGA and HGA component.

The comparison results in the fact that an HGA is required for high data-rate payload downlinks using an X-band frequency. The HGA will require a pointing mechanism to ensure proper communications but, in return, payload information (in this case, laser transmission performance data) will be communicated at high data transfer rates.

The choice of X-band (8.4 GHz) for the HGA was made based on its extensive use in scientific and deep-space missions. X-band provides a reliable and well-tested solution, balancing high data rates and moderate hardware complexity. Although higher frequencies such as Ku-band or Ka-band provide higher data rates, these frequencies can introduce problems such as stricter pointing accuracy requirements. Given the lunar mission requirements and the need for reliable performance, X-band has been determined as a low-risk and cost-effective solution. Furthermore, previous lunar spacecraft have utilized X-band as its high gain frequency, such as the Lunar Reconnaissance Orbiter [46].

Next, two LGAs are present for reliable telemetry and telecommand functions capable of providing communication with ground control [109]. S-band (2.3 GHz) is selected for the LGAs due to its robustness, lower power requirements and ability to maintain reliable communication without strict pointing accuracy. This frequency is a common choice for spacecraft communication, further simplifying ground system compatibility.

Thus, the antenna configuration of the SBSP system will consist of one HGA (8.4 GHz) and two LGAs (2.3 GHz). More specifically, the Rosetta radio subsystem shows a similar architecture that will be advantageous in the SBSP design [66]. A schematic for the TTC subsystem is shown in Figure 4.28. A parabolic dish HGA and two LGAs (positioned at the front and rear of the spacecraft) will be deployed in the SBSP system. Note that it was decided that no additional Medium-Gain Antenna (MGA) was required, as shown in the Rosetta schematic, since using three antennas will already be sufficient. Hence, a comprehensive list of components in the Telecommunications subsystem can be determined:

- One High-Gain Antenna (HGA): with a steerable parabolic dish.
- Two Low-Gain Antennas (LGAs), front and rear side.
- Two Transponders
- A Radio Frequency Distribution Unit (RFDU).

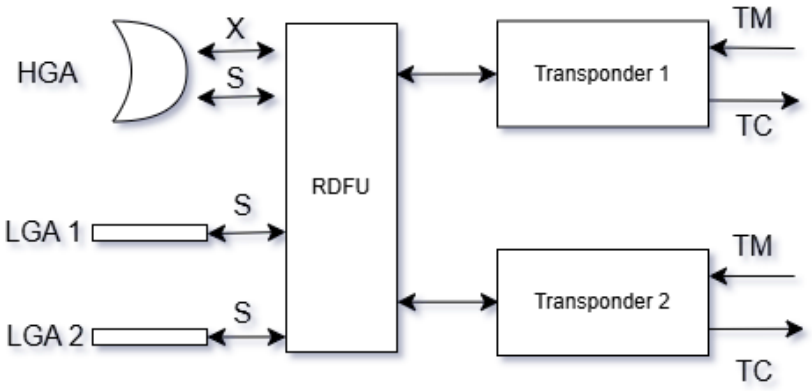

Figure 4.28: Principal block diagram of the TTC subsystem in the SBSP system.

The telecommunications subsystem differs from other subsystems in that a detailed trade-off analysis between COTS components was not conducted. This decision originates from specific challenges encountered during the component selection process. First, it proved difficult to identify COTS LGAs supporting S-band frequencies that were not explicitly designed for CubeSats. Most available options were either too small-scale for the SBSP satellite or lacked the required specifications for a larger platform. Furthermore, a review of Thales Alenia Space's detailed component list of transponders revealed that the only suitable transponder capable of supporting both S-band and X-band communication was the Spread Spectrum Transponder [96]. This significantly limited the options for a meaningful trade-off. Lastly, no COTS RFDU was found online, necessitating the conceptualization of this component in terms of mass, volume, and power requirements. These limitations rendered a trade-off analysis impractical for this subsystem. Concluding, the preliminary design of the telecommunication subsystem will use the above listed components that resulted from the concise telecommunication subsystem analysis.

Option	**HGA**	**LGA**
Gain and Directivity	High gain and directivity, ideal for high data-rate communications	Lower gain, suitable for routine communications
Beamwidth	Narrow beamwidth requiring precise pointing	Wide beamwidth. Easier to maintain communication
Size and Mass	Larger and heavier, impacting satellite design and launch costs	Compact and lightweight, easier to integrate
Power Consumption	Higher power requirements due to pointing mechanism	Lower power consumption
Deployment Complexity	Often complex deployment mechanisms needed	Simpler deployment, no moving parts
Frequency Band Utilization	Suitable for high-frequency bands (e.g., X-band) with high data rates	Suitable for lower-frequency bands (e.g., S-band) with lower data rates
Cost	Generally higher cost due to complexity and size	Generally lower cost, simpler design

Table 4.27: Comparison of the High-Gain Antennas (HGA) and Low-Gain Antennas (LGA).

4.8. Structural System Trade-off

The structure of the SBSP system is what ensures the overall satellite integrity throughout its mission lifetime. It plays the critical role of externally housing the LPT subsystem, deployable solar arrays and communication antennas. And, internally, it houses all other subsystems, including the PMAD, batteries, propulsion system and OBC. This subsystem must maintain stability and be designed to accommodate the dynamic loads which the satellite experiences during launch and in-orbit operations.

4.8.1. Structural System Objectives

The Structural subsystem has to fulfil a set of objectives to ensure mission success. These objectives have been listed in Table 4.28. The objectives range from stability goals to facilitating the integration of other subsystems of the SBSP system.

ID	Objective
STR-01	The structural subsystem should ensure adequate support and stability for the laser payload, minimizing deformations that could impact beam accuracy.
STR-02	The subsystem should minimize mass while maintaining structural integrity to meet the overall spacecraft mass constraints and reduce launch costs.
STR-03	The structure should accommodate deployable solar arrays and radiators, ensuring their smooth operation and integration into the overall bus design.
STR-04	The design should ensure compatibility with the thermal control subsystem to handle the high heat loads generated by the laser and power systems.
STR-05	The structural subsystem should be designed to withstand both launch loads and in-orbit operational stresses, including vibration and thermal cycling.
STR-06	The subsystem should facilitate the integration of other satellite subsystems.

Table 4.28: Structural subsystem objectives with corresponding ID.

4.8.2. Primary Structure System Trade-off

The structural subsystem of the satellite will consist of primary structures and secondary structures. Primary structures are load-bearing components (i.e. the central tube, honey-comb platforms and beams). Secondary structures are structures mounted on the primary structure such as solar arrays, antennas and thermal shielding. The selection of the optimal primary structural configuration directly impacts the total mass, ease of integration and performance of the system. Hence, this section will perform the trade-off between different primary structural configurations. More specifically, it will evaluate *Monocoque*, *Semi-Monocoque* and *Truss* designs:

- **Monocoque Structures**: Rely entirely on a stressed skin to bear the loads, providing a lightweight and stiff configuration. Skin may consist of a thin metallic sheet or sandwich panels. Offers minimal mass but monocoque designs are vulnerable to damage and limit modularity and subsystem flexibility. In Figure 4.29, a satellite using a honeycomb sandwich structure is displayed.
- **Semi-Monocoque Structures**: Combining a load-bearing skin with internal frames, this structure provides redundancy and improves modularity. It offers a balance between mass and flexibility, making it suitable for larger spacecraft that require moderate deployment and thermal management.
- **Truss Structures**: Trusses use an open framework of beams to bear the loads, offering high load capacity. This design excels in supporting large deployable systems like solar arrays but comes with increased complexity and mass. A design using truss structures is shown in Figure 4.30. Note, the truss structure is covered with a non-load-bearing skin which is not shown in Figure 4.30.

Figure 4.29: Satellite using a honeycomb sandwich structure [18].

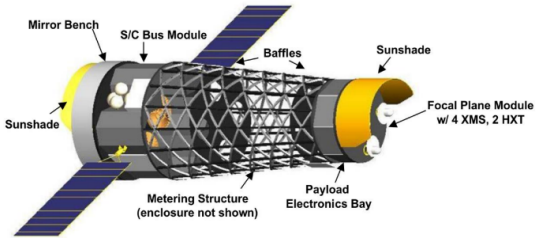

Figure 4.30: Satellite design using a truss structure [106].

For a comprehensive trade-off analysis, a set of criteria has been generated which will assess various aspects of the three primary structure options. In Table 4.29, the criteria have been listed with their corresponding rationale and weight.

Criteria	Rationale	Weight
Mass	Affects the overall spacecraft mass and launch costs. Lower mass structures reduce launch cost but must still maintain required structural integrity.	5
Structural Integrity	Ensures the structural subsystem can withstand the dynamic loads experienced during launch and in orbit.	4
Ease of Assembly	Reflects the complexity of assembling the structure and its adaptability for modifications.	3
Scalability	Scalability reflects the ability to accommodate growth or changes in mission requirements, such as increasing the spacecraft power transmission.	4
Deployment	Assess the capability to support and accommodate deployable mechanisms such as solar arrays and antennas.	5
Cost	Assess the estimated cost of these structural options, which will influence the mission budget	3

Table 4.29: Trade-off criteria for the Structural Subsystem with corresponding rationale and weight.

The *Monocoque* option comes with the advantage of minimal mass which is crucial for reducing launch costs. However, their vulnerability to skin damage and their limited capabilities of incorporating large deployable structures makes it less attractive for a SBSP mission. The *Semi-Monocoque* option provides a good balance between mass, structural integrity and scalability. The featured internal frames enhance structural integrity which is desirable when experiencing the loads during launch. Combining it with a sandwich panel skin, this configuration makes a strong candidate for the SBSP system. At last, the *Truss* option excels in structural integrity and incorporating deployment mechanisms but comes at the cost of higher mass and a higher complexity in assembly.

The trade-off matrix shown in Table 4.30 presents the results for all three options. When analyzing the results, it is concluded that the *Semi-Monocoque* option is the most suitable option for the SBPS system with a total score of 76 points. The primary reason being the option provides an excellent balance between mass, structural integrity and scalability. In second place is the *Truss* option, at 59 points total. Compared to the *Semi-Monocoque*, the *Truss* option comes with a higher mass and a higher system complexity. At last, the *Monocoque* option seems to have a higher risk in terms of skin failure and integration of deployable mechanisms. These characteristics are not critical for smaller satellites (CubeSats), but might become critical for a larger SBSP satellite.

To assess the validity of the trade-off results, a sensitivity analysis must be conducted using different weighting scenarios. The following weighting scenarios are used in the sensitivity analysis:

- **Original**: Emphasizes mass, structural integrity, ease of assembly, scalability, and deployment with a balanced focus.
- **Scenario A**: Prioritizes mass and deployment, reflecting a higher importance on minimizing mass and ensuring effective deployment mechanisms.
- **Scenario B**: Focuses on structural integrity and scalability, valuing robust structural performance and the ability to scale the design.
- **Scenario C**: Highlights structural integrity and deployment, balancing the need for a strong structure with effective deployment capabilities.
- **Scenario D**: Applies equal weighting across all criteria, providing a balanced view of each factor's impact.
- **Scenario E**: Concentrates on deployment and overall balance, considering effective deployment alongside a balanced assessment of other factors.
- **Scenario F**: Focuses on scalability and deployment, highlighting the ability to scale the design and support deployment mechanisms.
- **Scenario G**: Emphasizes mass and structural integrity, reflecting a priority on reducing mass while ensuring a robust structure.
- **Scenario H**: Prioritizes structural integrity, ease of assembly and cost, balancing a strong structure with ease of assembly considerations.

Structure / Criteria	**Monocoque**	**Semi-monocoque**	**Truss**
Mass	Lowest mass due to stressed-skin design, minimal internal supports.	Moderate mass with added internal frames.	Higher mass due to multiple support members and joints carrying all loads.
Structural Integrity	High stiffness, but failure of skin is critical.	Redundant load paths from internal frames, good for structural integrity.	High load-bearing capacity with robust structural stiffness and integrity.
Ease of Assembly	Simpler to assemble, fewer components.	Moderate complexity with internal frames, but flexible design.	Complex assembly with precise alignment of joints and beams.
Scalability	Limited scalability. Difficult to expand beyond initial design without significant redesign.	Moderate scalability. Capable of incremental size adjustments.	Moderate scalability. Capable of incremental size adjustments.
Deployment	Limited support for deployable mechanisms like solar arrays.	Moderate support for deployment of solar arrays and other subsystems.	Best suited for supporting large deployable structures like solar arrays.
Cost	Relatively cost-effective solution due to simple components.	Moderate cost with internal frames and skin component.	Complex assembly leads to high expected cost.

Excellent = 4	Good = 3	Medium = 1	Low = 0

Table 4.30: Trade-off analysis for different structural configurations for Laser SBSP system.

Analyzing the results of the sensitivity analysis, displayed in Figure 4.31, the final conclusion can be made that the *Semi-Monocoque* structure is the most suitable option for the SBSP across all weighting scenarios. In particular, an internal framework combined with the honeycomb sandwich panel skin offers the best performance for the lowest mass penalties.

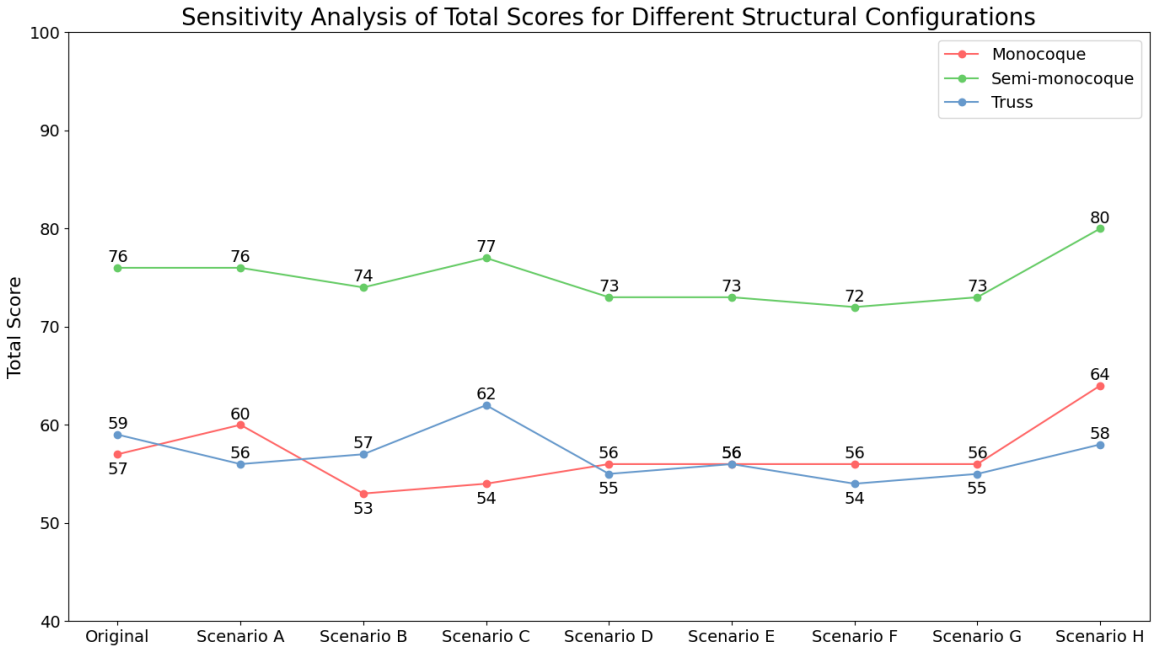

Figure 4.31: The results of each scenario in the sensitivity analysis for the Structure System trade-off.

4.9. Propulsion System Trade-off

The propulsion system is essential for the success of the lunar SBSP demonstration mission. It provides the satellite with the capability to achieve orbital maneuvers such as the lunar orbit insertion, maintain attitude control and perform station-keeping maneuvers. The propulsion system consists of the primary thruster(s) used for the lunar orbital insertion, orbital maneuvers and orbital maintenance and the ADCS thrusters to maintain correct satellite attitude during its mission lifetime. Corresponding propellant tanks and potential pressurant gas tanks are required to operate the propulsion system. Besides these primary components, secondary components such as pipes and valves are also part of the propulsion system. In this section, all these components are evaluated to decide what methods and configurations are the most suitable option for the SBSP system.

From the ADCS trade-off section, it was determined that eight thrusters are required for the ACS. Together with the reaction wheels, these thrusters enable full three-axis stabilization. In the following sections, further trade-offs will be performed to evaluate the best thruster option for these six ACS thrusters. Additionally, the thruster system used for the lunar orbit insertion will be determined as well as the corresponding propellant and pressurant gas tanks.

4.9.1. Propulsion System Objectives

The objectives for the propulsion system have been determined and listed in Table 4.31. The emphasis lies on precise control of the spacecraft attitude, reliable performance under the lunar environment and minimizing mass while ensuring sufficient velocity increments throughout the mission. The propulsion system objectives will be a baseline for the coming trade-off criteria.

ID	Objective
PROP-01	The propulsion subsystem should provide precise control of the spacecraft orbit and attitude, ensuring accurate positioning and stabilization of the satellite.
PROP-02	The propulsion subsystem should be capable of delivering sufficient velocity increments to achieve the required orbital insertion and adjustments throughout the mission lifetime.
PROP-03	The propulsion subsystem should operate reliably under the expected environmental conditions of the lunar environment, including extreme temperatures and radiation levels.
PROP-04	The propulsion subsystem should minimize mass and volume while maintaining performance.

Table 4.31: Propulsion subsystem objectives with corresponding ID.

4.9.2. Main Propulsion Method Trade-off

The performance of the main propulsion system is assessed by comparing various propulsion methods. These methods include cold gas, mono-propellant, bi-propellant and electrical propulsion. Each method is shortly elaborated:

- **Cold Gas:** A simple propulsion system that uses pressurized gas expelled through a nozzle to generate thrust. While it holds a low specific impulse, it is lightweight and requires no combustion, making it a safe option with low system complexity.
- **Mono-Propellant:** This method uses a chemical propellant, typically hydrazine, which decomposes through a catalyst to produce thrust. It offers moderate specific impulse and thrust, and is commonly used for small satellites due to its reliability and simplicity.
- **Bi-Propellant:** Using two separate chemicals, a fuel and oxidizer, bi-propellant systems are characterized with a higher specific impulse, making them suitable for missions requiring significant velocity increments. However, they are more complex and heavier due to the need for separate tanks.
- **Electrical Propulsion:** Electric propulsion systems, such as ion thrusters, offer extremely high specific impulse, making them very efficient. However, these thrusters produce low thrust and require significant electrical power, making them ideal for long-duration missions with gradual velocity changes.

The trade-off analysis will consider the criteria listed below to critically assess the different propulsion methods for the insertion and orbital maneuver thrusters. Each criterion is listed with its respective rationale and weight.

Criteria	Rationale	Weight
Specific Impulse	Higher specific impulse means a more efficient use of propellant and thus a reduced propellant mass for a velocity increment.	4
Thrust	Thrust is essential for maneuvers such as orbital insertion and attitude adjustments by rapidly providing a velocity increment or attitude change.	5
System Mass	The mass of the propulsion system affects the spacecraft mass budget and costs.	5
Power Consumption	The power needed for propulsion affects the spacecraft power budget.	3
Reliability	A reliable propulsion system minimizes the risk of mission failure, ensuring consistent performance under various operational conditions.	5
Propellant Type	The choice of propellant affects safety, handling, and environmental impact.	4
System Complexity	Simpler systems are easier to integrate and reduce overall risks of the spacecraft.	3
Operational Flexibility	The ability to perform a variety of maneuvers enhances the versatility of the spacecraft.	3

Table 4.32: Trade-off criteria for the Propulsion Method with corresponding rationale and weight.

The results of the propulsion method trade-off analysis are displayed in the trade-off matrix shown in Table 4.33. It indicates a clear preference for the *Mono-propellant* system which scored 88 points overall, outperforming all other options. This dominance shows the balanced performance of the mono-propellant system across multiple criteria such as specific impulse, thrust, reliability and operational flexibility.

The *Bi-propellant* option ranked as second with 80 points. Despite its high thrust capability and flexibility for large maneuvers, its system complexity and higher mass ultimately lowered its ranking to second place. Bi-propellant thrusters still remain a suitable option for missions that require large thrust capabilities, but in this case, it was outperformed by the Mono-propellant option.

Cold Gas propulsion ranks third overall with 77 points. The simplicity and the reliability of Cold Gas thrusters make it a suitable option in mission profiles where high thrust is not required. However, considering the fact that a lunar orbit insertion burn is required makes the cold gas thrusters not the right solution for that maneuver.

Electrical Propulsion came in last place with a total of 76 points. While the electrical propulsion system is highly efficient, it scores lower in thrust and operational flexibility. Incorporating electrical propulsion would lead to an extended mission lifetime of the SBSP system as it is only capable of providing large velocity increments over long periods of time. This feature was determined to be very undesirable for a demonstration mission as it prolongs the wait for useful results and in-flight demonstration.

Propulsion Method / Criteria	Cold Gas	Mono-propellant	Bi-propellant	Electrical Propulsion
Specific Impulse	55 - 65 s [109]. Low propellant efficiency.	206 - 235 s [109]. Moderate propellant efficiency	220 - 352 s [109]. Higher propellant efficiency	3000 - 19300 s [109] Highly efficient with propellant.
Thrust	Low thrust (0.001 - 266 N), not suitable for lunar insertion burns [109].	Moderate thrust (0.02 - 572 N), suitable for most operations [109].	High thrust (4 - 27000 N), effective for large maneuvers [109].	Very low thrust (0.000001 - 5 N), thrusters in top thrust range require immense amounts of power [109].
System Mass	Highest propellant mass due to low I_{sp}.	Moderate mass with added components.	Heavier due to dual propellants.	Moderate mass, but will increase power usage which will reflect in high power subsystem mass.
Power Consumption	Low power requirement.	Moderate power consumption.	Moderate power consumption.	High power consumption, (2 - 250 kW) [109].
Reliability	High reliability, simple and safe system. Proven in-flight.	Reliable and proven in-flight. But not as much as cold gas thrusters	Moderate reliability, more components to fail.	Proven technology but not as much as the other thrusters.
Propellant Type	Inert gas, non-toxic such as N2 gas.	Mostly Hydrazine (Toxic). Requires careful handling. Green propellants in development.	Mostly MMH as fuel (Toxic). Requires careful handling. Cryogenic propellants are more complex.	Uses non-toxic inert gases or ions such as Xenon and Argon.
System Complexity	Simple design, easy to integrate.	Moderate complexity with catalyst and a propellant tank systems.	More complex due to two propellant tanks.	Complex system, requires advanced technology. Reflects in higher costs.
Operational Flexibility	Limited operational capabilities.	Good operational flexibility.	High flexibility, suitable for various maneuvers.	High flexibility but only effective for long-duration missions.

Excellent = 4	Good = 3	Medium = 1	Low = 0

Table 4.33: Trade-off analysis for different propulsion methods for the SBSP system.

A sensitivity analysis was conducted and resulted in the following plot shown in Figure 4.32. Clearly, the *Mono-propellant* option is superior among all weighting scenarios. The other propulsion methods did change in ranking depending on the specific weighting scenario but nevertheless the mono-propellant option will be used for the SBSP system. Based on this result, further evaluation of the mono-propellant thruster options will be done in Section 4.9.3.

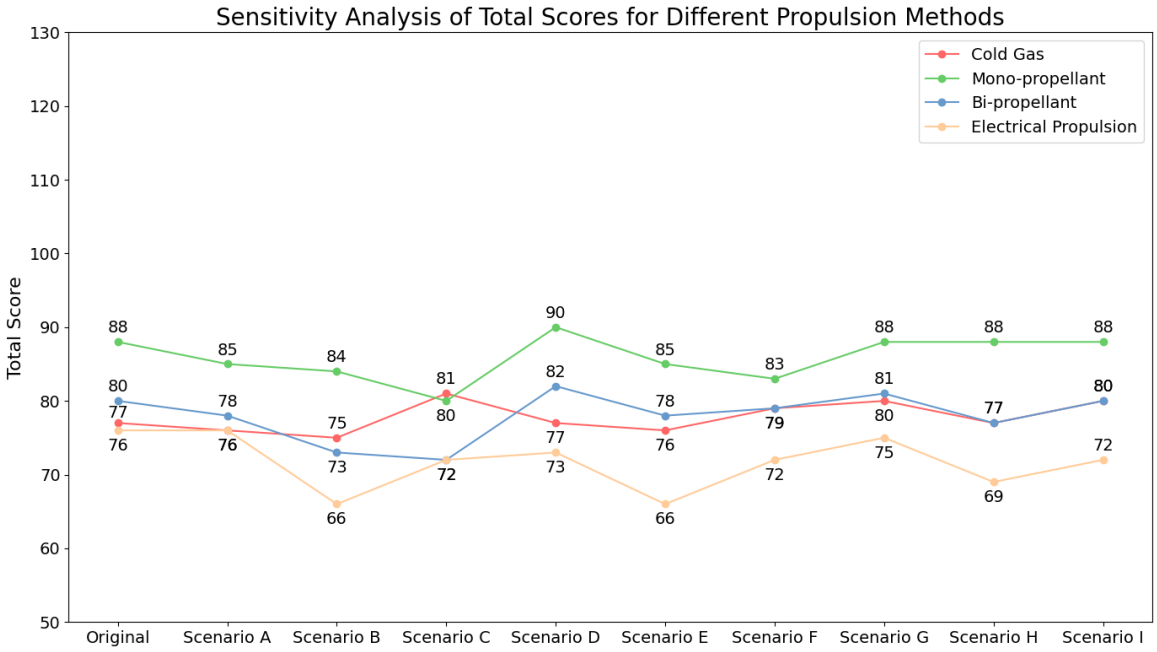

Figure 4.32: The results of each scenario in the sensitivity analysis for the Propulsion Method trade-off.

4.9.3. Main Propulsion Propellant Trade-off

This subsection will focus on the trade-off analysis for the mono-propellant used by the thrusters. As sustainability becomes an increasingly important aspect of spacecraft design, the implementation of non-toxic propellants is a vital consideration when designing a satellite. Traditional spacecraft designs have implemented hydrazine as the mono-propellant due to its reliable performance, but a major disadvantage of hydrazine is the propellant's toxicity. Hence, interest in greener alternatives have risen in the space industry. This trade-off will investigate the benefits and drawbacks of both hydrazine and green propellants for mono-propellant thrusters.

A set of criteria has been determined to assess hydrazine and green mono-propellants. It addresses the performance, toxicity and TRL of the propellants. The criteria with their corresponding rationale and weights are shown in Table 4.34.

Criteria	Rationale	Weight
Specific Impulse	A higher specific impulse leads to more efficient propellant use.	4
Thrust	Thrust is essential for maneuvers such as orbital insertion and attitude adjustments by rapidly providing a velocity increment or attitude change.	5
Propellant Density	Higher density allows for more propellant to be stored in a smaller volume, which is beneficial for compact spacecraft designs.	4
Toxicity	Lower toxicity improves safety for ground handling and its environmental impact.	4
Technology Readiness Level (TRL)	Higher TRL indicates that the propellant and thruster technology is more mature and has been tested extensively in real-world applications, reducing risks.	5
Handling and Storage Requirements	Simpler handling and storage processes reduce operational costs and risks during the spacecraft's development and integration phases.	3
Cost	The total cost of the propellant, including procurement, storage, handling, and potential mission-specific requirements, impacts the overall mission budget.	3

Table 4.34: Trade-off criteria for assessing hydrazine and green mono-propellants with corresponding rationale and weight.

Propellant Type / Criteria	**Hydrazine**	**Green Propellant**
Specific Impulse	206 - 235 s [109].	253 - 261 s [36].
Thrust	0.02 - 572 N [109].	1 - 22 N [91].
Propellant Density	1004 kg/m^3 [104].	1238 - 1470 kg/m^3 [104].
Toxicity	Highly toxic, carcinogenic.	Non-toxic, safe to handle.
Technology Readiness Level (TRL)	Very high, proven in many missions.	Proven in-flight, high thrust configurations still in development.
Handling and Storage Requirements	Complex and hazardous, requires protective gear.	Easier and safer to handle.
Cost	Relatively affordable, well-established thruster. Safety costs increase.	Higher development costs but potential savings.

Excellent = 4	Good = 3	Medium = 1	Low = 0

Table 4.35: Trade-off analysis for hydrazine and green mono-propellants.

The trade-off analysis for the hydrazine and green mono-propellant option has resulted in the matrix shown in Table 4.35. The various criteria have been evaluated for both propellant options and yielded the following results. The *Hydrazine* option is suggested to be the more favourable option for the lunar demonstration mission. Hydrazine offers a well-established performance profile with its corresponding specific impulse and thrust range. Its high TRL makes it an attractive option for a mission requiring reliable and immediate results. However, hydrazine has significant drawbacks in terms of toxicity and handling complexity. This will require strict safety protocols.

On the other hand, *Green Propellant* thrusters hold a higher specific impulse and are non-toxic which simplifies handling and storage and has negligible environmental impact. Green propellants also possess a higher propellant density, which could allow for smaller tank volumes. However, these benefits come at the cost of a low thrust range and a lower TRL as high thrust green mono-propellant thrusters are still in development.

When conducting the sensitivity analysis, the *Hydrazine* option performs more optimal 7 out of 10 times. Although the technology is not dominant in every scenario, hydrazine propellant showcases its benefits in the majority of the cases. The *Green Propellant* option becomes favourable only when the propellant toxicity and handling is emphasized, seen in Scenario B, C and E.

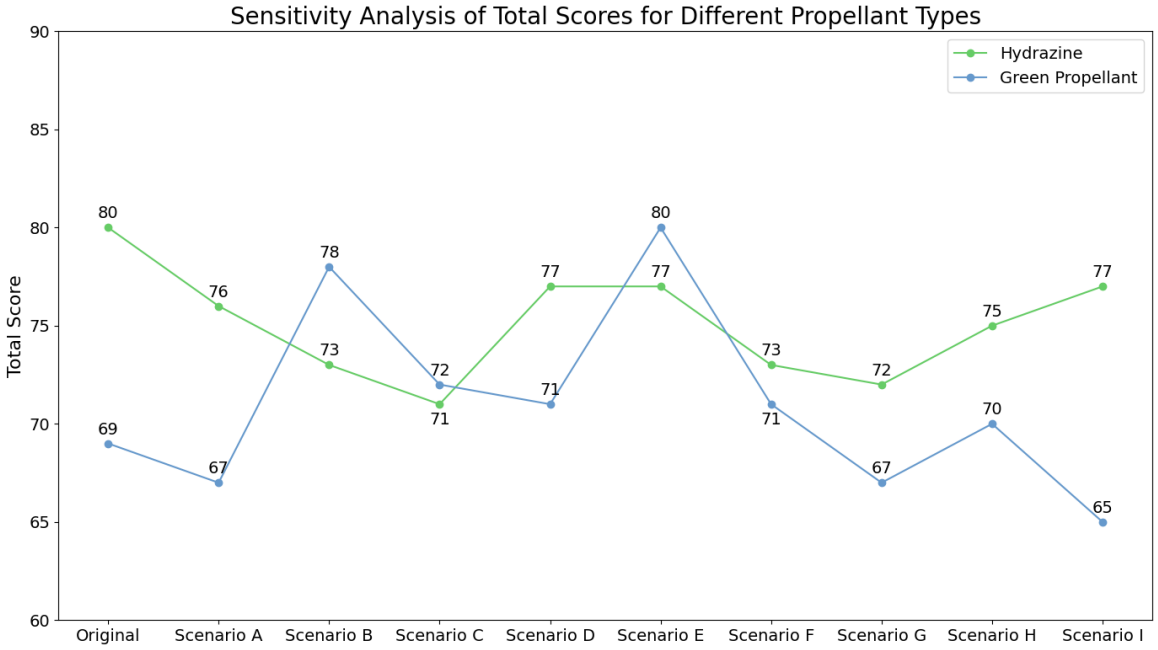

Figure 4.33: The results of each scenario in the sensitivity analysis for the Propellant trade-off.

While green propellant is safer and offers higher performance in specific impulse and propellant density, the technology is not yet mature enough to be confidently implemented in a lunar SBSP demonstration mission. The lower TRL combined with ongoing development for high thrust configurations suggest that the hydrazine option remains a more practical choice for the mission timeline. For this mission, its primary goal is to achieve reliable results in a short time frame. The proven track record of hydrazine outweighs the safety and environmental benefits of the green propellant option at this stage.

Nevertheless, it is important to note that once the green propellant technology has matured and high-performance mono-propellant thrusters become available, future missions could potentially transition to green propellants. For instance, the successor to this demonstration mission could investigate the implementation of green mono-propellant thrusters to enhance the safety and environmental impact features of the future, full-scale SBSP system without compromising on performance.

4.9.4. ADCS Propulsion Trade-off

The performance and suitability of thrusters for the ADCS are assessed through a dedicated trade-off analysis. This analysis evaluates similar thruster types as in the main propulsion trade-off based on a set of criteria listed in Table 4.36. While the primary propulsion system may prioritize high thrust for maneuvers such as orbital insertion, ADCS thrusters require finer control to perform small, precise adjustments to the SBSP system orientation. The criteria are in line with the criteria of the main propulsion trade-off. However, the ”Integration with Main Propulsion” criteria has been added which addresses the ability to integrate the ADCS thrusters into the main propulsion thruster loop. This could simplify the overall SBSP design, improving the overall reliability. Furthermore, ”Operational Flexibility” was removed as this criteria was more suitable for the main propulsion trade-off, assessing the ability to perform the insertion burn as well as smaller orbital maneuvers.

Criteria	Rationale	Weight
Specific Impulse	A higher specific impulse leads to more efficient propellant use.	4
Thrust	The ability to generate small, precise thrust levels is essential for accurate attitude control without overshooting.	5
System Mass	A lighter propulsion system reduces the overall spacecraft mass, contributing to launch cost savings and improved performance.	4
Integration with Main Propulsion	Using similar propellant or compatible systems simplifies spacecraft design and improves reliability.	5
Power Consumption	Lower power requirements minimize the load on the spacecraft's power budget, allowing allocation to other systems.	3
Reliability	A robust and dependable system ensures consistent performance under varying conditions, reducing mission risk.	5
Propellant Type	Propellants that are non-toxic or align with the main propulsion system reduce handling risks and simplify ground operations.	4
System Complexity	Lower complexity facilitates integration, reduces the risk of malfunctions, and simplifies testing and verification processes.	3

Table 4.36: Trade-off criteria for ADCS propulsion with corresponding rationale and weight.

In Table 4.37, the ADCS thruster trade-off can be observed. Mono propellant thrusters emerge as the top-performing choice, achieving the highest score of 96 points due to their balanced performance across all criteria. These systems provide moderate to high specific impulse, enabling efficient propellant use and deliver adequate thrust levels suitable for a wide range of ADCS operations, including precise maneuvers. Furthermore, their compatibility with the main propulsion system, utilizing hydrazine as a common propellant, reduces system complexity while maintaining reliability.

Cold gas thrusters follow closely behind with a score of 93 points. They offer high reliability, simplicity, and low power consumption, making them particularly safe and easy to operate. Additionally, the use of inert and non-toxic propellants, such as nitrogen gas, further enhances their safety profile. However, their low specific impulse significantly impacts propellant efficiency, resulting in higher propellant mass requirements. Despite this limitation, cold gas thrusters are well-suited for precise attitude adjustments.

Electrical propulsion systems, scoring 75 points, demonstrate an excellent specific impulse, making them highly efficient in terms of propellant usage. They also benefit from the use of non-toxic propellants, such as xenon or argon. However, their very low thrust levels render them unsuitable for rapid or large-scale attitude adjustments. Furthermore, their high power consumption, which can range from 2 to 250 kW, imposes significant demands on the power subsystem, leading to increased system mass and complexity.

Bi-propellant thrusters, with a score of 52 points, are the lowest-performing option in this trade-off. While they provide higher thrust and specific impulse compared to mono-propellant systems, their high complexity negatively impacts reliability and integration. These characteristics make bi-propellant systems better suited for large-scale orbital maneuvers rather than the precise and reliable functions required for ADCS.

In Figure 4.34, the results from the sensitivity analysis provide additional information on the performance of the evaluated propulsion methods. Among the 10 analyzed scenarios, the *Mono-propellant* option emerges as the optimal solution in four instances, demonstrating its consistent balance across criteria such as specific impulse, thrust, integration, and reliability. The *Cold Gas* option is the best solution in three scenarios, showcasing its reliability and simplicity in configurations where low thrust and high safety are prioritized. For the remaining three scenarios, both *Mono-propellant* and *Cold Gas* options are tied, reflecting their closely matched performance in specific trade-off conditions. Concluding, the *Mono-propellant* option demonstrates superior versatility and robustness, enhancing its position as the preferred propulsion method for the ADCS in the SBSP system. This also indicates that the ADCS thrusters will utilize hydrazine propellant such that it can be easily integrated into the main propulsion system.

Propulsion Method / Criteria	Cold Gas	Mono-propellant	Bi-propellant	Electrical Propulsion
Specific Impulse	55 - 65 s [109]. Low propellant efficiency.	206 - 235 s [109]. Moderate propellant efficiency	220 - 352 s [109]. Higher propellant efficiency	3000 - 19300 s [109] Highly efficient with propellant.
Thrust	Low thrust (0.001 - 266 N), suitable for attitude correction burns [109]. Precise burns are desired.	Moderate thrust (0.02 - 572 N), suitable for most operations [109].	High thrust (4 - 27000 N), only effective for large maneuvers [109].	Very low thrust (0.000001 - 5 N), thrusters in top thrust range require immense amounts of power [109].
System Mass	Highest propellant mass due to low I_{sp}.	Moderate mass with added components.	Heavier due to dual propellants.	Moderate mass, but will increase power usage which will reflect in high power subsystem mass.
Integration with Main Propulsion	Requires additional propellant besides the hydrazine propellant.	Can be integrated in the existing main propulsion system using hydrazine.	Would require an extra propellant and oxidizer.	Requires additional propellant besides the hydrazine propellant.
Power Consumption	Low power requirement.	Moderate power consumption.	Moderate power consumption.	High power consumption, (2 - 250 kW) [109].
Reliability	High reliability, simple and safe system. Proven in-flight.	Reliable and proven in-flight. But not as much as cold gas thrusters	Moderate reliability, more components to fail.	Proven technology but not as much as the other thrusters.
Propellant Type	Inert gas, non-toxic such as N2 gas.	Mostly Hydrazine (Toxic). Requires careful handling. Green propellants in development.	Mostly MMH as fuel (Toxic). Requires careful handling. Cryogenic propellants are more complex.	Uses non-toxic inert gases or ions such as Xenon and Argon.
System Complexity	Simple design, easy to integrate.	Moderate complexity with catalyst and a propellant tank systems.	More complex due to two propellant tanks.	Complex system, requires advanced technology. Reflects in higher costs.

Excellent = 4	Good = 3	Medium = 1	Low = 0

Table 4.37: Trade-off analysis for different ADCS propulsion methods for the SBSP system.

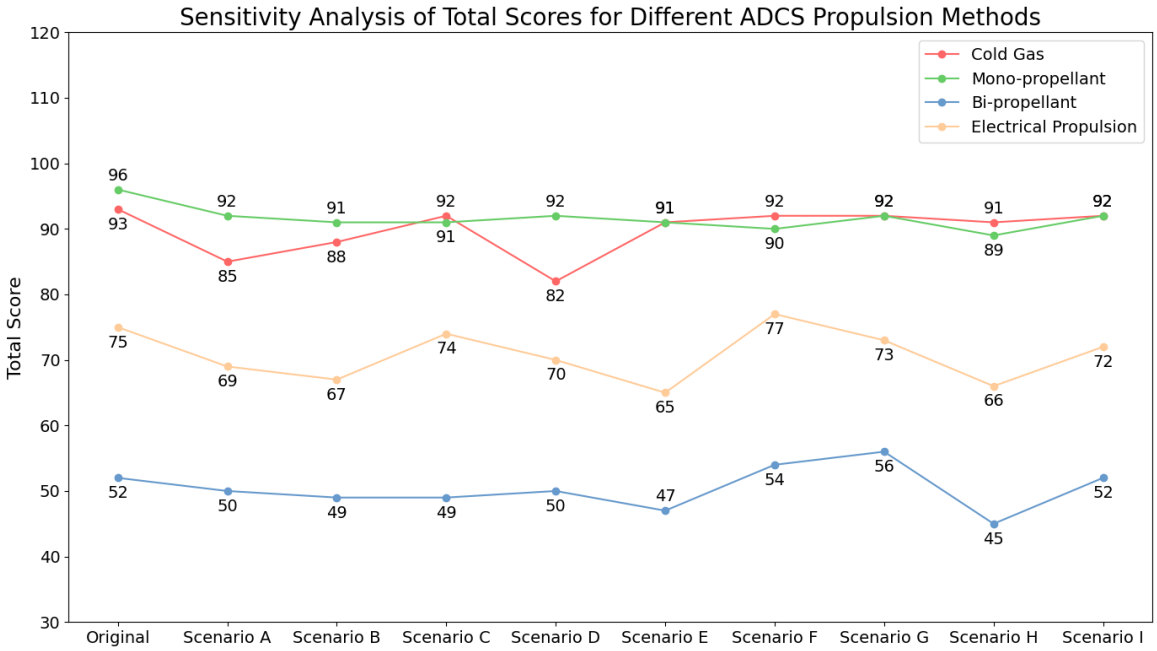

Figure 4.34: The results of each scenario in the sensitivity analysis for the ADCS Propulsion trade-off.

4.9.5. Propellant Tank Trade-off

This subsection investigates the hydrazine propellant configuration that is to be used in the SBSP system. The material of the propellant tank is an important feature which ensures the structural integrity and mass and volume efficiency of the propellant tank. Additionally, the material must be compatible with the propellant, in this case, hydrazine. The trade-off will assess three material options for the propellant tank; titanium alloys, aluminum alloys and composites.

- **Titanium Alloys**: Material with high strength-to-weight ratio. Titanium has an excellent corrosion-resistance, but is relatively heavy and expensive.
- **Aluminum Alloys**: Lightweight, cost-effective material. Lower tensile strength compared to titanium and requires coating for chemical compatibility. Easily manufacterable for various space applications.
- **Composites**: Composites such as carbon fiber reinforced polymers hold exceptional strength-to-weight ratios. High resistance to corrosion and thermal stress. However, complex to manufacture, and less proven in space applications.

The material of the propellant tank will be evaluated using the various criteria listed in Table 4.38. Among the criteria, the strength-to-weight ratio, the corrosion resistance and TRL are ranked as most important in the trade-off.

Criteria	Rationale	Weight
Strength-to-Weight Ratio	A high strength-to-weight ratio ensures that the propellant tank can withstand internal pressure without adding excessive mass, which is critical for optimizing spacecraft performance.	5
Density	Lower density materials reduce the overall mass of the propellant tank, which is beneficial for reducing launch costs and improving payload capacity.	4
Corrosion Resistance	Resistance to corrosion is essential to ensure long-term structural integrity, particularly for tanks exposed to reactive or corrosive propellants like hydrazine.	5
Manufacturability	Materials that are easier to manufacture or fabricate into complex shapes reduce production time and costs.	3
Cost	The cost of raw materials and manufacturing processes directly impacts the total budget of the spacecraft system.	3
Thermal Performance	Good thermal properties ensure that the material can withstand temperature fluctuations in space without significant degradation or structural failure.	4
Technological Readiness Level (TRL)	Materials with proven performance in previous missions reduce development risks and increase the likelihood of mission success.	5

Table 4.38: Trade-off criteria for assessing propellant tank materials with corresponding rationale and weight.

Based on the trade-off matrix in Table 4.39, *Titanium* emerges as the most suitable choice for the propellant tank. The combination of good strength-to-weight ratio, high corrosion resistance and an extensive flight heritage make titanium a reliable and robust propellant tank material for this respective SBSP system. Composites also excel due to its exceptional strength-to-weight ratio but have lower been flown less frequent as titanium propellant tanks. Hence, the trade-off analysis skewed more towards titanium. Aluminum as a propellant tank material holds its own benefits such as its low density and the material being affordable and easy to manufacture. However, in terms of performance, it got overruled by the other two options.

When analyzing the results from the sensitivity analysis in Figure 4.35, it becomes clear that *Titanium* remains the most suitable material for the propellant tanks. While *Aluminum* performs better in cost-conscious scenarios, such as scenarios B and F, Titanium consistently emerges as the optimal choice in a majority of the cases, making it the more reliable solution.

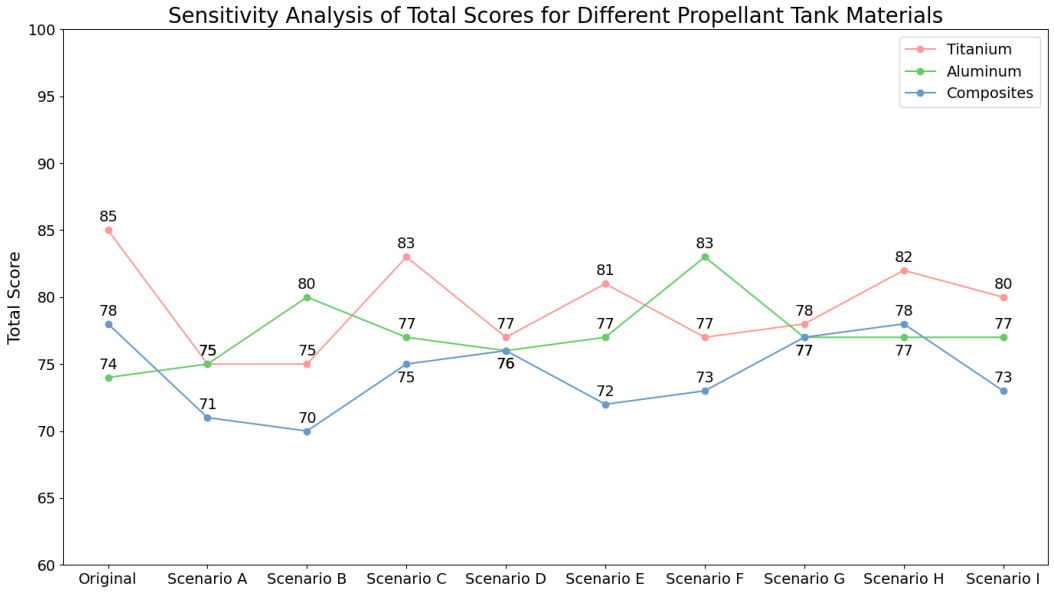

Figure 4.35: The results of each scenario in the sensitivity analysis for the Propellant Tank Material trade-off.

Material / Criteria	Titanium	Aluminum	Composites
Strength-to-Weight Ratio	High strength-to-weight ratio. Tensile strength of 345-1380 MPa [49].	Moderate strength-to-weight ratio. Tensile strength of 140 to 480 MPa [49].	Exceptional strength-to-weight ratio. Tensile yield strength of 4.62 to 3380 MPa [55].
Density	4550 kg/m^3 [75].	2710 kg/m^3 [75].	1150 - 2250 kg/m^3 [55].
Corrosion Resistance	Excellent, highly resistant to corrosion.	Moderate, susceptible to corrosion in space.	High, can be tailored with specific resins.
Manufacturability	Difficult to machine and weld, high cost.	Easy to machine, well-known fabrication processes.	Complex to manufacture, requires specialized manufacturing processes.
Cost	High cost of raw material and fabrication.	Affordable, widely used in aerospace.	High development cost, may reduce overall mass and cost over the mission.
Thermal Performance	Good thermal resistance, performs well in extreme environments.	Moderate thermal resistance, can deform at high temperatures.	Excellent thermal stability.
Technological Readiness Level (TRL)	Extensive flight heritage, proven in space missions.	Extensive flight heritage, widely used in aerospace.	Less heritage compared to metals, but increasing usage.

Excellent = 4	Good = 3	Medium = 1	Low = 0

Table 4.39: Trade-off analysis for propellant tank materials: Titanium, Aluminum, and Composites.

4.9.6. Pressurant Gas

Conventional spacecraft utilizing hydrazine mono-propellant thrusters typically require a pressurant gas to force the hydrazine from the propellant tank into the thrusters. This allows for a consistent flow and maintaining the correct pressure for combustion or decomposition. Since the majority of spacecraft implement helium as a pressurant gas due to its low density, this pressurant gas will also be integrated in the SBSP system to feed the propellant into both the ADS mono-propellant thrusters and the thrusters for large scale maneuvers.

4.10. Subsystem Trade-Off Summary and Conclusions

This section summarizes the SBSP conceptual design trade-offs performed in Chapter 4. The goal of these trade-offs was to identify the optimal SBSP system configuration which balances system performance, reliability and scalability while meeting the mission objectives. Table 4.40 provides a clear overview of each subsystem and their respective components in the SBSP design.

Table 4.40: Summary of the SBSP Conceptual Design Trade-offs.

Subsystem	Component	Description
Power Generation	Two deployable MegaFlex solar arrays	Deployable and scalable lightweight solar arrays.
Laser Power Transmission	Custom LPT system	Multiple low power laser units combined into one large LPT system.
Power Management and Distribution (PMAD)	2 Sequential Shunt Units (SSU)	Allow selective disconnection of specific loads of the solar arrays, maintaining a constant output voltage.
	2 DC Switching Units (DCSUs)	Route the power flow between the solar arrays, BCDUs, and downstream MBSUs and DDCUs.
	2 Main Bus Switching Units (MBSUs)	Distribute the primary power from channels downstream towards DDCUs.
	4 DC-DC Converter Units (DDCUs)	Adjust voltage levels of the primary power to meet the voltage requirements of the individual subsystems.
	2 Battery Charge Discharge Units (BCDUs)	Manages the charge and discharge cycles of the onboard batteries.
	TBD Li-ion Batteries	Store excessive power generated by the solar arrays and supply power during eclipse periods to keep the system operational.
Thermal Control (TCS)	Cold Plates	Collects heat of the spacecraft subsystems and components.
	Active Fluid Loops with Pumps	Transports the heat from the cold plates to the radiators.
	Radiators	Dissipates the transported heat into space through deployable radiators.
Attitude Determination (ADS)	2 Star Trackers	Provides high-precision attitude determination using star field imaging.
	4 Coarse Sun Sensors	Low-power sensor that determines the orientation of the spacecraft when the Sun is visible.
	2 3-axis Fiber Optic Gyroscopes (FOGs)	The FOG is capable of providing extremely high-performance rotation sensing data.
Attitude Control (ACS)	4 Reaction Wheels	Allow continuous control of the spacecraft attitude. One extra wheel included for redundancy.
	8 Hydrazine Mono-Propellant Thrusters	Used for large-scale maneuvers and momentum dumping.

Continued on next page...

Table 4.40 continued from previous page: Summary of the SBSP Conceptual Design Trade-offs.

Subsystem	Component	Description
On Board Computer (OBC)	ICDE-NG by Airbus Defense and Space	In-flight proven computer on extraterrestrial missions. Uses the OBC characteristics as an estimate for the preliminary design.
Telecommunication (TT&C)	1 High-Gain Antenna (HGA)	High data rate communication with Earth (X-band).
	2 Low-Gain Antennas (LGAs)	Used for routine communication with both the lunar receiver and Earth (S-band).
	2 Transponders	Handles frequency conversion, amplification and re-transmission of signals.
	1 Radio Frequency Distribution Unit (RFDU)	Manages and distributes the RF signals within the SBSP telecommunications subsystems.
Structure	Semi-Monocoque structure	Honeycomb sandwich panels reinforced with an internal frame.
Propulsion	Hydrazine Mono-propellant thrusters	Insertion thrusters (plus 8 ACS thrusters)
	2 Titanium Propellant Tanks	Two tanks purposed to store the hydrazine propellant.
	1 Helium Pressurant Gas Tank	Tank housing the helium pressurant gas which forces the propellant to the thrusters when necessary.
	Pressure regulators	Regulating the pressure of the propellant and pressurant gas.
	Pipes	Guiding the propellant towards the thrusters.
	Valves	Controlling the propellant access to the thrusters.

Following from the SBSP conceptual design trade-off analyses, the next step in the SBSP system development is to compute and size the actual system components in the preliminary design phase. This will use the identified configuration to create a detailed model that accurately calculates the SBSP characteristics. Moreover, a mass, volume and power budget will be extracted using the results of the model. Finally, the model will be used to assess the scalability of the system and identify key factors which may limit the system's ability to scale effectively.

5

Preliminary SBSP System Design

In this chapter, the SBSP conceptual design will transition to a preliminary design and marks a critical phase in the development of the SBSP system for the lunar demonstration mission. This chapter aims to refine the satellite design through preliminary sizing and computational analysis based on the previously established conceptual design trade-offs.

The first step is to elaborate on the systems engineering approach that underpins the preliminary design. This includes a detailed system architecture of the space segment and an overview of the subsystem interactions and dependencies. Then, the preliminary design requirements will be established which will guide the satellite sizing. Finally, the SBSP system sizing model will be presented, detailing the calculations and assumptions made throughout the process for each subsystem.

5.1. Preliminary System Architecture

The preliminary system architecture of the SBSP system is defined by the interactions and dependencies between its various subsystems. These interactions and dependencies will be visualized via an N2-chart shown in Table 5.1. This chart is a powerful tool for understanding the relations between subsystems and can illustrate how changes in one subsystem can influence the performance and functionality of other subsystems.

The solar arrays convert the solar flux into usable power. This power is transmitted to the PMAD subsystem. The solar arrays themselves use some of the generated power to point the arrays towards the sun. The excess heat is dissipated to the external environment. The PMAD subsystem manages and distributes the power received from the solar arrays to all other subsystems within the SBSP system. It sends PMAD related data to the OBC for further processing, and excess heat to the TCS subsystem. The payload, or the LPT subsystem, converts a part of that delivered power and transmits 3 kW of power to the external environment onto the lunar receiver. While doing so, heat is generated and is collected by the TCS subsystem.

The TCS subsystem is tasked with collecting, transporting and rejecting heat generated by various subsystems. It dissipates this heat to the external environment. Furthermore, it sends TCS related data to the OBC for further processing and receives commands from the OBC to tailor its thermal control operations. Similarly, the ADCS subsystem receives its ADS data from the external environment and sends this data to the OBC subsystem where it is processed and used to generate ACS commands. The OBC receives and processes all transmitted information in the system and turns this data into actionable commands. The TT&C subsystem is responsible for managing telecommands, telemetry and payload data. It sends TC data to the OBC to execute commands and receives TM data back from the OBC, which is then transmitted to the external environment, either to the Earth ground station or the lunar receiver. At last, the propulsion system receives thruster commands from the OBC, allowing it to initiate propellant burns to control the spacecraft.

Solar Arrays	Power				Solar Array Performance			Heat
Power	PMAD	Power	Power Heat	Power	Power PMAD Data	Power	Power	
		LPT	Heat		LPT Data			3 kW of power
			TCS		TCS Data			Heat
			Heat	ADCS	ADS Data			
Attitude Commands ADS Data	PMAD Commands	WPT commands	Heat TCS Commands	ACS Commands	OBC	ADS Data TM Data LPT Data	Thruster command	
			Heat		TC Data	TT&C		TM Data LPT Data
			Heat		Thruster & Propellant Data		Propulsion	Burned Propellant
Solar Flux		Beam Accuracy Data from Receiver		ADS Data		TC Data		EXTERNAL

Table 5.1: N2 Diagram of the entire SBSP system.

After creating an N2 chart to visualize the interactions and dependencies between subsystems, the preliminary architecture of the SBSP system is depicted in Figure 5.1. This diagram provides a compact and integrated visualization of all the key subsystems within the overall satellite design.
Each subsystem is presented in a concise layout, highlighting their components and functional roles. Notably, the power generation and PMAD subsystems have been combined into a single Electrical subsystem. In this subsystem, the arrows represent the flow of power through the SBSP system, illustrating how power is distributed from the solar arrays or batteries to the LPT subsystem or other subsystems via the DDCUs. The TCS subsystem illustrates its workflow, showing how excess heat is collected, transported, and rejected into the external environment. The ADCS subsystem incorporates its five key components, including eight 22 N thrusters that receive hydrazine propellant from the Propulsion subsystem to function. The TT&C subsystem depicts the communication flow between its components, ensuring robust communications with the ground segment. All subsystems are integrated through a MIL-STD-1553 interface, enabling the OBC subsystem to issue commands and manage subsystem operations. Lastly, the Structural subsystem comprises three key elements: the primary core structure, secondary honeycomb skin panels, and Multi-Layer Insulation (MLI) material, which together ensure the structural integrity and thermal protection of the SBSP system.

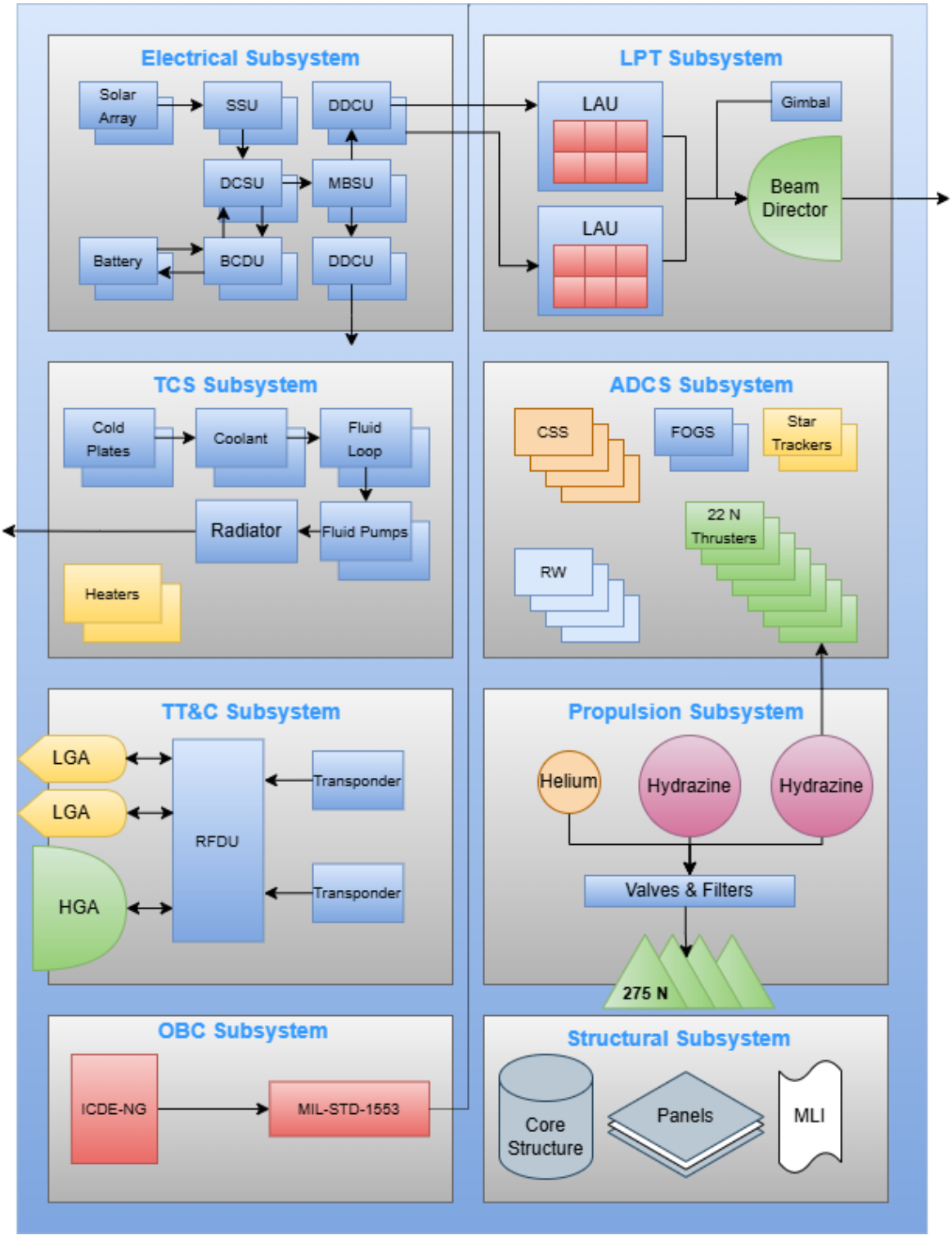

Figure 5.1: The preliminary SBSP system architecture.

5.2. COTS Hardware

This section outlines the different COTS hardware components integrated into the subsystems of the SBSP design. The selection of COTS hardware allows for a reduced development time, reduced cost and ensures reliability through the use of proven technologies. For some subsystems, the COTS components will be used together with a set of assumptions as a starting point for conceptualizing the subsystem and integrate it into the SBSP design. For other subsystems, this section will list subsystem characteristics used during the preliminary sizing of the SBSP system.

5.2.1. LPT Subsystem

The LPT subsystem will have two primary components: the laser assembly unit and the beam director. The laser assembly unit consists of multiple lasers, previously described as low powered lasers. The output of each laser is combined in the laser assembly unit as one coherent laser beam where it is directed towards the beam director. An on-axis Cassegrain telescope will be implemented as the beam director. This device uses a primary mirror and a secondary mirror which will allow for a compact design that efficiently focuses the laser beam onto the receiver.

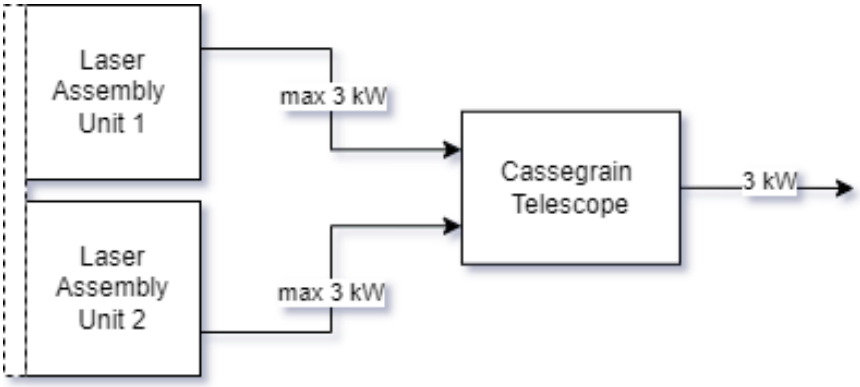

Figure 5.2: The LPT subsystem architecture.

Laser Assembly Unit

Two laser assembly units of 3 kW each will be integrated into the SBSP design to increase the redundancy and reliability of the system. Now, a set of assumptions must be made regarding the lasers. These assumptions will be related to the output power, efficiency, mass and volume of one laser. Note, these assumptions are estimations based on publicly available data and on terrestrial portable fiber laser COTS [71] [5]. These assumptions will serve as a baseline for the sizing of the SBSP satellite.

- Each laser has a total output power of **500 W**.
- Each laser has a conversion efficiency of **30%**.
- Each laser uses a wavelength of **1064 nm**.
- Each laser has a length of **0.5** meters, a width of **0.1** meter and a height of **0.1** meter.
- Each laser has a mass of **20 kg**.
- Each laser assembly unit requires a bus voltage of **300 V**.
- Each laser assembly unit has a maximum output power of **3 kW**.

Beam Director

For the beam director, an on-axis Cassegrain telescope with a dual-mirror system is proposed coupled with a highly accurate gimbal mechanism. This configuration would ensure precise aiming and stabilization of the laser beam. The Cassegrain telescope provides a relatively compact design with high optical performance. The system is sketched in Figure 5.3. The use of the Cassegrain design also allows for the integration of additional sensors, such as a beam guider. The beam guider will be equipped with sensors and an advanced algorithm designed to monitor the position of the beam on the receiver. The beam guider will then analyze the feedback data which is used for precisely correcting the beam director.

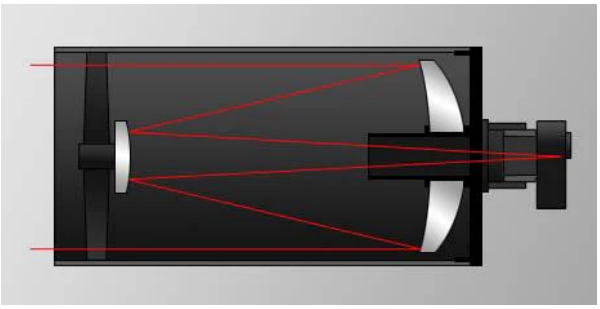

Figure 5.3: A classical Cassegrain Telescope [93].

To accurately direct the laser beam onto the receiver, a highly accurate gimbal mechanism will be deployed. This gimbal features two degrees of freedom, enabling fine adjustments to the orientation of the Cassegrain telescope. Implementing a closed-loop feedback system, the gimbal will compensate for any movement or vibrations of the satellite. From reference material [60], the following gimbal performance data is found and the assumption is made that the component used in the SBSP design holds the same performance characteristics:

- Output step angle on each axis is equal to **0.001** °.
- Power consumption of the gimbal is **10 W**.
- Total mass of the gimbal is **4.4 kg**.

5.2.2. PMAD Subsystem

The main components of the SBSP PMAD subsystem have been determined in Chapter 4. The next step is to establish the component characteristics. Previously, a set of assumptions was made:

- The mass of the components scales linearly with the percentage of power that passes through them, with the ISS performance being 100%.
- Using the density of a component, the new volume can be computed using the new mass of said component.
- The efficiency characteristics of each component are assumed to be constant.

Next, Table 5.2 is depicted, with the component characteristics such as specific mass, efficiency and density. The specific mass of each component is determined using the stated assumptions and the data in Figure 4.11. Specifically, the power which runs through the component is divided by the mass of the component to calculate the specific mass. The density is calculated by dividing the mass with the volume of the component. At last, the efficiencies in Figure 4.10 are used for the respective components. Table 5.2 will be used for the preliminary sizing of the PMAD subsystem. For the SSU component, no mass and volume characteristics were found. Hence, it is assumed to be similar to the MBSU unit parameters.

Component	Specific Mass (W/kg)	Density (kg/m^3)	Efficiency (%)
SSU	219	453	98
DCSU	447	490	95
BCDU	224	484	95
MBSU	219	453	98
DDCU	326	150	95
Li-ion Battery	200 (Wh/kg) [1]	200 (Wh/L) [52]	95

Table 5.2: PMAD component characteristics.

In terms of PMAD power consumption, it is assumed that besides the power efficiency losses, the PMAD system utilizes roughly 2% of the generated power in the SBSP system. This will affect the SBSP power budget.

5.2.3. Solar Array Subsystem

The solar array subsystem will implement the MegaFlex solar array, known for its high efficiency and compact design. The MegaFlex solar array specifications are displayed in Table 5.3, showcasing its specific mass, specific volume, efficiency and EOL bus voltage.

Characteristic	MegaFlex
Specific Weight (W/kg)	100
Specific Volume (kW/m^3)	40
Efficiency (%)	28.9
Bus Voltage (V)	160 EOL
Power Consumption (W)	10 W per array

Table 5.3: MegaFlex solar array characteristics.

Furthermore, both the MegaFlex arrays are assumed to be controlled by a gimbal. From reference material [58], the following gimbal performance data is found:

- Output step angle on each axis is equal to **0.009375** °.
- Power consumption of the gimbal is **10 W**.
- Total mass of the gimbal is **4.4 kg**.

5.2.4. TCS Subsystem

Heat Exchangers

For the TCS subsystem, cold plates/heat exchangers will be implemented to serve as the interface between the subsystems and the active thermal control loop. For this SBSP system, the heat exchangers are assumed to be made out of aluminum and will be sized accordingly to the individual subsystem components. With an assumed thickness of 3 cm and the density of aluminum, an accurate estimate for the heat exchangers mass can be computed. During the preliminary sizing phase, the total mass of the heat exchangers will be determined.

Active Fluid Loop

The active fluid loop with mechanical pumps will transport the coolant to the radiators where the heat is rejected into space. NLR has developed and tested an active fluid loop capable of rejected 3 kW of power [15]. This system weighs 45 kg, including piping, fluid pumps and the H-Galden Zt85 coolant fluid. For the SBSP system, the required heat rejection is initially estimated to be 9 kW of power. Therefore, the assumption is made that the fluid loop scales proportionally with the heat load. Given this assumption, a 9 kW power would require a fluid loop weighing 135 kg where the fluid pump consumes 171 - 471 W of power. Furthermore, a specific weight for the piping would be equal to 0.11 kg/m. This type of system uses 8 liters of coolant for a system length of 70 m. Hence, a specific volume for the coolant can also be determined, equaling to 0.11 L/m. Using these parameters, a preliminary design of the active fluid loop can be established. Since two fluid loops are used for increased redundancy, the total power consumed by the TCS subsystem accumulates to 342 - 942 W. Here the assumption is made that the lower value corresponds to the TCS's idle state or when it is maintaining lower power levels, while the higher value applies during active laser transmission.

Radiators

The radiators are dissipating the transported heat into the external environment. The required radiating area will be calculated during the preliminary sizing phase, but to make this possible, a few radiator parameters must be determined. According to Iwata et al., the average radiator area density was less than 7.0 kg/m^2 [44]. Hence, this value will be used to calculate the radiator mass. This also indicates that aluminum will be used as the radiator material.

Multi-Layer Insulation

Finally, the satellite will incorporate multi-layer insulation (MLI) as the external coating, serving as a passive thermal control solution. A typical emissivity of MLI is $= (0.05 - 0.007)$ [99]. Furthermore, it is assumed that the absorptivity of the MLI is also equal to 0.05.

5.2.5. ADCS Subsystem

The ADCS subsystem is divided into ADS and ACS components. First the ADS components, the Coarse Sun Sensors, Star Trackers and Fiber Optic Gyroscopes are elaborated. Then, the ACS reaction wheels and thrusters will be determined.

ADS Components

The ADS will integrate four Coarse Sun Sensors (CSS) developed by Bradford Engineering, which have been applied in a variety of different planetary and interplanetary missions, showcasing its reliability and robustness [21]. These sensors feature internal redundancy, enhancing their robustness. The accuracy of this CSS is $\pm 1.5°$ throughout its mission lifetime, making it a reliable and responsive sensor aboard the SBSP system, albeit at the cost of the sensor accuracy. This CSS is a passive sensor and therefore does not consume any power. Finally, the CSS excels in withstanding the extreme temperature fluctuations and high radiation levels in the lunar environment. In Table 5.4, the component characteristics of the Bradford CSS are depicted.

Additionally, two Hydra TC Star Trackers developed by Sodern will be integrated in the SBSP system. The Hydra TC Star Tracker is a high-end, off-the-shelf component known for its high performance and robustness, which makes it a highly suitable choice for demanding space environments like the lunar environment. The Hydra Star Tracker has successfully operated on several interplanetary spacecraft missions, such as the NASA's Lucy space probe and GOES-R mission and has therefore obtained an TRL of 9. Two Optical Heads (OH) will be connected to one fully redundant Electronics Unit (EU) via SpaceWire. These two Star Trackers will act as the high-accuracy sensor aboard the SBSP system. The performance characteristics of the Hydra Star Tracker are included in Table 5.4.

The SBSP system will also include two 3-axis Fiber-Optic Gyroscopes (FOGs) developed by Exail. These gyroscopes utilize solid-state FOG technology, which has been proven in the last decades with over 6 million cumulative flight hours on more than 40 major satellites [45]. This makes the FOG produced by Exail a suitable choice for challenging conditions of this lunar mission. The FOGs will play a key role in maintaining the satellite attitude by providing accurate rotational data. Their compact design and quick response time make them ideal for the SBSP system, where precise attitude control and reliable performance are critical. The characteristics of the FOGs will be presented in Table 5.4, alongside the other ADS components.

Characteristic	CSS [22]	Star Tracker [84]	3-axis FOG [45]
Mass (kg)	0.215	OH: 1.4 EU: 3.9	1.4
Dimensions (mm)	110 x 110 x 30	OH: D=147, H=283 EU: 194 x 166 x 159	100 x 100 x 100
Accuracy	Better than $\pm 1.5°$	<11 arcsec	0.0025 - 0.005 °/h
Power Consumption	Nil: CSS is passive	9.3 W total	8 (BOL)
Qualification Temperature	-80/+120°C	-30/+60°C	-20/+65°C

Table 5.4: The ADS component characteristics in the SBSP system.

ACS Components

The SBSP will integrate four reaction wheels to control its attitude. It will utilize reaction wheels similar to that of the Rosetta and BepiColombo spacecraft, namely the reactions wheels manufactured by Bradford Engineering [23]. These reaction wheel units are accompanied with publicly available data sheets as well as an excellent flight record such as on board Rosetta, a large satellite weighing approximately 3000 kg [33]. This heritage provides confidence in their reliability and performance for the SBSP mission. For this design, the largest reaction wheel developed by Bradford Engineering is implemented to ensure that it at least will be able to support missions in size similar to Rosetta. However, this assumption must be verified during later stages in the overall SBSP design when more information is known. Four reaction wheels are implemented in the SBSP design. Each reaction wheel unit (RWU) consists of a Reaction Wheel Assembly (RWA) and one Wheel Drive Electronics Box (WDE). Both component characteristics are shown in Table 5.5. Note, the depicted power characteristics are indicating the performance of the combined RWA+WDE configuration.

Characteristic	RWA	WDE
Mass (kg)	7.45	4.67
Dimensions (mm)	d = 365, h = 125	258x181x143
Max RPM	4000	-
Momentum Storage (Nms)	45	-
Peak Power Consumption, max torque and speed (W)	168	-
Steady state Consumption, max constant speed (W)	29	-
Quiescent Power Consumption (W)	7.6	-
Power Bus Interface	28Vdc or 50Vdc	-

Table 5.5: Bradford Reaction Wheel Characteristics [23].

Additionally, eight hydrazine thrusters are implemented for momentum dumping and large-scale maneuvers. The MR-106L 22N hydrazine thruster by Aerojet Rocketdyne has been selected due to its performance and proven reliability in space missions [6]. The 22 N variant of the thruster has been selected since the Lunar Reconnaissance Orbiter (LRO) has employed similar hydrazine thrusters capable of providing 22 N of thrust for ADCS maneuvers [34]. The usage of comparable thrust capabilities by the LRO showcases the suitability of this thrust class for the SBSP system design. However, it is essential to evaluate whether this thrust level is sufficient for this SBSP design.

The selection of the MR-106L provides a reliable solution based on past mission experiences. This ensures robust performance for the SBSP satellite operational needs. In Table 5.6, specific characteristics of the MR-106L thruster are provided.

Characteristic	MR-106L 22N
Thrust range (N)	10 - 34
Flow rate (g/s)	4.1 - 14
Specific Impulse (s)	228 - 235
Mass (kg)	0.59
Valve Power (W)	25.1
Valve Heater Power (W)	4
Cat. Bed Heater Power (W)	7.06
Power Bus Interface (Vdc)	28

Table 5.6: MR-106L Aerojet Rocketdyne characteristics [6].

5.2.6. OBC Subsystem

The ICDE-NG OBC will be integrated into the SBSP system, setting the foundation for the OBC subsystem [7]. This system, manufactured by Airbus Defense and Space, is a highly suitable option due to its robustness, flight heritage and full internal redundancy. The modular architecture of the ICDE-NG allows flexibility, which enables the integration of various sensors, actuators and power interface modules. The component characteristics are displayed in Table 5.7, showcasing important features such as component mass and dimensions.

Characteristic	ICDE-NG OBC
Processor	ERC32 (16 MIPS)
Memory	8 MB SRAM, 2 MB redundant
Power Consumption (W)	35 W
Mass (kg)	13.6
Dimensions (mm)	307 x 242 x 263
Telemetry Uplink	Up to 1 Mbit/s
Telemetry Downlink	Up to 10 Mbit/s
Power Bus Interface (Vdc)	18 - 50
Qualification Temperature	-25/+50°C

Table 5.7: ICDE-NG OBC characteristics [7].

5.2.7. TT&C Subsystem

The SBSP system will be equipped with two S-band LGAs for telemetry, tracking and control purposes. For this mission, the Helix Antenna variant of the S-band TTC antennas made by Beyond Gravity has been selected [16]. This type of antenna has been widely used in scientific and telecommunication satellites since the late 1970s, proving its reliability over decades of use. Furthermore, its compact size and low mass make it a suitable choice for the SBSP system. Its frequency bands range from 2000 MHz to 2300 MHz for TC/RX, 2200 MHz to 2300 MHz for TM/TX and 1700 MHz to 2000 MHz for low TC communications. This will ensure sufficient bandwidth for command and telemetry operations.

The selection process for the LGA and HGA is different due to their distinct functions within the SBSP system. The LGA will be a simple helix antenna operating in the S-band, primarily used for low-data-rate TM and TC functions. Helix antennas are standard for this purpose and do not require detailed sizing or gain calculations, as their performance is well-established for these applications. In contrast, the HGA, designed for transmitting high-data-rate communications, requires precise sizing to achieve the necessary gain. As such, its dimensions and characteristics will be determined during the preliminary sizing phase, guided by a link budget analysis. This approach ensures that each antenna is selected appropriately based on its specific role and design considerations. The component characteristics for LGAs have been listed in Table 5.8, alongside the already available information of the HGA.

Next, the SBSP system will integrate two SPREAD SPECTRUM Transponders manufactured by Thales Alenia Space [96]. These transponders offer multi-band functionality, including S- and X-bands, which is required to operate the LGAs and HGA. Each transponder uses approximately 44 W of power and weighs 4 kg and is able to operate at a downlink transmission power of 5 W for S-band and 4 W for X-band and has an uplink bit rate range of of 7.8125 - 128000 bps, downlink does not mention any specific data rates [96]. Hence it is assumed that the transponder supports a downlink of 1 Mbit/s. The required S-band uplink data rate for the SBSP system is assumed to be similar to that of the LRO, which operated at 4 kbps for TM/TC data [29]. The LRO utilized an X-band data rate of up to 100 Mbps for imaging the lunar surface [29]. However, such a high data rate is not necessary for the SBSP system. Instead, the X-band communication for the SBSP design is assumed to require only a fraction of this capacity, with a data rate determined to be 1 Mbps. For the Radio Frequency Distribution Unit (RFDU), unfortunately no specific COTS were found. Therfore, the RFDU characteristics are assumed to give an estimate for the preliminary design. The mass is assumed to be equal to 5 kg, and a volume of 0.005 m^3. Further, it is assumed that the RFDU consumes 20 W of power.

Characteristic	**LGA** [16]	**HGA**	**Transponder** [96]	**RFDU**
Frequency Band	2000 MHz - 2300 MHz	8400 MHz	S-band & X-band	X-band
Mass (kg)	0.235	TBD	4	5
Diameter (mm)	65	TBD	-	-
Dimensions (mm)	h < 289	TBD	150 x 282 x 195	500 x 200 x 50
Power (W)	-	-	44	20

Table 5.8: TTC component characteristics.

5.2.8. Structure Subsystem

The structural design for the SBSP system uses a semi-monocoque architecture, combining an internal frame with skin sheets in the form of sandwich honeycomb panels. At the core of the structure is a hollow structural cylinder made out of a Carbon Fiber Reinforced Polymer (CFRP) and aluminum sandwich structure, similar to the structure developed by Beyond Gravity [17]. This will act as the backbone of the satellite frame, the internal frame. This cylinder extends from the base to the top of the satellite, encompassing the propellant tanks. This configuration allows for a very rigid and stiff structure, allowing for precise pointing accuracy. The skin also consists of a CFRP and aluminum sandwich structure. These panels are attached to the core using similar honeycomb panels, effectively dividing the spacecraft into multiple compartments or sections.

In terms of panel characteristics, the panels come in different shapes and sizes. Therefore, a specific design for a panel will be determined such that its characteristics can be established. Hence, the CFRP density is found to be equal to 1600 kg/m^3. Additionally, the aluminum honeycomb is assumed to have a density of 72 kg/m^3 [10]. With these assumptions, the sandwich panel dimensions and combined density can be computed. In Table 5.9, the characteristics of the honeycomb structure and the CFRP sheet are displayed. With these parameters, the thickness of both the honeycomb structure and the CFRP sheet can be determined. Using both thicknesses, the combined density can be computed to eventually compute the mass of the structure in the preliminary sizing phase.

Characteristic	**Aluminum Honeycomb Panel**	**Carbon Fiber Reinforced Polymer (CFRP)**
Density (kg/m^3)	72 [10]	1600 [51]
Tensile Strength (MPa)	2.5 [65]	3400 [77]
Shear Strength (MPa)	1.4 [65]	
Modulus of Elasticity (GPa)	0.540 [65]	230 [77]
Shear modulus (MPa)	260 [65]	

Table 5.9: Typical characteristics of Aluminum Honeycomb Panels and CFRP structures used in space applications.

5.2.9. Propulsion Subsystem

The propulsion system of the SBSP system will implement four primary mono-propellant thrusters to perform the LLO insertion maneuvers. Out of the four thrusters, two will be operational while the other two will provide redundancy. This setup ensures that in the event of a failure of one or both primary thrusters, the backup thrusters can be activated to complete the insertion maneuvers. Specifically, the MR-107S hydrazine thruster manufactured by Aerojet Rocketdyne has been selected [6]. Each thruster is categorized as a 275 N thruster, however, a single thruster can provide a thrust range of 85 - 360 N. In Table 5.10, the component characteristics of the MR-107S thruster are displayed.

Characteristic	**MR-107S 275N**
Thrust range (N)	85 - 360
Flow rate (g/s)	36.3 - 154.7
Specific Impulse (s)	225 - 236
Mass (kg)	1.01
Valve Power (W)	34.8
Valve Heater Power (W)	4
Cat. Bed Heater Power (W)	13.2
Power Bus Interface (Vdc)	28

Table 5.10: MR-107S Aerojet Rocketdyne characteristics [6].

To ensure no single point of failure in the propellant storage system, two spherical hydrazine mono-propellant tanks will be used. This approach guarantees that if one tank malfunctions, the other propellant tank could still enable a part of the mission-critical burns. Moreover, the two spherical propellant tanks also increase the structural integrity of the whole SBSP system by providing a rigid structure in the middle of the spacecraft. Finally, the propellant tanks will be manufactured using titanium as its

material.

For the pressurization of the hydrazine tanks, the SBSP system uses a single helium pressurant tank. However, rather than adopting full redundancy with a second helium tank, partial redundancy will be implemented through multiple redundant valves. These valves ensure that if one fails, the remaining valves can continue to regulate the flow of helium to maintain the required pressure in the propellant tanks.

5.2.10. Preliminary Power Budget

Table 5.11 outlines the different power phases during the lunar mission for the SBSP system. Each phase corresponds to distinct operational requirements which is reflected in the total power budget of the spacecraft. In total, four phases have been identified and will be further elaborated.

Cruise Phase

The cruise phase begins after the spacecraft is placed into a Trans-Lunar-Injection orbit by the launch vehicle. Next, the spacecraft separates from the launcher and continues its cruise toward the lunar orbit. During this phase, the emphasize lies on maintaining attitude control, thermal management and communication with the Earth ground segment. The solar arrays have been deployed to provide the power during the cruise phase. Simultaneously, subsystems like the PMAD and TCS ensure for proper power distribution and heat rejection. The ADCS, OBC and Propulsion subsystems ensure for the proper spacecraft attitude and the TT&C system ensures for communication with the ground segment. For the TCS power consumption, the assumption is made that running one fluid pump at minimum power is sufficient to operate the subsystem during the cruise phase. Including a 10% margin, the total power consumption during this phase equals 624.4 W. The 10% margin acts as a safety factor, acknowledging the fact that the system is still in its preliminary design phase. Therefore, to ensure sufficient solar array area, the 10% margin is implemented. This phase requires maintaining essential functionality but the spacecraft is largely in a low-power state compared the operational phase.

Insertion Phase

The insertion phase is the phase when the satellite enters the lunar orbit. Particularly, the propulsion system is required to perform the insertion burn to enter the 100 km LLO. This is reflected in the propulsion power consumption. Instead of just providing power to the integrated heaters in the thrusters, the valves also have to be controlled and actuated. Additionally, the TCS subsystem is assumed to operate both fluid pumps at minimum power consumption. Also worth noting is the PMAD power consumption; this is higher compared to the cruise phase which is caused by the assumption made previously regarding the PMAD power consumption. It was determined that the PMAD consumes 2% of the total power consumption, hence the increase in required PMAD power. The insertion phase would require a total of 1198 W of power including the 10% margin.

Operational Phase

The operational phase is the main demonstrating period where the SBSP system will be transmitting power to the lunar receiver via the LPT subsystem. The operational phase is by far the most power-intensive phase, as the satellite is fully engaged in transmitting power and maintaining optimal operating conditions. This is directly noticeable in the power budget as the LPT subsystem consumes 10010 W of power where 10000 W is allocated to the laser system itself and 10 W is used to accurately point the beam director onto the receiver. In order to dissipate all heat to the external environment, the TCS can be required to operate both fluid pumps at maximum power. This results in the TCS subsystem consuming over 900 W of power. Furthermore, in order to accurately point the transmitting beam on the receiver, the satellite itself must also be highly stable during its orbit. Hence, the ADCS subsystem is might be required to fully operate all of its components, including the four reaction wheels at full speed resulting in a total ADCS power consumption of 996 W. The operational phase is predicted to consume a staggering 13671.1 W of power including a 10% margin.

Eclipse Phase
The eclipse phase corresponds to the periods when the satellite is either not transmitting power or is in a lower activity state. This eclipse period can occur when the satellite is located in the shadow of the moon where it must conserve power while maintaining essential functions. The eclipse phase power budget is equal to 1468.6 W where compared to the cruise phase an additional 255 W + 497.1 W is required for the internal heaters and MegaFlex array heaters, respectively.

Subsystem	P_{cruise} (W)	$P_{insertion}$ (W)	$P_{operational}$ (W)	$P_{eclipse}$ (W)
LPT	-	-	10010	-
Solar Arrays	20	20	20	20
PMAD	11.4	21.8	248.6	17.8
TCS	171	342	942	923
ADCS	153.5	153.5	995.9	153.5
OBC	35	35	35	35
TT&C	108	108	108	108
Propulsion	68.8	208	68.8	68.8
Total Power	567.6	1089.1	12428.2	1335.1
+ 10% margin	624.4	1198.0	13671.1	1468.6

Table 5.11: Preliminary Power Budget of a 3 kW SBSP system.

From the four different power budget phases, it can be concluded that the operational phase is the most power-demanding phase as the whole satellite is fully engaged in transmitting power to the lunar receiver. Hence, the MegaFlex solar arrays should be sized according to the power demands of this phase plus the power necessary to charge the onboard Li-ion batteries for when the satellite is experiencing the eclipse period.

5.3. SBSP System Preliminary Sizing

Now that the COTS components for each subsystem have been defined, the satellite can undergo preliminary sizing for its design. Figure 5.4 illustrates the sequence for this sizing process, beginning with the LPT power requirement, also referred to as the payload requirement. This power requirement, combined with the COTS components in Section 5.2 forms the basis of the satellite power budget.

From the power budget, the operational and eclipse modes, together with the maximum eclipse time, will be used to calculate the required battery size resulting in the battery capacity, mass and volume. Next, the MegaFlex solar array area can be determined using the operational power mode and the battery charging requirement, leading to the solar array mass and volume. After computing the solar arrays, it is essential to establish the diameter of the LPT beam director, as this dimension directly influences the size of the receiver on the lunar surface. The optimal configuration for the beam director will be defined in Section 5.3.3.

Once the generated power is determined, the PMAD components can be sized according to the assumptions specified in Section 5.2, resulting in specific mass and volume for each component. Subsequently, the TCS subsystem is sized, taking into account all components requiring active thermal management. This will yield details on the number of cold plates, the characteristics of the active fluid loop and the required radiator mass and dimensions.

Next, constant parameters such as the OBC, ADCS and TTC subsystems will be incorporated into the model. For the TTC subsystem, the dimensions of the HGA will also need to be computed, although this parameters will remain constant when the design is scaled for higher transmission power requirements.

Finally, an initial mass budget will be established which will facilitate the computation of the structural core of the satellite, along with the required mass for propellant, tanks and pressurant gas. These three parameters are all interdependent, requiring some sort of an optimization for these parameters. The outcome will be a preliminary mass budget, along with an preliminary volume budget for the SBSP satellite design.

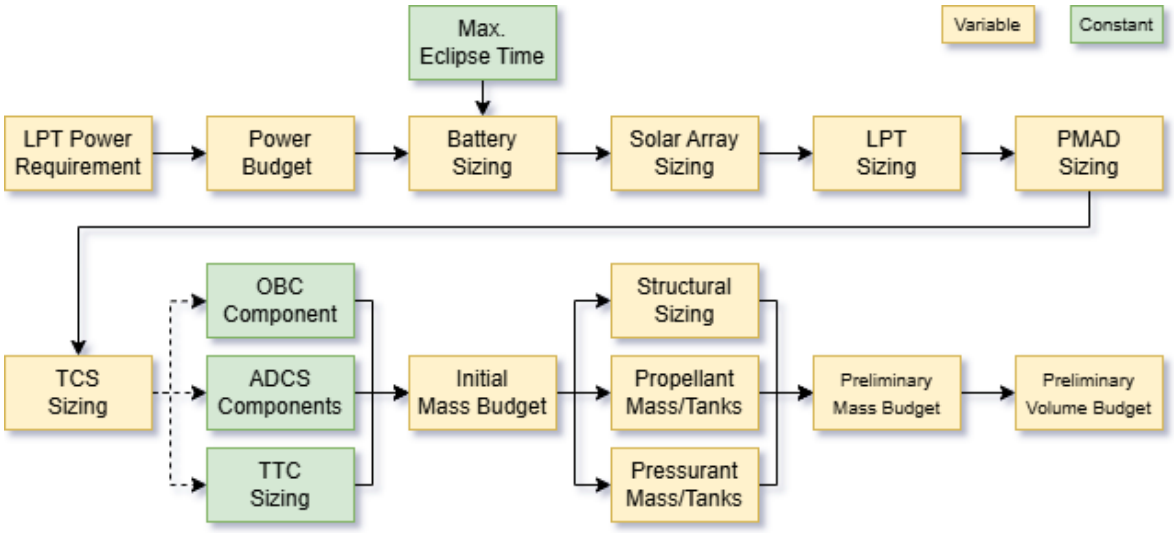

Figure 5.4: Flow diagram for the SBSP preliminary sizing sequence.

5.3.1. Battery Sizing

The purpose of battery sizing in a satellite power system is to ensure adequate energy storage to support satellite operations during eclipse periods when the solar arrays cannot generate power. The sizing process involves calculating the energy required to maintain essential functions during these eclipse periods, taking into account the satellite's eclipse power mode, the duration of the eclipse, and battery efficiency factors such as discharge and charge efficiencies.

Battery Capacity Calculation
To determine the required battery capacity, the energy needed during the eclipse must be calculated first. The required energy, E_{required} in Wh, can be calculated using the eclipse power in watts and eclipse duration in hours:

$$E_{\text{required}} = P_{\text{ecl}} \cdot t_{\text{e}} \tag{5.1}$$

Then, using E_{required} and factoring in the battery discharge and charge efficiencies, the required battery capacity C_{battery}, in Ah, can be expressed as:

$$C_{\text{battery}} = \frac{E_{\text{required}}}{DOD \cdot V_{\text{bat}} \cdot \eta_{\text{discharge}} \cdot \eta_{\text{charge}}} \tag{5.2}$$

Substituting E_{required} from Equation 5.1:

$$C_{\text{battery}} = \frac{P_{\text{ecl}} \cdot t_{\text{e}}}{DOD \cdot V_{\text{bat}} \cdot \eta_{\text{discharge}} \cdot \eta_{\text{charge}}} \tag{5.3}$$

where:

- P_{ecl} is the power consumed by the satellite during eclipse mode, in watts (W), representing the minimum operational power required to maintain critical systems.
- t_{e} is the maximum time the satellite will be in eclipse without solar power, in seconds (s).
- DOD is the allowable depth of discharge, representing the fraction of the battery capacity that can be safely used. Typically kept at 30% to preserve battery life in space applications [108].
- V_{bat} is the total voltage of the battery.
- $\eta_{\text{discharge}}$ is the efficiency of the battery during discharge, accounting for internal losses.
- η_{charge} is the efficiency of the battery during charging, influencing how much energy must be generated to fully recharge the battery.

In this case, P_{ecl} is equal to 1468.6 W. From LRO reference data, the maximum t_e for a LLO of the LRO is found to be approximately 48 minutes [14]. Furthermore, the DOD is assumed to be 30% [108] and V_{bat} is assumed to be 48 V [82]. Finally, $\eta_{\text{discharge}}$ and η_{charge} are both equal to 0.95 according to Table 5.2. Substituting these values in Equation 5.4 results in the following:

$$C_{\text{battery}} = \frac{1468.6 \cdot \frac{48}{60}}{0.3 \cdot 48 \cdot 0.95 \cdot 0.95} = 90.4\,\text{Ah} \tag{5.4}$$

This result indicates that a battery capacity of at least 90.4 Ah is needed to support the satellite power requirements during the eclipse period.

Battery Mass and Volume Sizing
After determining the required battery capacity, it is essential to size the battery in terms of both mass and volume to fit within the structural and mass constraints of the SBSP system. For this calculation, the specific energy (Wh/kg) and energy density (Wh/L) of the battery will be used. First, the total battery capacity has to be converted to watt-hours in order to determine the mass and volume of the batteries. This is done by multiplying the battery capacity with the battery voltage, resulting in a total battery energy of 4339.4 Wh.

The mass of the battery, m_{battery}, is calculated by dividing the required battery energy E_{battery} by the specific energy e_{specific}:

$$m_{\text{battery}} = \frac{E_{\text{battery}}}{e_{\text{specific}}} = \frac{4339.4}{200} = 21.70\,\text{kg} \tag{5.5}$$

Similarly, the volume of the battery, V_{battery}, can be calculated by dividing the required battery energy E_{battery} by the energy density e_{density}:

$$V_{\text{battery}} = \frac{E_{\text{battery}}}{e_{\text{density}}} = \frac{4339.4}{200} = 21.70\,\text{L} = 0.02170\,\text{m}^3 \tag{5.6}$$

where:

- e_{specific} is the specific energy, equal to 200 Wh/kg [1], which defines the energy storage capacity per unit mass of the battery.
- e_{density} is the energy density, equal to 200 Wh/L [52], which defines the energy storage capacity per unit volume of the battery.

These calculations indicate that the battery must have a mass of approximately 21.70 kg and a volume of 0.02170 m^3 to meet the satellite power requirements during eclipse periods. To meet the redundancy requirement, a fully redundant battery system will be in place. This would indicate that the total battery mass increases to 43.39 kg with a total volume of 0.04339 m^3.

5.3.2. MegaFlex Solar Arrays Sizing

To ensure continuous power availability, the solar array must generate sufficient energy during the sunlight period to support the operations of the SBSP system and recharge the batteries for use during eclipse periods. The sizing of the solar array is done by balancing the energy generated during sunlight with the energy required to meet the satellite load and the energy needed to charge the batteries for eclipse demands. This relationship can be described as follows:

$$P_{\text{SA,eff}} \cdot t_d = \frac{P_{\text{operational}} \cdot t_{\text{beam}}}{\eta_d} + \frac{(P_e - P_{\text{heaters}}) \cdot (t_d - t_{\text{beam}})}{\eta_d} + \frac{P_e \cdot t_e}{\eta_e} \tag{5.7}$$

where:

- t_d and t_e are the durations of the sunlight and eclipse periods, respectively.
- t_{beam} is the time the laser is being transmitted.
- $P_{\text{operational}}$ and P_e represent the power needed during the daylight and eclipse periods, respectively.
- P_{heaters} represent the power that is used during eclipse mode for the heaters, which is subtracted from the eclipse mode to get the idle power budget when in daytime.
- η_d and η_e are the efficiencies of the power system during day and night operations, respectively.

The third term on the right side of Equation 5.7 represents the energy that needs to be stored in the battery to cover the eclipse power consumption. From LRO reference data, the maximum t_e for a 100 km LLO is found to be approximately 48 minutes [14]. Further, the orbital period for a 100 km LLO is 117.8 minutes. Subtracting the maximum eclipse time from this orbital period gives the shortest time in sunlight where t_d equals 69.8 minutes. Furthermore, given a $\pm$ 45 ° beaming angle relative to the surface results in a 2 minute beaming period. Hence, $t_{\text{beam}} = 2\,\text{min}$. Although relatively short, this could give valuable performance parameters regarding the SBSP system.

To ensure the solar array can provide sufficient power during the beaming phase, a minimum required power is established based on the power needed to sustain the laser transmission, shown in Equation 5.14. If Equation 5.7 results in a lower power than the minimum required power, the minimum required power is used for further computations.

$$P_{\text{min}} = \frac{P_{\text{operational}}}{\eta_d} \tag{5.8}$$

Day and Night Efficiency Factors

Daytime and nighttime efficiencies are affected by different system efficiencies. Daytime efficiency η_d reflects the power transfer efficiency from the solar array directly to the subsystems, while nighttime efficiency η_e considers the efficiency losses in battery charging, discharging, and power conversion. These efficiencies are defined as follows [109]:

$$\eta_d = \eta_{\text{power conditioning}} \cdot \eta_{\text{distribution}} \tag{5.9}$$

$$\eta_e = \eta_{\text{power conditioning}} \cdot \eta_{\text{charge}} \cdot \eta_{\text{battery}} \cdot \eta_{\text{discharge}} \cdot \eta_{\text{distribution}} \tag{5.10}$$

where:

- $\eta_{\text{power conditioning}}$ is the efficiency of the power control system that conditions the energy from the solar panels.
- $\eta_{\text{distribution}}$ is the efficiency of the power distribution system.
- η_{charge} and $\eta_{\text{discharge}}$ represent the efficiencies of charging and discharging the battery, respectively.
- η_{battery} is the round-trip efficiency of the battery itself.

When substituting the PMAD efficiencies from Table 5.2 into Equation 5.9 and Equation 5.10, the following daytime and nighttime efficiencies are found:

$$\eta_d = \eta_{SSU} \cdot \eta_{DCSU} \cdot \eta_{MBSU} \cdot \eta_{DDCU} = 0.98 \cdot 0.95 \cdot 0.98 \cdot 0.95 = 0.8668 \tag{5.11}$$

$$\begin{aligned} \eta_e &= \eta_{SSU} \cdot \eta_{DCSU} \cdot \eta_{BCDU} \cdot \eta_{Bat} \cdot \eta_{BCDU} \cdot \eta_{DCSU} \cdot \eta_{MBSU} \cdot \eta_{DDCU} \\ &= 0.98 \cdot 0.95 \cdot 0.95 \cdot 0.95 \cdot 0.95 \cdot 0.95 \cdot 0.98 \cdot 0.95 = 0.706 \end{aligned} \tag{5.12}$$

Finally, to calculate the effective power to be generated by the solar arrays, the parameters in Equation 5.7 are substituted, resulting in:

$$P_{\text{SA,eff}} \cdot 69.8 \cdot 60 = \frac{13671.1 \cdot 2 \cdot 60}{0.8668} + \frac{(1468.6 - 255 - 497.1) \cdot (69.8 - 2) \cdot 60}{0.8668} + \frac{1468.6 \cdot 48 \cdot 60}{0.706} \approx 2685.33\,\text{W} \tag{5.13}$$

and where P_{min} is equal to:

$$P_{\text{min}} = \frac{P_{\text{operational}}}{\eta_d} = \frac{13671.1}{0.8668} \approx 15772\,\text{W}. \tag{5.14}$$

It becomes evident that the computed power in Equation 5.13 is lower than the minimum required power to enable the power transmission. Hence, for the rest of the computations, $P_{\text{min}} = P_{\text{SA}} = 15772\,\text{W}$.

Solar Array Size Calculation

The total array power requirement, $P_{\text{SA,tot}}$, can be calculated using the degradations factors in solar array efficiency due to aging, shadowing, and temperature effects. For a mission lifetime of 1 year, the following is assumed:

- Aging degradation factor, $\eta_{\text{aging}} = 1 - 0.006 \cdot 1 = 0.994$ (0.6% degradation per year) [69],
- Shadowing factor, $\eta_{\text{shadow}} = 0.80$ (20% reduction), this value is rather overestimated to ensure sufficient solar array area is available for the SBSP system.
- Temperature degradation factor, $\eta_{\text{temp}} = 0.98$ (2% reduction), also a conservative estimate (4x) based on general degradation rates in solar panels [13].

The combined degradation factor, η_{degrad}, is:

$$\eta_{\text{degrad}} = \eta_{\text{aging}} \cdot \eta_{\text{shadow}} \cdot \eta_{\text{temp}} = 0.994 \cdot 0.80 \cdot 0.98 = 0.7793$$

Taking into account the degradation factor as well as the solar incidence angle, which for the worst case is assumed to be equal to 45° [41], the effective required power can be expressed as:

$$P_{\text{SA,tot}} = \frac{P_{\text{SA}}}{\eta_{\text{degrad}} \cdot \cos(\theta_{\text{incidence}})} = \frac{15772}{0.7793 \cdot \cos(20)} = 28626.13\,\text{W} \tag{5.15}$$

The solar array area, A_{SA}, is then given by:

$$A_{\text{SA}} = \frac{P_{\text{SA,tot}}}{2 \cdot I_{\text{sun}} \cdot \eta_{\text{SA,BOL}}} = \frac{28626.13}{2 \cdot 1361 \cdot 0.289} = 36.39\,\text{m}^2 \tag{5.16}$$

Including the solar cell efficiency and the degradation factors, the required solar array area is equal to $36.39\,\text{m}^2$, accounting for efficiency losses due to aging, shadowing, and temperature effects.

The MegaFlex array includes a central structural section that does not contain solar cells, which expands the overall diameter of the solar array compared to an ideal circular array without this structural feature. Based on reference data from MegaFlex [62], the structural section is assumed to occupy approximately 14% of the total radius. With this assumption, the required radius for the MegaFlex arrays can be calculated using Equation 5.17. This radius can then act as an initial estimate of the length of the SBSP satellite.

$$R_{\text{SA}} = \sqrt{\frac{A_{\text{SA}}}{\pi(1-0.14)}} = \sqrt{\frac{36.39}{\pi(1-0.14)}} = 3.67\,\text{m} \tag{5.17}$$

The mass of one solar array, m_{SA}, is determined by dividing the generated power $P_{\text{SA,tot}}$ by the specific power of the solar array, p_{specific}, which is given as 100 W/kg:

$$m_{\text{SA}} = \frac{P_{\text{SA,tot}}}{2 \cdot p_{\text{specific}}} = \frac{28626.13}{2 \cdot 100} = 143.1\,\text{kg} \tag{5.18}$$

Similarly, the volume of one solar array, V_{SA}, can be calculated by dividing the generated power $P_{\text{SA,tot}}$ by the specific power density v_{specific} (in kW/m³), which is given as 40 kW/m³:

$$V_{\text{SA}} = \frac{P_{\text{SA,tot}}}{2 \cdot v_{\text{specific}}} = \frac{28.626}{2 \cdot 40} = 0.358\,\text{m}^3 \tag{5.19}$$

In these equations:

- $P_{\text{SA,tot}}$ is the total power generated by the solar array.
- p_{specific} is the specific power (100 W/kg) [59].
- v_{specific} is the specific power density (40 kW/m³) [59].

These formulas provide estimates for the mass and volume of the solar array based on the effective required power output and the specific power and volume characteristics of the MegaFlex array. Note that, for the remainder of the design process, $P_{\text{SA,eff}}$ (the effective power output of the solar arrays) is used, while the total power, $P_{\text{SA,tot}}$ was utilized exclusively to determine the area, mass and volume of the MegaFlex arrays.

5.3.3. LPT Sizing

The Laser Power Transmission (LPT) subsystem will be sized to fit the SBSP satellite design requirements, such that it is capable of delivering the required power from the satellite to the ground receiver on the lunar surface. To ensure system redundancy and reliability, two Laser Assembly Units (LAUs) will be integrated, each containing multiple laser modules. Both the primary and redundant LAUs are designed to support the full power output independently, ensuring that power transmission can continue if one LAU fails.

Number of Laser Modules Required

To determine the total number of laser modules required per LAU to achieve the desired output power of the LPT subsystem, the following formula is used:

$$N = \frac{P_{\text{output}}}{P_{\text{laser}}} \tag{5.20}$$

where:

- P_{output} is the total power output required from each LAU,
- P_{laser} is the output power of a single laser module, determined in Section 5.2.1.

Assuming each LAU must support the maximum output independently, and based on the requirement of **3 kW per LAU**:

$$N = \frac{3000\ \text{W}}{500\ \text{W}} = 6 \tag{5.21}$$

Thus, each LAU will contain **6 laser modules**.

Mass and Volume of the LPT Subsystem
With each laser module having a mass of 20 kg, the mass of one LAU can be calculated as follows:

$$M_{\text{LAU}} = N \cdot M_{\text{laser}} = 6 \cdot 20 = 120\,\text{kg} \tag{5.22}$$

For redundancy, two LAUs are included in the design, resulting in a total laser module mass of:

$$M_{\text{LPT}} = 2 \cdot 120 = 240\,\text{kg} \tag{5.23}$$

The volume of each laser module is calculated using its dimensions (assuming each laser module has a simple rectangular shape):

$$V_{\text{laser}} = l \cdot w \cdot h = 0.5 \cdot 0.1 \cdot 0.1 = 0.005\,\text{m}^3 \tag{5.24}$$

The volume of each LAU, with 6 laser modules, is:

$$V_{\text{LAU}} = N \cdot V_{\text{laser}} = 6 \cdot 0.005 = 0.03\,\text{m}^3 \tag{5.25}$$

With two LAUs in the system, the total volume for the LPT subsystem is:

$$V_{LPT} = 2 \cdot 0.03\ \text{m}^3 = 0.06\ \text{m}^3 \tag{5.26}$$

Beam Director Sizing
The spot size of a laser beam at a given distance is limited by diffraction effects. Light passing through a circular aperture forms a central diffraction pattern (Airy disk) in the far field. The angular half-angle divergence, θ, of this pattern is given by:

$$\theta = 1.22\frac{\lambda}{D_t} \tag{5.27}$$

where λ is the wavelength of the laser and D_t is the diameter of the transmitting aperture. At a distance L from the aperture, the beam radius, r_{spot}, is related to the divergence angle as:

$$r_{\text{spot}} = \theta \cdot L + r_t \tag{5.28}$$

where r_t is the radius of the aperture. The full spot size, D_{spot}, is twice the radius of the beam, giving:

$$D_{\text{spot}} = 2r_{\text{spot}} = D_t + 2 \cdot (1.22\frac{\lambda L}{D_t}) \tag{5.29}$$

To determine the minimum spot size diameter D_{spot}, Equation 5.29 is rewritten as a function of D_t:

$$D_{\text{spot}}(D_t) = D_t + \frac{2.44\lambda L}{D_t}$$

Taking the derivative of $D_{\text{spot}}(D_t)$ with respect to D_t, one gets:

$$\frac{dD_{\text{spot}}}{dD_t} = 1 - \frac{2.44\lambda L}{D_t^2}$$

To find the minimum value, the derivative is set to zero:

$$1 - \frac{2.44\lambda L}{D_t^2} = 0$$

Rearranging gives an equation to find the corresponding diameter of the transmitting aperture:

$$D_t^2 = 2.44\lambda L.$$

To ensure optimal power transmission even when the satellite is at a 45-degree ground visibility angle, the increased transmission distance must be considered. At this angle, the effective distance between the satellite and the receiver is:

$$L_{\text{max}} = \frac{100\,\text{km}}{\cos(45^\circ)} \approx 141\,\text{km} \tag{5.30}$$

Using this adjusted distance, the required beam director diameter, D_t, can be computed:

$$D_t = \sqrt{2.44\lambda L_{\text{max}}} = \sqrt{2.44 \cdot 1064 \cdot 10^{-9} \cdot 141 \cdot 10^3} = 0.606\,\text{m} \tag{5.31}$$

Then, substituting D_t in Equation 5.29 gives:

$$D_{\text{spot}} = 0.606 + \frac{2.44 \cdot 1064 \cdot 10^{-9} \cdot 141 \cdot 10^3}{0.605} = 1.21\,\text{m} \tag{5.32}$$

This value of D_t minimizes D_{spot}, providing the smallest spot size required for the given parameters.

However, thermal constraints must be considered to prevent overheating of the receiver. According to Grandidier et al., a power density of 12 kW/m^2 on the receiver is achievable [38]. Given the transmitted power of 3 kW, this constraint provides a lower limit on the spot size that can be achieved:

$$P_{\text{density}} = \frac{P_{\text{transmitted}}}{A_{spot,min}} \leq 12\,\text{kW/m}^2 \tag{5.33}$$

where $P_{\text{transmitted}}$ is the transmitted power, set to 3 kW, and A_{spot} is the area of the laser spot, which is related to D_{spot} by $A_{spot} = \frac{\pi D_{spot,min}^2}{4}$.
Rearranging for $D_{spot,min}$:

$$D_{spot,min} = \sqrt{\frac{4P_{\text{transmitted}}}{\pi \cdot 12\,\text{kW/m}^2}} \tag{5.34}$$

Substituting $P_{\text{transmitted}} = 3$ kW:

$$D_{spot,min} = \sqrt{\frac{4 \cdot 3}{\pi \cdot 12}} \approx 0.56\,\text{m} \tag{5.35}$$

Therefore, it can be concluded that the computed minimum spot size in Equation 5.32 exceeds the required minimum spot size diameter, confirming the feasibility of transmitting this power onto the receiver.

Beam Director Mass Estimation
The mass of the beam director can be estimated by scaling the mass of an existing Cassegrain telescope with similar structural characteristics. For this analysis, the ASA RC600 Cassegrain telescope, which has a tube mass of 105 kg, serves as the reference model [12]. The ASA RC600 has an aperture diameter of 600 mm.

An increase in output power would necessitate a corresponding increase in the minimum required receiver diameter due to the 12 kW/m² thermal constraint, ensuring sufficient surface area to safely manage and dissipate the additional power density. To scale the mass for a beam director with a different diameter, it is assumed that the mass scales approximately with the square of the diameter, as the mass of the beam director is simplified to $m_{\text{BD}} = 0.25\pi D_{\text{BD}}^2 L\rho$. This relationship can be expressed as:

$$m_{\text{BD}} = m_{\text{ref}} \left(\frac{D_{\text{BD}}}{D_{\text{ref}}} \right)^2 \tag{5.36}$$

where:

- m_{BD} is the estimated mass of the beam director for the required diameter D_{BD},
- m_{ref} is the reference mass, 105 kg for the ASA RC600,
- D_{BD} is the required beam director diameter,
- D_{ref} is the reference diameter, 600 mm for the ASA RC600.

This scaling formula provides an estimate for the beam director mass based on changes in diameter. The assumption is that the structural mass increases proportionally to the area of the beam director, which is reasonable for a telescope assembly where mechanical and structural elements are scaled uniformly. Using this method, the mass of a beam director can be computed with any desired diameter for the LPT system, ensuring an appropriately sized structure without extensive custom mass estimates.

Using the calculated beam director diameter of $D_{\text{BD}} = 0.65\,\text{m}$ from the previous section, it can be substituted into Equation 5.36:

$$m_{\text{BD}} = 105\,\text{kg} \cdot \left(\frac{0.606\,\text{m}}{0.6\,\text{m}}\right)^2 \approx 107\,\text{kg} \tag{5.37}$$

Thus, the estimated mass of the beam director for a diameter of 0.606 m is approximately 107 kg. This method allows for efficient scaling of the beam director mass to meet the specific diameter requirements of the LPT system.

5.3.4. PMAD Sizing

To estimate the mass of each component within the PMAD subsystem, the following general formula is used:

$$M_{\text{component}} = \frac{P_{\text{in,comp}}}{p_{\text{specific}}} \tag{5.38}$$

where:

- $M_{\text{component}}$ is the mass of the component (kg),
- $P_{\text{in,comp}}$ is the input power to the component (W),
- p_{specific} is the specific power of the component (W/kg).

In the SBSP satellite design, there are two distinct power chains, each designed to handle the total power generated by the solar arrays. This redundancy ensures that the PMAD system maintains operational integrity even in the event of a failure in one power chain, thereby enhancing system reliability.

To compute the volume of each component, the density of the component is also considered, which can be expressed as:

$$V_{\text{component}} = \frac{M_{\text{component}}}{\rho_{\text{component}}} \tag{5.39}$$

where:

- $V_{\text{component}}$ is the volume of the component,
- $M_{\text{component}}$ is the mass of the component calculated previously,
- $\rho_{\text{component}}$ is the density of the component.

By applying these formulas, the mass and volume of each PMAD component can be effectively estimated based on the power inputs from the solar arrays. This approach provides a systematic way to size the PMAD subsystem, such that it meets the operational demands of the SBSP system while also accommodating redundancy for enhanced reliability. Table 5.12 shows the results of this sizing method for each PMAD component, including the expected power running through the component. Note, the DCSUs, BCDUs and MBSUs are assumed to be designed for full redundancy capabilities, i.e. each component is capable of taking over the power demand of the other power chain. This results in a total PMAD subsystem mass of 382.1 kg with a corresponding total volume of 1.2231 m^3. Additionally, the maximum heat generated in each component is computed. Again, note that the heat generated by the DCSU, BCDU, MBSU, and DDCUs is only counted once in the total heat loss, as each component's heat corresponds to the scenario where it handles the entire power load through the power chain. Thus, while in operational mode, the PMAD subsystem generates 2205.5 W of heat which must be actively dissipated by the TCS.

Component	Max. Input Power (W)	Max. Heat Loss (W)	Mass (kg)	Volume (m^3)
SSU.01	7886.3	157.73	36.01	0.0795
SSU.02	7886.3	157.73	36.01	0.0795
DCSU.01	15457.14	772.86	34.58	0.0706
DCSU.02	15457.14	772.86*	34.58	0.0706
BCDU.01	2080.24	104.01	9.29	0.0192
BCDU.02	2080.24	104.01*	9.29	0.0192
MBSU.01	14684.3	293.69	67.05	0.148
MBSU.02	14684.3	293.69*	67.05	0.148
DDCU.01	11590.53	579.53	35.55	0.237
DDCU.02	11590.53	579.53*	35.55	0.237
DDCU.03	2800.1	140.0	8.59	0.0573
DDCU.04	2800.1	140.0*	8.59	0.0573
Total	15772	2205.5	382.1	1.2231

Table 5.12: PMAD component sizing results.

During the non-operational phase, the PMAD subsystem generates substantially lower heat loads. As a total of 1578.6 W is required during this phase, the PMAD subsystem generates the following amount of heat:

$$\begin{aligned} Q_{\text{PMAD,ecl}} &= \frac{P_{\text{ecl}}}{\eta_{DDCU} \cdot \eta_{MBSU} \cdot \eta_{DCSU} \cdot \eta_{BCDU}} - P_{\text{ecl}} \\ Q_{\text{PMAD,ecl}} &= \frac{1468.6}{0.95 \cdot 0.98 \cdot 0.95 \cdot 0.95} - 1468.6 = 279.26\,\text{W} \end{aligned} \tag{5.40}$$

Additionally, for the non-operational phase in daylight, the PMAD generates the following heat. The heater powers have been determined during the iterative design process and will be further elaborated in the TCS section.

$$\begin{aligned} Q_{\text{PMAD,non-op}} &= \frac{P_{\text{ecl}} - P_{\text{heaters}}}{\eta_{DDCU} \cdot \eta_{MBSU} \cdot \eta_{DCSU} \cdot \eta_{BCDU}} - (P_{\text{ecl}} - P_{\text{heaters}}) \\ Q_{\text{PMAD,non-op}} &= \frac{1468.6 - 252 - 497.1}{0.95 \cdot 0.98 \cdot 0.95 \cdot 0.95} - (1468.6 - 252 - 497.1) = 117.61\,\text{W} \end{aligned} \tag{5.41}$$

5.3.5. TCS Sizing

This subsection covers the calculations needed to estimate the total heat load in lunar orbit and the required radiator size and active fluid loop size with pumps and cold plates.

Total Heat Load

The total heat load Q_{total} on the satellite is the sum of internal and external heat loads:

$$Q_{\text{total}} = Q_{\text{external}} + Q_{\text{internal}} - Q_{\text{radiated}} \tag{5.42}$$

where:

- Q_{total} is the total heat that the thermal control system must manage (W).
- Q_{external} is the heat absorbed by the satellite from external sources (W).
- Q_{internal} is the heat generated internally by the satellite subsystems (W).
- Q_{radiated} is the heat radiated out into space by the satellite (W).

External Heat Calculation

The exposed area of the satellite bus is assumed to be the diagonal of the spacecraft, which takes the form of a rectangular box with dimensions where the length is L and the width and depth are both $0.6L$, where $L = 3.67\,\text{m}$. This length, L, represents the minimum required dimension to stow the undeployed

MegaFlex arrays on the side of the spacecraft bus. The diagonal of the spacecraft bus results in an exposed area:

$$A_{\text{exposed}} = 2 \cdot 0.6L \cdot \cos(45) \cdot L = 11.43\,\text{m}^2 \tag{5.43}$$

The external heat load Q_{external} is primarily derived from solar radiation, lunar albedo, and planetary infrared (IR) radiation. Each source contributes to the overall absorbed heat.

- **Direct Solar Radiation:** The incident solar flux on a lunar satellite is approximately 1361 W/m^2. The absorbed heat from this radiation depends on the exposed surface area and the absorptivity of the MLI surface material [99].

$$Q_{\text{solar}} = A_{\text{exposed}} \cdot I_{\text{solar}} \cdot \alpha_{\text{surface}} = 11.43 \cdot 1361 \cdot 0.05 = 777.63\,\text{W} \tag{5.44}$$

- **Albedo Radiation:** Albedo heat load is calculated based on the fraction of reflected solar radiation from the lunar surface. For a satellite in LLO around the Moon, this is typically around 33.6 W/m^2[109].

$$Q_{\text{albedo}} = A_{\text{albedo}} \cdot I_{\text{albedo}} \cdot \alpha_{\text{surface}} = (0.6 \cdot 3.67) \cdot (0.6 \cdot 3.67) \cdot 33.6 \cdot 0.05 = 8.15\,\text{W} \tag{5.45}$$

- **Lunar IR Radiation:** During lunar nighttime, the Moon emits IR radiation, which can be absorbed by the satellite. This IR radiation is significantly weaker than solar irradiance but still contributes to the thermal load. The lunar IR radiation in LLO is found to be equal to 423.4 W/m^2 [109].

$$Q_{\text{moon}} = A_{\text{moon}} \cdot I_{\text{moon}} \cdot \alpha_{\text{surface}} = (0.6 \cdot 3.67) \cdot (0.6 \cdot 3.67) \cdot 423.4 \cdot 0.05 = 102.65\,\text{W} \tag{5.46}$$

Combining Q_{solar}, Q_{albedo} and Q_{moon} results in Equation 5.47.

$$Q_{\text{external}} = Q_{\text{solar}} + Q_{\text{albedo}} + Q_{\text{moon}} = 777.63 + 8.15 + 102.65 = 888.43\,\text{W} \tag{5.47}$$

Internal Heat Calculation

The internal heat load Q_{internal} depends on the power consumed by the subsystems in the SBSP system. This heat is generated primarily by electronics, payloads, and power systems. To estimate Q_{internal}, the following equation can be used:

$$Q_{\text{internal}} = \sum_{i=1}^{n} P_{\text{sys},i} \cdot (1 - \eta_{\text{sys},i}) \tag{5.48}$$

where:

- $P_{\text{sys},i}$ is the power consumed by the i-th internal subsystem.
- $\eta_{\text{sys},i}$ is the thermal efficiency of the i-th internal subsystem, representing the fraction of power that is not converted to heat.
- n is the total number of internal subsystems in the satellite.

The most significant contributor to the total internal heat is the LPT system with its 30% efficiency. This causes the LPT subsystem to generate 7 kW of heat during operations. Moreover, the PMAD subsystem also generates significant amounts of heat, amounting to approximately 2.2 kW of heat. Nevertheless, since not enough information on the other individual component efficiencies was available, it is assumed that these subsystems all have an internal efficiency of 70%. Following the operational power budget, the subsystems produce a combined heat of 651 W during operations. Thus, the total internal heat generated by the SBSP system amounts to 9856.44 W of heat during operations.

Radiated Heat Calculation
This section calculates the heat radiated by the satellite into space using the Stefan-Boltzmann law. The amount of heat radiated is determined by the emissivity of the satellite surface, the surface area available for radiation, and the temperature of the radiating surface. The formula for the radiated heat (Q_{radiated}) is given by:

$$Q_{\text{radiated}} = \epsilon \sigma A T^4 \tag{5.49}$$

where:

- ϵ is the emissivity of the satellite surface, for MLI equaling to 0.05 [99],
- σ is the Stefan-Boltzmann constant, equal to 5.67×10^{-8} W/m^{2}K^4,
- A is the radiative surface area of the satellite, in square meters (m^2),
- T is the temperature of the radiating surface, in Kelvin (K).

The volume of the satellite bus is assumed to be $(0.6 \cdot L)^2 \cdot L$, resulting in a total area of $A = 4 \cdot (0.6L \cdot L) + 2 \cdot (0.6L)^2 = 42.02\,\text{m}^2$. Furthermore, the radiating temperature is assumed to be close to ambient temperature, 300 K. Thus, Equation 5.49 becomes:

$$Q_{\text{radiated}} = 0.05 \cdot 5.67 \times 10^{-8} \cdot 42.02 \cdot (300)^4 = 965.03\,\text{W} \tag{5.50}$$

Then, Q_{total} can be computed using Equation 5.42, resulting in:

$$Q_{\text{total}} = 888.43 + 9856.4 - 965.03 = 9779.85\,\text{W} \tag{5.51}$$

Radiator Sizing for Heat Dissipation
To balance the heat absorbed and generated by the satellite, radiators dissipate the excess heat into space. The required radiator area A_{radiator} depends on the total heat load, the desired radiator operating temperature, and the emissivity of the radiator surface. The radiator emissivity is assumed to be equal to 0.95 and the radiator operating temperature is assumed to be equal to 70 °C, or 343 °K [4].

$$A_{\text{radiator}} = \frac{Q_{\text{total}}}{\epsilon_{\text{radiator}} \cdot \sigma \cdot T_{\text{radiator}}^4} = \frac{9779.85}{0.95 \cdot 5.67 \times 10^{-8} \cdot (343)^4} = 14.43\,\text{m}^2 \tag{5.52}$$

where:

- $\epsilon_{\text{radiator}}$ is the emissivity of the radiator ,
- σ is the Stefan-Boltzmann constant (5.67×10^{-8} W/m^{2}K^4),
- T_{radiator} is the operating temperature of the radiator.

To ensure sufficient area for dissipating excess heat under varying operational conditions, the area of 14.43 m^2 is rounded up to 15 m^2. Each radiator panel is designed to be 5 m^2 (with dimensions of 2 m in width and 2.5 m in length), to achieve an optimized panel layout. Given a specific mass of 7 kg/m^2 for the radiator material, the total radiator mass is estimated at 105 kg.

Non-operational Heat Loads
In the non-operational case, the LPT subsystem is not active and does not generate the 7 kW of heat as in the operational case. Additionally, the PMAD subsystem operates at a reduced power load, resulting in a lower heat generation compared to the operational state. To estimate the heat load in the non-operational case, the following equations can be used to compute the total heat load:

$$Q_{\text{int,hot}} = Q_{\text{sub}} + Q_{\text{PMAD,non-op}} = 243.38 + 117.61 = 361\,\text{W} \tag{5.53}$$

$$Q_{\text{int,cold}} = Q_{\text{sub}} + Q_{\text{PMAD,ecl}} = 243.38 + 279.26 = 522.65\,\text{W} \tag{5.54}$$

$$Q_{\text{ext}} + Q_{\text{int}} = Q_{\text{rad}} = \epsilon \sigma A T_{\text{sat}}^4 \tag{5.55}$$

where Q_{ext} is the external heat load, Q_{int} is the internal heat load and Q_{rad} is the heat radiated into space by the satellite. Furthermore, the heat load of the subsystems is determined using the power budget of the eclipse phase and assuming a 70% efficiency in subsystem equipment.

For the hot case (when the satellite is in direct sunlight), the total external heat load will still be dominated by solar radiation, identical to Equation 5.47. The internal heat load is calculated based on the active subsystems, with the LPT system generating no heat and PMAD operating at a reduced power consumption. Following Equation 5.57, the equilibrium temperature of the satellite in the hot case is equal to 320K, or 46.8 °C.

$$T_{\text{sat,hot}} = \sqrt[4]{\frac{Q_{\text{ext}} + Q_{\text{int}}}{\epsilon \sigma A}} = \sqrt[4]{\frac{888.43 + 361}{0.05 \cdot 5.67 \cdot 10^{-8} \cdot 42.02}} = 320\,\text{K} \tag{5.56}$$

For the cold case (during lunar eclipse), the external heat load from solar radiation drops significantly, and only the lunar IR radiation contributes, while the internal heat load, similar to the hot case, is lower due to the reduced power consumption of the subsystems. This results in an equilibrium temperature of 269.16 K, or -3.99 °C.

$$T_{\text{sat,cold}} = \sqrt[4]{\frac{Q_{\text{ext}} + Q_{\text{int}}}{\epsilon \sigma A}} = \sqrt[4]{\frac{102.65 + 522.65}{0.05 \cdot 5.67 \cdot 10^{-8} \cdot 42.02}} = 269.16\,\text{K} \tag{5.57}$$

From these computations, it can be concluded that the satellite does not stay within the operational equilibrium of the most sensitive equipment, in this case the hydrazine propellant (15 - 40 °C [105]) using the MLI material. Therefore, a set of heaters must be implemented in order for the satellite to stay within this temperature range as well as the TCS should be utilized during the hot case to remove excess heat. For an equilibrium temperature of 20 °C, or 293.15 K, the combined power from the heaters should equal:

$$P_{\text{heaters}} = \epsilon \sigma A T_{\text{min}}^4 - Q_{\text{ext}} - Q_{\text{int}} = 0.05 \cdot 5.67 \cdot 10^{-8} \cdot 42.02 \cdot 293.15^4 - 102.65 - 522.65 \approx 255\,\text{W} \tag{5.58}$$

This required heater power is therefore implemented into the power budget, specifically in the eclipse power mode. This feature has affected the battery capacity which on its own affects the required solar panel power and area. Thus, adding these heaters had a snowball effect on the whole satellite design. The heaters have been included in the design since the start as this is the final design from the iterative design process. Additionally, the mass of these heaters are estimated using the typical watt densities of heaters (6 W/cm^2) and the heater weight (2 kg/m^2) [109]. Given the heater power, the heaters will have an area of 42.5 cm^2. Multiplying this area with the heater weight and by 2 for a full redundancy strategy provides the estimated heater mass of $M_{\text{heaters}} = 0.017$ kg.

Non-operational Heat Loads for Solar Arrays

In the non-operational case, the solar arrays are assumed to be thermally isolated from the spacecraft bus, with no significant thermal interactions between the two. Each solar array has a radius of 3.67 m, corresponding to an area of 36.39 m^2. The thermal balance for the solar arrays is analyzed separately to ensure their temperature remains within an acceptable range during both hot and cold cases. The following equations outline the thermal balance:

$$Q_{\text{int,SA}} = Q_{\text{rad,SA}} = \epsilon_{\text{SA}} \sigma A_{\text{SA}} T_{\text{SA}}^4 \tag{5.59}$$

where $Q_{\text{int,SA}}$ is the internal heat generated by the solar panels and $Q_{\text{rad,SA}}$ is the heat radiated into space by the solar arrays. The values of emissivity (ϵ_{SA}) and absorptivity (α_{SA}) are specific to the solar array coating and are assumed to be $\epsilon_{\text{SA}} = 0.80$ and $\alpha_{\text{SA}} = 0.75$ based on typical values for space-grade solar array materials [42].

For the hot case, the solar arrays are exposed to direct solar radiation and 28.9% is converted into usable power. The rest is converted into heat, thus, the external heat load is computed as:

$$Q_{\text{int,SA}} = I_{\text{sun}} A_{\text{SA}} (1 - \eta_{\text{SA}}) = 1361 \cdot 36.39 \cdot (1 - 0.289) = 35213.55\,\text{W} \tag{5.60}$$

The equilibrium temperature for the hot case is then determined using Equation 5.59:

$$T_{\text{SA,hot}} = \sqrt[4]{\frac{Q_{\text{int,SA}}}{\epsilon_{\text{SA}}\sigma \cdot 2A_{\text{SA}}}} = \sqrt[4]{\frac{35213.55}{0.80 \cdot 5.67 \cdot 10^{-8} \cdot 2 \cdot 36.39}} \approx 321.37\,\text{K}\,(48.2\text{C}) \tag{5.61}$$

Note that this is using the total solar array area but in reality the solar array will never fully utilize all its area due to varying solar incidence angles and shadowing effects. Hence, the it is safe to assume that the solar arrays falls within the temperature limits of -150 to 110 °C [105] during operations.

For the cold case, during the lunar eclipse, the solar arrays receive no direct solar radiation. To survive the eclipse period, the solar arrays should be above -200 °C [105]. A safety margin is added such that the minimum required temperature is equal to -180 °C (93.15 °K) . The required heater power to accommodate that temperature is then equal to:

$$Q_{\text{heaters,SA}} = \epsilon_{\text{SA}}\sigma \cdot 2A_{\text{SA}} \cdot T_{\text{SA}}^4 = 0.80 \cdot 5.67 \cdot 10^{-8} \cdot 2 \cdot 36.39 \cdot 93.15^4 = 248.56\,\text{W} \tag{5.62}$$

These results show that the solar arrays experience extreme temperatures in both the hot and cold cases. To maintain the MegaFlex solar arrays, each solar array is equipped with a heater capable of delivering 248.56 W of power. This corresponds to an area of 41.42 cm^2. Adding full redundancy, this adds up to 82.84 cm^2 per MegaFlex array. This corresponds to a heater mass $M_{\text{heater,SA}}$ of 0.0166 kg per array. Double this and one gets 0.033 kg for the total mass in the SBSP system. This additional power requirement is considered in the eclipse power budget and integrated into the overall thermal control subsystem design.

Active Fluid Loop Sizing
The active fluid loop, equipped with mechanical pumps, will be responsible for transporting H-Galden Zt85 fluid to the radiators for heat rejection into space. According to the development by NLR [15], an active fluid loop designed to reject 3 kW of power weighs approximately 45 kg, including piping, fluid pumps, and the coolant itself. For the SBSP system, an estimated heat rejection requirement of 9779.85 W is found. Assuming proportional scaling with the heat load, the mass of the fluid loop can be estimated as follows:

$$M_{\text{FL}} = 2 \cdot \left(\frac{P_{\text{required}}}{P_{\text{base}}}\right) \cdot M_{\text{base}} \tag{5.63}$$

where:

- M_{FL} is the mass of the fluid loop,
- P_{required} is the required heat rejection power,
- P_{base} is the base power of the tested system,
- M_{base} is the mass of the base fluid loop.

In Equation 5.63, the multiplication by two accounts for the two-loop system. This results in a calculated mass for the fluid loop of:

$$M_{\text{FL}} = 2 \cdot \left(\frac{9779.85}{3000}\right) \cdot 45\,\text{kg} = 293.40\,\text{kg} \tag{5.64}$$

Additionally, the power consumption of the fluid pump is estimated to range from 171 W to 471 W, resulting in a total power consumption for the TCS subsystem (considering two fluid loops for redundancy) of approximately 342 W to 942 W.

5.3.6. TT&C Sizing

In this subsection, the gain of the HGA on the satellite is computed to determine its required diameter. The downlink budget is analyzed step-by-step, after which the uplink budget is established using a similar method.

Received Power

To compute the received power P_{R}, first the energy per bit to noise density ratio, $(E_{\mathsf{b}}/N_{\mathsf{o}})_{\text{received}}$, must be determined. This can be done using Equation 5.65, where the combination of $(E_{\mathsf{b}}/N_{\mathsf{o}})_{\text{required}}$ [109], the internal losses of the receiver and a 3 dB link margin are used to compute $(E_{\mathsf{b}}/N_{\mathsf{o}})_{\text{received}}$. The losses from the receiver are estimated to be 1 dB [105]. This results in a $(E_{\mathsf{b}}/N_{\mathsf{o}})_{\text{received}}$ of 5 dB .

$$\left(\frac{E_{\mathsf{b}}}{N_{\mathsf{o}}}\right)_{\text{received}} = \left(\frac{E_{\mathsf{b}}}{N_{\mathsf{o}}}\right)_{\text{required}} - L_{\text{receiver}} + L_{\text{margin}} = 1 - (-1) + 3 = 5\,\text{dB} \tag{5.65}$$

Then, the system noise density can be computed by first estimating the system noise temperature for X-band communications, which is assumed to be equal to 30 K [105]. With Equation 5.66, a system noise density of $N_0 = -183.3$ dBm/Hz is found [105] using the Boltzmann constant k and the system noise temperature T_s.

$$N_0 = 10\log_{10}(kT_s) = -183.3\,\text{dBm/Hz} \tag{5.66}$$

$$P_{\mathsf{R}} = 10\log_{10}\frac{E_{\mathsf{b}}}{N_{\mathsf{o}}}_{\text{received}} + N_{\mathsf{o}} + 10\log_{10}(R) - 10\log_{10}\sin^2\beta \tag{5.67}$$

Using $10\log_{10}\sin^2\beta = -0.6$ dB [105], $R = 1$ Mbps set by the maximum downlink bit rate of the transponder [96], and $N_0 = -183.3$ dBm/Hz, the received power is:

$$P_{\mathsf{R}} = 5 + (-183.3) + 10\log_{10}(1 \cdot 10^6) - (-0.6) = -118.9\,\text{dBm}$$

Free-Space Path Loss

Next, the free-space path loss L_{space} is determined as:

$$L_{\text{space}} = 10\log_{10}\left(\frac{4\pi d}{\lambda}\right)^2 = 10\log_{10}\left(\frac{4\pi \cdot 407000000}{0.0357}\right)^2 = -223.12\,\text{dB} \tag{5.68}$$

For a downlink distance $d = 407000000$ m [109] and wavelength $\lambda = 0.0357$ m (X-band 8.4 GHz), $L_{\text{space}} = -223.12$ dB.

EIRP and HGA Gain

The effective isotropic radiated power (EIRP) is calculated from the received power, path loss, atmospheric loss L_{a}, and ground station gain G_{R}:

$$EIRP = P_{\mathsf{R}} - L_{\text{space}} - L_{\mathsf{a}} - G_{\mathsf{R}} \tag{5.69}$$

Assuming a 10 m ground station antenna with 50% efficiency [105], the ground station antenna gain can be computed using Equation 5.70:

$$G_{\mathsf{R}} = 10\log_{10}\left(\left(\frac{\pi d}{\lambda}\right)^2 \cdot \eta\right) = 10\log_{10}\left(\left(\frac{\pi \cdot 10}{0.0357}\right)^2 \cdot 0.5\right) = 55.88\,\text{dBic} \tag{5.70}$$

Substituting the parameters in Equation 5.69 results in $EIRP = 58.64$ dBm,

$$EIRP = -118.9 - (-223.12) - (-0.3) - 55.88 = 48.64\,\text{dBm}$$

The transmitted power, 4 W, can be converted to dBm using Equation 5.71

$$P_{\mathsf{T}} = 10\log_{10}(P_{\mathsf{T}}) = 10\log_{10}(4000) = 36\,\text{dBm} \tag{5.71}$$

The HGA gain, G_{HGA}, is then computed using Equation 5.72:

$$G_{\text{HGA}} = EIRP - P_{\mathsf{T}} - L_{\mathsf{P}} \tag{5.72}$$

For a transmit power $P_{\mathsf{T}} = 36$ dBm and transmit passive loss $L_{\mathsf{p}} = -2$ dB [105]:

$$G_{\text{HGA}} = 48.64 - 36 - (-2) = 10.62\,\text{dBic}$$

HGA Diameter

Finally, the diameter of the HGA is derived from its gain using [105]:

$$D_{\text{HGA}} = \sqrt{\frac{10^{G_{\text{HGA}}/10}}{\eta}} \cdot \frac{\lambda}{\pi} \tag{5.73}$$

With $G_{\text{R}} = 10.62$, $\eta = 0.5$ (efficiency) and $\lambda = 0.0357$, the diameter of the transmitting antenna is:

$$D_{\text{HGA}} = \sqrt{\frac{10^{\,10.62/10}}{0.5}} \cdot \frac{0.0357}{\pi} = 0.06\,\text{m}$$

Table 5.13 summarizes all relevant parameters of downlink budget into a concise overview. The downlink budget results in a HGA diameter of approximately 0.05 m. Up next is establishing the uplink budget to verify if an 0.05 m diameter is sufficient.

TT&C Downlink Budget	**Value**	**Unit**
Frequency	8.4×10^9	Hz
Wavelength	0.0357	m
Distance (d)	4.07×10^8	m
Data Rate (R)	10^6	bits/s
Satellite Antenna		
Transmitter Power (P_{T})	36	dBm
Transmitter Loss (L_{P})	-2	dB
High-Gain Antenna Gain (G_{HGA})	10.62	dBic
Antenna Diameter (D_{HGA})	0.05	m
Effective Isotropic Radiated Power (EIRP)	48.64	dBm
Propagation Range		
Space Loss (L_{space})	-223.12	dB
Atmospheric Loss (L_{a})	-0.3	dB
Ground Receiver		
Receiver Antenna Diameter (D_{receiver})	10	m
Receiver Efficiency (η_{receiver})	0.5	-
Receiver Antenna Gain (G_{R})	55.88	dBic
Received Power (P_{R})	-118.9	dBm
Data-to-Total Power Ratio	-0.6	dB
System Noise Temperature (T_{s})	30	K
Noise Power Spectral Density (N_{o})	-183.30	dBm/Hz
Received $E_{\text{b}}/N_{\text{o}}$	5.00	dB
Required $E_{\text{b}}/N_{\text{o}}$	1.00	dB
Receiver Loss (L_R)	-1	dB
Link Margin	3	dB

Table 5.13: TT&C Downlink Budget.

Using a similar approach, the receiver antenna (in this case the HGA) can be computed. However, for the uplink budget, the transmitting side will be the ground station and the receiving side will be the satellite. Since this is the uplink budget, a few parameters have changed, listed in Table 5.14. The data rate, R, is equal to 128 kbps [96] as determined by the transponder. Next, it is assumed that the transmitter power has been increased to 20 W, or 43 dBm. Furthermore, the system noise temperature would also be different compared to the downlink budget but accurately estimating this temperature for the uplink budget turned out to be more difficult than expected. Therefore, a rough estimate of 250 K has been implemented, resulting in $N_{\text{o}} = -174.6$ dBm/Hz. Furthermore, the receiver loss and transmitter loss have swapped which affects $(E_{\text{b}}/N_{\text{o}})_{\text{received}}$. For the uplink budget, $(E_{\text{b}}/N_{\text{o}})_{\text{received}}$ equals 6 dB. Table 5.14 shows the full uplink budget for the SBSP system.

Calculating the corresponding receiver antenna gain gives $G_{\text{HGA}} = 7.41$ dBic. To produce such a gain, the diameter of the HGA should be 0.03 m. Thus it can be concluded that the downlink budget is the main driver for the HGA diameter, necessitating a diameter of 0.05 m.

However, the 0.05 m HGA seems too small to be integrated onboard the SBSP system. Hence, the diameter will be increased to 0.25 m. This would allow for easier integration into the SBSP system as well as provide greater performance in terms of signal to noise ratio. To determine the mass of the HGA, an specific antenna mass of 5 kg/m^2 is assumed [109]. Together with the diameter, the mass of the antenna can be estimated by:

$$M_{\text{HGA}} = \rho \cdot 0.25\pi D_{\text{HGA}}^2 = 5 \cdot 0.25\pi \cdot 0.25^2 = 0.245\,\text{kg} \tag{5.74}$$

TT&C Uplink Budget	**Value**	**Unit**
Frequency	8.4×10^9	Hz
Wavelength	0.0357	m
Distance (d)	4.07×10^8	m
Data Rate (R)	128 $\cdot 10^3$	bits/s
Ground Antenna		
Transmitter Power (P_{T})	43	dBm
Transmitter Loss (L_{P})	-1	dB
Ground Antenna Gain (G_{HGA})	55.88	dBic
Antenna Diameter (D_{HGA})	10	m
Effective Isotropic Radiated Power (EIRP)	97.89	dBm
Propagation Range		
Space Loss (L_{space})	-223.12	dB
Atmospheric Loss (L_{a})	-0.3	dB
Satellite Receiver		
Receiver Antenna Gain (G_{R})	7.41	dBic
Receiver Antenna Diameter (D_{HGA})	0.03	m
Receiver Efficiency (η_{HGA})	0.5	-
Received Power (P_{R})	-118.1	dBm
Data-to-Total Power Ratio	-0.6	dB
System Noise Temperature (T_{s}) [105]	250	K
Noise Power Spectral Density (N_{o}) [105]	-174.6	dBm/Hz
Received $E_{\text{b}}/N_{\text{o}}$	6.00	dB
Required $E_{\text{b}}/N_{\text{o}}$	1.00	dB
Receiver Loss (L_R)	-2	dB
Link Margin	3	dB

Table 5.14: TT&C Uplink Budget.

5.3.7. Initial Mass Budget

Given that all subsystems have been sized besides the structure and the propulsion subsystem of the satellite, an initial mass budget can be established to provide an estimate for the structure and propellant mass sizing.

Additionally, mass margins have been added to each component in the subsystems, depicted in Table 5.15. Depending on the maturity of the component, a specific margin has been included. If a component has to be custom designed for the mission, a margin of 20% has been set. If a component is a COTS but requires additional modifications for the specific mission, a 10% margin has been added. Finally, if a component is fully COTS without any modifications, a margin of 5% is implemented.

For the next sizing computations, Equation 5.75 will be used to estimate the SBSP system dry mass. It makes use of the subsystem mass which has already been determined in Table 5.15 as well as the propellant tank masses and the propellant mass. In this equation, it is assumed that tank mass can be subdivided into the tank shell structure mass of both the propellant tank and the pressurant tank plus pressurant gas mass, in this case the mass of the helium.

$$M_{\text{dry}} = M_{\text{sub}} + M_{\text{tank}} + M_{\text{structure}} \tag{5.75}$$

Next, the assumption is made that the M_{tank} and the $M_{\text{structure}}$ are equal to $0.1 \cdot M_{\text{sub}}$. This enables the first estimation of the propellant mass, which is a significant contributor to total satellite mass and is used to size the structural core of the satellite.

Table 5.15: Initial Mass Budget of a 3 kW SBSP system.

Subsystem	Mass (kg)	Margin (%)	Corrected Mass (kg)
Power Generation			
MegaFlex Left	143.1	10	157.45
MegaFlex Right	143.1	10	157.45
Gimbal Left	4.4	10	4.84
Gimbal Right	4.4	10	4.84
LPT			
LAU.1	120	20	144
LAU.2	120	20	144
Beam Director	111	20	133.8
PMAD			
SSU.1	36.01	20	43.21
SSU.2	36.01	20	43.21
DCSU.1	34.58	20	41.50
DCSU.2	34.58	20	41.50
MBSU.1	67.05	20	80.46
MBSU.2	67.05	20	80.46
DDCU.1	35.55	20	42.66
DDCU.2	35.55	20	42.66
DDCU.3	8.59	20	10.31
DDCU.4	8.59	20	10.31
BCDU.1	9.29	20	11.15
BCDU.2	9.29	20	11.15
4 Li-ion Batteries	43.39	10	47.73
TCS			
Active Fluid Loops with Pumps and Cold Plates	293.4	20	352.07
Radiators	105	20	126
Heaters	0.050	20	0.06
ADS			
2 Star Trackers	10.6	5	11.13
4 Coarse Sun Sensors	0.86	5	0.90

Continued on next page...

Table 5.15 continued from previous page: Initial Mass Budget.

Subsystem	Mass (kg)	Margin (%)	Corrected Mass (kg)
2 3-axis FOGs	2.8	5	2.94
ACS			
4 Reaction Wheels	48.48	10	53.33
8 MR-106L Thrusters	4.72	5	4.96
OBC			
ICDE-NG	13.6	10	14.96
TT&C			
1 HGA	0.245	20	0.294
2 LGAs	0.47	5	0.494
2 Transponders	8	10	8.8
1 RFDU	5	20	6
Structure			
Core Structure	**TBD**	20	
Panel Structure	**TBD**	20	
MLI	**TBD**	20	
Propulsion			
4 MR-107S thrusters	4.04	5	4.24
Propellant Mass	**TBD**	2	
2 Titanium Propellant Tanks	**TBD**	20	
Pressurant Gas Mass	**TBD**	20	
1 Helium Pressurant Gas Tank	**TBD**	20	
2 Filters	0.3	10	0.33
2 Isolation Valves	1	10	1.1
2 Pressure Transducers	0.4	10	0.44
2 N2H4 Fill/Drain Valves	0.2	10	0.22
He Fill/Drain Valve	0.1	10	0.11
Tubing & Fittings	2	10	2.2
Brackets	4.6	10	5.06
Thermal Equipment	1.4	10	1.54
Electrical	2.2	10	2.42
Total Subsystem Mass	1581.56		1852.27
Total Dry Mass	**TBD**		
Total Wet Mass	**TBD**		

The initial estimate for both M_{tank} and $M_{\text{structure}}$, equal to $0.1 \cdot M_{\text{sub}}$, results in $M_{\text{tank}} = 185.23\,\text{kg}$ and $M_{\text{structure}} = 185.23\,\text{kg}$. This estimation enables a baseline for sizing the structure and propulsion subsystem. Through an iterative process, the actual structural and propulsion masses are recalculated based on the updated estimates. This iteration continues until the total wet satellite mass converges, such that the estimated and actual values for both the structural and propulsion masses are consistent. The next two subsections cover the results for the structural and propulsion masses after the iterative process.

5.3.8. Structure Sizing

The structural subsystem can be subdivided in the core structure and into the panel structure acting as a secondary structure of the satellite.

The Core Structure

The axial launch loads for common launch vehicles, such as the Falcon 9, are assumed to be equal to $6g$, while the lateral launch loads are assumed to be $1.5g$. Using the total mass of the SBSP system, the axial force experienced by the spacecraft can be calculated using Equation 5.76, and the bending moment caused by lateral loads can be determined using Equation 5.77.

In Equation 5.76, F_{axial} represents the axial force experienced by the spacecraft, M_{sat} is the satellite mass, g is the gravitational acceleration ($9.81\,\text{m/s}^2$), n_{axial} is the axial load factor, and SF is the safety factor, which accounts for design uncertainties and is equal to 1.5. The total satellite mass, derived from the iterative process, corresponds to the total satellite mass in the final solution and is used in the following calculations.

$$F_{\text{axial}} = M_{\text{sat}} \cdot g \cdot n_{\text{axial}} \cdot SF = 4057.42 \cdot 9.81 \cdot 6 \cdot 1.5 = 358230.03\,\text{N} \tag{5.76}$$

In Equation 5.77, M_{lateral} represents the bending moment caused by lateral loads, n_{lateral} is the lateral load factor, and L is the effective length of the satellite structure.

$$M_{\text{lateral}} = M_{\text{sat}} \cdot g \cdot n_{\text{lateral}} \cdot \frac{L}{2} \cdot SF = 4057.42 \cdot 9.81 \cdot 1.5 \cdot \frac{3.67}{2} \cdot 1.5 = 164340.84\,\text{Nm} \tag{5.77}$$

The structural design of the satellite's core must withstand both axial and lateral loads during launch, which are translated into stresses in the primary load-bearing structure. The axial stress, σ_{axial}, combines the contributions from the axial force, F_{axial}, and the bending moment, M_{lateral}, as shown in Equation 5.78. In this equation, A is the cross-sectional area of the structure, I is the moment of inertia, R_{tank} is the average radius of the cylindrical structure, and t_{CFRP} is the thickness of the CFRP material.

$$\sigma_{\text{axial}} = \frac{F_{\text{axial}}}{A} + \frac{M_{\text{lateral}}}{I} = \frac{F_{\text{axial}}}{2\pi R_{\text{tank}} t_{\text{CFRP}}} + \frac{M_{\text{lateral}}}{\pi R_{\text{tank}}^3 t_{\text{CFRP}}} \tag{5.78}$$

The required CFRP thickness, t_{CFRP}, can then be determined by rearranging the stress equation, as expressed in Equation 5.79. This equation ensures that the structure can withstand the maximum stress without failure, where σ_{axial} is the allowable axial stress of the CFRP material. With $R_{\text{tank}} = 0.628\,\text{m}$ and $\sigma_{\text{axial}} = 3400 \cdot 10^6$ Mpa, the thickness of the CFRP sheets can be computed.

$$t_{\text{CFRP}} = \frac{F_{\text{axial}}}{4\pi R_{\text{tank}} \sigma_{\text{axial}}} + \frac{M_{\text{lateral}}}{2\pi R_{\text{tank}}^3 \sigma_{\text{axial}}} = 4.44 \cdot 10^{-5}\,\text{m} = 0.0444\,\text{mm} \tag{5.79}$$

The aluminum honeycomb structure is designed to withstand the lateral forces, F_{lateral}, encountered during the launch sequence. These forces are calculated using Equation 5.80, where M_{sat} is the satellite's mass, g is the gravitational acceleration, n_{lateral} is the lateral load factor, and SF is the applied safety factor to account for design uncertainties.

$$F_{\text{lateral}} = M_{\text{sat}} \cdot g \cdot n_{\text{lateral}} \cdot SF = 4057.42 \cdot 9.81 \cdot 1.5 \cdot 1.5 = 89557.51\,\text{N} \tag{5.80}$$

The lateral force produces a shear stress, τ, in the aluminum honeycomb material, which can be expressed using Equation 5.81. Here, R_{tank} represents the radius of the cylindrical structure, and t_{aluminum} is the thickness of the aluminum honeycomb layer.

$$\tau = \frac{2F_{\text{lateral}}}{2\pi R_{\text{tank}} t_{\text{aluminum}}} \tag{5.81}$$

Rearranging Equation 5.81, the required thickness of the aluminum honeycomb structure can be determined as:

$$t_{\text{aluminum}} = \frac{2F_{\text{lateral}}}{2\pi R_{\text{tank}} \tau} = \frac{2 \cdot 89557.51}{2 \cdot \pi \cdot 0.628 \cdot 1.4 \cdot 10^6} = 0.0324\,\text{m} \tag{5.82}$$

Using the thicknesses of the CFRP sheet and the aluminum honeycomb, the structural core's mass can be computed. Since the radius of the cylindrical structure (R) is significantly larger than the thicknesses (t) of the materials, the area of the CFRP sheets and aluminum honeycomb can be approximated using Equation 5.83. Here, A is the surface area, r is the radius, and t is the material thickness.

$$A = 2\pi r t \tag{5.83}$$

The volume of each material can then be determined by multiplying the surface area by the length of the cylindrical structure (L), as shown in Equation 5.84.

$$V = A \cdot L = 2\pi r t L \tag{5.84}$$

Finally, the mass of each component is calculated by multiplying the volume by the material's density (ρ), as expressed in Equation 5.85.

$$M = V \cdot \rho = 2\pi r t L \cdot \rho \tag{5.85}$$

These equations provide a straightforward approach to determining the mass of the CFRP sheets and the aluminum honeycomb. Substituting the respective material properties from Table 5.9 and dimensions, the total core mass can be accurately estimated. As a result, $M_{\text{core,CFRP}} = 2.11\,\text{kg}$ and $M_{\text{core,Al}} = 34.68\,\text{kg}$. Combining these masses gives $M_{\text{core}} = 36.79\,\text{kg}$

The Skin Panels

The skin panels of the satellite structure are composed of two CFRP sheets sandwiching an aluminum honeycomb core. The satellite has four rectangular sides, each with an area of $0.6L \times L$, and two square sides, each with an area of $(0.6L)^2$, where $L = 3.67\,\text{m}$ represents the length of the satellite. These panels provide structural rigidity and protection for the internal components. The area of the four rectangular sides is computed as:

$$A_{\text{rect}} = (0.6L \cdot L) = 0.6L^2 = 8.08\,\text{m}^2 \tag{5.86}$$

The area of the two square sides is given by:

$$A_{\text{square}} = (0.6L)^2 = 0.36L^2 = 4.85\,\text{m}^2 \tag{5.87}$$

The total area of the skin panels is then:

$$A_{\text{total}} = 4 \cdot A_{\text{rect}} + 2 \cdot A_{\text{square}} = 42.02\,\text{m}^2 \tag{5.88}$$

The volume of the aluminum honeycomb core (V_{Al}) and the CFRP sheets (V_{CFRP}) can be computed using their respective thicknesses (t_{Al} and t_{CFRP}) and the total area of the panels:

$$V_{\text{Al}} = A_{\text{total}} \cdot t_{\text{Al}} \tag{5.89}$$

$$V_{\text{CFRP}} = 2 \cdot A_{\text{total}} \cdot t_{\text{CFRP}} \tag{5.90}$$

The masses of the aluminum honeycomb core (M_{Al}) and the CFRP sheets (M_{CFRP}) are calculated by multiplying the respective volumes by their material densities (ρ_{Al} and ρ_{CFRP}):

$$M_{\text{Al}} = V_{\text{Al}} \cdot \rho_{\text{Al}} = A_{\text{total}} \cdot t_{\text{Al}} \cdot \rho_{\text{Al}} = 42.02 \cdot 0.0324 \cdot 72 = 98.02\,\text{kg} \tag{5.91}$$

$$M_{\text{CFRP}} = V_{\text{CFRP}} \cdot \rho_{\text{CFRP}} = 2 \cdot A_{\text{total}} \cdot t_{\text{CFRP}} \cdot \rho_{\text{CFRP}} = 2 \cdot 42.02 \cdot 4.44 \cdot 10^{-5} \cdot 1600 = 5.97\,\text{kg} \tag{5.92}$$

The total mass of the skin panels is the sum of the masses of the CFRP sheets and the aluminum honeycomb:

$$M_{\text{panels}} = M_{\text{CFRP}} + M_{\text{Al}} = 98.02 + 5.97 = 104.1\,\text{kg} \tag{5.93}$$

Finally, the mass of the MLI material is computed by assuming that the $A_{\text{MLI}} = A_{\text{total}}$. Given the specific weight of the MLI material, $e_{\text{MLI}} = 0.6\,\text{kg/m}^2$, the total mass of the MLI material is equal to 25.21 kg.

Combining the mass of the core structure, the panels and the MLI provides the total structural mass of the SBSP satellite:

$$M_{\text{structure}} = M_{\text{core}} + M_{\text{panels}} + M_{\text{MLI}} = 36.79 + 104.1 + 25.21 = 166.08\,\text{kg} \tag{5.94}$$

5.3.9. Propulsion Sizing

This subsection computes all the parameters related to the propulsion subsystem. First, the delta-V budget for the mission is established. Then, the propellant mass is computed which on its own can be used to compute the propellant tank characteristics. Finally, the pressurant gas mass and tank characteristics can be found.

Delta-V Budget

From the previously flown LRO mission, an accurate delta-V estimation has been established which will be used to compute the required propellant mass [34]. In Table 5.16, the different burns for the LRO has been identified with their corresponding velocity increment plus the EOL burn required for a controlled lunar impact. Furthermore, a margin similar to the LRO mission has been implemented in the delta-V budget. The total velocity increment, $1191\,\text{m/s}$ will serve as an estimation for the trajectory of the SBSP system. Note, the TLI burn is not in this delta-V budget as this maneuver is performed by the launcher vehicle.

Maneuver	ΔV (m/s)
Mid-Course Correction	28
LOI 1	567
LOI 2	185
LOI 3	133
LOI 4	41
Station Keeping	150
EOL	48
Margin	39
Total	**1191**

Table 5.16: Delta-V Budget for the SBSP system.

Propellant Mass Sizing

To determine the required propellant mass (M_{P}), the dry mass of the spacecraft ($M_{\text{dry+margin}}$), the specific impulse of the propulsion system (I_{sp}), the gravitational acceleration constant (g), and the total velocity increment (ΔV) must be considered. The relationship is given by:

$$M_{\text{P}} = M_{\text{dry+margin}} \cdot \left(e^{\frac{\Delta V}{I_{\text{sp}} g}} - 1\right) = 1856.93\,\text{kg} \tag{5.95}$$

For this design, the specific impulse is $I_{\text{sp}} = 225\,\text{s}$, and the total ΔV required is $1191\,\text{m/s}$. After the iterative design process, the dry mass of the spacecraft was determined to be $M_{\text{dry}} = 2163.36\,\text{kg}$. Adding a 20% margin on the dry mass gives $M_{\text{dry+margin}} = 2596.03\,\text{kg}$. Substituting these values into the equation provides the required propellant mass of 1856.93 kg. After adding a 2% margin required by ESA [102], the total propellant mass is equal to 1894.07 kg. Given a density of 1004 kg/m^3, the propellant volume is equal to 1.887 m^3. An additional 10% margin has been used to account for the ullage volume in the propellant tank, resulting in a total propellant tank volume of 2.075 m^3 [102].

For redundancy reasons, the total propellant tank volume is split into two separate tanks, resulting each tank having a volume of 1.038 m^3. Next, the radius of the propellant tank can be computed using:

$$R_{\text{tank}} = \left(\frac{3V}{4\pi}\right)^{\frac{1}{3}} = 0.628\,\text{m} \tag{5.96}$$

The thickness of a spherical tank, t_{tank}, can be computed using the following relation:

$$t_{\text{tank}} = \frac{P_{\text{prop}} \cdot R_{\text{tank}}}{2\sigma_{\text{titanium}}} \cdot SF = \frac{22 \cdot 10^5 \cdot 0.628}{2 \cdot 1380 \cdot 10^6} \cdot 1.5 = 0.000751\,\text{m} = 0.751\,\text{mm} \tag{5.97}$$

where $P_{\text{prop}} = 22\,\text{bar}$ is the internal pressure, R_{tank} is the radius of the tank, and $\sigma_{\text{titanium}} = 1380\,\text{Mpa}$ is the yield strength of the tank material. Next, using the thin-walled assumption, the volume of each tank, V_{tank}, can be computed with:

$$V_{\text{tank}} \approx 4\pi R_{\text{tank}}^2 t_{\text{tank}} \approx 0.003722\,\text{m}^3 \tag{5.98}$$

Using the density of titanium, $\rho_{\text{titanium}} = 4550\,\text{kg/m}^3$, the mass of the propellant tanks can be calculated. This results in two propellant tanks, each with a mass of 16.93 kg.

Pressurant Gas Sizing

The helium pressurant gas will be stored at 140 bar and the propellant at 22 bar. Furthermore, the storage temperature of the helium is assumed to be 298 K. The specific gas constant of helium is equal to 2077.1 J/kg K [98] and the specific heat ratio for helium has been found as 1.66 [97].

$$M_{\text{gas}} = \frac{P_{\text{tank}} \cdot V_{\text{tank}}}{R \cdot T_{\text{i}}} \cdot \frac{\gamma}{1 - \frac{P_{\text{f}}}{P_{\text{i}}}} = 7.26\,\text{kg} \tag{5.99}$$

Adding a 20% margin, the pressurant gas mass is equal to 8.72 kg. To calculate the volume of the helium gas, n_{helium} is calculated using the molecular weight of helium, $M_{\text{helium}} = 4.0026\,\text{g/mol}$.

$$n_{\text{helium}} = \frac{M_{\text{gas}}}{M_{\text{helium}}} = \frac{8720}{4.0026} \approx 2177.54\,\text{mol} \tag{5.100}$$

With n_{helium} known, the volume of the helium gas can be computed using the ideal gas law:

$$V = \frac{nRT}{P} = \frac{2177.54 \cdot 8.314 \cdot 298}{140 \cdot 10^5} = 0.3854\,\text{m}^3 \tag{5.101}$$

For the pressurant gas tank, a 30% margin has been considered for the ullage volume [102]. This is to ensure enough volume is available for the gas and that explosive hazards regarding the pressurant tank are mitigated. Hence, the volume of the pressurant gas tank is equal to $V_{\text{tank,he}} = 0.5010\,\text{m}^3$. Substituting this value into Equation 5.96, a pressurant gas tank radius of 0.493 m is found. Next, a 140 bar tank pressure corresponds to the following pressurant gas tank thickness:

$$t_{\text{tank,he}} = \frac{P_{\text{he}} \cdot R_{\text{tank,he}}}{2\sigma_{\text{titanium}}} \cdot SF = \frac{140 \cdot 10^5 \cdot 0.493}{2 \cdot 1380 \cdot 10^6} \cdot 1.5 = 0.003749\,\text{m} = 3.749\,\text{mm} \tag{5.102}$$

Lastly, to compute the volume of the spherical pressurant gas tank, Equation 5.98 can be used, resulting in a pressurant tank structure volume of 0.01144 m^3. Multiplying by the density of titanium gives the pressurant tank mass, $M_{\text{tank,he}} = 52.03\,\text{kg}$. Thus, the total mass of the combined tanks plus the pressurant gas mass is equal to $M_{tank} = 93.16\,\text{kg}$.

5.3.10. Preliminary Mass Budget

The preliminary mass budget is established after the iterative design process of the structural, propellant and tank masses. In Table 5.17, the finalized preliminary mass budget is depicted. The SBSP system will have a wet mass, including margins, of 4057.42 kg where 1894.07 kg is dedicated to the hydrazine propellant.

The LPT subsystem, also classified as the payload of the satellite, can be used to define the payload mass fraction. For the LPT subsystem capable of transmitting 3 kW of power, a payload mass fraction of 10.4% is established. Furthermore, the propellant mass fraction is equal to 46.7% of the total satellite mass.

Table 5.17: Preliminary Mass Budget of a 3 kW SBSP system.

Subsystem	Mass (kg)	Margin (%)	Corrected Mass (kg)
Power Generation			
MegaFlex Left	143.1	10	157.45
MegaFlex Right	143.1	10	157.45
Gimbal Left	4.4	10	4.84
Gimbal Right	4.4	10	4.84
LPT			
LAU.1	120	20	144
LAU.2	120	20	144
Beam Director	111	20	133.8
PMAD			
SSU.1	36.01	20	43.21
SSU.2	36.01	20	43.21
DCSU.1	34.58	20	41.50
DCSU.2	34.58	20	41.50
MBSU.1	67.05	20	80.46
MBSU.2	67.05	20	80.46
DDCU.1	35.55	20	42.66
DDCU.2	35.55	20	42.66
DDCU.3	8.59	20	10.31
DDCU.4	8.59	20	10.31
BCDU.1	9.29	20	11.15
BCDU.2	9.29	20	11.15
4 Li-ion Batteries	43.39	10	47.73
TCS			
Active Fluid Loops with Pumps and Cold Plates	293.4	20	352.07
Radiators	105	20	126
Heaters	0.050	20	0.06
ADS			
2 Star Trackers	10.6	5	11.13
4 Coarse Sun Sensors	0.86	5	0.90
2 3-axis FOGs	2.8	5	2.94
ACS			
4 Reaction Wheels	48.48	10	53.33
8 MR-106L Thrusters	4.72	5	4.96
OBC			
ICDE-NG	13.6	10	14.96
TT&C			
1 HGA	0.245	20	0.294
2 LGAs	0.47	5	0.494
2 Transponders	8	10	8.8
1 RFDU	5	20	6
Structure			
Core Structure	36.79	20	44.15
Panel Structure	104.07	20	124.89
MLI	25.21	20	30.26
Propulsion			
4 MR-107S thrusters	4.04	5	4.24
Propellant Mass	1856.93	2	1894.07
2 Titanium Propellant Tanks	33.87	20	40.64
Pressurant Gas Mass	7.26	20	8.72
1 Helium Pressurant Gas Tank	52.03	20	62.44

Continued on next page...

Table 5.17 continued from previous page: Preliminary Mass Budget.

Subsystem	Mass (kg)	Margin (%)	Corrected Mass (kg)
2 Filters	0.3	10	0.33
2 Isolation Valves	1	10	1.1
2 Pressure Transducers	0.4	10	0.44
2 N2H4 Fill/Drain Valves	0.2	10	0.22
He Fill/Drain Valve	0.1	10	0.11
Tubing & Fittings	2	10	2.2
Brackets	4.6	10	5.06
Thermal Equipment	1.4	10	1.54
Electrical	2.2	10	2.42
Total Subsystem Mass	1581.56		1852.27
Total Dry Mass	2163.36	20	2596.03
Total Wet Mass	3697.73		4057.43

In Figure 5.5, a pie chart is presented, which offers a clearer visualization of the subsystem percentages relative to the total satellite mass. It can be concluded that the propulsion subsystem constitutes to the largest portion of the mass budget at 49.9%, followed by the PMAD, TCS and LPT subsystems. This outcome is reasonable, as the PMAD, TCS and LPT subsystems play important roles in supporting the critical function of power transmission.

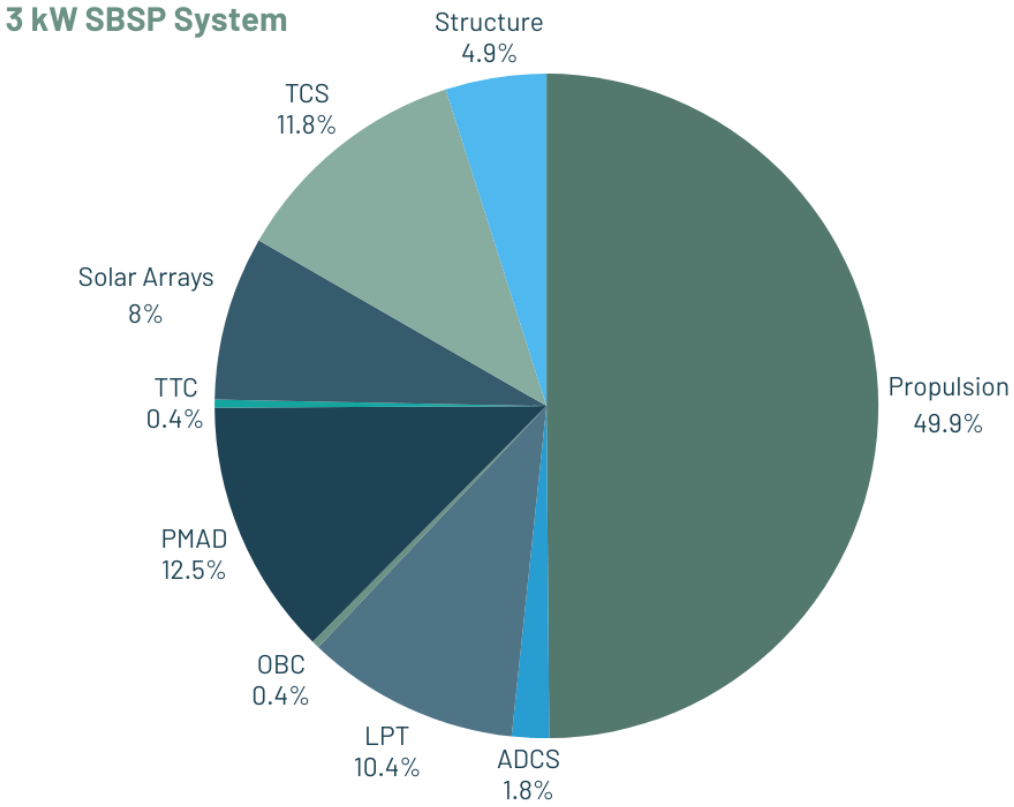

Figure 5.5: Subsystem mass percentages for a 3 kW SBSP system.

5.3.11. Preliminary Volume Budget

The preliminary volume budget for the 3 kW SBSP system gives an estimate of the internal and external volumes for each subsystem. Most component volumes have been determined via the specified data of the COTS manufacturers but others required some computations. Notably, the beam director volume was approximated by multiplying the area of its aperture by its length, giving a reasonable estimate for the volume budget. Similarly, the HGA volume is computed by multiplying the area of the dish by its thickness, resulting again in an approximation of the HGA volume.

However, some component volumes could not be accurately estimated. The active fluid loop did not have any detailed information regarding its volume, including pumps and cold plates. This made the estimation difficult and to mitigate this, the spacecraft bus volume was rather over-designed to accommodate the TCS thermal loop volume. After the 3D model was established, it turned out that sufficient volume was available, reducing the risk of the TCS not fitting in the spacecraft bus.

Secondly, the gimbals did not have any reliable data regarding the gimbal volumes. Nevertheless, their relatively small size indicates that their exclusion as a relatively small impact on the overall design. Next, the MLI volume was also not computed due to the variety of MLI configurations. Since MLI layers are very thin and flexible, their impact on the spacecraft bus's volumetric constraints was deemed negligible. Finally, the individual components of the propulsion hardware were not estimated. However, sufficient space has been left within the spacecraft to accommodate these components. The specific volumes will have to be verified during the detailed design phase.

Table 5.18: Preliminary Volume Budget of a 3 kW SBSP system.

Subsystem	Internal Volume (m^3)	External Volume (m^3)
Power Generation		
MegaFlex Left	-	0.358
MegaFlex Right	-	0.358
Gimbal Left	unknown	-
Gimbal Right	unknown	-
LPT		
LAU.1	0.03	-
LAU.2	0.03	-
Beam Director	-	0.2019
PMAD		
SSU.1	0.0795	-
SSU.2	0.0795	-
DCSU.1	0.0706	-
DCSU.2	0.0706	-
MBSU.1	0.1480	-
MBSU.2	0.1480	-
DDCU.1	0.2370	-
DDCU.2	0.2370	-
DDCU.3	0.0573	-
DDCU.4	0.0573	-
BCDU.1	0.0192	-
BCDU.2	0.0192	-
4 Li-ion Batteries	0.04339	-
TCS		
Active Fluid Loops with Pumps and Cold Plates	unknown	-
Radiators	-	0.375
Heaters	unknown	-
ADS		
2 Star Trackers	0.0756	-
4 Coarse Sun Sensors		0.0015

Continued on next page...

Table 5.18 continued from previous page: Preliminary Volume Budget.

Subsystem	Internal Volume (m^3)	External Volume (m^3)
2 3-axis FOGs	0.002	-
ACS		
4 Reaction Wheels	0.1700	-
8 MR-106L Thrusters	-	0.0013
OBC		
ICDE-NG	0.0195	-
TT&C		
1 HGA	-	0.0002
2 LGAs	-	0.002
2 Transponders	0.0164	-
1 RFDU	0.005	-
Structure		
Core Structure	0.4843	-
Panel Structure	-	1.366
MLI	-	unknown
Propulsion		
4 MR-107S thrusters	-	0.0029
Propellant Mass	2.08	-
2 Titanium Propellant Tanks	0.01	-
Pressurant Gas Mass	0.39	-
1 Helium Pressurant Gas Tank	0.011	-
Propulsion Hardware	unknown	-
Total SBSP Volume	4.579	2.667

The total internal volume of the SBSP system is 4.579 m^3, with an external volume of 2.667 m^3. Given that the spacecraft bus has an internal volume of $3.67 \cdot 2.20 \cdot 2.20 = 17.80\,m^3$, the current design leaves a significant portion of the volume unused within the bus. Even considering the unknowns in the volume budget it is safe to say that this design is rather inefficient in terms of volume.

Future work should focus on reiterating the spacecraft bus size, when more accurate data becomes available on the volumes of the active fluid loop, propulsion hardware and other miscellaneous components (electrical and data wiring). This will ensure the design is optimized for volume, which could save significant mass and cost.

5.3.12. ADCS Verification

The verification of the ADCS ensures that the thrusters are capable momentum management. The following approach was adopted to validate the system's performance:

Reaction Wheel Momentum Dumping Capability

The maximum angular momentum stored in the reaction wheels, $H_{\text{max}} = 45\,\text{Nms}$ per wheel, requires momentum dumping via the ADCS thrusters. Preliminary analysis was conducted assuming:

- Torque arm: $d = 1.83\,\text{m}$ (half the satellite length) or $d = 1.1\,\text{m}$ (half the satellite width).
- Thruster capability: $F = 10\,\text{to}\,34\,\text{N}$ per thruster.

Using two thrusters for a burn indicates that a minimum thrust of two times 10 N is possible along an arm of 1.83 m, resulting in a moment of 36.6 Nm. To dump the maximum momentum of one wheel, the thruster would need to burn for 1.22 seconds. For the shorter arm, namely $d = 0.5 \cdot 2.20 = 1.1\,\text{m}$, a burn time of 2.05 seconds is required to dump the maximum momentum stored in one wheel. Thus it can be confirmed that the 22 N thrusters, when operated in pairs, are sufficient for the momentum dumping process. To dump the momentum stored in all reaction wheels, the combined ADCS thrusters will have to burn three times as long.

5.4. Model Verification

To validate the accuracy and reliability of the developed system sizing model, a comparison was made against another lunar SBSP concept designed by Cougnet et al. to output 40 kW of power [25]. The laser transmission system of the reference system was composed of 4 Nd-Yag lasers, each able to output 10 kW. As a result, the reference system is reported to have a total mass of 25 tons. Initially, when given the power requirement of 40 kW, the model gave a total system mass of 52 tons. The primary reason for this significant mass difference is due to the differences in the orbital assumptions. The 40 kW SBSP concept is designed to be stationed in the Moon's L2 location and traveling to this point requires substantially less ΔV than a 100 km LLO. To reach the Earth Moon L2 point, a ΔV of roughly 350 m/s is assumed. After revising the model to account for this change in ΔV requirement, the estimated system mass was reduced to approximately 33.8 tons. Then, the model computes a more reasonable result compared to the reference system with a difference of 35.2% which could be the result of the usage of different margins in the design.

Table 5.19 compares system characteristics of the reference SBSP system with the outputs of the model. While the outputs of the model align reasonably well with the reference SBSP system, certain differences are observed.

Characteristic	Reference SBSP	Model Output
Total Mass (tons)	25	33.8
Solar Array Area (m^2)	720	930.2
Total Generated Power (kW)	285	202
Radiator Area (m^2)	480	188
Total System Efficiency (%)	14.2	19.8

Table 5.19: Characteristics of the reference SBSP and the model output.

The total mass predicted by the model is 33.8 tons, compared to 25 tons for the reference system. This difference in mass can be attributed to differences in assumptions regarding subsystem architectures. For instance, the reference system might make use of a more advanced PMAD subsystem with a reduced mass. The model uses a PMAD architecture that has been developed for the ISS and is relatively outdated. It is possible that the designers of the reference SBSP system have included a more optimized PMAD subsystem. However, no additional information on the mass budget can be found to confirm this hypothesis.

The solar array areas are very similar, with the reference system using 720 m^2 and the model outputting 930.2 m^2. The difference in numbers can most likely be explained because of the various assumptions that have been included in computing the solar array area. The model takes into account shadow factors, temperature factors, solar cell degradation and a maximum incidence angle of 45°. It is hard to tell whether or not the reference design has employed similar margins. What can be stated is that the efficiency of the solar cells are different. Notably, the reference model uses solar panels with a 12.3% efficiency whereas the model uses the MegaFlex arrays with an efficiency of 28.9%.

For the radiator area, the model estimates a required area of 188 m^2, significantly lower than the reference value of 480 m^2. This difference is due to the reference design including individual radiators for each laser module, each sized at 120 m^2, most likely for redundancy purposes. In contrast, the model only accounts for the required radiator area with a safety factor, assuming it is a passive device integrated with an active fluid loop for heat dissipation.

The total system efficiency differs as well. The reference system efficiency is stated as 14.2%. With including the receiver efficiency of 50%, the true end-to-end system efficiency of the reference SBSP system is 7.1%. The efficiency of the model, calculated without the receiver, is 19.8%, reflecting its higher performance in thermal management and power conversion.
Concluding, when comparing the model outputs with the reference system, they show reasonable agreement. The differences highlight the impact of varying design assumptions and subsystem redundancy considerations.

5.5. SBSP System Scalability

This section addresses the SBSP system scalability by analyzing the numerous SBSP configurations in Table 5.20. The comparison includes systems ranging from a 3 kW demonstration mission to a 100 kW operational system with a lifetime of 5 years. These configurations can be used to address the progression of system characteristics and design requirements as power and operational needs increase.

5.5.1. Overview of Scalability Parameters

The scalability of the SBSP system is driven by specific parameters such as mass, solar array and radiator area, satellite dimensions and operational lifetimes. Scaling the power output requirement requires larger solar arrays, radiators which impacts the dry mass and total mass of the SBSP system. The results below, computed with the SBSP model, demonstrate how these parameters evolve to support higher power outputs and longer mission durations.

Characteristic	3 kW 1Y	10 kW 1Y	10 kW 5Y	45 kW 5Y	100 kW 1Y	100 kW 5Y
Dry Mass (tons)	2.60	7.52	8.04	41.77	86.11	98.76
Total Mass (tons)	4.06	11.77	16.95	98.36	145.10	232.54
Solar Array Area (m^2)	72.78	225.62	231.12	1071.54	2320	2377.14
Satellite Length (m)	3.67	6.46	6.54	14.08	20.72	20.97
Total Generated Power (kW)	15.77	48.90	48.90	226.69	502.90	502.90
Radiator Area (m^2)	15	47	47	211	468	468
Operational Lifetime (year)	1	1	5	5	1	5
Total System Efficiency (%)	19.0	20.5	20.5	19.9	19.9	19.9
Specific Power (W/kg)	0.74	0.85	0.59	0.46	0.69	0.43

Table 5.20: Characteristics of the 3 kW, 10 kW, 45 kW and 100 kW SBSP system.

5.5.2. Mass and Propulsion Scalability

Increasing the power output directly influences a significant rise in the dry mass of the SBSP system. Since the LPT subsystem is scaled to meet the required output power, other subsystems must be scaled to support the higher power transmission requirements. For example, scaling from 3 kW to 100 kW requires more laser output power, which in its turn, demands larger MegaFlex arrays, PMAD and TCS subsystems. This is clearly seen in the dry mass increase from 2.60 tons for the 3 kW system to 86.11 tons for the 100 kW system.

The increased dry mass leads to the need for more propellant mass to achieve and maintain the desired orbit, which further requires larger propellant tanks and structural mass. The increase in propellant mass can be evidently seen when comparing the 3 kW system with the 100 kW system. The total mass grows from 4.06 tons for the 3 kW system to 145.10 tons for the 100 kW system.

Additionally, the increased SBSP system mass requires the scaling of other COTS components, such as the propulsion thrusters and the ADCS reaction wheels, to achieve similar performance with the higher system mass. For instance, the propulsion thrusters have been upgraded to the MR-80B thrusters [6], providing a thrust range of 31 to 3603 N for inserting the SBSP system into the 100 km LLO. Similarly, larger and more power-demanding reaction wheels are required to maintain attitude control for the expanded SBSP system. For this computation it is assumed that the reaction wheels scale linearly with the SBSP output power. These changes are all reflected in the increased dry mass and total mass of the satellite in Table 5.20.

5.5.3. Mission Duration Considerations

The mission duration of the demonstration mission was determined to be one year. This would allow for sufficient time to demonstrate and test the SBSP system in a realistic lunar environment. However, the mission lifetime of operational SBSP systems are expected to be much longer than one year. Therefore, two SBSP systems have been computed given a five year mission duration by substituting the ΔV for station-keeping for a five year mission. In Table 5.20 the total mass of the 100 kW system with a one year mission is equal to 145.10 tons. When extending the mission to five years, the total mass of the 100 kW system increases to 232.54 tons. The primary reason is the increased propellant mass which in its turn increases the propellant tank mass and the structural mass of the SBSP system. Furthermore, the increased mission duration will also increase the degradation in the solar arrays, requiring larger MegaFlex arrays. This is also reflected in the dry mass of the system.

5.5.4. System Efficiency and Specific Power

The total system efficiency, defined as the output power divided by the total generated power, improves slightly when increasing the output power of the SBSP system. From 19.0% for the 3 kW system to 19.9% for the 100 kW system. However, the specific power, defined as the output power divided by the total system mass, decreases for larger systems, with the highest value of 0.85 W/kg for the 10 kW system and the lowest of 0.43 W/kg for the 100 kW 5-year system. This decline is mostly the result of the increased mass of the subsystems which scale disproportionally compared to the output power. This highlights the trade-off between scalability and efficiency and emphasizes the need for investigating the possibility of deploying numerous lower output power SBSP systems to meet the high power demand for future lunar habitats.

5.5.5. Feasibility of Large-Scale Systems

The feasibility of the SBSP systems, specifically large-scale systems, depends on several factors. First, the SBSP system should lie within the payload constraints of existing or potential future launchers. Existing launchers such as the Falcon Heavy or the Ariane 6 could potentially launch SBSP systems up to 10 kW in a trans-lunar injection orbit (TLI). Specific details on the maximum payload capacity of the Falcon Heavy for TLI are not readily available. However, the Falcon Heavy can carry 16.8 tons to Trans Mars Injection (TMI) [89]. Since TLI requires less ΔV than TMI, the Falcon Heavy can be expected to carry at least 16.8 tons to TLI. However, the 45 kW SBSP system with a five year mission duration is too heavy for either the Falcon Heavy or the Ariane 6. Hence, an alternative launch solution must be found. As of now, Starship is still in development by SpaceX but is in the future supposedly capable of launching 100 tons to the lunar surface [90]. This would indicate that the 45 kW SBSP system, at 98.36 tons, falls within Starship's payload requirement. In terms of length, the satellites should also fit in the payload bay given a payload bay length of 18 meters [30]. Both 100 kW systems are too heavy to fit in any launchers, making it difficult to enable the deployment of these SBSP systems.

Secondly, the fact that larger systems have a diminishing return in mass-efficiency suggests that while larger SBSP systems enable higher power outputs, their reduced specific power raises challenges for efficient deployment and transportation to the lunar orbit. Large-scale SBSP systems not only increase launch costs but also demand more robust propulsion, ADCS and structural systems in order to support the satellite operations. Hence, the potential deployment of numerous lower-output SBSP systems can act as an alternative solution. Multiple 3 kW or 10 kW systems could reduce the overall mass and cost per kW of power delivered. Additionally, a distributed network of smaller SBSP satellites could provide redundancy and greater flexibility which may be advantageous for sustaining future lunar habitats.

However, the feasibility of deploying a fleet of SBSP systems must take into account the complexity of managing such a constellation around the Moon. Given that the power transmission starts at a 45 ° angle, a minimum of 60 satellites are required to enable a continuous power supply and for redundancy purposes, 60+ satellites are advised such that the power transmission phases overlap, mitigating any potential power outages. Future studies should investigate the optimal balance between constellation size, scalability, cost and efficiency to address the high-power demands for lunar habitats.

5.6. 3D CAD Model

This section provides a series of visualizations of the SBSP system design created in AutoCAD. These visualizations, including isometric, front and back internal views are intended to illustrate the general layout and integration of the subsystems. It should be noted that the design is purely conceptual and represents a visualization of the system architecture rather than a fully functional SBSP system. As such, the model does not include detailed deployment mechanisms, and other detailed features such as wiring, pipes and valves.

5.6.1. Isometric Top View

In Figure 5.6, the two prominent MegaFlex arrays are clearly visible, extending outward to convert sun light into power. Between the arrays lies the spacecraft bus where all essential equipment and subsystems are stored. On the top left front panel, a yellow component can be seen. This is a Coarse Sun Sensor part of the ADCS subsystem. The top panel features four propulsion thrusters used for the insertion burn to achieve LLO. A small black circular component on the top panel marks the location of the Star Tracker, for precise attitude determination, while the red component is one of the two LGAs onboard the SBSP system.

At the bottom of the system, the beam director is positioned such that it can direct the transmitted beam onto the lunar receiver. Also, another LGA is located on the bottom side, close to the edge to avoid physical interference with the beam director. Additionally, ADCS thrusters are distributed along the bottom edges. This allows for proper control and orientation during operations.

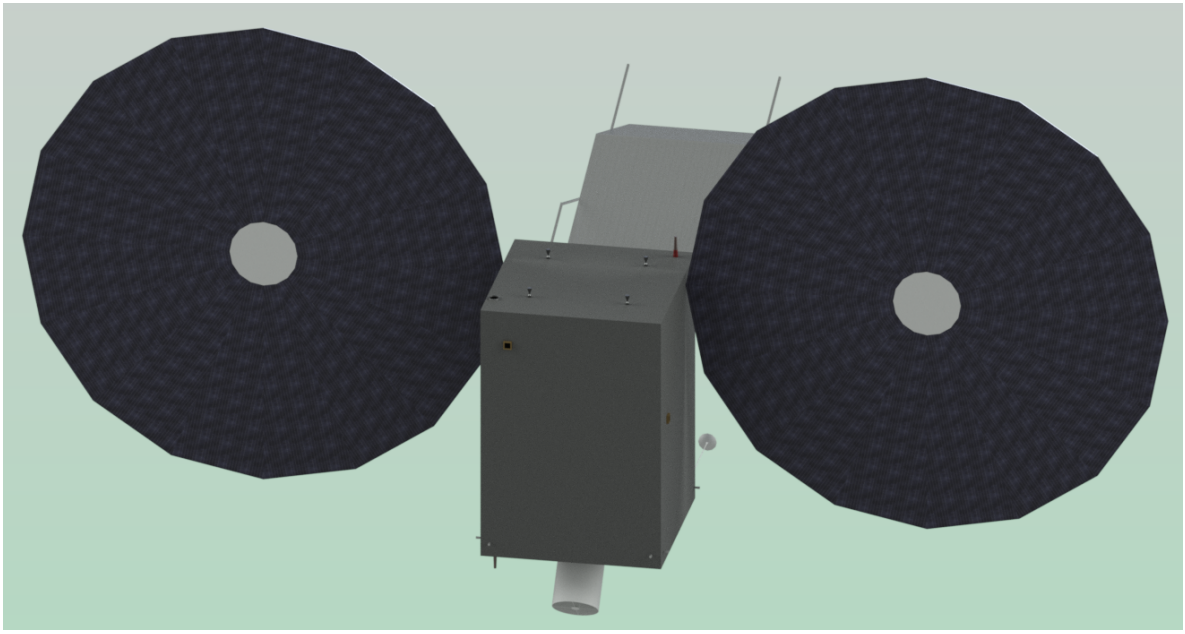

Figure 5.6: Isometric front view of the SBSP system.

In Figure 5.7, the TCS radiator is clearly visible, mounted on the back panel to dissipate heat efficiently. Another black circular component is also located on the back panel. Just below the radiator on the right side, another Coarse Sun Sensor can be seen. A small extended rod with a communication dish, positioned at the bottom of the satellite, is the HGA shown here in its deployed configuration, enabling X-band communication. Furthermore, the structural panels are constructed as sandwich panels and are layered with MLI on the surface for extra thermal protection.

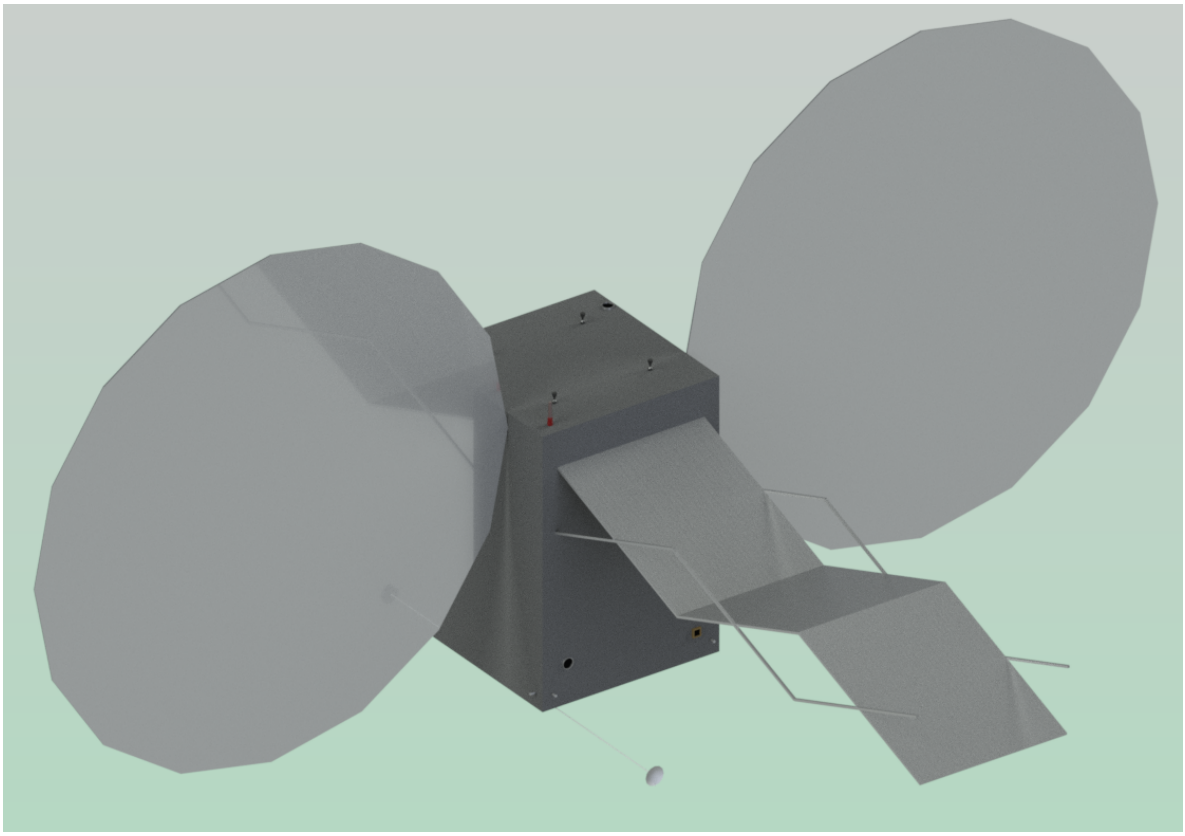

Figure 5.7: Isometric back view of the SBSP system.

5.6.2. Front and Back Internal View

With the front panel removed, the internal structure of the SBSP system becomes visible in Figure 5.8. At the bottom of the spacecraft bus, two light grey boxes represent the two LAUs part of the LPT subsystem, hosting the laser components for the power transmission.

The spacecraft bus is centered around a core cylindrical structure that functions as the primary structure of the SBSP system. Mounted on its sides are numerous components and inside the core structure, the two hydrazine propellant tanks and the helium pressurant gas tank are located (not visible in these images). At the top of the core cylinder, four circular reaction wheels are positioned along with their power units. The larger rectangular boxes surrounding the core are part of the PMAD subsystems. In the middle of the core, a small box is found which represents a 3-axis FOG, part of the ADCS subsystem.

Figure 5.9 shows the system with the back panel removed, revealing additional internal components. Next to the MegaFlex arrays, the brown-greyish components represent the SSUs, part of the PMAD subsystem. In the center, the BCDU and batteries are visible. Next, at the bottom, just above the beam director, the transponders and the RFDU components are located which are part of the TT&C subsystem.

Additionally, the TCS pumps are symmetrically positioned just underneath the reaction wheel, attached to the core. It is important to note that the active fluid loop is not displayed in this visualization due to the current uncertainties regarding its exact volume and layout. Consequently, sufficient space has been allocated to accommodate the active fluid loop, which should be implemented in a future detailed design study.

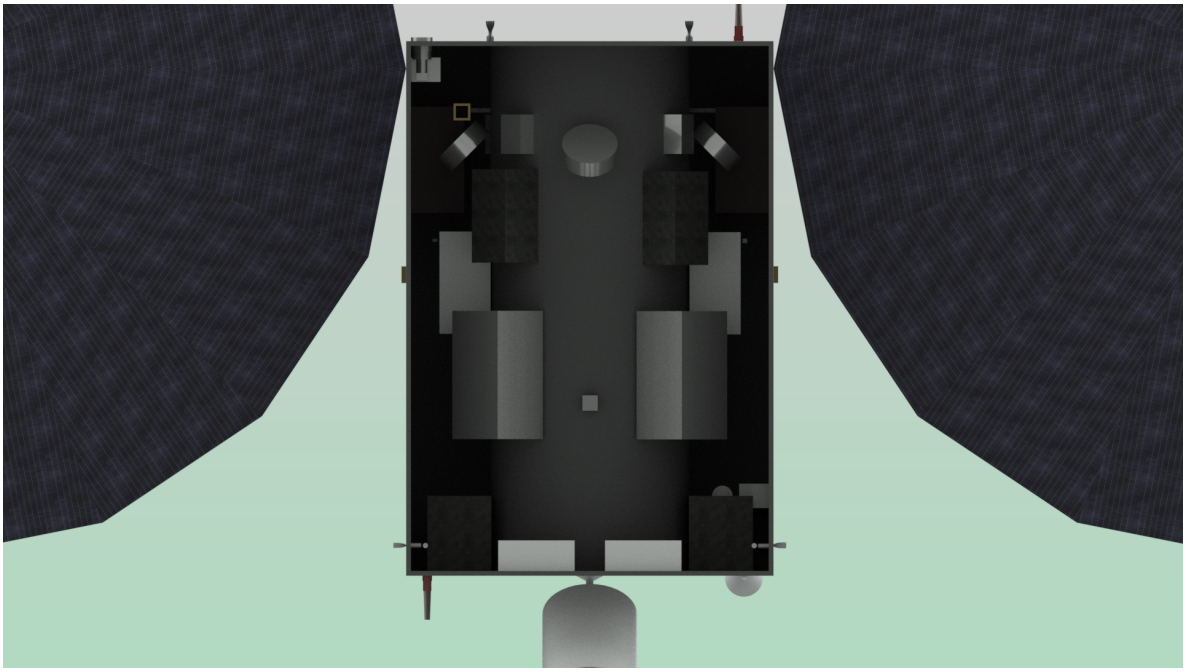

Figure 5.8: Front internal view of the SBSP system.

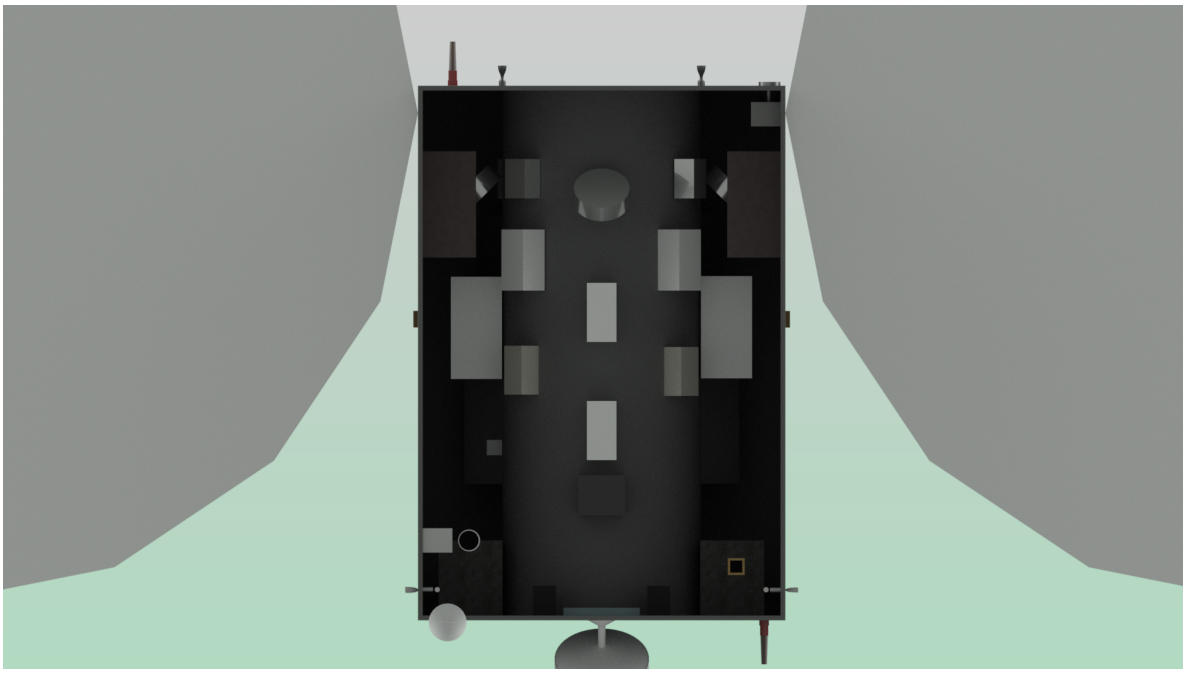

Figure 5.9: Back internal view of the SBSP system.

Finally, a visualization of the SBSP system in a realistic environment has been rendered shown in Figure 5.10. Note that the altitude of the satellite is not to scale as it is merely just a visualization.

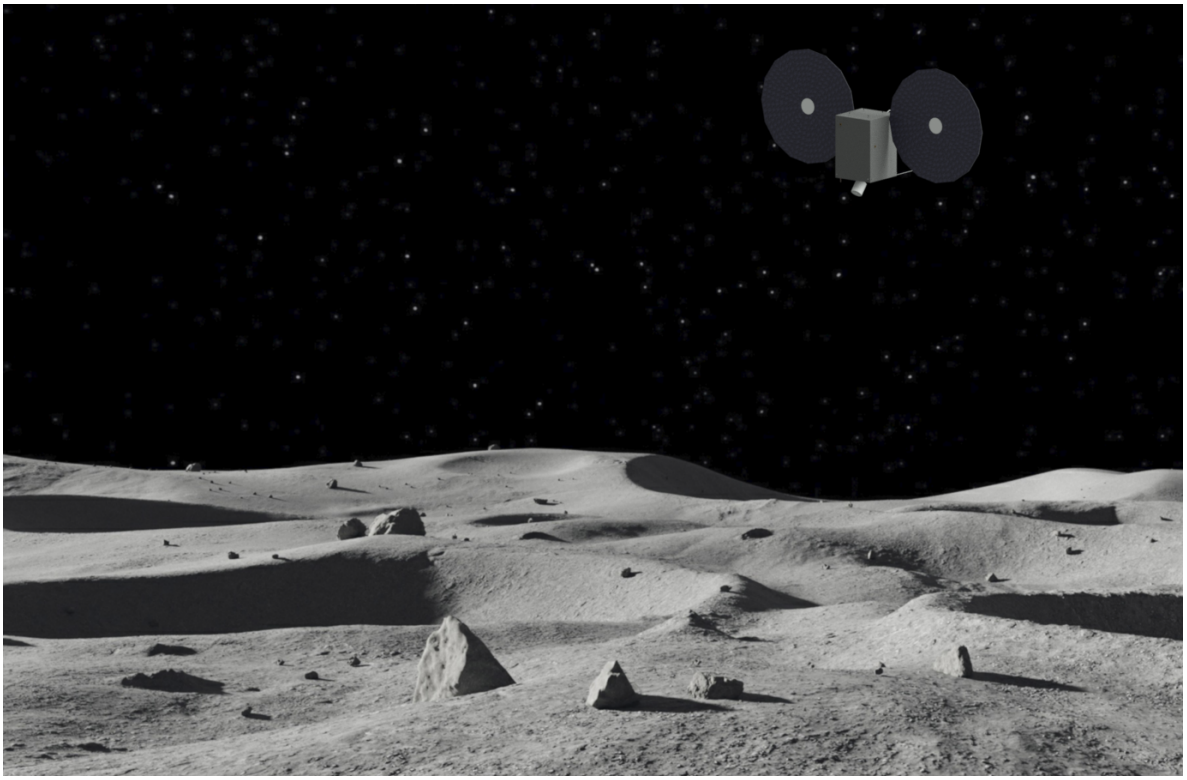

Figure 5.10: SBSP system in the lunar environment [107].

6

Conclusion

This thesis aimed to investigate a promising solution of conceptual design for a lunar-based SBSP demonstration mission, covering system architecture, transmission techniques and corresponding SBSP subsystems. The research question was further divided into four sub-questions to address specific components of the main research questions. These sub-questions will be discussed below after which the main research question can be addressed. Then, the validity of the SBSP design will be discussed and future research will be recommended.

6.1. Research Questions

SQ-1: What are the mission objectives for the lunar SBSP demonstration mission guaranteeing a successful mission?

The mission objectives for the lunar SBSP demonstration mission are derived from the mission statement, which focuses on demonstrating the feasibility and effectiveness of SBSP technology and wireless energy transmission from lunar orbit to a designated receiver on the lunar surface. The primary objectives are validating the efficiency and performance of the solar power generation system in the lunar environment, assessing the impact of lunar environmental factors on power generation, and demonstrating the transmission of the generated power from the satellite to the lunar surface receiver. Additionally, the efficiency and accuracy of power transmission will be measured and analyzed.

The system scalability and redundancy will also be assessed, evaluating the ability to scale up for increased power generation and transmission, while also maintaining system functionality in the event of individual component failures. Successful orbital maneuvers will be executed to achieve and maintain optimal satellite positioning for power generation and transmission, and the thermal control system will be validated to ensure proper thermal regulation of the satellite. The power management system will be validated to handle the generated power, combined with power storage and distribution. The communications system will be validated to ensure robust communication between the satellite, lunar receiver, and Earth ground control. Finally, the mission will demonstrate the system's ability to operate continuously and sustainably over an extended period, identifying and addressing any long-term operational challenges.

Together, these mission objectives ensure that the lunar SBSP demonstration mission is successfully executed and provide a clear framework to assess the SBSP readiness level for future SBSP operations on the Moon.

SQ-2: What is the most effective method for transmitting solar power to the lunar surface?

The trade-off analysis between laser and RF SBSP systems has highlighted a number of factors that impact their suitability for the lunar SBSP demonstration mission. Despite its lower end-to-end effi-

ciency, laser SBSP exhibits greater performance in beam precision, smaller mass and volume, higher power density and lower deployment complexity. These characteristics make laser SBSP the most effective method for transmitting solar power to the lunar surface, where compactness, precision are of paramount importance.

Nevertheless, RF SBSP systems are known for their higher technical maturity, with a TRL of 6, making them less risky for near-term deployment. Still, their larger size, lower beam precision and higher deployment costs due to their highly modular nature make RF SBSP systems less optimal for lunar applications. Additionally, RF systems require larger rectenna areas which would require more mass to be sent to the lunar surface, leading to increased mission costs.

Concluding, laser SBSP presents itself as a more optimal solution for the lunar demonstration mission, since laser SBSP systems balance cost-effectiveness, compactness and precision making it the preferred choice for future lunar SBSP operations.

SQ-3: What redundancy and reliability measures should be integrated into the design of a lunar SBSP system to ensure mission success?

The design of the SBSP system has integrated a list of redundancy and reliability measures that will ensure mission success for the lunar demonstration mission. Almost every subsystem has included redundancy measures by adding additional components that could replace other malfunctioning components within that particular subsystem.

The ADCS subsystem utilizes a configuration that combines two Star Trackers, four Coarse Sun Sensors, and two 3-axis FOGs. Implementing this feature allows for sensor diversity and redundancy. The OBC subsystem has included hardware redundancy and fault-tolerant software in the COTS component itself. Additionally, the PMAD subsystem has been designed such that two power flow chains are available and in the case of a malfunctioning component within one chain, the back-up component in the other chain takes over, ensuring continuous operations even when components fail in the PMAD subsystem.

The TT&C subsystem has incorporated two LGAs but only one HGA. However, the HGA functionalities can be reassigned to one of the LGAs in case the HGA experiences a failure. This would result in a decreased communication data rate but in return the satellite is still able to communicate with the Earth ground segment. Additionally, two transponders are included in the design for redundancy purposes. The propulsion system has integrated two independent spherical hydrazine tanks, each equipped with their own feed system to the thrusters, allowing for uninterrupted operations, even in the event of a malfunction in one of the tanks.

The TCS subsystem has integrated two active fluid loops such that the TCS is always able to regulate the temperatures within the SBSP system. However, the TCS radiator does not have a redundant counterpart which could lead to a single-point-of-failure if it suddenly malfunctioned. Deployment issues could pose a threat to the TCS radiator, but these were assumed to be unlikely due to the technical maturity of TCS radiators.

Furthermore, the LPT subsystem exists of two independent LAU modules, each capable of providing the required 3 kW of power output for power transmission. However, the beam director, precisely pointing the beam onto the receiver also does not have a redundant part in the design. This could also lead to a single-point-of-failure.

In summary, these redundancy measures collectively improve the operational reliability of the lunar SBSP system. Across critical subsystems, redundancy and fault-tolerant mechanisms have been implemented, such that the design is able to cope with individual component failures. This allows the system to achieve its objectives and demonstrate the ability to deliver power to the lunar surface. Nevertheless, this SBSP design still holds single-point-of-failures, such as the TCS radiator and the LPT beam director and must be carefully monitored during the mission to mitigate risks and ensure system

reliability.

SQ-4: How can the design of a lunar SBSP demonstration mission be scaled up for future SBSP operations on the Moon?

The design of a lunar SBSP demonstration mission can be scaled up for future lunar SBSP operations by addressing the challenges associated with mass scalability, mission duration, system efficiency and deployment feasibility. Scaling up the output power of the SBSP system, substantially increases the dry mass and total system mass to accommodate larger subsystems, including the MegaFlex arrays and components in the LPT, PMAD, TCS, ADCS and Propulsion subsystems. For example, scaling from a 3 kW to a 100 kW system increases the dry mass from 2.60 tons to 86.11 tons and the total system mass increases from 4.06 tons to 145.10 tons for a one year mission duration. It becomes clear that increasing the output power requirement has cascading effects on the total system design.

To operate for an extended period, such as five years, the SBSP system will require additional propellant. This cascades into the design by further increasing the propellant tank size, structural mass and dry mass. For the 100 kW system, a mission duration of five years would increase the total system mass from 145.10 to 232.54 tons. This example illustrates the impact of the operational lifetime on system scalability. Additionally, the degradation in the solar cells over time requires larger initial MegaFlex arrays such that the sustained power output can be ensured.

While scaling up the SBSP system improves the overall system efficiency, from 19.0% for the 3 kW system to 19.9% for the 100 kW system, the specific power (output power per unit mass) decreases with size. Thus, scaling up the SBSP system results in diminishing returns in mass efficiency. For example, the specific power decreases from 0.85 W/kg for the 10 kW system to 0.69 for the 100 kW system, both for a mission duration of one year. This result indicates that alternative strategies must be explored, such as deploying numerous smaller SBSP systems instead of a single large-scale system. This way, the high power demand of future lunar habitats can be addressed using more mass efficient, and thus cost-effective strategies.

Furthermore, the feasibility of large-scale SBSP systems depends on the capabilities of existing and future launch vehicles. Launchers such as the Falcon Heavy and Ariane 6 can support smaller SBSP systems, up to 10 kW. Larger systems would have to rely on emerging launch vehicle solutions such as Starship developed by SpaceX. Starship is expected to incorporate payloads of up to 100 tons to the lunar surface. With a total system mass of 98.36 tons, the 45 kW SBSP falls within the payload capacity of this launcher. Thus, making it feasible to deploy systems up to 45 kW using Starship. However, a 100 kW system would face significant deployment challenges due to their mass and size, making SBSP systems of this scale as of now not feasible.

The strategy of deploying multiple lower-output SBSP systems could result in a more mass efficient, redundant and flexible solution. For instance, a distributed network of 3 kW of 10 kW satellites could reduce the overall mass and cost per kW of delivered power. Through the usage of a SBSP constellation, continuous power could be delivered to a lunar habitat near the Shackleton's Crater. Continuous operations would require a minimum of 60 satellites and, for reliable operations, 60+ satellites are recommended to ensure redundancy and overlap in power transmission phases. Future studies should focus on investigating the optimal balance between constellation size, scalability, cost and efficiency to address the high-power demands for lunar habitats.

RQ: What is a promising conceptual design for a lunar-based SBSP demonstration mission, covering system architecture, transmission techniques, and corresponding SBSP subsystems?

A promising conceptual design for a lunar-based SBSP demonstration mission involves a laser-based SBSP system capable of delivering 3 kW of power from a low lunar orbit to a surface receiver. The SBSP design has integrated scalable and redundant subsystems, including the LPT, PMAD ADCS, TCS, OBC, TT&C and Propulsion subsystems. The SBSP architecture is designed with scalability in mind to accommodate systems up to 45 kW, such that these are compatible with launch vehicles

such as the Falcon Heavy or future vehicles such as Starship. The lunar demonstration mission would validate key technologies for wireless power transmission, potentially paving the way for supporting lunar habitats through a distributed SBSP constellation.

6.2. Discussion

The SBSP design in this thesis is based on a set of assumptions regarding various subsystems. For one in particular, the LPT subsystem, its properties have been assumed and acted as the foundation for this SBSP design. However, it must be noted that these values have not been verified and can only be confirmed once a detailed LPT design is presented. Furthermore, the beam director has been based on a Cassegrain telescope. While this approach provides a starting point, the effectiveness of such telescopes in the context of wireless power transmission may not be optimal. Further development, testing and optimization will be necessary to ensure that the beam director meets the performance requirement for the lunar SBSP demonstration mission.

The PMAD subsystem has been derived from the ISS PMAD subsystem, since it is the only existing system capable of handling high power loads in space. However, the ISS PMAD subsystem is a relatively old technology, which indicates that this design may not be the most efficient and compact solution for the lunar SBSP mission. Given the fact that the PMAD subsystem is not specifically designed for SBSP applications, further research and development in the PMAD area are required to create a more efficient, compact and tailored subsystem for the SBSP system.

Next, the TCS has been computed in a relatively simplistic manner based on a reference active thermal control loop. As volumetric data was not available during the design process, the CAD model does not incorporate the active fluid loop. Nevertheless, sufficient space has been reserved for the active fluid loop. It can even be concluded that the amount of available space in the CAD model may be too great for the TCS, indicating that the internal volume of the spacecraft has been over-designed. This should be reiterated in the design once more detailed information is available on the TCS active fluid loop.

Finally, each subsystem in this design requires a more comprehensive and detailed design process to refine the assumptions made in this study. The current design constitutes a conceptual framework, but it will have to be iterated as more detailed data and operational requirements emerge.

6.3. Recommended Future Research

Looking forward, future research should focus on several key areas for advancing the lunar SBSP design. First, the LPT subsystem design should be initiated. This subsystem acts as the payload of the satellite and is therefore integral to the entire SBSP system. The LPT performance will directly influence the efficiency of wireless power transmission from low lunar orbit to the surface. Hence, a detailed LPT subsystem is required such that the beam director and other optical components are optimized and verified for lunar operations.

Additionally, future research should focus on designing the PMAD and TCS subsystems, as these two subsystems are directly supporting the LPT subsystem in delivering power to the lunar surface. As discussed, the PMAD subsystem is based on older ISS technology and therefore future work should focus on developing a more modern and efficient solution specifically designed for SBSP applications. Similarly, the TCS subsystem should be further designed such that volumetric unknowns can be incorporated into the SBSP design.

The lunar receiver, which is not included in this study, must also be designed in a separate study. Without the lunar receiver, the SBSP system will not have anything to transmit its power to. Furthermore, understanding the specific requirements and limitations of the lunar receiver could demand certain changes in the SBSP system such that both systems are compatible with each other.

Lastly, the operations of the SBSP system during the demonstration mission must be planned and organized. The operational timeline can cause additional constraints on the SBSP design. To minimize risk and ensure mission success, these operations will have to be carefully coordinated. Future research should focus on mapping a detailed mission operations plan.

In conclusion, the detailed design and testing of critical subsystems such as the LPT, PMAD and TCS are of paramount importance for the next steps in advancing the lunar SBSP demonstration mission. These future steps will enable the way for the deployment of scalable, efficient SBSP systems for future lunar habitats.

Bibliography

[1] A. Baez. *Design Considerations for High Power Spacecraft Electrical Systems*. 2015. URL: https://ntrs.nasa.gov/api/citations/20150010178/downloads/20150010178.pdf (visited on 09/23/2024).

[2] Abhishek Ghosh. *Space-Based Solar Power: A Comphrehensive Exploration*. 2024. URL: https://thecustomizewindows.com/2024/09/space-based-solar-power-a-comprehensive-exploration/ (visited on 12/10/2024).

[3] Able Engineering. *UltraFlex Solar Array: Enabling Light Weight Low Volume Technology*. 2003. URL: https://satelliteobservation.net/wp-content/uploads/2024/02/ultraflex-solar-array.pdf (visited on 09/02/2024).

[4] Advanced Cooling Technologies. *Spacecraft Radiator Design*. URL: https://www.1-act.com/resources/learning-center/case-studies/spacecraft-radiator-design/#:~:text=Typical%20spacecraft%20radiators%20use%20aluminum,280%C2%B0C%20temperature%20range. (visited on 11/05/2024).

[5] Advanced Fiber Resources. *500 W Fiber to Free Space Isolater*. 2025. URL: https://www.fiber-resources.com/1064-nm-500-w-fiber-to-free-space-isolator_p316.html (visited on 01/13/2025).

[6] Aerojet Rocketdyne. *In-Space Propulsion Data Sheets*. 2020. URL: https://satcatalog.s3.amazonaws.com/components/847/SatCatalog_-_Aerojet_Rocketdyne_-_MR-107S_275N_-_Datasheet.pdf?lastmod=20210710010118 (visited on 10/10/2024).

[7] Airbus Defence and Space. *Integrated Control and Data EquipmenT (ICDE) NG*. 2022. URL: https://satsearch.co/products/airbus-defence-and-space-integrated-control-and-data-equipment-icde-ng (visited on 09/09/2024).

[8] American Solar Energy Society. *Thin-Film Solar Panels*. 2021. URL: https://ases.org/thin-film-solar-panels/#:~:text=Thin%2DFilm%20solar%20panels%20are%20less%20efficient%20and%20have%20lower,%25%20and%20up%20to%2018%25. (visited on 08/19/2024).

[9] S. Angelucci et al. "LUNARSAT ADCS EUROPEAN ORBITER TO THE MOON ATTITUDE DETERMINATION AND CONTROL SYSTEM". In: *European Control Conference (ECC)* (1999).

[10] APCO Technologies. *Panels CFRP/Aluminum*. 2018. URL: https://www.apco-technologies.eu/wp-content/uploads/2023/02/Data-Sheet-PdV-LR-CFRP-AL-Panels-1.pdf (visited on 10/10/2024).

[11] Argotec S.r.l. *FERMI Deep Space On-Board Computer*. 2024. URL: https://satsearch.co/products/argotec-fermi-deep-space-on-board-computer (visited on 09/09/2024).

[12] ASA. *ASA RC600*. URL: https://www.astrosysteme.com/products/rc600_1/ (visited on 11/01/2024).

[13] B. Mow. *STAT FAQs Part 2: Lifetime of PV Panels*. 2025. URL: https://www.nrel.gov/state-local-tribal/blog/posts/stat-faqs-part2-lifetime-of-pv-panels.html?utm_source=chatgpt.com (visited on 01/14/2025).

[14] M. Beckman. "Mission Design for the Lunar Reconnassaince Orbiter". In: *29th Annual AAS Guidance and Control Conference* (2006).

[15] R. C. van Benthem et al. "Development of a Mechanically Pumped Fluid Loop for 3-6 kW Payload Cooling". In: *NLR-TP-2009-459* (2010).

[16] Beyond Gravity. *S-band TTC Antennas*. 2024. URL: https://www.beyondgravity.com/sites/default/files/media_document/2024-07/S-band_TTC_Antennas_R-1308999-RSE_01-24.PDF (visited on 10/08/2024).

[17] Beyond Gravity. *Satellite Central Structures*. 2022. URL: https://www.beyondgravity.com/sites/default/files/media_document/2024-01/Beyond-Gravity-Satellite-Central-Structures.pdf (visited on 10/22/2024).

[18] Beyond Gravity. *Satellite Structures*. URL: https://www.beyondgravity.com/en/satellites/mechanical-solutions/satellite-structures (visited on 09/16/2024).

[19] Boeing. *Active Thermal Control System (ATCS) Overview*. 2006. URL: https://www.nasa.gov/wp-content/uploads/2021/02/473486main_iss_atcs_overview.pdf (visited on 09/04/2024).

[20] Boeing. *International Space Station Electric Power System (EPS)*. 2012. URL: https://gandalfddi.z19.web.core.windows.net/Shuttle/Misc_Space_Non-Shuttle/ISS_EPS.pdf (visited on 09/23/2024).

[21] Bradford Engineering. *Coarse Sun Sensor*. 2024. URL: https://www.bradford-space.com/products/css (visited on 10/07/2024).

[22] Bradford Engineering. *Coarse Sun Sensor*. 2024. URL: https://fra1.digitaloceanspaces.com/bradford/media/Coarse%20Sun%20Sensor%20Datasheet%20(2017) (visited on 10/07/2024).

[23] Bradford Engineering. *Reaction Wheel Unit*. 2019. URL: https://fra1.digitaloceanspaces.com/bradford/media/Reaction%20Wheel%20Datasheet%20(2019) (visited on 10/01/2024).

[24] D. Butler, J. Ku, and T. Swanson. “Loop Heat Pipes and Capillary Pumped Loops - an Applications Perspective”. In: *NASA/GSFC, Code 545* (2002).

[25] C. Cougnet et al. “Solar Power Satellites For Space Applications”. In: *55th International Astronautical Congress* IAC-04-R-3-06 (2004).

[26] D. B. Coyle. *Applications of Fiber Amplifiers for Space: Laser Altimetry and Mapping*. 2005. URL: https://nepp.nasa.gov/DocUploads/F6EB577B-9A9E-4EF1-BAB27D314EB490E7/Coyle.pdf (visited on 08/31/2024).

[27] Deployable Space Systems. *ROSA Flight Demonstration Hardware Successfully Deploys on ISS*. 2017. URL: https://redwirespace.com/wp-content/uploads/2021/05/ROSA-deployment-ISS-2017-scaled-1-1200x799.jpg (visited on 09/02/2024).

[28] Eagle-Group. *Fiber vs CO2 laser*. URL: https://eagle-group.eu/en/fiber-vs-co2-laser (visited on 08/25/2024).

[29] eoPortal. *LRO (Lunar Reconnaissance Orbiter)*. 2013. URL: https://www.eoportal.org/satellite-missions/lro#launch (visited on 01/15/2025).

[30] eoPortal. *Starship of SpaceX*. 2021. URL: https://www.eoportal.org/other-space-activities/starship-of-spacex#starship-of-spacex (visited on 01/03/2025).

[31] ESA. *How Hubble got its wings*. 2010. URL: https://www.esa.int/Enabling_Support/Space_Engineering_Technology/How_Hubble_got_its_wings (visited on 08/20/2024).

[32] ESA. *Hydra Star Tracker Pillars*. 2012. URL: https://www.esa.int/var/esa/storage/images/esa_multimedia/images/2012/11/hydra_startracker/12111960-3-eng-GB/Hydra_startracker_pillars.jpgr (visited on 09/06/2024).

[33] European Space Agency. *The Rosetta Orbiter*. 2025. URL: https://www.esa.int/Science_Exploration/Space_Science/Rosetta/The_Rosetta_orbiter (visited on 01/13/2025).

[34] M. D. Fiebig and C. M. Zakrzwski. “LRO Propulsion System Design On-Orbit Operations”. In: *48th Join Propulsion Conference Exhibit* (2012).

[35] E. B. Gietl et al. “The Electric Power System of the International Space Station - A Platform for Power Technology Development”. In: *NASA/TM-2000-210209* (2000).

[36] A. S. Gohardani et al. “Green space propulsion: Opportunities and prospects”. In: *Progress in Aerospace Sciences* 71 (2014), pp. 128–149.

[37] J. Grandidier et al. “Laser Power Beaming for Lunar Night and Permanently Shadowed Regions”. In: *Jet Propulsion Laboratory* (2020).

[38] J. Grandidier et al. “Power Beaming for Deep Space and Permanently Shadowed Regions”. In: *The 2nd Optical Wireless and Fiber Power Transmission Conference* (2020).

[39] Gyroscope.com. *Control Moment Gyroscope Platform*. URL: https://www.gyroscope.com/d.asp?product=CMG (visited on 09/06/2024).

[40] H. M. Remi. *ROSA: The Rollable Solar Arrays of NASA International Space Station*. URL: https://www.ccinnolab.org/solarcare/en/SolarAroundTheWorldPost/TheRollableSolarArrays#:~:text=They%20can%20hit%20around%2034,reach%2015%2D20%25%20efficiency. (visited on 09/02/2024).

[41] M. El-Heddeiny et al. "Optimal Orbit Parameters for Power Subsystem of LEO Satellites". In: *8th International Conference on Electrical Engineering* EE156.1 (2012).

[42] J. H. Henninger. "Solar Absorptance and Thermal Emittance of Some Common Spacecraft Thermal Control Coatings". In: *NASA-EP-1121* (1984).

[43] Isaac Ost. *Space-Based Solar vs. Conventional Solar - How Are They Different?* 2023. URL: https://www.solar.com/learn/space-based-solar-vs-conventional-solar-how-are-they-different/ (visited on 08/19/2024).

[44] N. Iwata et al. "Thermal Performance Evaluation of Space Radiator for Single-Phase Mechanically Pumped Fluid Loop". In: *Journal of Spacecraft and Rockets* 59.1 (2022).

[45] ixBlue. *Astrix NS The new 3-axis Fiber-Optic Gyroscope for space applications*. 2023. URL: https://www.ixblue.com/wp-content/uploads/2021/12/datasheetastrix-ns-ixblue.pdf (visited on 09/07/2024).

[46] J. Garrick and J. Simpson and N. Shah. *Lunar Reconnaissance Orbiter (LRO) Guidance, Navigation and Control (GNC) Overview*. 2010. URL: https://ntrs.nasa.gov/api/citations/20100014254/downloads/20100014254.pdf (visited on 09/07/2024).

[47] P. Jaffe et al. "Opportunities and Challenges for Space Solar for Remote Installations". In: *NRL/MR/8243–19-9813* (2019).

[48] JAXA. *IKAROS Small Scale Solar Powered Sail Demonstration Satellite*. 2021. URL: https://www.isas.jaxa.jp/en/missions/spacecraft/current/ikaros.html (visited on 08/20/2024).

[49] Jiga. *Titanium vs Aluminum*. URL: https://jiga.io/articles/titanium-vs-aluminum/#:~:text=Titanium%20generally%20exhibits%20a%20higher,(20%2C000%20to%2070%2C000%20psi). (visited on 09/21/2024).

[50] M. Kaczmarzyk and M. Musial. "Power to survive the Lunar night: An SPS Application". In: *59th International Astronautical Congress,* Paper IAC-08-C.3.1.2 ().

[51] K. A. Kamarudin and I. A. Hamid. "Effect of High Velocity Ballistic Impact on Pretensioned Carbon Fibre Reinforced Plastic (CFRP) Plates". In: *IOP Conference Series Materials Science and Engineering* 165 (2016).

[52] F. M. Khan et al. "Maximizing energy density of lithium-ion batteries for electric vehicles: A critical review". In: *7th International Conference on Renewable Energy and Conservation* (2022).

[53] K. Kumar and R. Noomen. "Stability of Highly Elliptical Orbits at the Moon". In: *Astrodynamics Specialist conference and Exhibit* AIAA 2008-7069 (2008).

[54] J. C. Mankins. "SPS-ALPHA: The First Practical Solar Power Satellite via Arbitrarily Large Phased Array". In: *NIAC Phase 1 Final Report* IAC-04-R-3-06 (2012).

[55] MatWeb. *Overview of materials for Epoxy/Carbon Fiber Composite*. URL: https://www.matweb.com/search/datasheet.aspx?matguid=39e40851fc164b6c9bda29d798bf3726&ckck=1 (visited on 09/21/2024).

[56] J. O. McSpadden and J. C. Mankins. "Space Solar Power Programs and Microwave Wireless Power Transmission Technology". In: *IEEE Microwave Magazine* ISSN 1527-3342/02 (2002).

[57] J. I. Minow et al. "Evidence for Arcing on the International Space Station Solar Arrays". In: *15th Spacecraft Charging Technology Conference* (2018).

[58] Moog. *Type 33 Biaxial Gimbal*. URL: https://www.moog.com/content/dam/moog/literature/sdg/space/actuationmechanisms/moog-type33-biaxial-thruster-gimbal-datasheet.pdf (visited on 10/01/2024).

[59] D. M. Murpy et al. "UltraFlex and MegaFlex - Development of Highly Scalable Solar Power". In: *978-1-4799-7944-8/15* (2015).

[60] R. Nalbandian. “Enhanced Pointing Gimbal Mechanisms for Next Generation Communication Antennas”. In: *15th European Space Mechanisms Tribology Symposium* ESMATS 2013 (2013).

[61] NASA. *NASA Space Science Data Coordinated Archive: Vanguard 1*. URL: https://nssdc.gsfc.nasa.gov/nmc/spacecraft/display.action?id=1958-002B (visited on 09/02/2024).

[62] NASA, Chris Lynch. *PHOTOS: ATK Validates New MegaFlex Solar Array Technology for NASA's Future Solar Electric Propulsion Missions*. 2014. URL: https://www.americaspace.com/2014/05/04/photos-atk-validates-new-megaflex-solar-array-technology-for-nasas-future-solar-electric-propulsion-missions/ (visited on 09/02/2024).

[63] New Space Economy. *Satellite Components: Reaction Wheels*. URL: https://newspaceeconomy.ca/2023/10/24/satellite-components-reaction-wheels (visited on 09/05/2024).

[64] NorthropGrumman. *Spacecraft Components*. URL: https://www.northropgrumman.com/space/spacecraft-components (visited on 09/02/2024).

[65] J. K. Paik, A. K. Thayamballi, and G. S. Kim. “The strength characteristics of aluminum honeycomb sandwich panels”. In: *Thin-Walled Structures* 35 (1999), pp. 205–231.

[66] M. Pätzold et al. “Rosetta Radio Science Investigations (RSI)”. In: *Space Science Reviews* 128 (2007), pp. 599–627.

[67] R. Nave. *Lagrange Points of the Earth-Moon System*. URL: http://hyperphysics.phy-astr.gsu.edu/hbase/Mechanics/lagpt.html (visited on 07/22/2024).

[68] R. Paschotta. *Diode Pumped Lasers*. URL: https://www.rp-photonics.com/diode_pumped_lasers.html (visited on 08/25/2024).

[69] T. Rahman et al. “Investigation of Degradation of Solar Photovoltaics: A Review of Aging Factors, Impacts, and Future Directions toward Sustainable Energy Management”. In: *Advances in Solar Cells and Photocatalysis,* II (2023).

[70] Rami Arieli. *The Laser Adventure*. URL: https://perg.phys.ksu.edu/vqm/laserweb/Ch-6/F6s2t2p3.htms (visited on 08/25/2024).

[71] Raycus. *Global Version Continuous-Wave Fiber Laser User Guide*. 2023. URL: https://en.raycuslaser.com/upload/20230829/1h902lf2plkt7aao.pdf (visited on 09/03/2024).

[72] Raytheon. *Raytheon Hel6 Panel Data*. 2023. URL: https://prd-sc102-cdn.rtx.com/raytheon/-/media/ray/what-we-do/integrated-air-and-missile-defense/hel/pdf/ray_hel6-panel_data_ic23.pdf?rev=d79c063a461246b7bb752674d3534cb0&hash=D3597E8AA47D344FF8CC1465B5C75C1B (visited on 08/25/2024).

[73] Redwire. *Solar Arrays - Roll Out Solar Array (ROSA)*. 2021. URL: https://redwirespace.com/wp-content/uploads/2023/06/redwire-roll-out-solar-array-flysheet.pdf (visited on 09/02/2024).

[74] W.T. Reynolds. “Architecture analysis of wireless power transmission for lunar outposts”. In: *Calhoun: The NPS Institutional Archive* (2015).

[75] RoyMech. *Titanium Alloy Properties*. URL: https://roymech.org/Useful_Tables/Matter/Titanium.html#:~:text=Titanium%20is%20a%20light%20metal,Aluminium%20at%202710kg%2Fm3. (visited on 09/21/2024).

[76] S. Clark. *Astronauts install new solar array outside International Space Station*. 2022. URL: https://spaceflightnow.com/2022/12/03/iss-eva-82/ (visited on 09/02/2024).

[77] R. Salih et al. “Experimental Investigation of Reinforced Concrete Beam with Openings Strengthened Using FRP Sheets under Cyclic Load”. In: *Materials* 13.3127 (2020).

[78] Sat Now. *Top Satellite Reaction Wheels in 2023*. 2023. URL: https://www.satnow.com/news/details/1455-top-satellite-reaction-wheels-in-2023 (visited on 09/06/2024).

[79] Sat Search. *Bradford Space Coarse Sun Sensor*. 2024. URL: https://satsearch.co/products/bradford-coarse-sun-sensor (visited on 09/06/2024).

[80] Sat Search. *Satellite OBC products on the global market*. 2024. URL: https://blog.satsearch.co/2020-03-11-an-overview-of-on-board-computer-obc-systems-available-on-the-global-space-marketplace (visited on 09/09/2024).

[81] Satnow. *Control Moment Gyroscope for Earth Observation and Science Missions*. URL: https://www.satnow.com/products/control-moment-gyroscopes/airbus/43-1213-cmg-75-75-s#:~:text=The%20CMG%2075%2D75%20S,10%20years%20in%20LEO%20orbit. (visited on 09/05/2024).

[82] SatSearch. *COTS Satellite Battery*. 2025. URL: https://satsearch.co/products/eaglepicher-technologies-cots-satellite-battery (visited on 01/14/2025).

[83] SITAEL. *Digital Earth Sensor*. 2025. URL: https://www.satcatalog.com/component/digital-earth-sensor/ (visited on 01/12/2025).

[84] Sodern. *Hydra M*. 2023. URL: https://sodern.com/wp-content/uploads/2023/12/2023-12-Hydra-family.pdf (visited on 10/07/2024).

[85] S. Somers-Neal et al. "Experimental investigation of a 10 kW-class flat-type loop heat pipe for waste heat recovery". In: *International Journal of Heat and Mass Transfer 231* 125865 (2024).

[86] L. T. Soto and L. Summerer. "Power to survive the Lunar night: An SPS Application". In: *59th International Astronautical Congress,* Paper IAC-08-C.3.1.2 ().

[87] Space Operations Command. *First In-Space Laser Power Beaming Experiment Surpasses 100 Days of Successful On-Orbit Operations*. 2023. URL: https://www.spoc.spaceforce.mil/News/Article-Display/Article/3457469/first-in-space-laser-power-beaming-experiment-surpasses-100-days-of-successful (visited on 07/15/2024).

[88] SpaceNews. *ATK Awarded* $20 Million Ultra Flex(TM) Solar Array Contract from Orbital$. 2011. URL: https://spacenews.com/atk-awarded-20-million-ultraflextm-solar-array-contract-from-orbital/ (visited on 09/02/2024).

[89] SpaceX. *Falcon Heavy*. 2024. URL: https://www.spacex.com/vehicles/falcon-heavy/ (visited on 01/03/2025).

[90] SpaceX. *Starship*. 2024. URL: https://www.spacex.com/vehicles/starship/ (visited on 01/03/2025).

[91] R. A. SPores et al. "GPIM AF-M315E Propulsion System". In: *50th Joint Propulsion Conference and Exhibit* (2013).

[92] S. R. Starin and J. Eterno. "Attitude Determination and Control Systems". In: *GSFC Book 3882* (2011).

[93] Starizona.com. *Classical Cassegrain Design*. 2020. URL: https://starizona.com/blogs/tutorials/classical-cassegrain-design (visited on 10/01/2024).

[94] M. Straubel, M. Hillebrandt, and C. Hühne. "Evaluation of Different Architectural Concepts for Huge Deployable Solar Arrays for Electric Propelled Space Craft". In: *14th European Conference on Spacecraft Structures, Materials and Environmental Testing (ECSSMET)* (2016).

[95] L. Summerer and O. Purcell. "Concepts for Wireless Energy Transmission via Laser". In: *ACT-RPR-NRG-2009-SPS-ICSOS* (2008).

[96] Thales Alenia Space. *Deep Space Secure Transponders*. 2012. URL: https://www.thalesgroup.com/sites/default/files/database/d7/asset/document/Deep_Space_Secure_Transponders.pdf (visited on 10/10/2024).

[97] The Engineering Toolbox. *Helium - Thermophysical Properties*. URL: https://www.engineeringtoolbox.com/helium-d_1418.html (visited on 11/11/2024).

[98] The Engineering Toolbox. *Universal and Individual Gas Constants*. URL: https://www.engineeringtoolbox.com/individual-universal-gas-constant-d_588.html (visited on 11/11/2024).

[99] ThermalEngineer. *Effective Emittance Multi-Layer Insulation (MLI)*. URL: https://www.thermalengineer.com/library/effective_emittance.htm#:~:text=Typical%20spacecraft%20MLI%20blankets%20only,layers)%20no%20lower%20than%200.001.&text=where%20n%20%3D%20number%20of%20mylar,of%20surfaces%201%20and%202. (visited on 11/04/2024).

[100] Y. Ulybyshev. "Long-Term Station Keeping of Space Station in Lunar Halo Orbits". In: *Journal of Guidance, Control, and Dynamics* (2014).

[101] Unibap AB. *SpaceCloud iX5-106*. 2024. URL: https://satsearch.co/products/unibap-ix5100 (visited on 09/09/2024).

[102] Valispace. *How to calculate Mission Specified Propulsion System Parameters – Part III*. 2019. URL: https://www.valispace.com/how-to-calculate-mission-specified-propulsion-system-parameters-part-iii/ (visited on 11/11/2024).

[103] WallpapersWide. *High Resolution Photo of the Moon*. 2025. URL: https://wallpaperswide.com/high_resolution_photo_of_the_moon-wallpapers.html (visited on 01/07/2025).

[104] L. Werling et al. “Experimental Performance Analysis (c□ c□ efficiency)of a Premixed Green Propellant consisting of N2O and C2H4”. In: *American Institute of Aeronautics and Astronautics* (2017).

[105] J. R. Wertz, D. F. Everett, and J. J. Puschell. *Space Mission Engineering: The New SMAD*. Icrocosm Press, 2015.

[106] N. E. White, J. Bookbinder, and A. Hornschemeier. “The status of the Constellation-X mission -art. no. 6686oB”. In: *Proceedings of SPIE - The International Society for Optical Engineering* (2007).

[107] Yamato3D. *Moon Surface*. 2024. URL: https://www.turbosquid.com/3d-models/3d-moon-surface-model-2072947 (visited on 12/20/2024).

[108] J. Yang et al. “State-of-health estimation for satellite batteries based on the actual operating parameters – Health indicator extraction from the discharge curves and state estimation”. In: *Journal of Energy Storage* 31 (2020).

[109] B.T.C. Zandbergen. “Aerosapce Design Systems Engineering Elements I Part: Spacecraf (bus) design and sizing”. In: *Delft University of Technology* Faculty of Aerospace Engineering (2021).